Universities of Glasgow and
Strathclyde

Department of Naval Architecture
and Marine Engineering

Probability of brittle fracture for a cracked ship

by

John Kent

A thesis presented in fulfilment of the
requirements for the degree of
Doctor of Philosophy

2007

Acknowledgements

The author would like to extend his considerable thanks to Dr. John Sumpter for his help and advice at all stages of this work. It is fair to say that without John's involvement the study would have never progressed to the stage it is at today.

Thanks are also due to Professors Nigel Barltrop and Purnendu Das who have been involved in the supervision of the project since its initial conception as an MSc study at the University of Glasgow.

Abstract

Fatigue cracking is a common problem in ships and can potentially lead to a catastrophic brittle fracture. This thesis presents a methodology to quantify the risk of leaving these cracks unrepaired while a ship remains in service. The most important variable affecting the probability of failure is the material fracture toughness. Test results carried out on samples taken from a number of ship steel plates are fitted using a modified 'master curve' approach. The approach links fracture mechanics toughness (characterised by K_{jc} in MPa$\sqrt{m}$) to the Charpy 27 joule temperature. A major innovation in the work is the use of time-dependent reliability to account for the variation in toughness as the crack extends by fatigue. The loading applied to the crack tip comprises three components: still water bending; wave induced bending; and residual stress. A number of methods used to calculate the probability of failure are compared, with the convolution integral identified as the most suitable. The methodology is successfully benchmarked against the trend in actual failure statistics from the Liberty ships to date. Target probabilities of failure are used to estimate crack lengths for repair. Taking a figure of 5×10^{-4} events per year as broadly typical of the observed frequency of brittle fracture in merchant ships the methodology suggests that this is equivalent to a crack length of 300 mm in grade A steel at $0^{o}C$. Given that cracks are unlikely to be found until they reach 200mm this provides a small margin of safety. For grade D steel the repair length is increased to over 1000mm potentially allowing the repair to be delayed to coincide with scheduled maintenance periods.

List of contents

Acknowledgements ..... **III**

Abstract ..... **IV**

List of contents ..... **V**

List of figures ..... **VIII**

List of tables ..... **XIV**

Notation ..... **XV**

1 Introduction **1**

1.1 Overview 1
1.2 Examples of brittle fracture 1
1.3 Factors influencing brittle fracture 9
1.4 Thesis contents 10

2 Literature review **12**

2.1 Background 12
2.2 Hodgson and Boyd 12
2.3 Sumpter 13
2.4 Ship Structure Committee 15
2.5 SINTAP 20
2.6 Classification societies 21
2.7 Discussion 22

3 Problem definition **25**

3.1 Overview 25
3.2 Stress intensity factor 25
3.3 Fatigue crack growth 28
3.4 Limit state function 30
3.5 Time-dependent reliability 33

4 Applied loading **37**

4.1 Overview 37
4.2 Measured data 38
4.3 Wave induced bending stress – fracture 40
4.4 Wave induced bending stress – fatigue 50
4.5 Still water bending stress 52
4.6 Combining the still water and bending stress 53
4.7 Residual stress 55

5 Material fracture toughness **57**

5.1 Overview 57
5.2 Test procedure 58

5.3 QinetiQ test programme 60
5.4 Fitting the toughness distribution 64
5.5 Defining a region of constant toughness 79

6 Structural reliability methods 85

6.1 Background 85
6.2 Example calculation 86
6.3 Limit state function 88
6.4 First-order reliability methods 89
6.5 Monte Carlo simulation 94
6.6 Monte Carlo simulation with importance sampling 97
6.7 Lower bound on fracture toughness 99
6.8 Comparison of methods 106
6.9 Discussion 108

7 Results 110

7.1 Overview 110
7.2 Parametric Study 112
7.3 Comparison with reference casualty statistics 114
7.4 Example safe crack lengths 122

8 Conclusions and discussion 124

8.1 Summary 124
8.2 Areas of further work 127

9 References 133

10 Publications 140

A Selected Lloyd's Register material specifications 141

B Program flowchart 142

B.1 Overview 142

C Summary of distributions 146

C.1 Normal distribution 146
C.2 Weibull distribution 146
C.3 Rayleigh distribution 147
C.4 Exponential distribution 147
C.5 Extreme Type 1 distribution 147

D Sea state fits 149

D.1 Flowchart of fitting procedure 149
D.2 Sea state fit parameters 150
D.3 Least squares methodology 151
D.4 Least squares fits for long-term operation 152
D.5 Combined still water and bending stress distribution 153

E Material fracture toughness 154

E.1 Example trace of toughness tests 154
E.2 Toughness data 155
E.3 Master curve fit to plate 1 test data 158
E.4 Master curve fit to plate 2 test data 159
E.5 Master curve fit to plate 3 test data 160
E.6 Master curve fit to plate 4 test data 161
E.7 Master curve fit to plate 4 weld and HAZ test data 162
E.8 Master curve fit to plate 5 test data 163
E.9 Master curve fit to plate 6 test data 164
E.10 Master curve fit to plate 7 test data 165
E.11 Master curve fit to plate 7 weld and HAZ test data 166
E.12 Master curve fit to all test data 167
E.13 Master curve with censored specimens 168
E.14 Bimodal master curve 169
E.15 Zerbst modified lower bound approach 170
E.16 Bimodal master curve and Zerbst approach 171
E.17 Master curve with random inhomogeneities 172
E.18 Wide plate analysis 173

F Standard calculation parameters 175

G Structural reliability methods 177

G.1 Example calculation at first time step 177
G.2 Inclusion of lower bound on fracture toughness 186

H Results 190

H.1 Parametric study 190
H.2 Safe crack length as a function of steel grade 196

List of figures

Figure 1-1 Brittle fracture of Liberty ship whilst at sea 2

Figure 1-2 Example of Liberty ship suffering brittle fracture whilst in dock 3

Figure 1-3 Recovered stern section of M.V. Kurdistan 5

Figure 1-4 Forward section of Flare following brittle fracture 6

Figure 1-5 Lake Carling awaiting assistance from tug following brittle fracture 7

Figure 1-6 Brittle fracture in sideshell of Lake Carling 8

Figure 2-1 Example of failure assessment diagram 19

Figure 3-1 Geometry factor as a function of characteristic crack length for superstructure detail 27

Figure 3-2 Diagram of crack propagating from assumed area of damage 27

Figure 3-3 Geometry factor as a function of ratio of characteristic crack length to radius of damage 28

Figure 3-4 Example of crack growth in steel 29

Figure 3-5 Example load resistance plot at time step 1 31

Figure 3-6 Calculation of probability of failure at each time interval 34

Figure 4-1 Mechanical strain gauge recorder 38

Figure 4-2 Mechanical strain gauge data plotted using median ranking 39

Figure 4-3 Example fit to sea state 8 44

Figure 4-4 Example fit to sea state 5 44

Figure 4-5 Relationship between probability of exceedance per cycle and per 4 hour period 47

Figure 4-6 Comparison of long-term fit with measured data 48

Figure 4-7 Extreme type-1 distribution derived for maximum measured hog and sag stress 49

Figure 4-8 Distribution of still water bending stress 53

Figure 4-9 Plot of combined probability density function for still water bending stress and wave induced bending stress 54

Figure 4-10 Plot of stress intensity due to residual stress 56

Figure 5-1 All toughness results plotted against test temperature 62

Figure 5-2 All toughness results plotted against test temperature relative to Charpy 27J temperature 62

Figure 5-3 All toughness results plotted against temperature relative to Charpy 27J temperature indexed by plate identifier 67

Figure 5-4 Comparison of mixed-mode distribution with basic master curve approach fitted to all test data 68

Figure 5-5 Master curve fit to all test data 69

Figure 5-6 Plot of engineering lower bound approach 72

Figure 5-7 Effect of toughness model on probability of failure 77

Figure 5-8 Wide plate test set-up 80

Figure 5-9 Close-up showing cold temperature tests 80

Figure 5-10 Applied stress intensity as a funciton of crack length plotted against material fracture toughness data 82

Figure 5-11 Effect of sampling interval on cumulative probability of failure 83

Figure 6-1 Joint probability density function of wave induced bending stress and material fracture toughness 87

Figure 6-2 Joint probability density function showing limit state function 88

Figure 6-3 Joint probability density function showing limit state function 90

Figure 6-4 Limit state function mapped into standard normal space 91

Figure 6-5 Limit state function showing design point in standard normal space 94

Figure 6-6 Convergence of Monte Carlo simulation 96

Figure 6-7 Convergence of Monte Carlo simulation with importance sampling 98

Figure 6-8 Probability density function of material fracture toughness modified to account for lower bound cut-off 100

Figure 6-9 Effect of lower bound on material fracture toughness distribution on limit state function 101

Figure 6-10 Convergence of FOR algorithm with lower bound on material fracture toughness distribution 102

Figure 6-11 Design point calculated using simple geometry 103

Figure 6-12 Convergence of Monte Carlo simulation 104

Figure 6-13 Convergence of Monte Carlo simulation with importance sampling .. 105

Figure 6-14 Effect of increasing crack length on shape of limit state function 108

Figure 7-1 Construction of traffic light regions 111

Figure 7-2 Spread of Charpy 27J temperature as a function of date of manufacture 115

Figure 7-3 Fitted distribution of Charpy 27J temperature as a function of date of manufacture 116

Figure 7-4 Distribution of operating temperature for normal operation 117

Figure 7-5 Probability of brittle fracture as a function of the date of manufacture of plate 118

Figure 7-6 Comparison of reference casualty statistics with predicted risk of brittle fracture 119

Figure 7-7 Comparison of reference casualty statistics with predicted risk of brittle fracture 120

Figure 7-8 Assumed distribution of Charpy 27J transition temperature as a function of steel grade 122

Figure 8-1 Shift in T_0 as a function of the stress intensity rate 128

Figure 8-2 High frequency component of applied loading superimposed on low frequency wave bending 129

Figure D-1 Long term sagging fit to Lloyd's Register operational profile 152

Figure D-2 Long term hogging fit to Lloyd's Register operational profile 152

Figure D-3 Effect of bin size on combined distribution 153

Figure E-1 Example test traces of material fracture toughness tests 154

Figure E-2 All toughness results plotted against test temperature 155

Figure E-3 All toughness results plotted against test temperature showing effects of rolling direction 155

Figure E-4 All toughness results plotted against test temperature relative to Charpy 27J temperature 156

Figure E-5 All toughness results plotted against test temperature relative to FATT156

Figure E-6 All toughness results plotted against test temperature relative to Charpy 27J temperature – mode of failure 157

Figure E-7 Master curve fit to plate 1 test data 158

Figure E-8 Normalised scatter plot of master curve fit to plate 1 test data 158

Figure E-9 Master curve fit to plate 2 test data 159

Figure E-10 Normalised scatter plot of master curve fit to plate 2 test data 159

Figure E-11 Master curve fit to plate 3 test data 160

Figure E-12 Normalised scatter plot of master curve fit to plate 3 test data 160

Figure E-13 Master curve fit to plate 4 test data 161

Figure E-14 Normalised scatter plot of master curve fit to plate 4 test data 161

Figure E-15 Master curve fit to plate 4 weld and HAZ test data 162

Figure E-16 Normalised scatter plot of master curve fit to plate 4 weld and HAZ test data 162

Figure E-17 Master curve fit to plate 5 test data 163

Figure E-18 Normalised scatter plot of master curve fit to plate 5 test data 163

Figure E-19 Master curve fit to plate 6 test data 164

Figure E-20 Normalised scatter plot of master curve fit to plate 6 test data 164

Figure E-21 Master curve fit to plate 7 test data 165

Figure E-22 Normalised scatter plot of master curve fit to plate 7 test data 165

Figure E-23 Master curve fit to plate 7 weld and HAZ test data 166

Figure E-24 Normalised scatter plot of master curve fit to plate 7 weld and HAZ test data 166

Figure E-25 Master curve fit to all test data 167

Figure E-26 Normalised scatter plot of master curve fit to all test data 167

Figure E-27 Censored master curve fit to all test data 168

Figure E-28 Normalised scatter plot of censored master curve fit to all test data ... 168

Figure E-29 Bimodal master curve fit to all test data 169

Figure E-30 Normalised scatter plot of bimodal master curve fit to all test data 169

Figure E-31 Zerbst modified lower bound approach fit to all test data 170

Figure E-32 Normalised scatter plot of Zerbst modified lower bound approach fit to all test data..... 170

Figure E-33 Bimodal Zerbst and Master Curve fit to all test data..... 171

Figure E-34 Normalised scatter plot of bimodal Zerbst and master curve fit to all test data 171

Figure E-35 Master curve with random inhomogeneities fit to all test data..... 172

Figure E-36 Normalised scatter plot of master curve with random inhomogeneities fit to all test data 172

Figure E-37 Master curve fit to wide plate test results 173

Figure E-38 Normalised scatter plot of Master Curve fit to wide plate test results. 174

Figure H-1 Acceptable crack length as a function of temperature relative to Charpy 27J temperature (residual stress)..... 190

Figure H-2 Effect of temperature relative to Charpy 27J temperature on number of days until repair (residual stress)..... 190

Figure H-3 Acceptable crack length as a function of temperature relative to Charpy 27J temperature (no residual stress)..... 191

Figure H-4 Effect of temperature relative to Charpy 27J temperature on number of days until repair (no residual stress)..... 191

Figure H-5 Effect of thickness on acceptable crack length..... 192

Figure H-6 Effect of thickness on number of days until repair..... 192

Figure H-7 Effect of operational profile on acceptable crack length..... 193

Figure H-8 Effect of operational profile on number of days until repair..... 193

Figure H-9 Effect of location on acceptable crack length..... 194

Figure H-10 Effect of location on number of days until repair..... 194

Figure H-11 Effect of damage on deck on acceptable crack length 195

Figure H-12 Effect of damage on keel on acceptable crack length 195

Figure H-13 Safe crack lengths for grade A steel as a function of external temperature..... 196

Figure H-14 Safe crack lengths for grade D steel as a function of external temperature..... 196

Figure H-15 Safe crack lengths for grade E steel as a function of external temperature..... 197

List of tables

Table 4-1 Discretisation of records into sea states 42

Table 4-2 Summary of long-term fits 45

Table 4-3 Summary of stress range as a function of sea state 51

Table 4-4 Summary of still water bending stress values 52

Table 5-1 Summary of Charpy and tensile properties for the plates tested 60

Table 5-2 Summary of T_0 parameters for master curve approach 67

Table 5-3 Summary of fitted parameters for combined engineering lower bound and original master curve fit 74

Table 5-4 Summary of maximum likelihood estimates for each fit method 76

Table 5-5 Fracture mechanics tests results from cold temperature test 81

Table 6-1 Input parameters for sample problem 86

Table 6-2 Comparison of predicted probabilities of failure estimated using a number of structural reliability methods 106

Table 7-1 Input variables analysed in parametric study 112

Table 7-2 Reduction in incidence of brittle fracture 115

Table A-1 Summary of material specifications (Lloyd's Register 2005b) 141

Table D-1 Weibull co-efficients describing per cycle distribution of wave induced bending stress for hog response 150

Table D-2 Weibull co-efficients describing per cycle distribution of wave induced bending stress for sag response 150

Table D-3 Effect of bin size on area under combined distribution 153

Table E-1 Summary of fit parameters for wide plate toughness results 173

Table F-1 Summary of standard calculation parameters 176

Notation

The following list defines the main symbols appearing in this thesis.

K_{1D}	=	Dynamic fracture toughness for mode 1 loading
σ_{yD}	=	Dynamic yield stress
K	=	Elastic stress intensity factor
Y	=	Geometry factor
σ	=	Remotely applied stress
UTS	=	Ultimate tensile strength
a	=	Characteristic crack length
N	=	Number of cycles
r	=	Radius of circular hole
A_Y	=	Geometry factor constant
B_Y	=	Geometry factor exponent
ΔK	=	Range of cyclic stress intensity
da/dN	=	Crack growth per cycle
C	=	Paris law crack growth constant
M	=	Paris law crack growth exponent
G( )	=	Limit state function
$\mathbf{X}$	=	Random vector of variables in real space
X_i	=	Random value of variable i in real space
x_i	=	Variable i in real space
y_i	=	Variable i in standard normal space
$\mathbf{x}^*$	=	Design point in real space
$\mathbf{y}^*$	=	Design point in standard normal space
p_f	=	Probability of failure
h( )	=	Hazard function
μ	=	Mean value
σ	=	Standard deviation
u	=	Modal value of extreme type-1 distribution
a	=	Measure of dispersion of extreme type-1 distribution
p( )	=	Probability density function
P( )	=	Cumulative distribution function
P_e( )	=	Probability of exceedance
P_{4hr}( )	=	Probability of exceedance in a 4-hour period

A	=	Weibull scale factor
B	=	Weibull shape factor
E[ ]	=	Expected value
$\Delta\sigma_{eq}$	=	Equivalent cyclic stress
σ_{SWBS}	=	Stress due to still water bending
σ_{wave}	=	Stress due to wave induced bending
K_{res}	=	Residual stress intensity factor
Y_{res}	=	Residual stress geometry factor
σ_y	=	Yield stress
c	=	Point at which residual stress changes from tensile to compressive
K_{mat}	=	Material fracture toughness
$K_{mat(25mm)}$	=	Equivalent material fracture toughness for 25 mm thick specimen
K_{min}	=	Minimum material fracture toughness
K_0	=	Material fracture toughness corresponding to a 63.2% probability of exceedance of K_{mat}
T	=	External temperature
T_0	=	Reference temperature for indexing material fracture toughness
T_{27J}	=	Charpy 27J transition temperature
L	=	Maximum likelihood estimator
b_0	=	Initial ligament size of material fracture toughness test specimen
E	=	Young's modulus of elasticity
ν	=	Poisson's ratio
p_a	=	Parameter used to indicate the probability of a value lying within the first distribution of a bimodal distribution
J_0	=	J integral related to material fracture toughness corresponding to a 63.2% probability of exceedance of K_{mat}
J_{LB}	=	J integral related to lower bound of material fracture toughness
J_c	=	J integral related to material fracture toughness
K_{LB}	=	Material fracture toughness at assumed lower bound of 0.1 % cumulative probability
μ_{K0}	=	Mean of distribution of K_0 variable
σ_{K0}	=	Standard deviation of K_0 variable
K_{SWBS}	=	Stress intensity due to still water bending stress
β	=	Reliability index

$\Phi( )$	=	Standard normal cumulative distribution function
$\Phi^{-1}( )$	=	Inverse of standard normal cumulative distribution function
$\phi( )$	=	Standard normal density function
J	=	Jacobian matrix
c_i	=	Components of outward normal vector to limit state equation in standard normal space
l	=	Length of outward normal vector in standard normal space
α_i	=	Direction cosines for each variable in standard normal space
I[ ]	=	Indicator function
r	=	Randomly generated number in the range 0 to 1
$h_v( )$	=	Probability density function of importance sampling function
$\Gamma( )$	=	Gamma function
N_H	=	Number of cycles per hour
$f_{x1}( )$	=	Probability density function for strength variable
$f_{x2}( )$	=	Probability density function for load variable
$F_{x1}( )$	=	Cumulative distribution function for strength variable

1 Introduction

1.1 Overview

Fatigue cracking has been a persistent problem in ship structures since welding processes were introduced during World War II. Small flaws are introduced into the structure during the weld process, which then develop into through-thickness cracks under the cyclic action of the loading acting on a ship's hull. These cracks propagate from highly stressed localised areas, adjacent to the weld, into plate and stiffeners.

A crack propagates relatively slowly under fatigue. However, under certain conditions a brittle fracture can occur. This is an extremely fast propagating crack which rapidly extends through the structure resulting in a dramatic loss of section.

Current classification society policy is to repair all fatigue cracks as soon as they are discovered. However, in a structure as complicated as a ship there are likely to be many small fatigue cracks which remain undetected. Therefore, the approach adopted by the classification societies is somewhat confusing. It is clear that there are many ships sailing around safely containing fatigue cracks. However, classification societies do not appear to acknowledge this fact in their rules.

If it can be demonstrated that the cracks are much smaller than the critical crack length, at which a brittle fracture would occur, and are propagating relatively slowly under fatigue, then it would be possible to delay the repair of the crack. This 'living with cracks' philosophy would reduce costs for the ship's operator, as the repair could be delayed to coincide with scheduled maintenance periods, and reduce time out of service.

1.2 Examples of brittle fracture

The problem of brittle fracture in ship structures came to the fore during the Second World War with the well publicised failures of the Liberty ships. Since then there has been a gradual reduction in the number of brittle fractures, although the examples given in the following sections highlight a number of recent incidents.

The following sections discuss examples of brittle fracture, which help to set the aims of the thesis in context and highlight the consequences of brittle fracture.

1.2.1 Liberty ships

Perhaps the most widely used examples of brittle fracture are the Liberty ships. Approximately 2700 of these lightly armed cargo vessels were built between 1942 and 1945 to transport goods across the North Atlantic. They were among the first ships to use welding rather than riveting to fabricate the ship's structure. This dramatically reduced the construction time and by the end of the war an entire vessel could be constructed in less than five days.

However the use of new welding technology caused problems: 15% of the ships suffered brittle fractures, often catastrophic. Figure 1-1 shows the SS John P Gaines which suffered a brittle fracture near Aleutians, completely breaking the ship in two. Figure 1-2 shows a T-2 tanker, also of welded construction, which suffered a brittle fracture in dock after returning from sea trials.

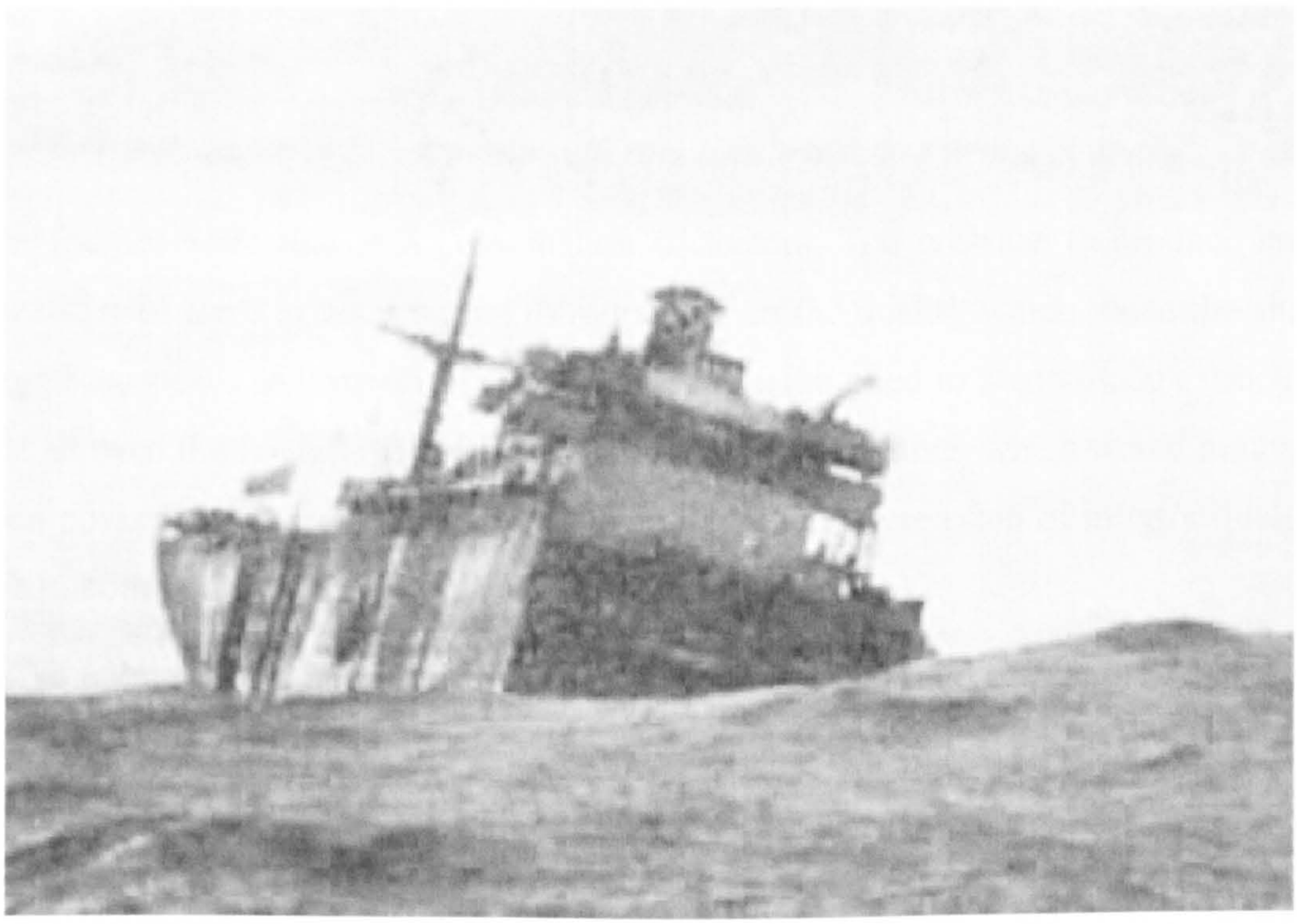

Figure 1-1 Brittle fracture of Liberty ship whilst at sea

Figure 1-2 Example of Liberty ship suffering brittle fracture whilst in dock

The failures were due to a combination of factors. The pressure to produce huge quantities of steel in wartime led to reductions in the quality which made the ships more susceptible to brittle fracture. The use of welding led to a continuous structure that allowed the fracture to propagate throughout the structure, which would not have been possible in a riveted ship. The welds themselves were often of inferior quality, due to both poor workmanship and materials.

These failures prompted a great deal of research into the field of fracture mechanics and moved it from a purely theoretical research topic into a specific engineering discipline.

1.2.2 Concorde

The Concorde was the largest tanker afloat in 1953 when it broke in two during heavy seas in the Irish Channel. Prior to the accident the ship had taken on extra ballast and reduced speed. The master reported a 'mountainous' wave which caused the ship to crash heavily into the following trough, at which point a second wave broke over the deck. Following this a loud rumbling was reported and the ship was

found to have broken in two at midships. Both halves of the vessel were salved and taken to the Clyde for analysis. The temperature at the time of the accident was 10°C, not particularly low.

A study of the vessel was undertaken (MacCallum, 1981) and found that the fracture had initiated in the keel of the vessel, at the intersection of the longitudinal with either the shell plate or the bulkhead bracket. The workmanship was generally reported to be of a high standard, although a slight lack of penetration was noted.

The vessel was constructed of special quality steel with a controlled carbon content. Subsequent testing of samples from the area of the fracture found high Charpy transition temperature and high crystallinity in the keel area. The steel would therefore have been brittle and susceptible to fracture at the time of the accident.

A number of factors are highlighted as contributory to the brittle fracture: the dynamic nature of the slam loading; the high still water bending moment; and the poor quality of the steel in the fracture initiation site.

1.2.3 Kurdistan

On 15th March 1979 the motor tanker M.V. Kurdistan broke in two while sailing through the Cabot Strait. At the time of the incident the vessel was fully laden in heavy seas (sea state 8) with an air temperature of approximately 0°C and a sea temperature of -0.7°C (Corlett, 1987). The vessel was pitching heavily in the high seas and the Master reported hitting a submerged object, although a subsequent investigation found that the bow had slammed into a wave (Stone, 1981).

Oil was seen to be leaking into the sea from a vertical wing tank. At 18:40 the vessel was re-ballasted in an effort to limit oil leakage. At this point a second shudder was felt by the crew, similar to the first one. At 21:30 there was a further shudder and the vessel broke in two at midships.

The stern of the vessel was salvaged and taken to New Brunswick. In an effort to reduce pollution the bow of the vessel was sunk by gunfire. The salvaged stern section is shown in Figure 1-3.

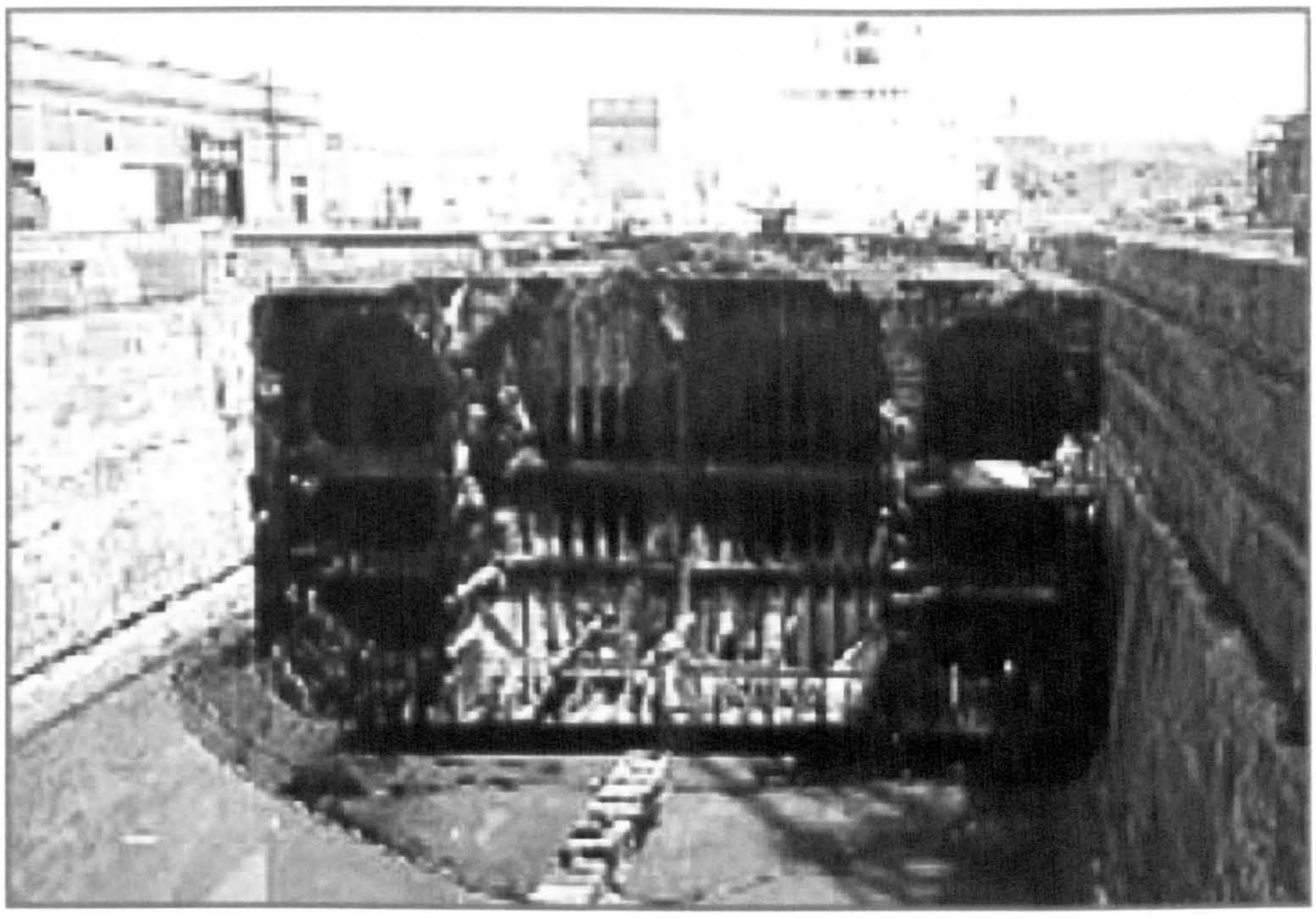

Figure 1-3 Recovered stern section of M.V. Kurdistan

The initiation site of the fracture was determined to be a weld defect in the port side flat bar butt weld (Stone, 1981) on the bilge keel. The flat bar was replaced following a grounding incident two years previously. The repaired section also failed to contain a crack arrest hole which was shown on the ship's diagrams. The repaired section was not inspected by the classification surveyor.

Samples were taken from the initiation site for testing, carried out by The Welding Institute (Garwood, 1980). It found that the materials conformed to Lloyd's Register requirements. However, the Kurdistan was constructed almost entirely of grade A steel which, at that time, had no minimum requirement for Charpy 27J temperature. The weld in which the fracture initiated had a Charpy 27J transition temperature of +20°C and the adjacent plate had a Charpy 27J transition temperature of +10°C. At the time of the incident the material would therefore have been 20°C below its Charpy 27J transition temperature.

1.2.4 Flare

The Flare was a Lloyd's Register classed bulk carrier built in 1972, constructed principally from grade A steel with grade D used for the deck and sheer strake. On the 15th of January 1998 the Flare sank after suffering a brittle fracture in the Cabot Strait. At the time of the incident the air temperature was -3°C with a sea temperature of 2°C (TSBC, 1998).

At approximately midnight a loud bang was heard by the ship's crew as the bow of the vessel experienced a severe slam. Four and a half hours later a second loud bang was heard, at which point the vessel split in two at approximately midships. The stern section sank in about half an hour, while the bow section stayed afloat for four days and is shown in Figure 1-4. At the time of the incident the seas were described as exceptionally high, with an estimated significant wave height of between 6 and 9 m.

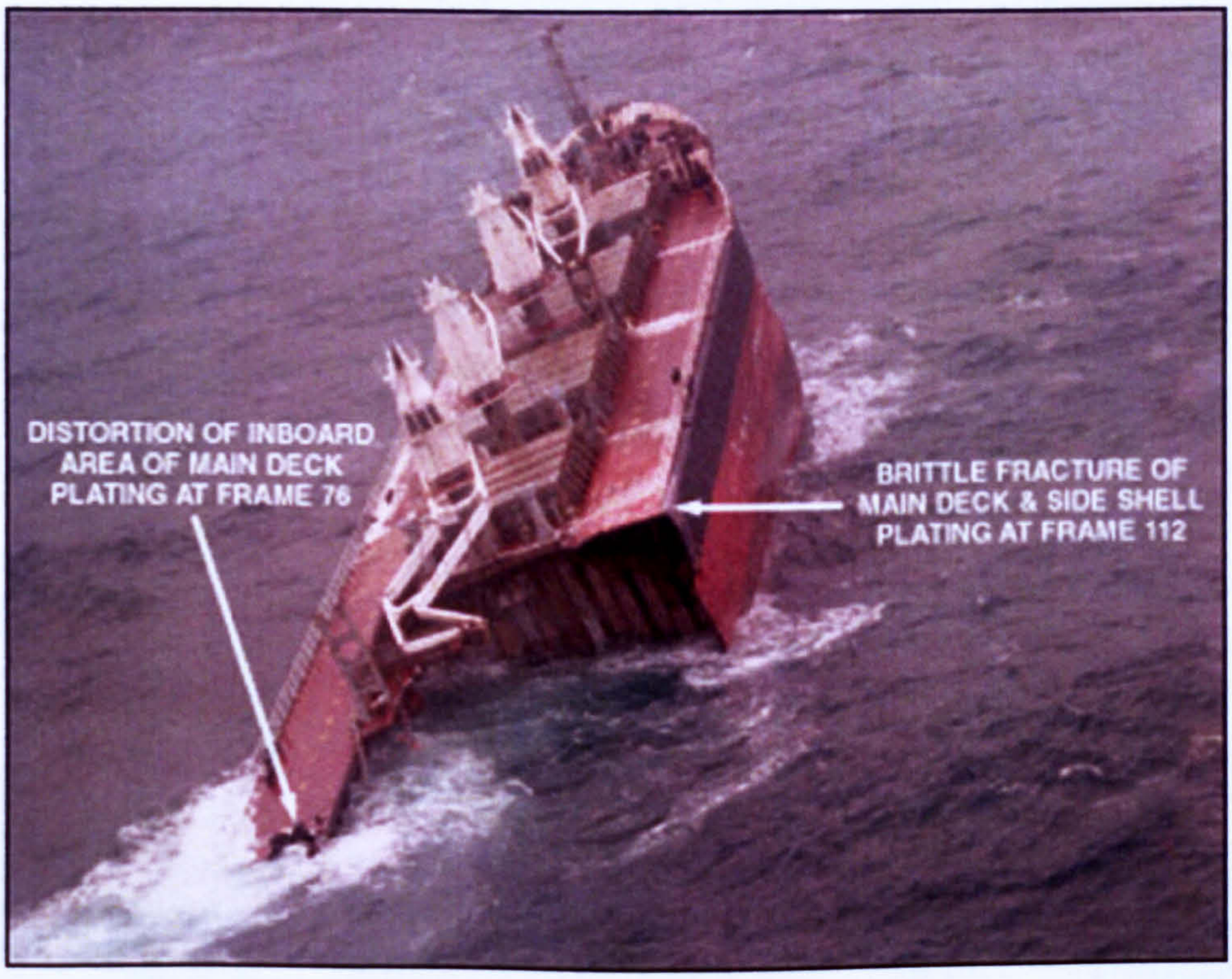

Figure 1-4 Forward section of Flare following brittle fracture

The cause of the brittle fracture was attributed to the slamming caused by the high seas, which increased the loading on the hull girder (TSBC, 1988). The nature of the

slamming was heightened by the draft, which was lower than that recommended by Lloyd's Register to minimise forefoot slamming.

The increased loading rate due to the slamming incident would have reduced the material's fracture toughness, making it more susceptible to brittle fracture. No samples were taken from the vessel and the report of the incident does not identify the initiation site.

1.2.5 Lake Carling

The Lake Carling was a "handy-sized" bulk carrier built in 1992 classified by DNV to ice class 1C. It is constructed principally of grade A steel with a shear strake and strength deck of grade E steel.

On the 18th of March 2002 a 6m long crack was found in the port side No. 4 hold during a routine inspection, due to water ingress into the hold. At the time of the incident the sea state was unexceptional, with a hindcast wave height of 1.5-2.5m. The weather was cold with an air temperature of -6°C and a water temperature of 0°C.

A salvage tug arrived to aid the vessel, supplying additional pumps to allow the hold to be pumped dry. The tug is shown alongside the Lake Carling in Figure 1-5. The exterior of the hold was then caulked by a diver to reduce water ingress.

Figure 1-5 Lake Carling awaiting assistance from tug following brittle fracture

The vessel was re-ballasted to reduce the still water bending moment and proceeded to Baie de Gaspe. Crack growth during transit was negligible due to a crack arresting hole drilled at the crack tip. Figure 1-6 shows the fracture in the side shell.

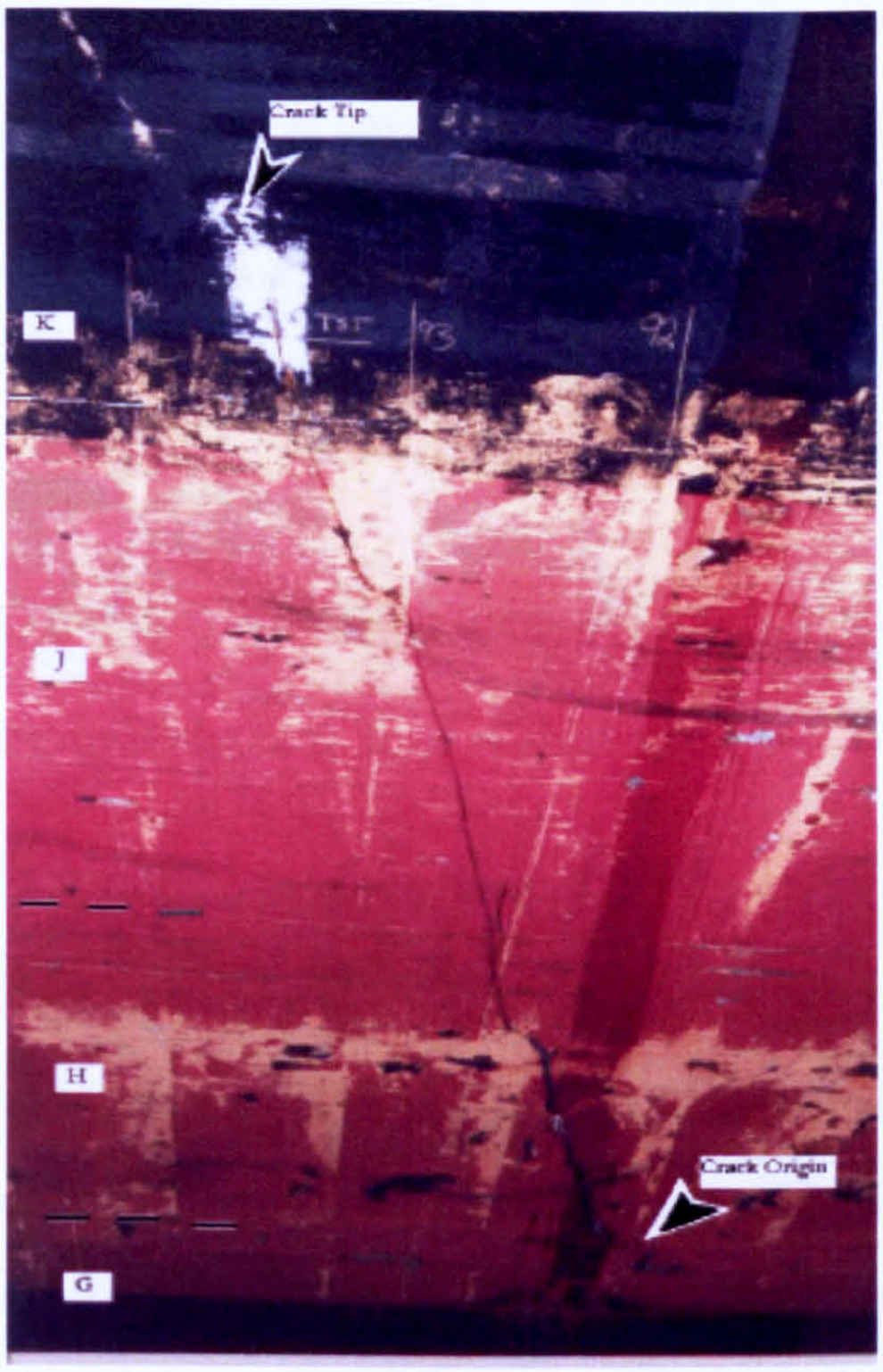

Figure 1-6 Brittle fracture in sideshell of Lake Carling

Inspection of the fracture indicated that it had initiated from a small fatigue crack at the toe of a weld at the base of a side shell frame. Cracks were also discovered at similar details, some of which had superficial weld repairs. No record of these repairs were documented by DNV surveyors.

Material near to the origin of the fracture was removed for analysis and indicated that the Charpy 27J transition temperature was approximately +15°C, with a fracture appearance transition temperature (FATT) of +32°C. At the time of the incident the steel would have been approximately 20°C below the Charpy 27J transition temperature.

The cause of the initial fatigue crack is attributed to the poor structural detail and heavy weather encountered on two previous voyages. It was also discovered that during one of the voyages the seagoing still water bending moment was 107% of the

allowable maximum. However, the crack initiated close to the neutral axis where the section modulus would be considerably lower than on the deck or keel. The critical crack length is estimated to be as short as 100mm, presumably due to the localised residual stresses near to the welded detail.

1.3 Factors influencing brittle fracture

The examples given in the previous sections have indicated a number of contributory factors to an incidence of brittle fracture. These are:

- presence of an initial flaw;
- applied loading (possibly including localised residual stress);
- loading rate (how quickly peak load is applied);
- low temperature;
- poor quality steel.

A brittle fracture occurs when the stress at the crack tip exceeds the critical cleavage stress. Exceeding the cleavage stress, which is far above yield stress for ship steels, requires the presence of a sharp crack tip to cause a local stress elevation. As the applied loading is increased the material local to the crack tip quickly reaches yield and attempts to contract, due to Poisson's effects. However, the material surrounding the crack tip is not subjected to the stress concentration and has not reached yield. It resists this contraction, which allows stress at the crack tip to further increase and approach the cleavage stress. Consequently, without a crack-like flaw a brittle fracture could not occur.

The remaining factors contribute to a brittle fracture. However, they are not all required to be present; nor does the presence of all the factors automatically result in a brittle fracture, it simply increases its likelihood. The applied loading obviously increases the probability of attaining the cleavage stress. Applying the load more quickly results in an increase of the yield stress of surrounding material, which prevents material at the crack tip from contracting, which would help to relieve the stress concentration. Low temperature or poor quality steel reduces the critical value of cleavage stress, allowing a brittle fracture to be triggered at a lower applied load.

There is a wealth of anecdotal evidence of ships that have continued to operate for many years in the presence of cracks. However, the cases given in this chapter highlight that if the contributory causes do coincide to result in the required conditions for a brittle fracture to initiate then the consequences are extremely severe.

1.4 Thesis contents

The thesis is divided into eight chapters with supporting appendices. A summary of the chapter contents is given below:

- Chapter 1 is a general introduction to the thesis, covering background to the problem and gives examples of brittle fracture.
- Chapter 2 is the literature review. Suggested approaches available in published literature are discussed and evaluated. Current state of the art thinking is discussed and shortfalls in methods are highlighted.
- Chapter 3 introduces the background equations used to quantify the conditions at the crack tip and fatigue crack growth rates. The limit state function used to define the boundary between the safe region and failure is defined.
- Chapter 4 discusses the applied loading acting on the crack tip. The distributions used and assumptions made are discussed.
- Chapter 5 examines the material fracture toughness. Considerable effort has been made to fit a realistic distribution with an appropriate lower bound. Time dependent reliability is used to account for the variation in material fracture toughness as a crack propagates across a plate.
- Chapter 6 evaluates several methods of solving the limit state function to calculate the probability of failure. The most suitable method should combine both accuracy and efficiency.
- Chapter 7 presents the results of the study. Published failure statistics are used to determine an acceptable level of risk. This can be used to determine suitable repair lengths for fatigue cracks.

- Chapter 8 presents the main conclusions and discussion of the thesis. Possible areas of further work are discussed and shortfalls of the current methodology are discussed.

2 Literature review

2.1 Background

This chapter provides an overview of previous work carried out in the field of brittle fracture research. The chapter starts with the empirical measures introduced following the dramatic failures of the Liberty ships. As understanding of the mechanisms of brittle fracture increased the approaches became increasingly more sophisticated, developing into fully probabilistic models.

Perceived shortfalls in the methodologies are highlighted and discussed, establishing the basis for the methodology presented in this thesis. The chapter concludes with a discussion of the areas which will be focussed on in this thesis.

2.2 Hodgson and Boyd

Hodgson and Boyd (Hodgson, 1958) carried out a comprehensive investigation of incidences of brittle fracture in merchant shipping covering the period from 1945 to 1958 on behalf of Lloyd's Register. In total, records from 182 vessels were analysed. It was found that welded ships had sustained 18% more incidences of fracture than riveted ships. It is acknowledged in the discussion that this figure would be even higher if more emphasis had not been placed in the design of local details for welded ships.

It is also interesting to note that the fractures in riveted ships had not arrested at the seams between plates. A common explanation of the sudden increase in incidence of brittle fracture in welded ships is due to the continuous nature of welded ships, which allow a fracture to propagate throughout the structure. Instead, Hodgson and Boyd attribute the lower incidence of fracture in riveted ships to the flexibility of riveted connections which allow stress concentrations to relieve.

The principal causatory factors of brittle fracture were determined to be: cold temperature; the presence of an initial defect; high applied loading; and poor material. The effect of high loading rate is also alluded to, due to a number of incidences being preceded by heavy slamming effects but is not specifically highlighted. In 1958 Lloyd's Register rules only specified simple tensile and bend requirements. American welded ships were subject to control of high sulphur and

phosphorus contents and limited the magnese to carbon ratio to 2.5. Increasing the carbon content increases the hardness and strength of the steel but also causes it to become brittle, due to the formation of martensite in the microstructure. Controlling the carbon content causes the steel to have a ferritic-pearlite structure. This has a much finer grain size, which leads to an increase in fracture toughness. Manganese is added to prevent hot-cracking during the manufacturing process.

It was found that despite these content controls fractures were still occurring. Consequently, Hodgson and Boyd decided to control the quality of steel through testing procedure. The Charpy impact test was used, primarily for its simplicity. Based on an analysis of data taken from known casualties the minimum Charpy temperature at 0°C was set at 35 ft.lb. (47J), together with a limit to the crystallinity of 70%.

The proposals made by Hodgson and Boyd were partially adopted by the class societies. The Charpy requirement was used in the specification of what was then grade D steel. Due to difficulties in determining the degree of crystallinity the 70% limit was not introduced. However, their work had little impact as the vast majority of shipping continued to be manufactured from grade A steel.

2.3 Sumpter

Sumpter published the first of a series of papers into the problem of brittle fracture in ships in 1989 (Sumpter, 1989), pointing out that in the 30 years since Hodgson and Boyds' landmark paper brittle fracture still remained a concern; highlighted by the recent failure of MV Kurdistan (Section 1.2.3).

The concern was furthered following a number of brittle fractures in the bow sections of naval frigates following collisions during the cod war. These areas had not been thought to be at risk of brittle fracture, due to the thinness of the plate. At the time of writing (1989) there was still no toughness requirement for grade A steel, which allowed a ship less than 250m to be constructed entirely from a steel with no specified toughness.

The first paper in the series (Sumpter, 1989) attempted to quantify the applied stress intensity at the crack tip. Two components of loading were considered, wave loading

and residual stress. It appears that the effects of still water bending were omitted. The loading at the crack tip was determined under two scenarios: a short crack embedded in the residual stress field; and a 1 m long crack which had propagated clear of the localised residual stress field. Based on these scenarios it was calculated that a toughness of 125 MPa$\sqrt{m}$ would provide a high safety factor against brittle fracture.

The temperature and loading rate at which this criterion should be met is discussed. 0°C is estimated to be the lowest temperature for normal ship operation. Loading rates applicable to collision, slamming, and wave action were considered. Dynamic crack tip opening displacement (CTOD) tests are used to demonstrate that at high loading rates of 10^4 MPa$\sqrt{m}$/s, equivalent to local plate slamming, the toughness requirement is met by grade D plate. Grade A plate only meets the requirement at lower loading rates, less than 10^2 MPa$\sqrt{m}$/s. Consequently, grade A steel is considered unsuitable for the outer hull. It is highlighted in the discussion that steel is neither homogeneous nor isotropic, and the result of a toughness test relates only to a single location within a plate. However, no discussion is made of the relative degree of scatter nor of the number of repeat tests required to satisfy the requirement.

A follow up paper (Sumpter, 1991) addressed the issue of weld toughness, which was found to meet the 125 MPa$\sqrt{m}$ requirement. This was due to the Charpy 27J requirements being higher than the parent plate.

The final paper in the series (Sumpter, 1995) translated the 125 MPa$\sqrt{m}$ requirement into an equivalent Charpy Fracture Appearance Transition Temperature (FATT). A toughness requirement based on a Charpy test is very desirable, being more common and much cheaper than a full CTOD test. However, it does have a number of drawbacks: the test is carried out at a dynamic loading rate; and the crack tip has a blunt notch, as opposed to a sharp crack. The FATT is preferred over the Charpy energy as it is insensitive to the rolling direction of the steel and is a more reliable estimate of the resistance of a steel to cleavage fracture.

It is concluded that to ensure that the material toughness requirement of 125 MPa$\sqrt{m}$ is met at a loading rate of 10^4 MPa$\sqrt{m}$/s and a temperature of 0°C the FATT for plate, weld, and heat-affected zone (HAZ) should be below 0°C. The paper also highlights

the significant effect of loading rate. Reducing the loading rate from 10^4 to 10^2 MPa$\sqrt{m}$/s is equivalent to a reduction of 30°C in the ductile to brittle transition.

The approach adopted by Sumpter has a number of drawbacks. The scenarios used to derive the toughness requirement make a number of unconservative simplifying assumptions. The short crack scenario assumes a geometry factor of 1. Short cracks are likely to propagate from a region of high local stress which would have a geometry factor in excess of 1. The long crack scenario is also based on a geometry factor of 1, which is felt to be reasonable, but the applied stress is only 100 MPa. Given that the effects of still water bending are also omitted, this is felt to be very low. With these considerations, the proposed 125 MPa$\sqrt{m}$ requirement would require to be increased.

The use of the FATT, rather than the Charpy energy test, is also questionable. The FATT is based on a visual inspection of the failure surfaces. It is considered that the Charpy energy test would have been more suitable as it does not require a subjective judgement by the operator.

2.4 Ship Structure Committee

The Ship Structure Committee (SSC) was formed in the 1940s. Its primary aim was to eliminate ship failures, principally through steering research into a number of different areas. Over the years it has published a number of reports on the issue of brittle fracture, together with research into many aspects of ship design including: wave loading; damage assessment; and material properties.

A major viewpoint of the SSC work is that cracks will always be present in a structure as large and complicated as a ship. The use of welding means that high residual stresses are present in the vicinity of a weld, often up to yield point. Consequently, the emphasis of SSC work has been to control these cracks using notch tough steel, combined with crack arrestor strakes.

Early work carried out by the SSC on the problem of brittle fracture investigated a number of projects undertaken by other research organisations (Drucker, 1954). The basic concepts of fracture mechanics are noted: sharpness of crack; loading rate effects; and the influence of secondary stress. The influence of stress triaxiality at the

crack tip on the likelihood of brittle fracture is also noted. However, at the time there was no way to link these parameters to a critical material parameter. Consequently, a lot of effort appears to have been placed in what is termed 'crack propagation'; the nature of how a brittle fracture runs through a plate and how it could be arrested.

This was followed by a notable publication, SSC-244 (Rolfe, 1974), which summarised developments in fracture mechanics and how they related to ships. The concept of the stress intensity factor had now been established and allowed the applied loading, flaw size, and geometry to be related to the material fracture toughness.

The most commonly used grades of steel, A and B, still had no minimum toughness requirements and although the number of brittle fractures had reduced since the Liberty ships, it was still considered to be unacceptably high. SSC-244 recommended that the most economical way to minimise the problem of brittle fracture was through material control. This was preferred over metallurgical controls as it allowed the steel mill more flexibility over the steel contents as long they met the minimum required standards.

The ship was divided into primary load-carrying structure on the extremities of the hull girder, with the remainder defined as secondary structure. Somewhat confusingly, the stiffeners on the extremities are not defined as primary structure as they are not connected to each other. However, the stiffeners will carry a greater proportion of the applied loading than the plating and a fatigue crack or brittle fracture occurring in a stiffener would certainly propagate into the parent plate.

The minimum fracture toughness was based on the assumption of yield point residual stress applied at a dynamic loading rate, given in Equation 2-1.

$$\frac{K_{1D}}{\sigma_{yD}} > 0.9 \qquad \textit{Equation 2-1}$$

with the input variables selected to give a result in $\sqrt{inch}$.

where K_{1D} is the dynamic fracture toughness for mode 1 loading and σ_{yD} is the dynamic yield stress. For secondary structure the criteria was lowered to 0.6.

A major drawback in the requirement was that the criteria could not be tested using any of the testing methods available at the time. The limit for plane-strain behaviour for steels below 25mm thick is approximately 0.6 of yield. Consequently, the criterion was established in terms of the nil-ductility temperature (NDT) to ensure that the ductile to brittle transition fell well below 0°C, the estimated lower bound of temperature for normal ship operation. This criterion was relaxed to 20°C for secondary structure.

A noted drawback of toughness testing is that the result only applies to a single location in the plate, and that there can be a significant difference in the results between the weld, heat-affected zone, and the parent plate. However, there is no discussion of the likely degree of scatter in the measured values or the number of tests required to determine if the test requirement was met by the entire plate.

A number of subsequent SSC publications attempted to meet the NDT requirement for ship steel and weld. SSC-248 (Hawthorne, 1974) tested existing ship steel grades A, B, C, D, and E and found that only grades D and E could meet the requirements. SSC-276 (Francis, 1978) drew similar conclusions from tests on weld and the heat affected zone.

This apparent contradiction is highlighted in SSC 307 (Pense, 1981): grade A is by far the most common shipbuilding steel and fails to meet Rolfe's criteria, yet these ships continue to operate relatively safely. It is concluded that the requirement given in Equation 2-1 was reasonable, but the required loading rate was in excess of normal ship operation. Material fracture toughness decreases as the loading rate is increased, caused by an increase in yield stress with loading rate. This allows a greater stress to build at the crack tip before local yielding occurs, increasing the likelihood of a cleavage failure.

The effect of loading rate was investigated in SSC-275 (Francis, 1978) by carrying out tests at three loading rates: static; dynamic; and impact. It was concluded that the effect of loading rate could be modelled as an equivalent shift in transition temperature, with the effect more noticeable moving from intermediate to dynamic than static to intermediate. The loading rate applicable to normal ship operation was estimated to be 200-440 ksi$\sqrt{}$in/sec (220-440 MPa$\sqrt{}$m/s), equivalent to an

intermediate loading rate. Note that this is considerably lower than the loading rate used by Sumpter. At this loading rate grades B and C met Rolfe's criteria, unfortunately grade A was not tested. This is felt to be a major omission as the vast majority of ships are constructed principally from grade A steel.

In recent years the focus of SSC work has shifted to more sophisticated calculation methodologies. This is attributed to a change in attitude from a 'safe-life' approach, where there is a low probability of failure during the service life, to a 'fail-safe' approach, where the structure is designed with multiple load paths. The 'fail-safe' approach is developed into a damage-tolerant context, which carries out an assessment of the structure assuming that damage is present.

SSC-409 (Glen, 1999) proposed a methodology to determine the critical crack length for repair of crack-type defects. This approach allows repairs to be scheduled to coincide with maintenance periods, reducing the cost and time out of service to the operator. The approach is principally developed for tankers, and considerable effort is placed in the calculation of the various load components.

The load components are calculated for the desired return period, incorporating a risk parameter. The risk parameter is the probability of exceedance that the load will be exceeded in the return period, and is commonly set to 1%. The material fracture toughness is determined through the standard ASTM test (ASTM, 2005). The toughness value used depends on the number of repeat tests, but is intended to be the 33^{rd} percentile.

The methodology utilises a failure assessment diagram (FAD) to determine if a failure has taken place through either of two mechanisms: brittle fracture or plastic collapse. The main concept of the FAD is to provide a boundary curve that represents the locus of predicted failure points. Calculated points lying inside the boundary curve are assumed to be safe, any points lying outside the boundary curve are considered to be unsafe and have failed. An example of a FAD is shown in Figure 2-1.

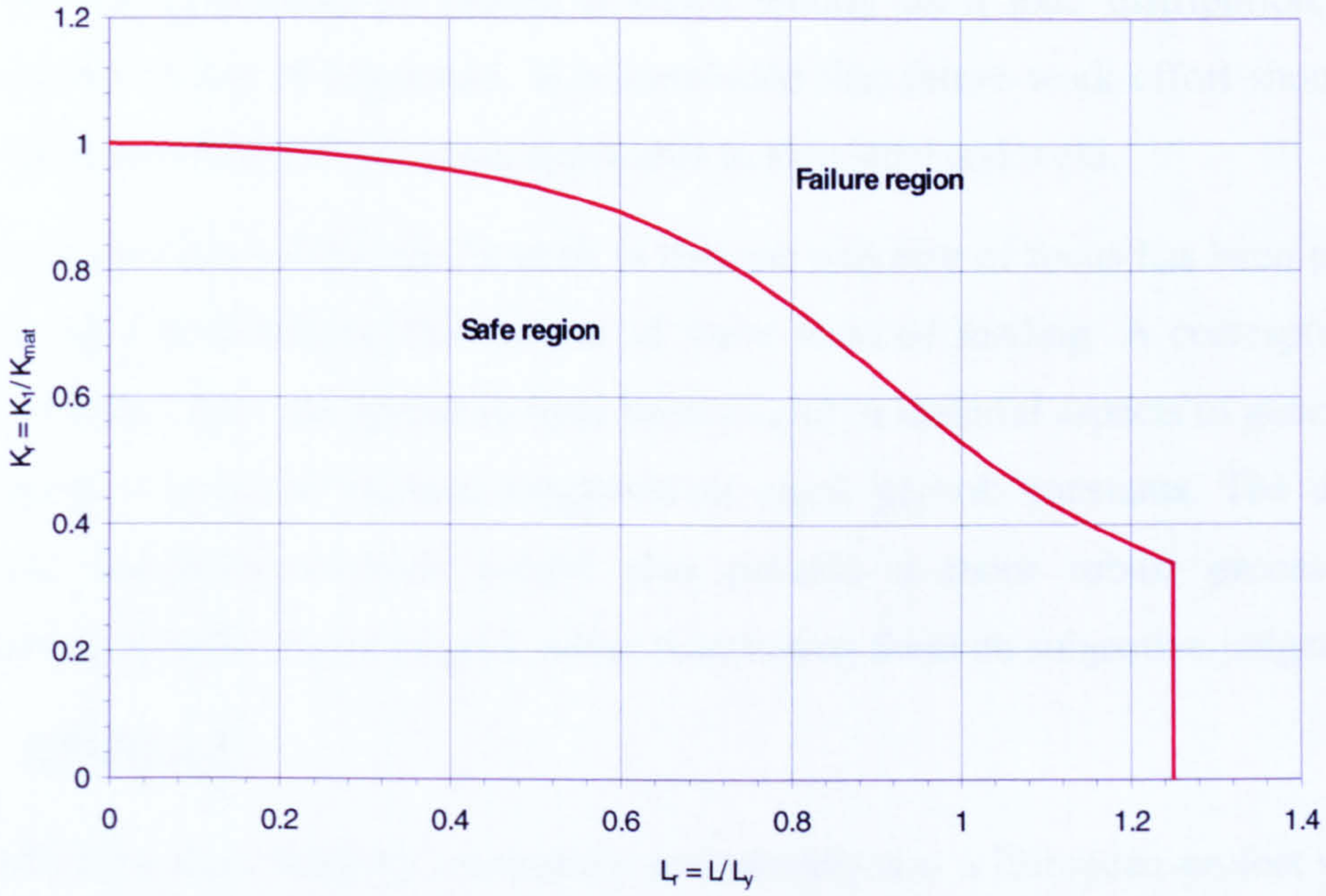

Figure 2-1 Example of failure assessment diagram

One of the most commonly used FADs is given by BS7910 (BS7910, 2005) for the assessment of flaws in metallic structures. BS7910 is divided into three layers of refinement. Level 1 is based on the original CTOD curve, Level 2 uses a strip yield approach, and Level 3 involves the reference stress approach. Different flaw types are accounted for by relating them to an equivalent through thickness effective crack length.

The SSC methodology is demonstrated for a number of sample problems. The defect sizes used in the study are relatively small: a 20 mm through thickness crack; and a 15 mm long weld undercut. The critical crack sizes are determined to lie between 20 mm and 50 mm, not particularly long. The short critical sizes are surprising given that the 33rd percentile is assumed for the toughness value and are likely to have been caused by assuming design values for the applied loading. However, given the small initial crack sizes this would allow the repair to be delayed for up to four years. The advice for the operator is then couched in terms of 'very likely' and 'highly unlikely', but these terms are not quantified and appear to be based on a subjective judgement.

SSC-428 (Tiku, 2003) reviews the methodology to determine the focus of future work. A parametric study is used to determine the influence of input parameters.

However, the probability of failure is based wholly on a load distribution, with deterministic values of toughness. It is concluded that future work effort should be focussed on deriving a distribution applicable to ship steel and weld.

The major criticism of the SSC's work is that the majority of focus has been placed on deriving a probabilistic distribution of wave induced loading. A corresponding degree of effort does not appear to have been placed in material aspects to generate a distribution of material fracture toughness or crack growth constants. The use of structural reliability methods would also provide a more robust process for determining suitable repair lengths, rather than basing them on subjective judgement.

2.5 SINTAP

SINTAP (Structural integrity assessment procedures) was a European project which aimed to provide a method to evaluate the safety of a given flaw against brittle fracture, ductile tearing, and plastic collapse (Ainsworth, 2000). The SINTAP procedure is very similar to BS7910, using failure assessment diagrams. The main advance is the incorporation of the master curve approach to describe the scatter in material fracture toughness. The master curve uses a Weibull distribution to describe the scatter in fracture toughness at a given temperature, combined with a mean line to describe the change in mean toughness across the ductile to brittle transition. The master curve concept was principally developed by Wallin and will be discussed in more detail in Chapter 5.

The SINTAP methodology has been incorporated into a probabilistic software tool, PROSINTAP (Dillström, 2000). This program allows a user to input distributions of fracture toughness, yield strength, ultimate tensile strength, applied loading, and defect size. The SINTAP procedure is then used to determine a probability of failure. The method does not incorporate a crack growth equation and as such represents only an instantaneous solution. The approach currently allows the user a choice of two reliability methods: a Monte Carlo simulation; and first-order reliability methods.

Wallin (Wallin, 2002) applied the SINTAP procedure to DNV's brittle fracture criteria for ships and mobile offshore units, which are based on Charpy energy requirements. Wallin used the master curve correlation between T_{27J} and fracture

toughness to estimate the failure probability as a function of the plate grade. However, the applied loading is assumed to be deterministic in the calculation method and the probability of failure is simply calculated by determining the probability of the toughness falling below the applied loading. In addition, the applied loading is assumed to be 60% of yield, which is considered to be extremely high.

The flaw size assumed in the study was extremely small: an elliptical flaw 3 mm deep and 15 mm in length. However, due to the high level of applied loading this gives an estimated probability of failure of 6 – 14%. Wallin argues that this is a realistic figure, given that the flaw has a 70% probability of detection. However, the probability of detection looks wildly optimistic. A similar study undertaken by the SSC-389 (Demsetz, 1996) found that a through thickness crack of 25 mm in length had less than 25 % probability of being detected, and it was only when cracks reached 200 mm in length that they were likely to be detected. In a structure as complicated as a ship, there are likely to be hundreds of undetected surface defects. If every flaw had a 6% probability of failure then a brittle fracture would be almost certain to occur during the life of every vessel, which is clearly not the case. It is believed that the master curve correlation between T_{27J} and fracture toughness is over-pessimistic for ship steel, leading to a high value of the assessed probability of failure. This is discussed in more detail in Chapter 5.

2.6 Classification societies

The International Association of Classification Societies (IACS) provides a minimum set of requirements to which the major classification societies adhere. Current IACS requirements state that ships less than 250 m can be constructed entirely in grade A plate, provided the thickness is less than 25 mm, and operated at temperatures down to -20°C (IACS URS6, 2003). In addition, grade A plate less than 50 mm thick has no minimum required T_{27J}, with steel quality controlled through material properties alone (IACS URW11, 2004).

Lloyd's Register's requirements are more stringent than IACS. Grade A is allowed for operation at temperatures of 0°C and above. However, below 0°C grade B is the minimum required, allowing operation down to -30°C (Lloyd's Register, 2000a). In

addition, Lloyd's grade A material requires in-house checks by the manufacturer to ensure it meets T_{27J} of +20°C. This test is only required every 250 tonnes, as opposed to three tests for every 25 tonnes for grade D steel (Lloyd's Register, 2000b). A summary of material requirements specified by Lloyd's Register for grades A, B, D, and E is given in Appendix A.

Det Norske Veritas (DNV) follows IACS guidelines in controlling grade A quality through material properties alone (DNV, 1998a). However, the minimum operational temperature for grade A ships is not well defined. Instead, if "ships intended to operate for longer periods in areas with low air temperature (i.e. regular service during winter to Arctic or Antarctic waters)" then rules for refrigerated spaces are applied. In contrast with Lloyd's rules, grade E steel would be required for operation at -30°C (DNV, 1998b).

A recent study funded by the Health and Safety Executive examined the fracture properties of grade A steel (Kapoor, 2000). In an attempt to find 'worst-case' properties seven plates were sourced from stockists as possible alternatives to grade A. However, all of the plates were found to be considerably better than the Lloyd's Register requirement, with a T_{27J} of 0°C or lower. In addition, four plates were tested to see if they met Sumpter's requirement of 125 MPa$\sqrt{m}$. It was found that three of the plates met the requirement at 0°C. The thickest of the plates, 20 mm, only met the requirement at +18°C.

2.7 Discussion

The literature review has highlighted a number of inconsistencies between academic studies and the physical actuality. Studies by the SSC and Wallin have indicated a very high risk of brittle fracture from very short crack lengths or weld defects. Given that there are over 50 miles of welding in a typical ship it is almost inevitable that there will be some undetected cracking or weld defect in every in-service ship. This would imply that every ship would suffer some form of brittle fracture during its service life, which is clearly not the case.

It is the author's opinion that the distributions used in the studies are very conservative. The SSC methodologies focus heavily on loading components but use

deterministic values from the lower regions of the toughness distribution to determine the critical crack lengths, leading to very short critical crack lengths.

In contrast, the SINTAP project focuses heavily on the material fracture toughness distribution and does not include a crack growth algorithm. Consequently, a critical crack length calculation would require considerable iteration by the user, unless simplifying assumptions are made. The PROSINTAP software tool is the only approach to utilise structural reliability methods but requires the user to enter a distribution of applied loading.

Wallin assumed that the primary stresses were 60% of the nominal strength level, combined with yield point residual stress in his analysis of the DNV rules. This is considered to be extremely conservative, given the safety factors on strength. The material toughness distribution is also conservative, compared to the distribution that will be fitted in Chapter 5. These factors combine to give high probabilities of failure for small surface flaws.

Despite the high degree of scatter in material fracture toughness none of the studies attempt to account for the variation in toughness as a crack propagates through a plate, although the variation in toughness, even within a single plate, is noted by Sumpter and Rolfe. As the crack tip propagates through the material it is essentially sampling a new toughness value over some interval. Each interval represents a new toughness test and has an associated probability of failure, which is a function of the toughness and the time required to propagate through the region. The overall probability of failure is then the combined probability of each region. To the best of the author's knowledge no study in the literature attempts to account for this variation.

This thesis will attempt to account for this effect using time-dependent reliability to analyse results from a number of wide plate tests. In addition, perceived shortcomings in current studies published in the literature in the calculation of the loading and material fracture toughness distribution will be addressed by using realistic loading and fracture toughness distributions derived from measured data.

A drawback of this approach is that the results are somewhat ship-dependent. However, the results are intended to demonstrate that fatigue cracks can be safely left

unrepaired for relatively long periods of time. This will allow ship operators to delay repairs to coincide with scheduled maintenance periods, reducing both cost and time out of service.

3 Problem definition

3.1 Overview

This chapter provides an introduction to the basic fracture mechanics parameter, the stress intensity factor, which is used to characterise the conditions at the crack tip. The probability of failure is then represented by, but not equal to, the area of overlap between the applied stress intensity and the material fracture toughness.

The original methodology written as part of this thesis (Kent, 2002) used the BS7910 Failure Assessment Diagram (FAD) described in the previous chapter combined with a Monte Carlo simulation to estimate the probability of brittle fracture. It was found that the failures were principally brittle fractures, with very few mixed mode failures and no plastic collapse cases. It was subsequently decided to simplify the Limit State Function (LSF) to consider only brittle fracture.

The methodology described in this thesis has been incorporated into a software program, called "Probability of Ship Fracture" or POSF. A flowchart summarising the major program steps can be found in Appendix B.

3.2 Stress intensity factor

The stress intensity factor, K, is the most commonly used parameter to characterise the conditions at the crack tip. Cracked structures can be loaded to various levels of K in an analogous manner to which uncracked structures can be loaded to various levels of applied stress. The stress intensity factor is usually given a subscript to denote the mode of loading. Cracks in naval ships are principally loaded in tension, as the vertical bending moment is the dominant load for slender vessels (Clarke, 1987). Consequently, in this thesis only mode 1, opening, will be considered.

The program uses the elastic stress intensity factor, K, as the crack characterising parameter for fatigue and fracture. K is defined as:

$$K = Y\sigma\sqrt{\pi a} \qquad \textit{Equation 3-1}$$

where a is the characteristic crack length, σ is the remote stress, and Y is the geometry factor which takes account of the stress distribution on the crack.

For a through-thickness crack propagating transversely in an infinitely wide plate the geometry factor would be equal to 1. For some simple geometries analytical solutions are available which give Y as a function of crack length but as the complexity increases finite element (FE) solutions are required. The values used in this report are taken from an FE model used to assess cracks growing from the corner of a superstructure block into deck plate. This is a common cracking location due to the local stress concentration and poor alignment due to relative complexity of the detail. The geometry factor is given in the form:

$$Y = \frac{A_Y}{a^{B_Y}} \qquad \textit{Equation 3-2}$$

where A_Y and B_Y are user inputs which define adjacent stress concentrations and a is the half crack length in mm. This gives a value of 3.425 for A_Y and 0.232 for B_Y with the crack length defined in millimetres.

This form reflects a high value of Y adjacent to a local stress concentration where the crack starts (as the crack length tends to zero Y tends to infinity). Y reduces as the crack moves away from the stress concentration and is perhaps crossed by stiffeners. The lower limit of Y would be 1.0 in unstiffened plate. If the crack is held shut by a heavy stiffener this reduces the effective crack length and a lower limit of $1/\sqrt{2}$ could be used. However, this depends on the stiffener remaining completely uncracked. Therefore, a lower limit of 1 is assumed in this study. The geometry factor as a function of crack length for the superstructure detail is shown in Figure 3-1.

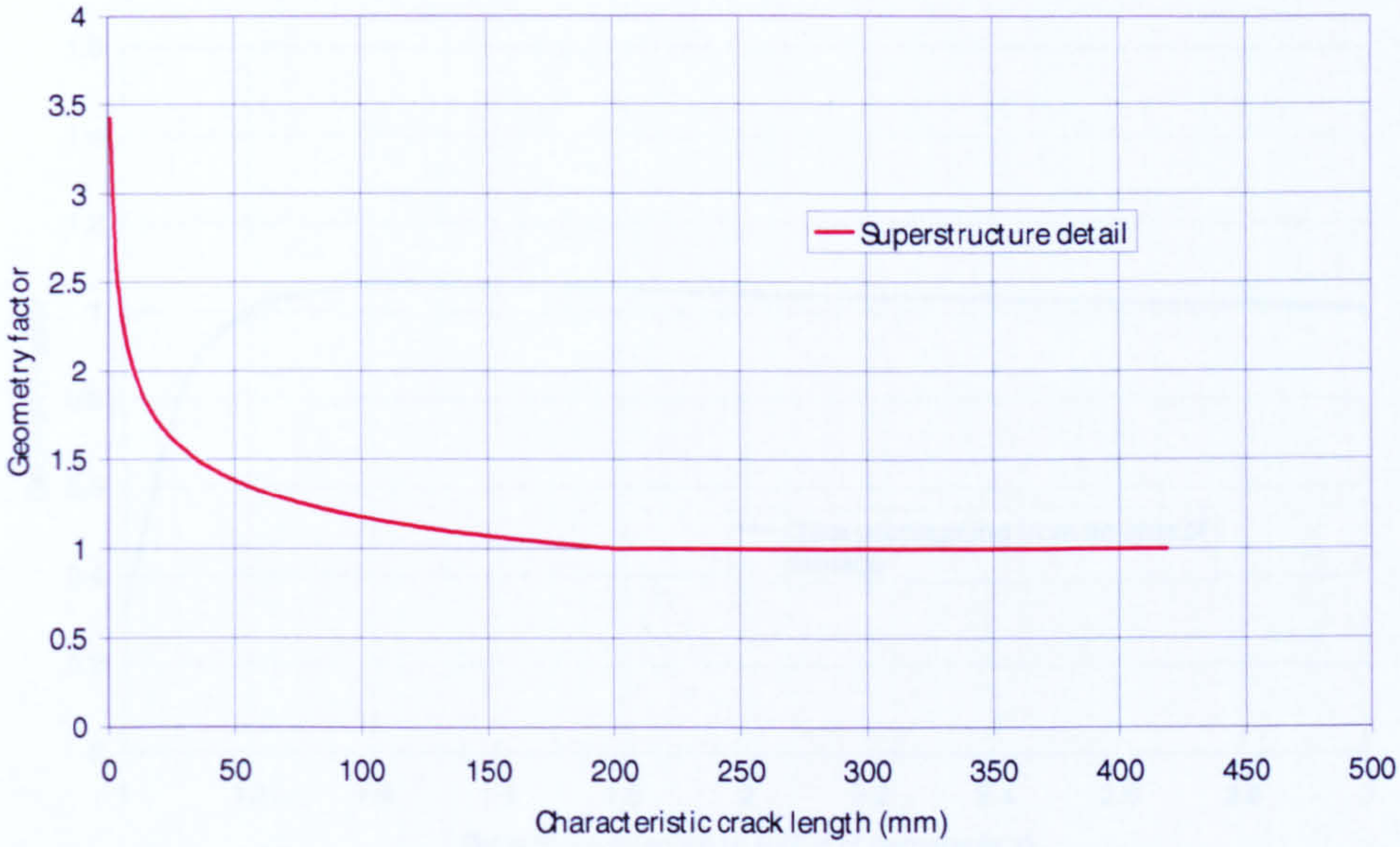

Figure 3-1 Geometry factor as a function of characteristic crack length for superstructure detail

In addition, an attempt will be made to model the effects of cracks growing from areas of damage to the deck or keel. This could help to provide advice to a ship's operator of the most suitable course of action in the event of damage. The damage is modelled as a circular hole, in either the deck or the keel, with a crack growing transversely. This is shown in Figure 3-2.

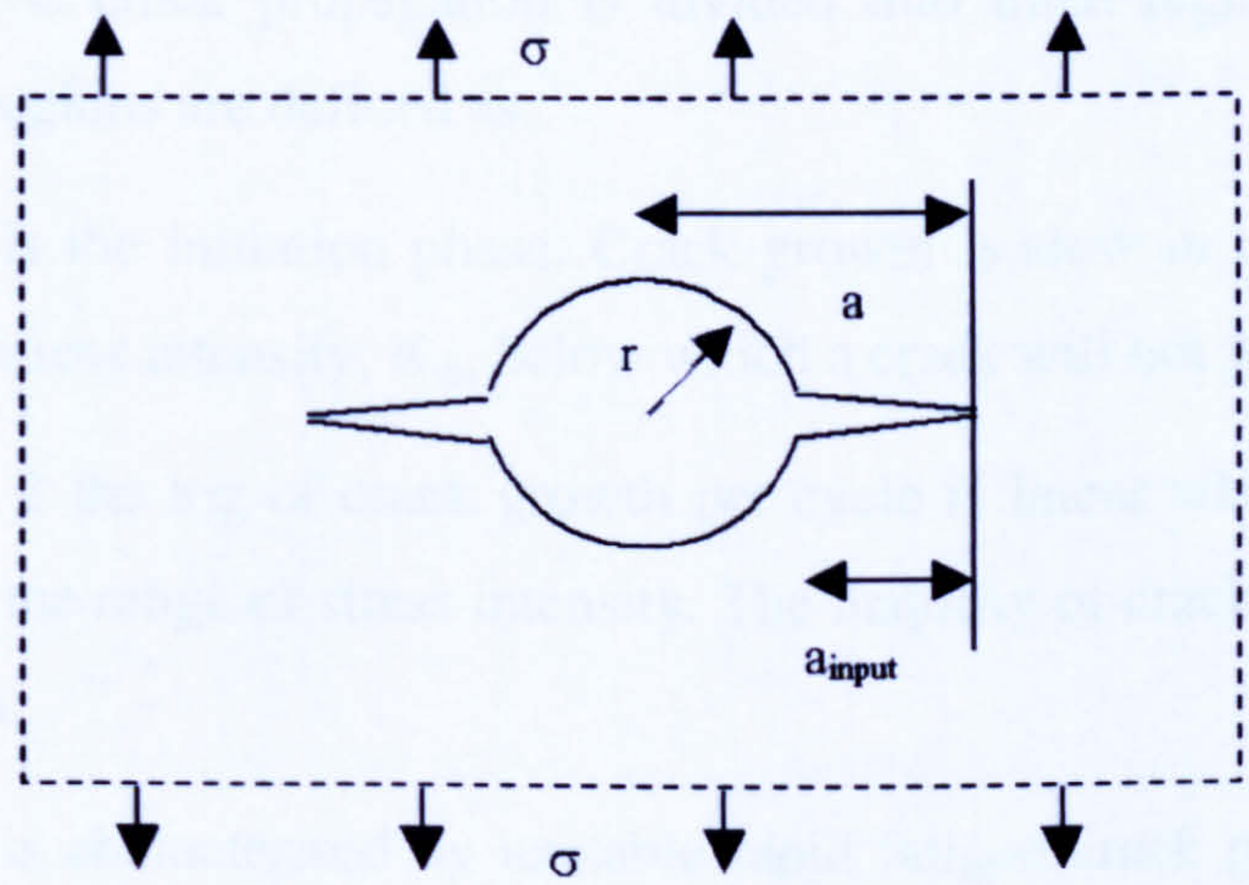

Figure 3-2 Diagram of crack propagating from assumed area of damage

The geometry factor for this scenario is taken from a published solution (Rooke, 1996). The geometry factor as a function of the ratio of the crack length to the radius of the damage, r, is shown in Figure 3-3.

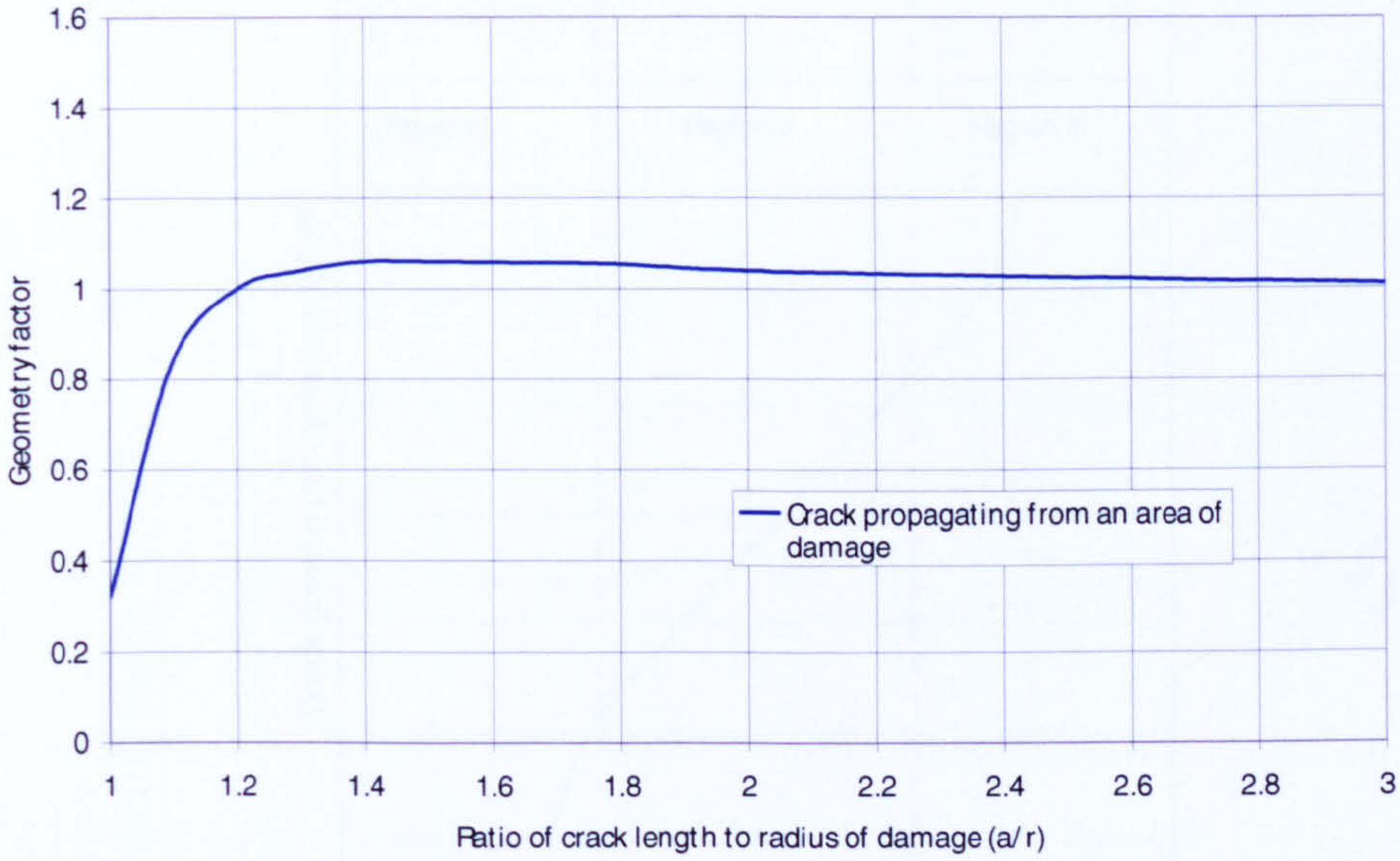

Figure 3-3 Geometry factor as a function of ratio of characteristic crack length to radius of damage

It can be seen that if the crack length is large relative to the dimension of the damaged area the solution tends to that of a centre cracked plate.

3.3 Fatigue crack growth

The most commonly used method to model fatigue crack growth is Paris Law (Paris, 1963). The fatigue crack propagation is divided into three regions, as shown in Figure 3-4. The regions are defined as:

- Region 1 is the initiation phase. Crack growth is slow in this region with a threshold stress intensity, K_{th}, below which a crack will not propagate.
- In Region 2 the log of crack growth per cycle is linear when plotted against the log of the range of stress intensity. The majority of crack growth occurs in this region.
- Region 3 is characterised by unstable rapid fatigue crack growth. It is often referred to as the static failure region as failure occurs after relatively few cycles.

The three regions are shown on log-log axes in Figure 3-4.

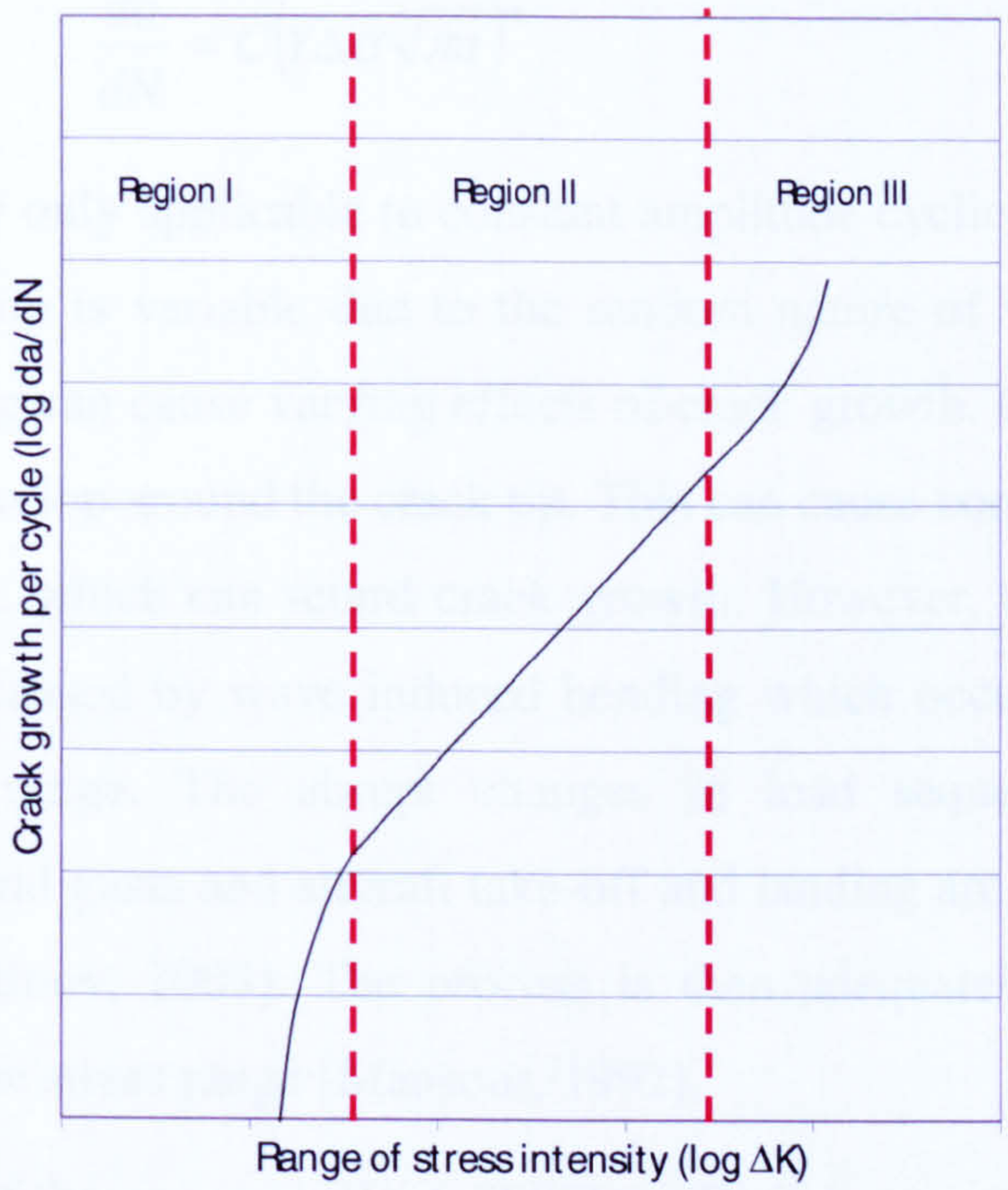

Figure 3-4 Example of crack growth in steel

Fatigue crack growth per stress cycle, da/dN, in Region 2 is described by Paris Law.

$$\frac{da}{dN} = C(\Delta K)^m \qquad \textit{Equation 3-3}$$

where C and m are material constants and ΔK is the change in stress intensity factor during the load cycle. Recent wide plate fatigue tests carried out at QinetiQ on ship steels have been well described with a C value of 24×10^{-9} and m = 3 (ΔK in MPa√m). These values compare well with constants suggested by Yazdani & Albrecht (Yazdani, 1989) to describe crack growth in a marine environment.

It is generally believed that a wholly tensile load will cause more crack growth than a part tensile – part compressive load. Paris Law gives an equivalent crack growth rate for the same cyclic stress, regardless of the magnitude of the maximum. Some fatigue crack growth models also include a term to account for the ratio of the applied stress, known as the R ratio. In this thesis the effects of R ratio will be ignored.

Equation 3-1 can then be substituted into Equation 3-3 to relate the fatigue crack growth to crack length and applied loading.

$$\frac{da}{dN} = C\left(Y\Delta\sigma\sqrt{\pi a}\right)^m \qquad \textit{Equation 3-4}$$

Paris Law is strictly only applicable to constant amplitude cyclic loading. However, the loading on a ship is variable due to the random nature of waves. The random nature of the loading can cause varying effects of crack growth. Overloads can cause a plastic zone to develop around the crack tip. This can cause compressive stresses to occur on unloading, which can retard crack growth. However, the vast majority of fatigue damage is caused by wave induced bending which occurs with a relatively narrow frequency range. The abrupt changes in load sequence seen in other structures due to wind gusts and aircraft take-off and landing are not as applicable to ship structures (Petinov, 2003). The process is then adequately described by the expected value of the stress range (Mansour, 1992).

In earlier versions of the program (Kent, 2002) the Paris Law was integrated over the number of cycles to calculate the crack length at the end of a time period, which could be taken as days, months, or years. This resulted in a different probability of failure depending on the selected time period. In the current version, a region of assumed constant toughness is defined and the corresponding number of cycles required to propagate the crack through the region is calculated. This issue is discussed in Chapter 5.5. Equation 3-4 is then re-arranged as:

$$\int_{a_0}^{a_n} da = \int_0^N C\left(Y\Delta\sigma\sqrt{\pi a}\right)^m dN \qquad \textit{Equation 3-5}$$

where the geometry function, Y, is a function of the crack length. This means that Equation 3-5 cannot be given in a closed form and requires a numerical solution.

3.4 Limit state function

A brittle fracture is assumed to occur when the applied stress intensity is greater than the material fracture toughness. This represents the failure region, with the safe region being defined as material fracture toughness being greater than the applied stress intensity. The material fracture toughness is designated the strength variable and denoted x_1, and the applied stress intensity the load variable, which is denoted x_2.

The limit state function defines the boundary between these two regions, which can be expressed as:

$$G(\mathbf{X}) = X_1 - X_2 \qquad \textit{Equation 3-6}$$

where **X** represents a random vector of material fracture toughness and applied stress intensity and:

- G(**X**)<0 represents a failure condition;
- G(**X**)=0 represents the boundary between safe and failure conditions;
- G(**X**)>0 represents a safe condition.

The applied stress intensity is a combination of the applied loads at the crack tip. These consist of wave induced bending stress, still water bending stress and residual stress. The applied stress intensity and the material fracture toughness are known as the basic variables as they form the fundamental input values to the problem.

The basic variables are defined in terms of probability distributions, often using the expected values or means and the co-variances (the first and second moments). The probability of failure is represented by, but not equal to, the area of overlap between the load and strength distributions. An example plot is shown in Figure 3-5.

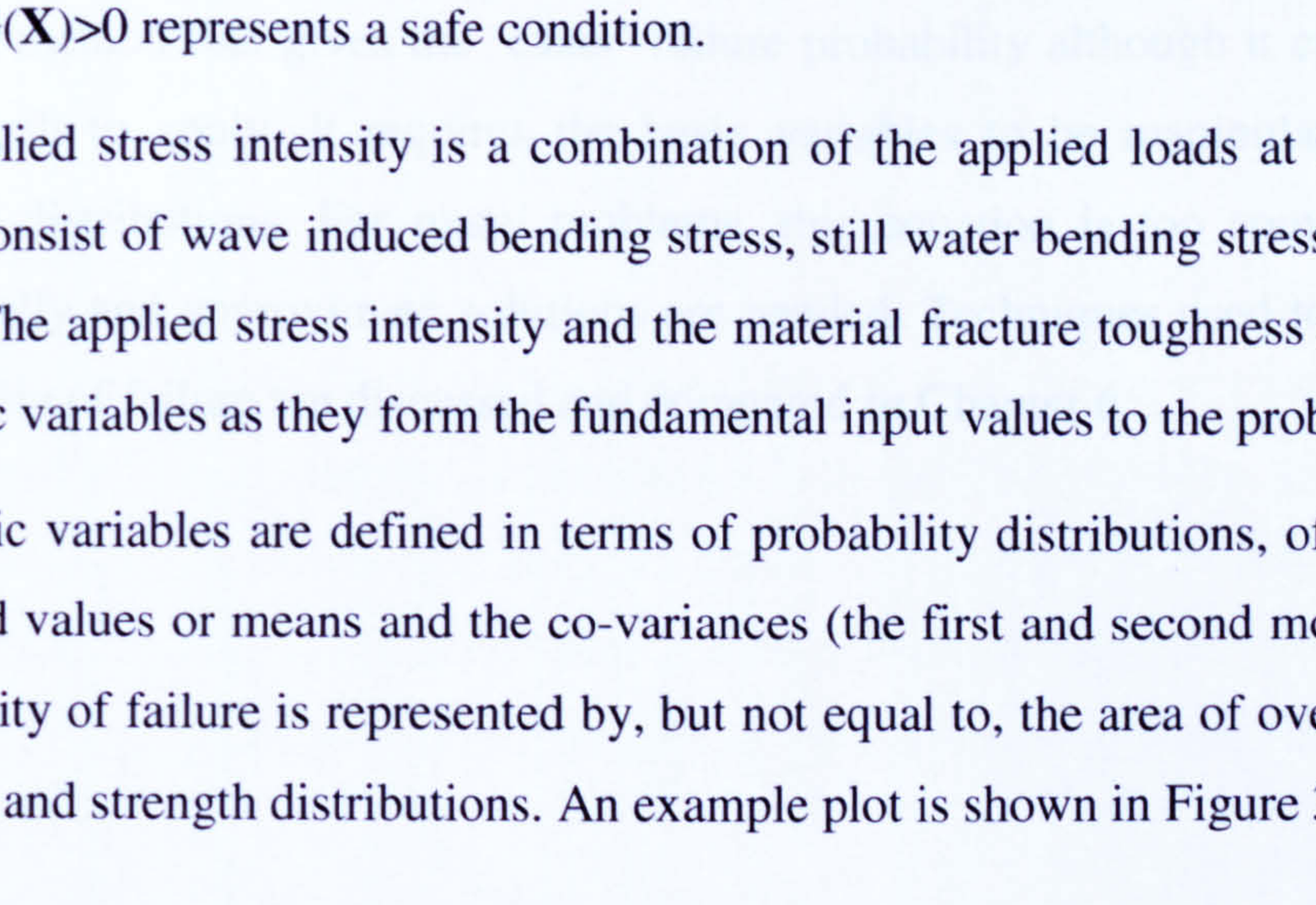

Figure 3-5 Example load resistance plot at time step 1

The probability of failure can then be expressed as:

$$p_f = P[G(\mathbf{X}) \leq 0] = \int_{G(\mathbf{X})\leq 0} \int f_{x_1 x_2}(x_1, x_2) dx_1 dx_2 \qquad \textit{Equation 3-7}$$

If the load and resistance variables are statistically independent then the order of integration can be reduced by one (Melchers, 1999). The assumption of independence is an important issue and is discussed in more detail in Chapter 6.

$$p_f = \int_0^\infty F_{x_1}(x) f_{x_2}(x) dx \qquad \textit{Equation 3-8}$$

Equation 3-8 is more commonly known as the convolution integral. This is an efficient method that gives the 'exact' failure probability although it can sometimes be difficult to apply. It requires the basic variables to be manipulated to fit the required distributions. For many problems, this equation is too complex to solve numerically and approximate solutions are needed. Techniques used to estimate the probability of failure are discussed and compared in Chapter 6.

3.5 Time-dependent reliability

If the material fracture toughness and the applied stress intensity vary with time, i.e. 'stochastic' variables, then the probability of failure at time t is given by (Melchers, 1999):

$$p_f(t) = P[G(\mathbf{X}(t) \leq 0)] = P[X_1(t) - X_2(t) \leq 0] \qquad \textit{Equation 3-9}$$

If the probability density functions of x_1 and x_2 are known at some time instant, t, then Equation 3-9 can be used to calculate the instantaneous probability of failure. Equation 3-9 is only valid if the load is re-applied or increasing, otherwise a brittle fracture would have occurred at an earlier time. In addition, the probability of failure over successive time intervals is correlated unless the value of t is sufficiently high to ensure that the load distributions can be considered to be independent.

The traditional method of overcoming these drawbacks is to generate a load distribution which is assumed to represent a time period (Melchers, 1999). This can be accomplished using the statistics of extremes to give a distribution of maximum values over a sufficiently long time interval. The probability of failure is then assumed to represent that for the time period. This is shown in Figure 3-6.

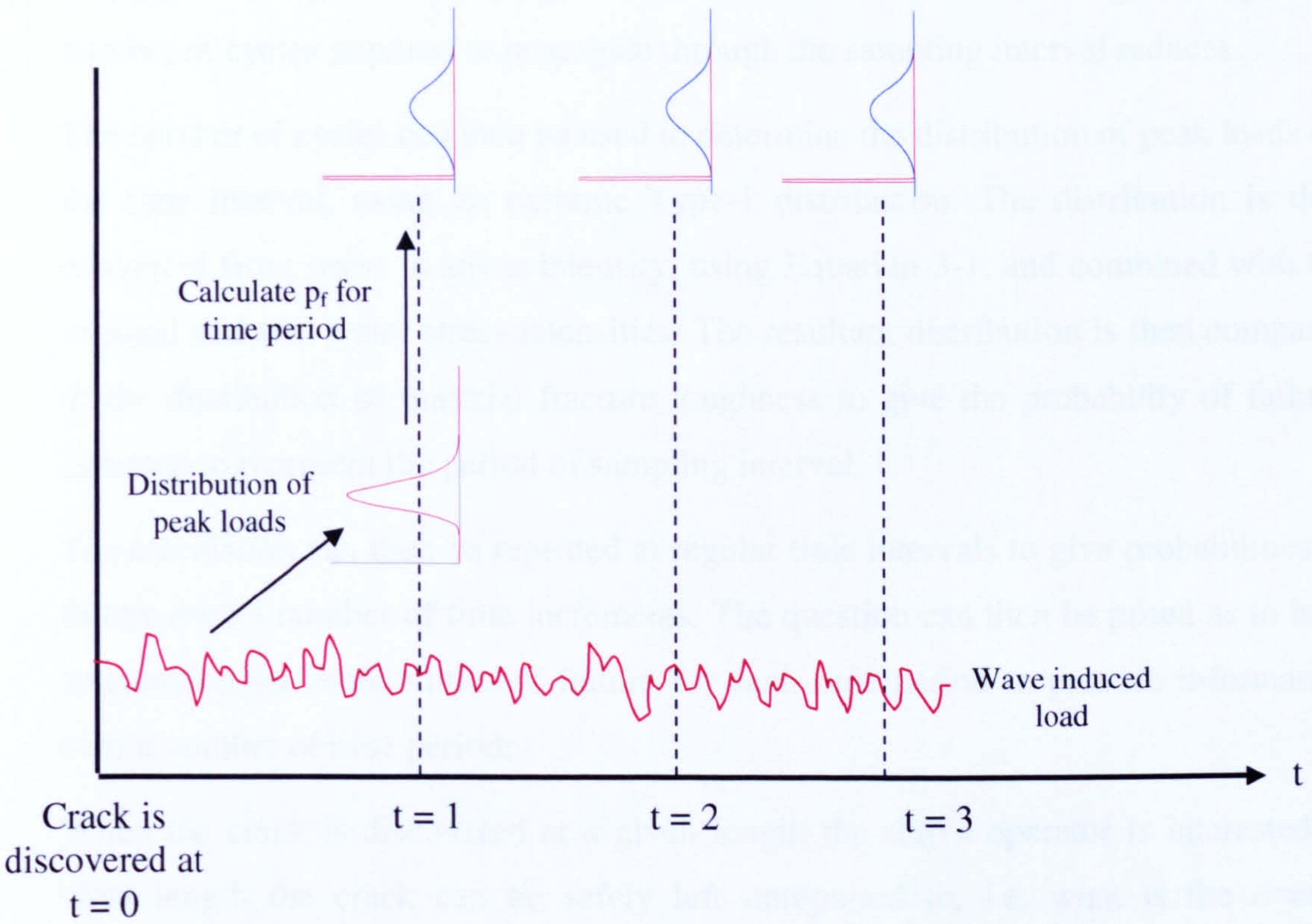

Figure 3-6 Calculation of probability of failure at each time interval

Traditionally, the time period is taken as a fixed increment of time such as days, weeks or more commonly years. However, in this thesis the material fracture toughness is assumed to vary over a fixed increment, termed the sampling interval, Δ. This is the distance over-which the toughness is assumed to remain constant. In the next time period the toughness value is re-sampled and is assumed to be completely uncorrelated, i.e. it can take a new value from anywhere within the toughness distribution.

Assuming a sampling interval over too long a distance will lead to unconservative results, as it is changing more quickly than modelled, increasing the probability of the load variable exceeding the strength. Estimation of a suitable value to use to represent the sampling interval is discussed in Chapter 5.5.

Equation 3-5 is then used to determine the number of cycles required for the crack to propagate through the sampling interval. Note that as the crack gets longer the number of cycles required to propagate through the sampling interval reduces.

The number of cycles can then be used to determine the distribution of peak loads for the time interval, using an extreme Type-1 distribution. The distribution is then converted from stress to stress intensity, using Equation 3-1, and combined with the residual and still water stress intensities. The resultant distribution is then compared to the distribution of material fracture toughness to give the probability of failure, assumed to represent the period of sampling interval.

The calculation can then be repeated at regular time intervals to give probabilities of failure over a number of time increments. The question can then be posed as to how to combine the probabilities of failure for each time period to provide information over a number of time periods.

When the crack is discovered at a given length the ship's operator is interested in what length the crack can be safely left unrepaired to, i.e. what is the overall probability of failure over a number of increments of crack growth or sampling intervals.

This could be calculated by simply summing the probability of failure for each time increment. However, this would over-estimate the overall probability of failure as a brittle fracture cannot occur in successive time periods. To compensate for this the probability of the crack fracturing in both time periods is removed. This can be expressed mathematically as:

$$P_f(t) = p_f(t) + P_f(t-1) - \left\lfloor p_f(t).P_f(t-1) \right\rfloor \qquad \textit{Equation 3-10}$$

where $P_f(t)$ represents the probability of failure from time period t = 0 to time period t = t and is termed the cumulative probability of failure, and $p_f(t)$ represents the probability of failure for the time period t = t.

Note that Equation 3-10 relies on the assumption that the toughness is completely uncorrelated over successive time periods. If the toughness were correlated the probability of failure in subsequent time periods would be dependent on the previous time period and Equation 3-10 would be invalid.

One further definition of probability of failure is also used in this thesis. To allow comparison with failure statistics the probability of failure for a given time period is factored to an equivalent per year value. This is effectively the risk of operating the ship for a year with a crack of a constant length.

To summarise three definitions of the probability of failure will be used in this thesis:

- probability of failure for time period t and is denoted $p_f(t)$;
- cumulative probability of failure, which represents the probability of failure over a number of time periods and is denoted $P_f(t)$;
- equivalent probability of failure per years, which factors $p_f(t)$ to a corresponding annual probability of failure and is denoted $p_{eq}(t)$.

Note that these definitions of the probability of failure are subtly different from another definition widely adopted in the literature, termed the hazard function. The hazard function can be expressed as (Ayyub, 1990):

$$h(t_i) = \frac{p_f(t_i)}{1 - \sum_{j=i-1}^{j=1} p_f(t_j)} \qquad \textit{Equation 3-11}$$

The hazard function calculates the probability of failure in a time period given that the crack has survived to reach the time period. The cumulative probability of failure calculates the probability of the crack failing over any of the time periods, but gives no information on when that failure exists.

It is assumed that the cumulative probability of failure will be of more use to the ship's operator who will be basing decisions on the risk of a particular voyage or the time until the next maintenance period. For this reason the hazard function will not be used in this thesis.

4 Applied loading

4.1 Overview

The applied loads are used to analyse both fatigue and fracture. Fluctuating loads cause the crack to propagate by fatigue, while peak loads can result in a brittle fracture. For a crack growing across the deck the main components of loading are considered to be: wave induced vertical bending stress; still water bending stress; and residual stress. Cracks growing in other locations may be subjected to additional loads. For example, a crack in the sideshell would be subjected to fluctuating pressure due to wave action.

All three components will be used to assess fracture. However, still water and residual stress are assumed to be static loads, as the still water value varies over a long time period. Therefore, the wave induced bending is the only cyclic stress acting on the crack tip.

An increasingly common method of calculating wave induced loading is to use a numerical load prediction tool. The advantage of this approach is that it can be used to assess novel hull designs and take into account the operational profile of the vessel. The sophistication and accuracy of these tools is increasing with computational power, which allows calculation to be performed in the time domain, as opposed to a frequency domain calculation. A time domain solution is better equipped to deal with the effects of non-linearities, such as slamming and Froude-Krylov forces, but can be computationally expensive.

The approach adopted in this work utilises measurements taken from the deck of a naval frigate. It is hoped that by making use of real data the wave induced bending stress can be more accurately predicted, through a reduction in the modelling uncertainties. The wave load analysis has been divided into two sections: fracture stresses and fatigue stresses. The peak values are used in the calculation of the probability of brittle fracture and the more frequent, but smaller, stresses used in the fatigue crack growth calculation.

4.2 Measured data

The extreme strain recorders were developed at the Naval Construction Research Establishment (NCRE) in the 1950s and deployed extensively across the British naval fleet. The recorder measures the maximum hogging and sagging strain over a given time period, normally set to four hours. An example of the recorder is shown in Figure 4-1.

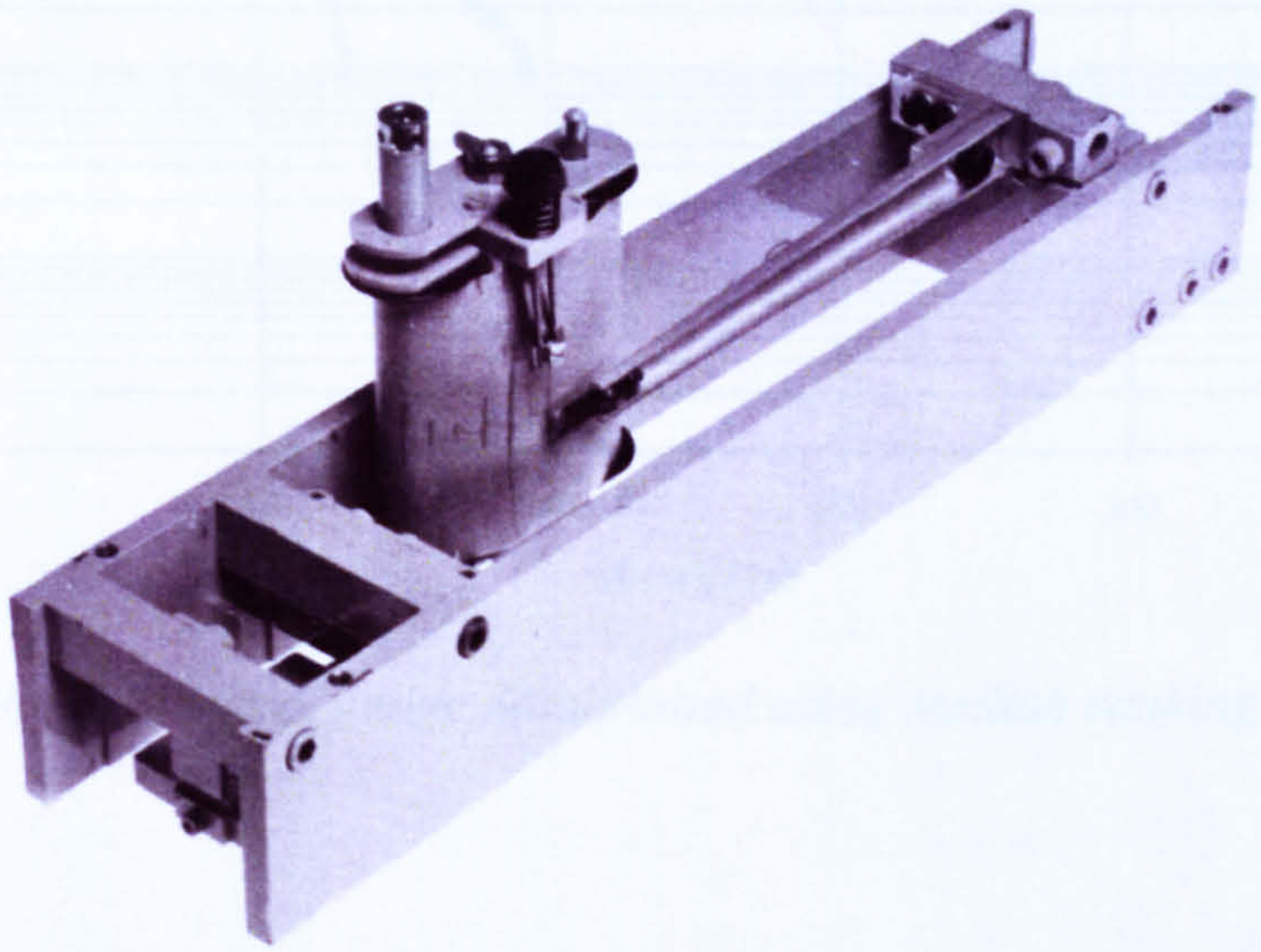

Figure 4-1 Mechanical strain gauge recorder

The recorders were located on the webs of longitudinal girders under the strength deck, as close as possible to the neutral axis of the plate stiffener combination to minimise the effects of lateral load on the deck. The recorder was also located clear of any structural discontinuities to avoid the effects of local stress concentrations.

The extreme strain recorders scribe a vertical line on a paper record. Every four hours the recorders wound on the paper and continued recording. The paper records were then used to determine the maximum hog and sag wave induced strains in each four hour period.

The extreme strain recorders were deployed on a number of vessels from the same class over a period of several years. The databank contains 13626 records, equating to over 6 years of continuous operation. Assuming that only 1/3 of life is spent at sea

then the databank corresponds to a nominal ship life. The measured data are plotted using median ranking in Figure 4-2.

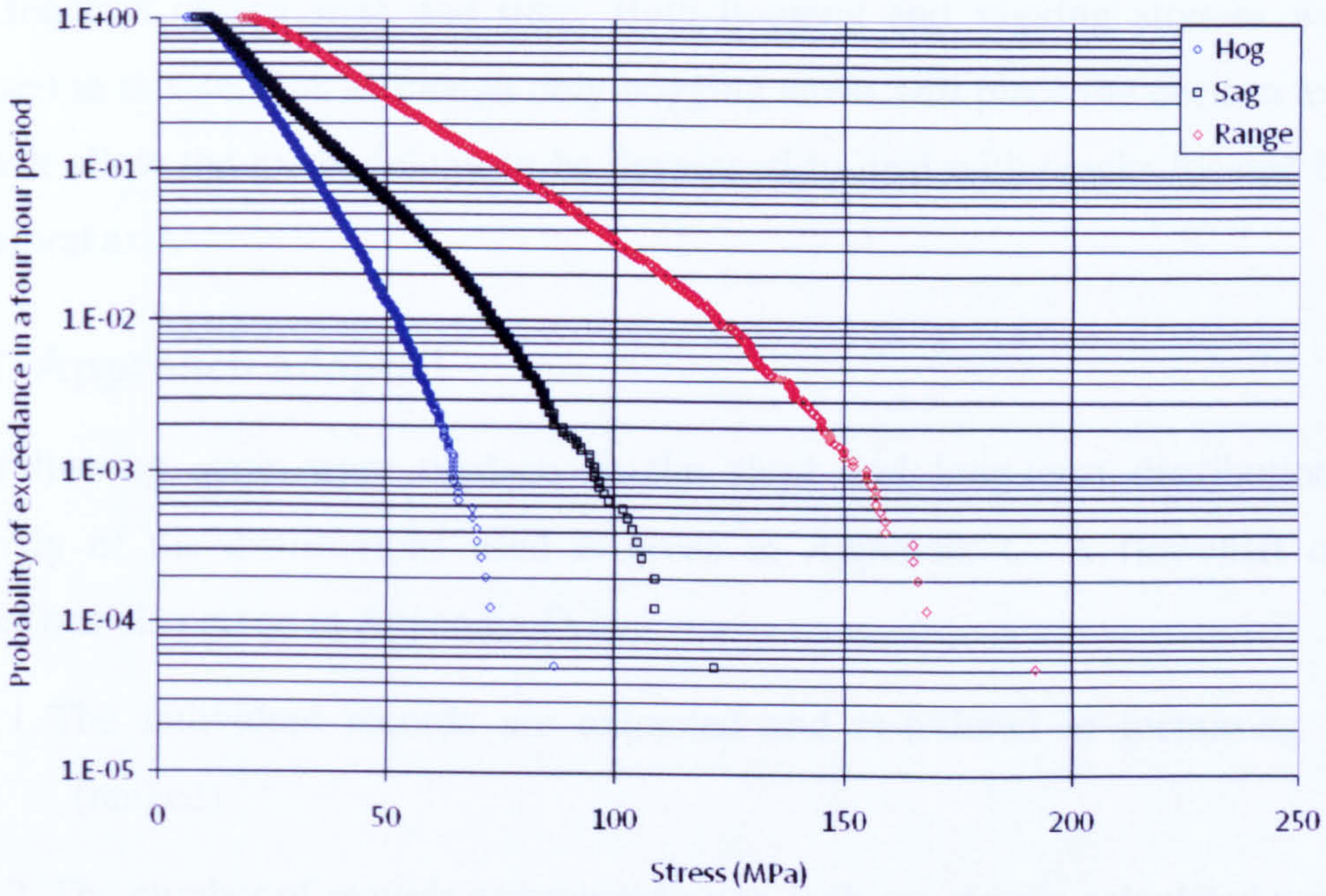

Figure 4-2 Mechanical strain gauge data plotted using median ranking

4.3 Wave induced bending stress – fracture

The objective of this section is to express the extreme wave induced bending stress as a function of sea state and time. Both hogging and sagging stresses will be analysed in this section. Although only hogging stress will place the deck in tension this will allow the methodology to be developed to deal with cracks located below the neutral axis.

4.3.1 Approach adopted

The following steps were used to fit the short and long-term distributions. A summary of the distributions used is given in Appendix C. A flowchart of the approach is also given in Appendix D.1.

1. The individual records are extracted and re-ordered in increasing value (ranked).
2. The number of records corresponding to each sea state is calculated using an assumed operational profile (discussed in Section 4.3.2).
3. The individual records are converted to a probability density function for each sea state. This is assumed to represent the extreme distribution for a 4-hour period for that sea state.
4. The parent distribution is fitted, based on the mean and standard deviation of the extreme distribution. This step converts the 4-hour maxima to an equivalent per cycle distribution.
5. The parent distributions for each sea state are then grouped together based on their associated probability of occurrence.
6. A least squares fit is carried out to give the long-term distributions for hog and sag.
7. The per cycle long-term distribution is then converted to a probability of exceedance in a 4-hour period to compare with the measured data.
8. The equivalent stress for each sea state and long-term operation is calculated by combining hogging and sagging distributions (Section 4.4).

4.3.2 Assumptions

A number of assumptions were made during the fit procedure. The implications of each are discussed below.

- The stress increases with sea state

  It seems intuitive that the load increases with increasing wave height, and hence sea state. However, while linear theories assume a linear relationship between wave height and ship response, they also take into account the effect of encounter frequency. Baarholm (Baarholm, 2003) showed that the maximum response occurred in the region of wavelength equal to ship length. As wave height increases there is a corresponding increase in wave period. This could result in a reduction in load compared to lower, but shorter, waves.

  The trend is also affected by operational considerations. It is commonly assumed that the ship's master will reduce speed in higher seas and avoid heading directly into waves. However, a recent SSC study (Glen, 1998) found that there was no correlation between ship's speed and heading with sea state.

- Operational profile

  The extreme distribution for each sea state is dependent on the assumed operational profile. The accuracy of the fits will therefore rely on the operational profile following the actual distribution over which the readings were taken.

  Lloyd's Register Naval Ship rules (Lloyd's Register, 2002) give a probability of each sea state. This information is believed to be taken from a table in STANAG (NATO, 1983), which is based on North Atlantic data. This data is thought to provide a reasonable estimate of the operational profile but is clearly a major assumption in the methodology.

- Number of cycles in a 4-hour period

  The fits are based on the assumption of 500 waves/hour, equating to a encounter period of 7.2 seconds. In reality, the number of waves is likely to be a complex function of sea state, area of operation, ship speed, and ship

heading. The use of the extreme distribution counteracts this effect to some degree. Increasing the number of cycles would move the extreme distribution to the right and reduce the parent distribution.

4.3.3 Extraction of individual sea states

The measured data were re-ordered into increasing value and the number of 4-hour periods spent in each sea state was calculated using the assumed operational profile. The assumed operational profile is taken from Lloyd's Register Naval ship rules (Lloyd's Register, 2002).

	Lloyd's Register operational profile	
Sea state	**Probability (%)**	**Number of readings**
8	1.16	158
7	6.05	824
6	13.15	1792
5	20.64	2813
4	27.8	3788
3	23.7	3229
2	7.5	1022
Σ=	100.00	13626

Table 4-1 Discretisation of records into sea states

The individual sea states were extracted for both hog and sag. The readings were then converted to an equivalent probability density function. This allowed a distribution to be fitted to describe the individual sea states.

4.3.4 Fitting individual sea state distributions

The objective of this section is to define distributions which describe the probability of all stress values in a sea state. It is assumed that in a 4-hour period there are 2000 cycles (500 per hour), equating to an encounter period of 7.2 seconds. It is further assumed that the distribution of maximum cycles follows an extreme type 1 distribution. This can be fitted to the measured data and used to derive the parent distribution, which gives describes the per cycle distribution.

The Weibull distribution has been used to describe both the long and short term stresses. This distribution has also been shown to provide a good fit to long-term data (Mansour, 1990). It is a general distribution and should also provide a good fit to the short-term data.

The mean of the extreme type-1 distribution is given by:

$$\mu = u + \frac{0.5772}{a} \qquad \textit{Equation 4-1}$$

where u is the mode of the extreme type-1 distribution and a is a measure of the dispersion. The standard deviation of the extreme type-1 distribution is given by:

$$\sigma = \frac{\pi}{\sqrt{6}a} \qquad \textit{Equation 4-2}$$

where u and a are given by:

$$u = A(\ln N)^{1/B} \qquad \textit{Equation 4-3}$$

$$a = Np_{weibull}(u) \qquad \textit{Equation 4-4}$$

u and a can be found by calculating the mean and standard deviation of the extracted data. This defines the extreme type-1 distribution. Solving Equation 4-3 and Equation 4-4 simultaneously then gives A and B, which define the parent distribution. To accomplish this Equation 4-3 is re-arranged in terms of A, giving:

$$A = \frac{u}{(\ln N)^{1/B}} \qquad \textit{Equation 4-5}$$

Equation 4-5 is then substituted into Equation 4-4 to give a as a function of the shape parameter:

$$a = \frac{NB(\ln N)^{1/B}}{u}\left[(\ln N)^{1/B}\right]^{B-1}\exp(-\ln N) \qquad \textit{Equation 4-6}$$

Equation 4-6 requires a iterative solution. Equation 4-1 and Equation 4-2 are used to calculate u and a from the measured data. The value of B is then iterated until the right hand side of the Equation 4-6 is equal to a. The value of B can then be

substituted into Equation 4-5 to find A. An example of the hog fits for Sea State 8 and 5 are shown in Figure 4-3 and Figure 4-4 respectively.

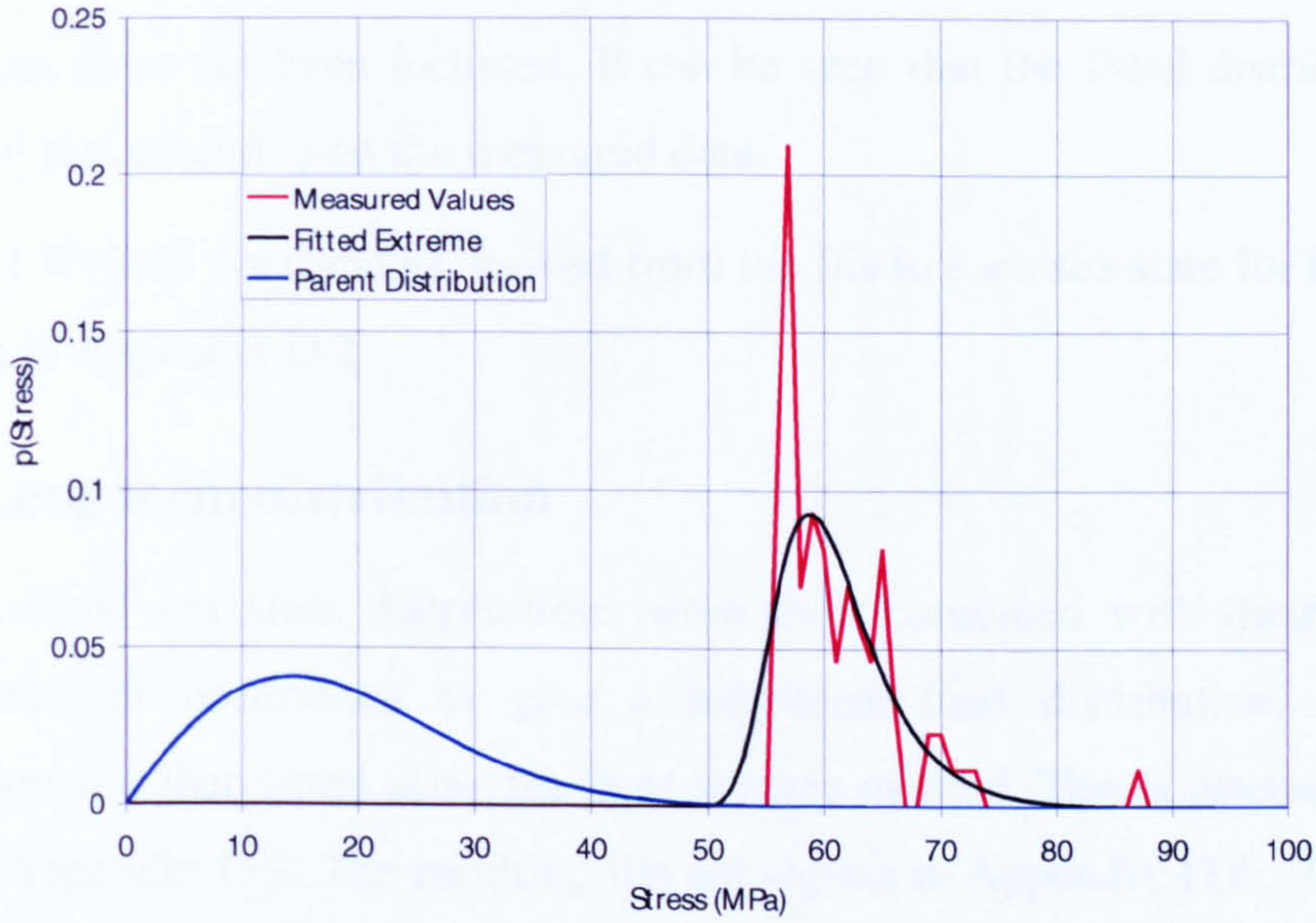

Figure 4-3 Example fit to sea state 8

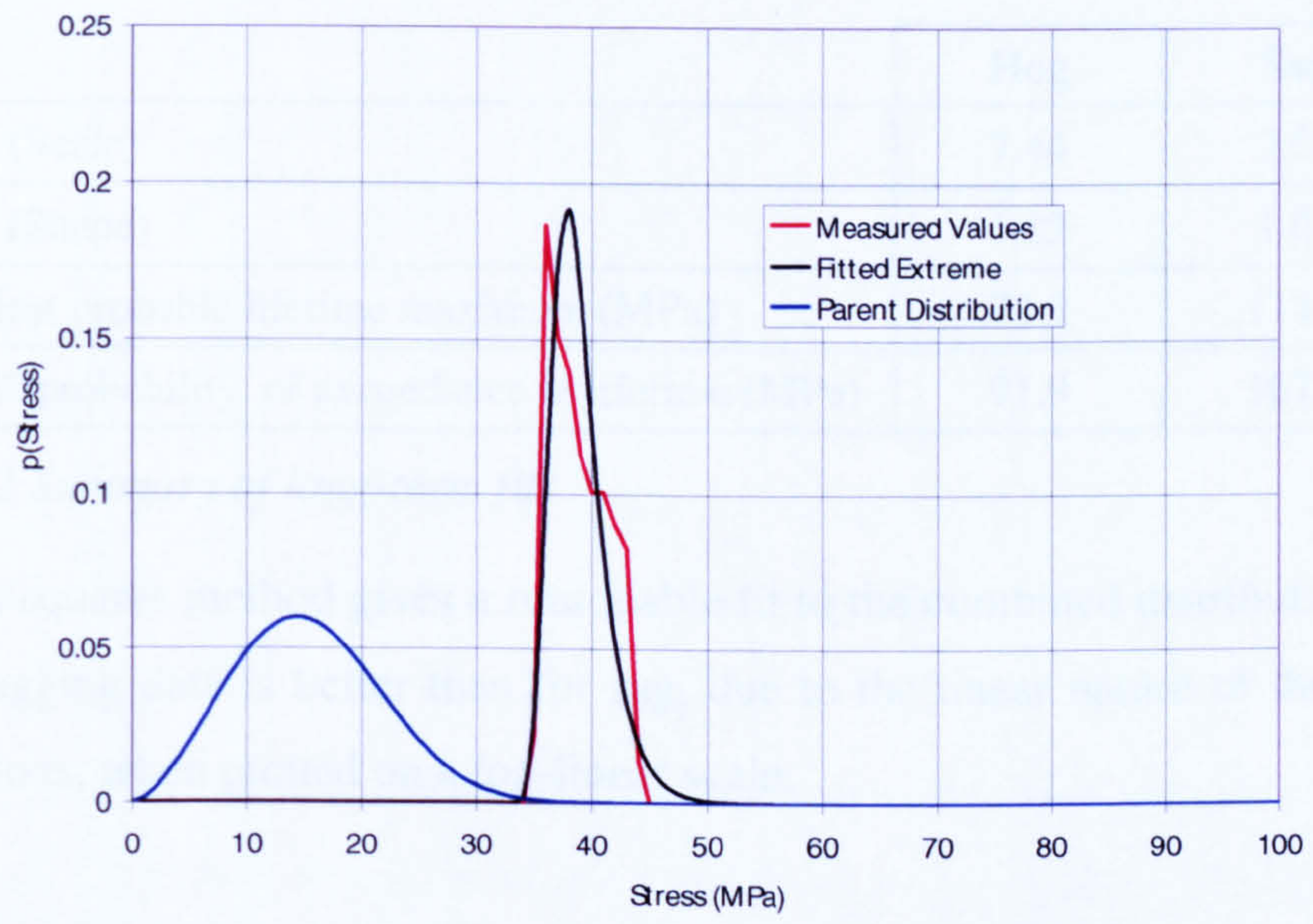

Figure 4-4 Example fit to sea state 5

The fit to sea state 8 shows the spread of the tail of the extreme distribution. There is an isolated high value at 87MPa. The fitted distribution does give a finite probability of this occurring but it is spread over the surrounding values.

The lower sea state histograms do not show this wide spread. This is because the values were ranked in increasing order so any high values have been included at the lower end of the next sea state. The large dataset should offset the fact that a few high values have not been included. It can be seen that the fitted distribution does have a tail that extends past the measured data.

The fitted Weibull coefficients derived from the fits to each sea state for hog and sag are given in Appendix D.2

4.3.5 Long term distribution

The individual sea state distributions were then combined with their associated probabilities of occurrence to give a long-term load distribution. A Weibull distribution was then fitted using the least squares method. This is discussed in more detail in Appendix D.3. The resulting fits are shown in Appendix D.4. The Weibull parameters for the fits are given in Table 4-2. The most probable and 1% probabilities of exceedance values for a lifetime are also given ($3.3x10^7$ cycles).

	Hog	**Sag**
A (Scale)	7.44	7.08
B (Shape)	1.23	1.04
Most probable lifetime maximum (MPa)	78.3	114.6
1% probability of exceedance in lifetime (MPa)	91.9	167.7

Table 4-2 Summary of long-term fits

The least squares method gives a reasonable fit to the combined distributions. The fit to the hogging data is better than for sag, due to the linear nature of the combined distributions, when plotted on a log-linear scale.

4.3.6 Converting to probability of exceedance in 4-hours

The probability of exceedance per cycle needs to be converted to an equivalent probability of exceedance in a 4-hour period to allow a comparison between the fitted distributions and the 4-hour maximum values.

A theoretical relationship is discussed by Clarke (Clarke, 1987).

$$P_{4hr} = 1 - (1 - P_e)^{2000} \qquad \textit{Equation 4-7}$$

where P_{4hr} and P_e are the probability of exceedance in 4-hours and per cycle respectively. This relationship assumes 500 waves per hour.

This relationship assumes that all cycles are independent and could occur at any time in the ship's life. However, high stresses will occur in storm conditions and the low stresses will be grouped in calmer seas. Consequently, this relationship over predicts the probability of low stress values occurring (Clarke, 1987).

There is a smaller dataset of continuous strain gauge readings for the same class of frigates. For these trials the entire strain histogram was recorded, as well as the 4-hour maximum. Rainflow counting techniques were then used to estimate the probability of strain range per wave encounter.

To establish a relationship between the 4-hour probability of exceedance to the probability of exceedance per wave encounter the data were grouped and plotted in Figure 4-5. The data appear to follow a straight-line relationship for higher probabilities before tending to Equation 4-7 below a probability of exceedance of 10^{-6} per wave encounter.

It is well known that the relationship between two variables can be expressed as $y=ax^n$, if they follow a straight-line relationship on a log-log plot. The data appear to be best fitted by a combination of two lines at higher probabilities.

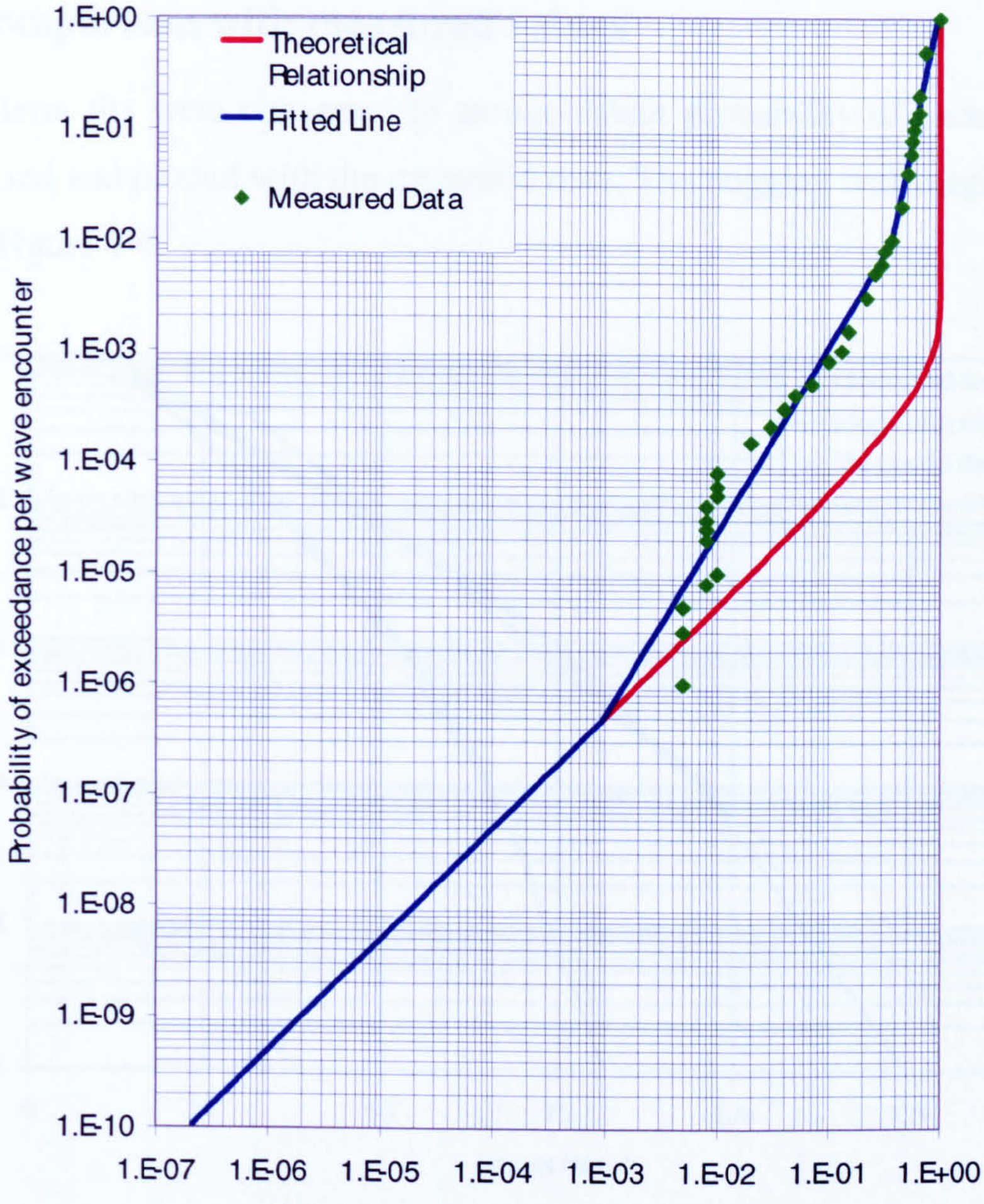

Figure 4-5 Relationship between probability of exceedance per cycle and per 4 hour period

4.3.7 Comparison with measured values

The long-term fits were converted to an equivalent probability of exceedance in a 4-hour period and plotted with the measured data. The hogging and sagging plots are shown in Figure 4-6.

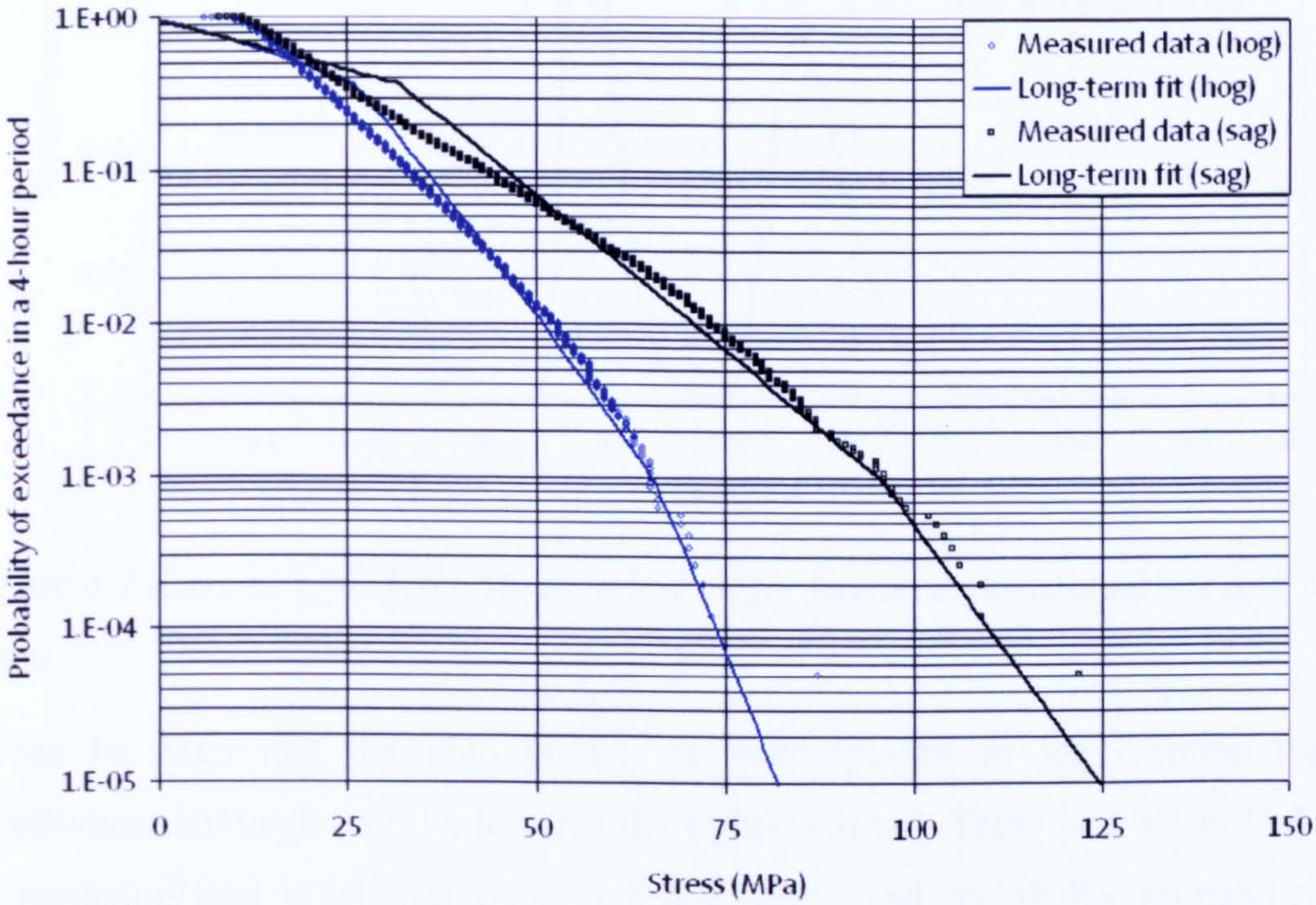

Figure 4-6 Comparison of long-term fit with measured data

The fits made using in the previous section give a very good fit to the measured data. There is a single high value on both the hogging and sagging fit, which lies above the fitted line. It should be noted the line describes the most probable maximum and there is a 63% probability of exceeding the value obtained from a Weibull distribution. The extreme type-1 distribution derived from the Weibull distributions at the probability of exceedance corresponding to the single high values is shown in Figure 4-7.

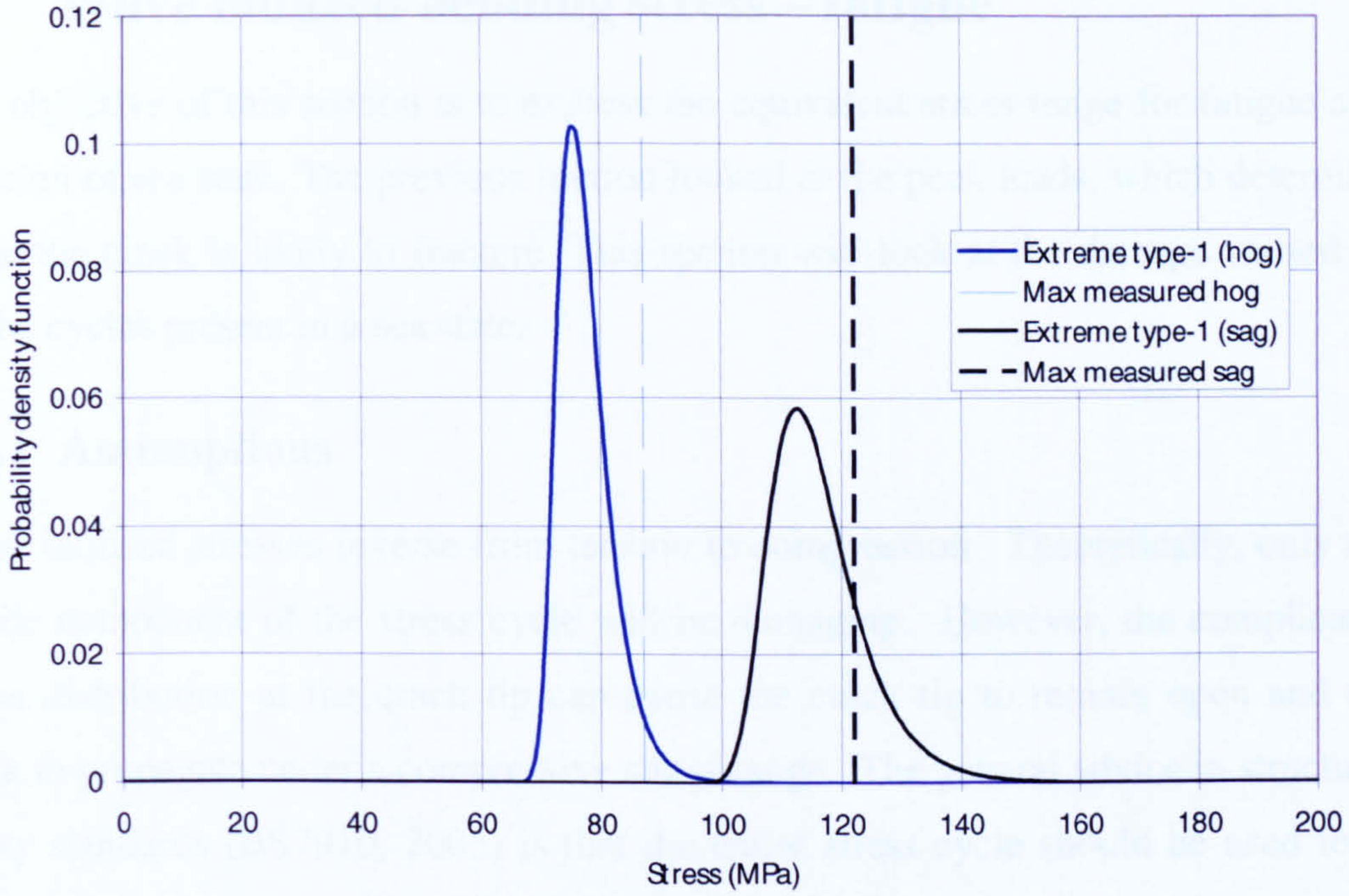

Figure 4-7 Extreme type-1 distribution derived for maximum measured hog and sag stress

It can be seen that the high points are encompassed in the extreme type-1 distribution, although both lie towards the right-hand tail. There is a 3% probability of exceeding the maximum measured hog value and an 18.5% probability of exceeding the maximum measured sag value.

Significance testing is a technique used in statistics to test the hypothesis that measured data has a significant probability of having resulting from the proposed distribution. The significance level is commonly set at 5% (Hinton, 2004), i.e. if there is a probability of 5% or less of the measured value occurring the distribution would be rejected. In a two-tailed test, where the value could occur either higher or lower than the proposed distribution, the significance level is reduced to 2.5% in either tail to give the same overall significance level. On this basis, the highest measured value for hog would fall just within the upper significance level and the proposed distribution would be considered to be acceptable.

4.4 Wave induced bending stress – fatigue

The objective of this section is to express the equivalent stress range for fatigue as a function of sea state. The previous section looked at the peak loads, which determine when the crack is likely to fracture. This section will look at the damage caused by all the cycles present in a sea state.

4.4.1 Assumptions

Wave induced stresses reverse from tension to compression. Theoretically, only the tensile component of the stress cycle will be damaging. However, the complicated stress distribution at the crack tip can cause the crack tip to remain open and the crack to propagate under a compressive stress range. The general advice in structural safety standards (BS7910, 2005) is that the entire stress cycle should be used for a welded structure.

4.4.2 Equivalent stress range

Fatigue crack growth was discussed in Section 3.3. Paris Law is used to describe the fatigue crack growth. The fluctuating loads at the crack tip are adequately described by the m-th expected moment of the stress range. This is defined as:

$$E\left[\Delta\sigma_{eq}{}^{m}\right] = \int_{0}^{\infty} \Delta\sigma^{m} f_{eq}(\Delta\sigma) d\Delta\sigma_{eq} \qquad \textit{Equation 4-8}$$

where σ_{eq} is the equivalent stress range. If we assume that the whole of the stress cycle is damaging then the stress range distribution is obtained by combining the hog and sag peak stress distributions.

Threshold effects, where the crack will not propagate if the applied stress intensity is below a certain value, are ignored in this approach. This effect will be important for short crack lengths, where a considerable portion of the applied stress intensity distribution could fall below the threshold level. However, it is felt for the longer crack lengths of interest in this thesis this effect will be minimal.

4.4.3 Individual sea state fits

The equivalent stress range for each sea state was calculated using the hog and sag peak stress fits carried out in the previous section. These fits gave a distribution of all peak cycles present in a sea state. The stress range is defined as the magnitude of the stress reversal.

The equivalent stress for each sea state is summarised in Table 4-3. The severity of the loading can be compared based on $N_h\Delta\sigma_{eq}^3$, where N_h is the number of cycles per hour.

	Proposed fit		
Sea state	**Δ_{eq} (MPa)**	**N_h**	**$N_h\Delta\sigma_{eq}^3$**
2	8.1	500	$2.66\text{x}10^5$
3	9.5	500	$4.29\text{x}10^5$
4	11.5	500	$7.60\text{x}10^5$
5	15.7	500	$1.93\text{x}10^6$
6	20.0	500	$4.00\text{x}10^6$
7	26.1	500	$8.89\text{x}10^6$
8	39.0	500	$2.97\text{x}10^7$

Table 4-3 Summary of stress range as a function of sea state

4.4.4 Long term data

The long-term equivalent stress can also be calculated by combining the long-term hog and sag peak stress distributions. This gives a long-term equivalent stress of 15.3 MPa, assuming 500 cycles per hour.

4.5 Still water bending stress

The still water bending moment (SWBM) depends on the ship loading conditions and can vary widely. This is discussed in more detail by Sun (Sun, 2003), who fits a Rayleigh distribution for sagging and an exponential distribution for hogging for FPSO vessels. Soares (Soares, 1989) states that the SWBM for warships is subject to considerably less uncertainty, as they are normally loaded in a similar manner for each voyage, and can even be taken as a deterministic value. SSC-368 (Mansour, 1992) proposes the use of a normal distribution with a coefficient of variation (COV) of 5%.

The still water bending moment for the naval frigate used in the previous section was extracted from the stability books. This was then converted to a stress on the deck using simple beam theory. Table 4-4 summarises the values. Note that although called the sagging condition the deck remains in tension and is, in effect, the minimum hogging value.

	Max BM (MNm)	**Stress (MPa)**
Hogging condition	110	45.0
Deep water condition	95	38.7
Sagging condition	60	24.5

Table 4-4 Summary of still water bending stress values

The mid-point between the hogging and sagging values is 35MPa, close to the deep-water condition. Fitting a normal distribution to the mid-point with a COV of 5% gives a 0% probability of exceeding the maximum and minimum values. Increasing the COV to 10% gives a 0.2% and 0.13% probability of exceeding the maximum and minimum conditions respectively. This is shown in Figure 4-8.

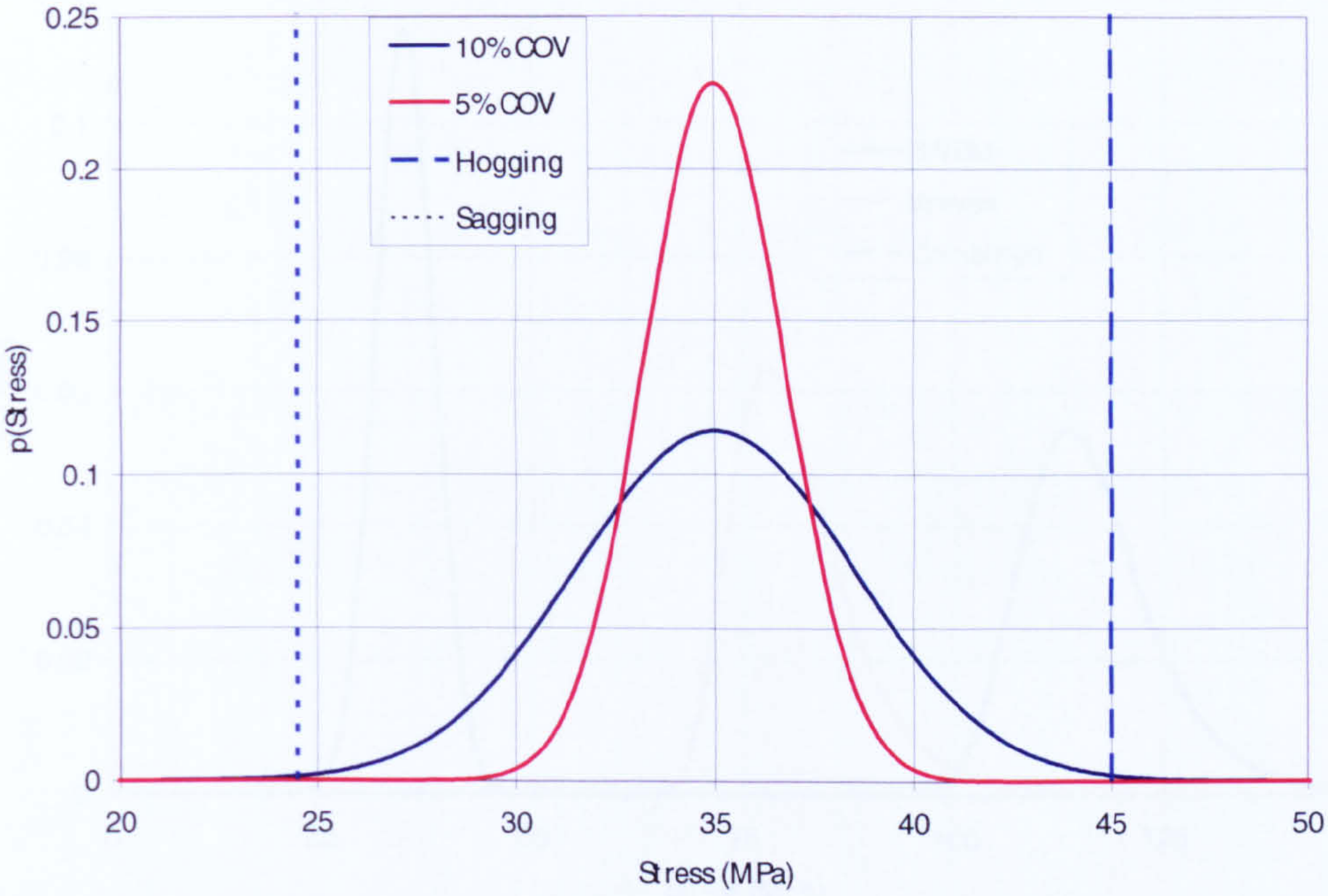

Figure 4-8 Distribution of still water bending stress

4.6 Combining the still water and bending stress

To enable the use of some of the reliability methods evaluated in Chapter 6 the wave induced stress and the still water bending stress need to be combined into a single applied load distribution.

The conditional probability of two independent variables is given as (Melchers, 1999):

$$p(\sigma_{SWBS} + \sigma_{wave}) = p(\sigma_{SWBS})p(\sigma_{wave}) \qquad \textit{Equation 4-9}$$

Equation 4-9 calculates the probability of a particular still water stress value occurring with each extreme wave stress. By repeating this calculation for every combination of still water bending stress and wave induced stress and summing the probability the overall probability density function can be calculated. An example of this is shown in Figure 4-9.

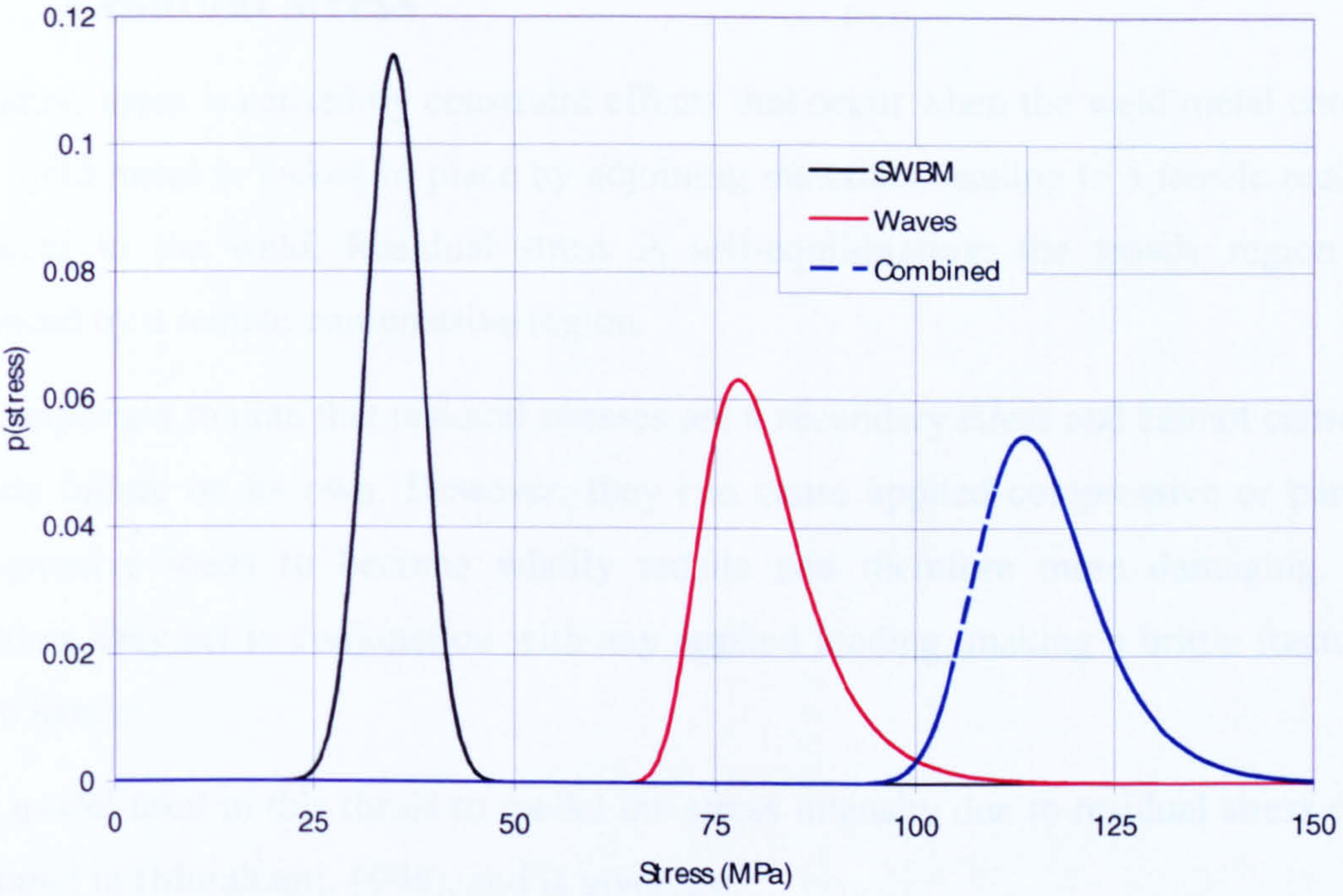

Figure 4-9 Plot of combined probability density function for still water bending stress and wave induced bending stress

The calculation is repeated at every time step as the extreme distribution is a function of the number of cycles, which can be computationally expensive. The effects of this are analysed in Appendix D.5. The same approach is applied when the still water bending stress and wave loading have opposite signs (i.e. a crack in the keel with a hogging still water value). The still water bending stress is subtracted from the wave bending stress to obtain the joint distribution.

Note that Equation 4-9 assumes that the still water and wave induced loading are independent values. In practice, it would be expected that there would be a degree of correlation between the components. Masters are advised to take on additional ballast in high seas to avoid forefoot slamming (Bishop, 1991). However, given the relatively small change in still water bending for naval ships this is not thought to have a significant effect in this study.

4.7 Residual stress

Residual stress is caused by constraint effects that occur when the weld metal cools. The weld metal is locked in place by adjoining materials, leading to a tensile region adjacent to the weld. Residual stress is self-equilibrating; the tensile region is balanced by a remote compressive region.

It is important to note that residual stresses are a secondary stress and cannot cause a plastic failure on its own. However, they can cause applied compressive or partly compressive loads to become wholly tensile and therefore more damaging. In addition, they act in conjunction with any applied loading, making a brittle fracture more likely.

The model used in this thesis to model the stress intensity due to residual stress can be found in (Murakami, 1996), and is given as:

$$K_{res} = Y_{res}\sigma_y\sqrt{\pi a} \qquad \textit{Equation 4-10}$$

where σ_y is the yield stress of the material and a is the characteristic crack length. Y_{res} is the geometry factor, given below:

$$Y_{res} = \left[\frac{\sqrt{1+\left(\frac{a}{c}\right)^4}-\left(\frac{a}{c}\right)^2}{1+\left(\frac{a}{c}\right)^4}\right]^{1/2} \qquad \textit{Equation 4-11}$$

where c is the point at which the stress intensity due to residual stress changes from tensile to compressive, normally taken as twice the plating thickness. A plot of stress intensity due to residual stress as a function of crack length for a 15 mm thick plate (c = 30 mm) and a yield stress of 265MPa is given in Figure 4-10.

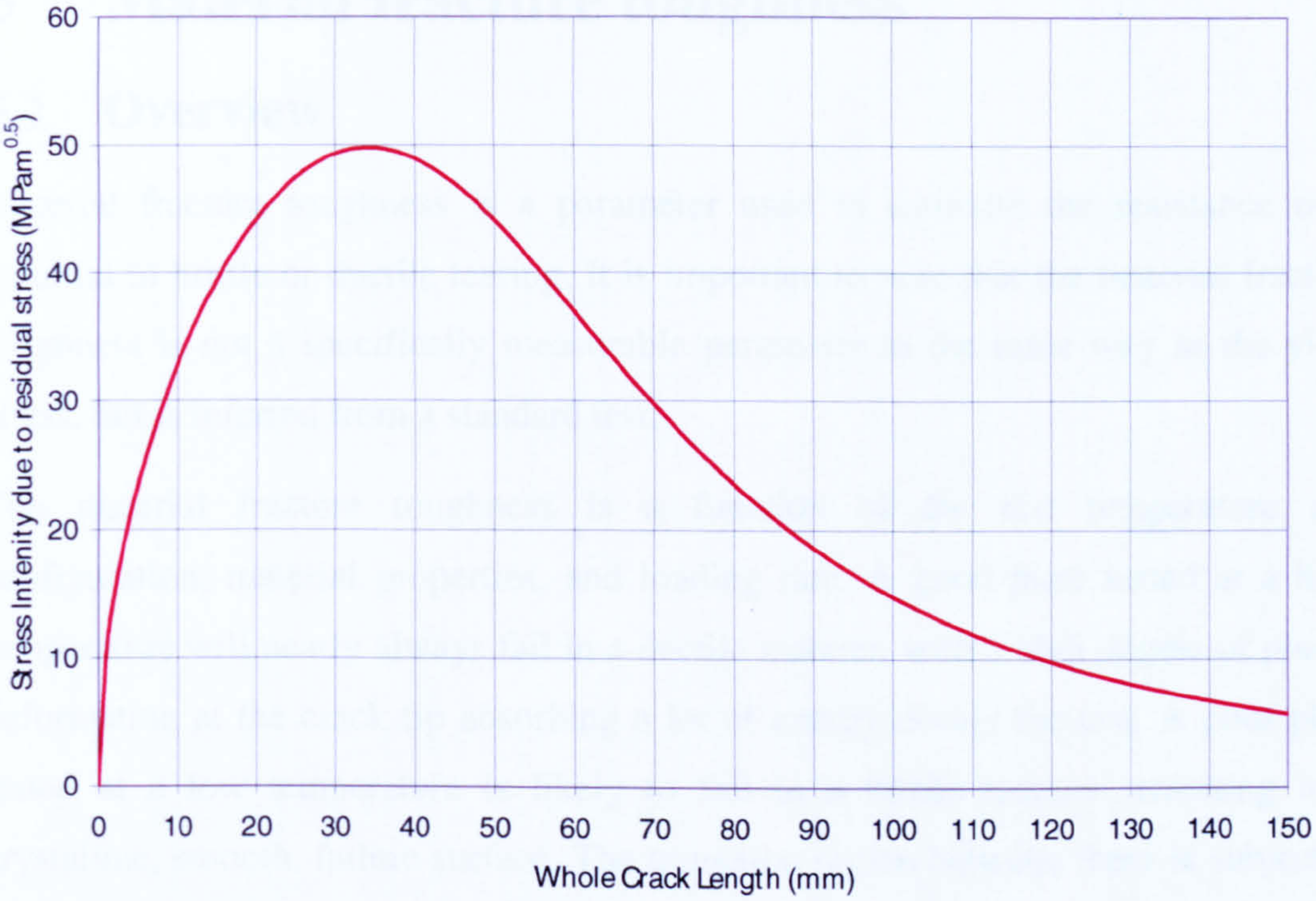

Figure 4-10 Plot of stress intensity due to residual stress

The stress intensity due to residual stress has been assumed to be a deterministic value and is simply added to the combined distribution shown in Figure 4-9. In practice, there will be some variation due to changes in the yield stress of the plate. However, as the influence of stress intensity due to residual stress falls as the crack propagates this effect is considered to be minimal for the types of cracks that are of interest in this study.

In theory, stress intensity due to residual stress is reduced in service due to shakedown effects. On application of a high load the material reaches it elastic limit so that plastic flow occurs. Load is then shed to adjacent material that is still elastic. When the load is removed the whole specimen unloads elastically and the peak residual stress is reduced. However, the advice in BS7910 (BS7910, 2005) is to assume yield point residual stress and does not allow any account to be made of relaxation due to prior overloading.

5 Material fracture toughness

5.1 Overview

Material fracture toughness is a parameter used to estimate the resistance of a material to brittle or ductile tearing. It is important to note that the material fracture toughness is not a specifically measurable parameter in the same way as the yield stress, but is inferred from a standard test.

The material fracture toughness is a function of the test temperature and configuration, material properties, and loading rate. A good plate tested at a high temperature will nearly always fail in a ductile manner, with a high degree of plastic deformation at the crack tip absorbing a lot of energy during the test. A poor plate tested at a low temperature is likely to fail in a brittle manner, resulting in a crystalline, smooth, failure surface. The transition region between these is subject to a high degree of scatter.

This chapter will describe the test procedure and the results of a test programme carried out at QinetiQ Rosyth on a number of modern steel plates. The master curve approach is commonly used to characterise the scatter in the fracture toughness over the ductile to brittle transition. A number of methods based on the master curve approach are evaluated.

It was discussed in Chapter 2 that all studies in the literature have assumed implicitly that the material fracture toughness remains constant as the crack propagates through the plate. It is the author's opinion that the predicted probability of brittle fracture will then be underestimated as the variability in material fracture toughness has not been correctly accounted for. Recent wide plate fatigue tests carried out at QinetiQ Rosyth will be used to attempt to quantify the variability in toughness.

5.2 Test procedure

The standard test procedure to determine material fracture toughness is defined in ASTM-E 1921 (ASTM, 2005) and involves testing a number of standardised specimens to give an estimate of the reference temperature, T_0. T_0 corresponds to the temperature where the median fracture toughness for a 25 mm thick specimen has a value of 100 MPa$\sqrt{m}$. An estimate of a suitable test temperature is given through correlation with the Charpy 27J temperature. Testing above the T_0 temperature has been demonstrated to considerably reduce the uncertainty in the estimate of T_0 (Wallin, 1998).

A number of different specimen types are commonly used to test for material fracture toughness: compact specimens (CT); disk-shaped compact specimens (DCT); and single-edge notched bend specimens (SEB). The most commonly used method is the SEB specimens, which are rectangular, with a span S, width W and breadth B. A starter crack is machined into the specimen and fatigued until the crack length reaches approximately half the width of the specimen. Fatiguing the machined crack ensures that there is a sharp tip at the crack front.

The SEB specimen is then placed in a test rig which applies a bending load at either end of the specimen. A clip gauge is used to measure the displacement of the specimen at the crack tip. The toughness is very sensitive to the applied loading rate, which should closely model the loading rate applicable to the real structure.

The results of the test are plotted as a load-displacement curve. The material fracture toughness can then be calculated from the area under the curve, using the J-Contour integral (Sumpter, 2006a). Some examples of test traces are shown in Figure E-1. The mode of failure is given by the subscript:

- m indicates that the test specimen reached maximum load;
- mc indicates that the test specimen reached maximum load, but cleaved as the load was being reduced. The material fracture toughness is calculated at the point of maximum load;
- c indicates that the specimen cleaved as the load was being increased.

The specimen size specified in the standard limits the ratio of the length of the crack to the thickness of the specimen to ensure that conditions of plane strain are maintained at the crack tip. A number of further checks are required to ensure that only small scale yielding has taken place.

Under plane strain the condition of stress triaxiality is maintained at the crack tip. The material close to the crack tip reaches yield stress and attempts to contract due to Poisson's effect. However, material surrounding the crack tip remains elastic and prevents this contraction resulting in a plane strain condition. This stops the material at the crack tip from yielding, elevating the stress at the crack tip and making a brittle fracture more likely.

If the plastic zone approaches the free surface in the thickness direction of the test specimen then yielding will occur as the material is free to contract, in a similar fashion to the necking of a tensile specimen, resulting in a large plastic zone and a plane stress condition. The formation of the large plastic zone allows the stresses at the crack tip to relax. The specimen can therefore carry more load before failure, resulting in a higher toughness value.

It is important that the constraint applied to the test specimen matches those attained in a real structure. For example, if the material in the real structure is prevented from attaining a condition of plane stress then the material fracture toughness values calculated from a series of test results may be artificially high, leading to an under-estimate in the risk of a brittle fracture.

5.3 QinetiQ test programme

QinetiQ Rosyth has recently carried out a significant test programme on a total of seven steel plates. The plates were procured from a variety of sources. Two of the plates were purchased under Lloyd's grade A specification, four of the plates under grade D, and one plate under grade DH. In the case of the two grade A plates: these were both purchased from the same source, one with a Lloyd's grade A specification and one without. It appears that the supplier provided two plates from the same batch, but Charpy tested the Lloyd's designated plate to demonstrate its conformance with the 27 Joule at +20°C requirement. A summary of the Charpy and tensile properties of the plates tested is given in Table 5-1.

Plate grade	Identifier	Charpy T_{27J} (°C)	Charpy FATT(°C)	Yield Strength (MPa)	UTS (MPa)
A	1	-24	0	338	512
A	2	-23	2	338	512
D	3	-34	-10	416	504
D	4	-35	-15	327	480
D	5	-45	-34	354	460
D	6	-79	-54	403	526
DH	7	-45	-35	409	548

Table 5-1 Summary of Charpy and tensile properties for the plates tested

All of the plates tested were well above their required Charpy and strength specifications, which are given in Appendix A. Since the grade A plates just meet the minimum grade D requirements they could be regarded as representative of the minimum toughness likely to be encountered in a grade D ship plate.

A number of different welds were made by the submerged arc and metal inert gas processes in one of the grade D plates (identifier 4) and in the grade DH plate (identifier 7). Charpy specimens were taken from the weld and heat-affected zone and tested at -20°C. Results for the grade D welds were in the same range as the parent plate. The grade DH welds were slightly degraded compared to the parent plate. In both cases the Charpy values at -20°C were mostly above 27J, but there were isolated values in the 15-20J range.

The SEB test specimens were slightly non-standard having a thickness of 15mm, width of 50mm, and a crack length of 15mm. These dimensions give a 'plane stress' ligament which is thought to closely model the constraint conditions in a ship structure, which have large in-plane dimensions compared to the thickness of the plate. All plates tested had a nominal thickness of 15 mm, with the majority of specimens taken in LT direction.

All specimens were tested at a loading rate of 250 MPa$\sqrt{m}$/sec, which is thought to model the loading rate applicable to a 1 metre long crack in the deck of a ship under storm conditions. Up until the late 1990s fracture toughness tests at QinetiQ Rosyth were carried out at a loading rate of 10^4 MPa$\sqrt{m}$/sec. This was estimated to be the loading rate applicable to a slam in the keel of a ship. It is demonstrated by Sumpter (Sumpter, 1995) that the material fracture toughness is extremely sensitive to the applied loading rate.

In total 183 toughness tests have been carried out: 99 on plain plate and 84 on weld and HAZ areas. 165 tests were carried out in the LT direction. The effect of rolling direction is shown in Figure E-3. There is perhaps a slight tendency for the TL specimens to have lower toughness values, although there are a number of occurrences at high toughness values. It would difficult to extract trends with rolling direction due to the limited number of tests in the TL directions and consequently the potential effects of rolling direction are ignored. All test results are plotted against test temperature in Figure 5-1.

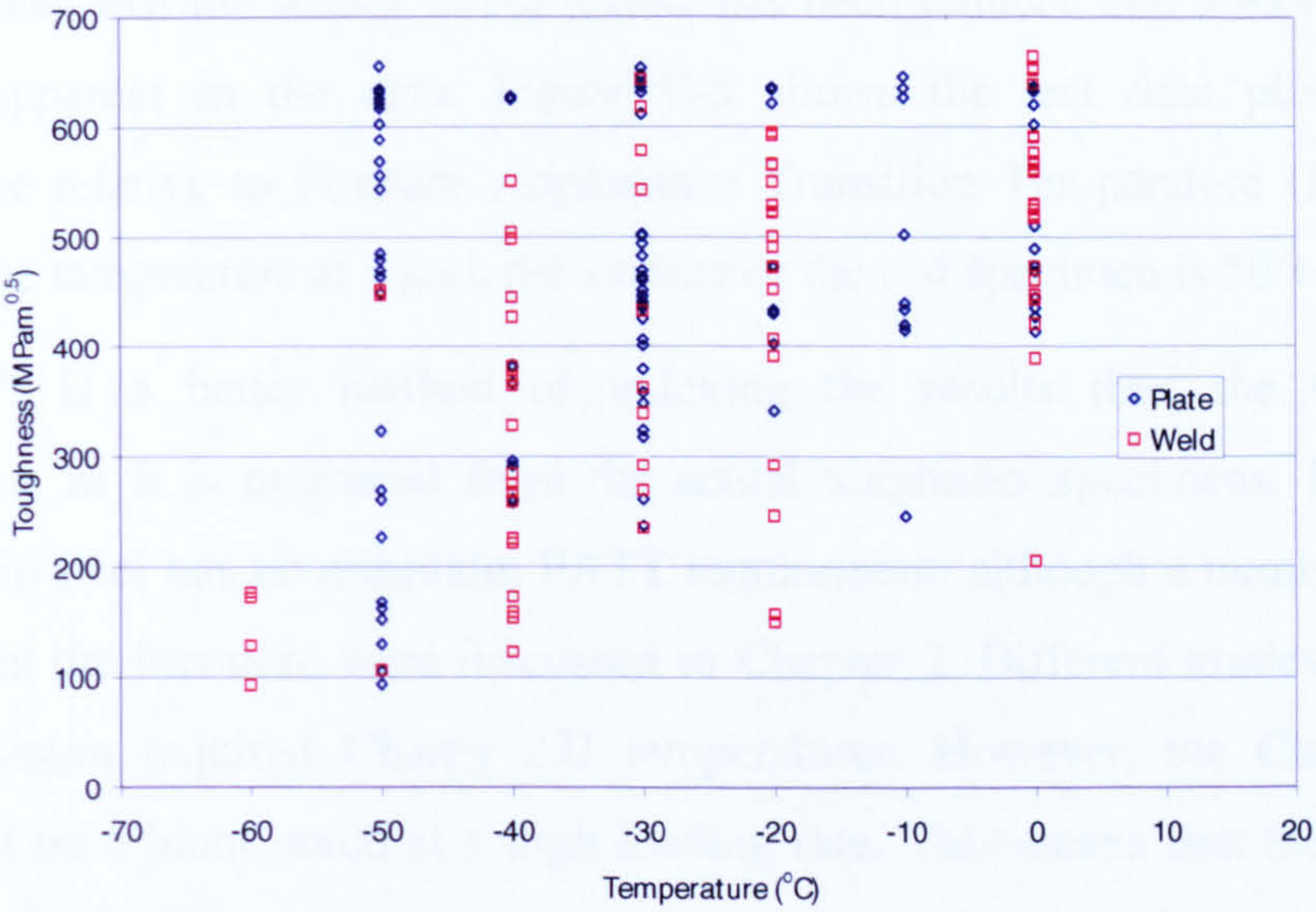

Figure 5-1 All toughness results plotted against test temperature

It can be seen that there is considerable scatter in the data. There is a trend for increasing toughness with temperature but there are still some isolated low toughness results at higher test temperatures. The weld results also appear to be slightly worse.

In an attempt to produce a more distinctive trend of toughness with temperature it was decided to plot the results against temperature relative to the Charpy 27J temperature. This is shown in Figure 5-2.

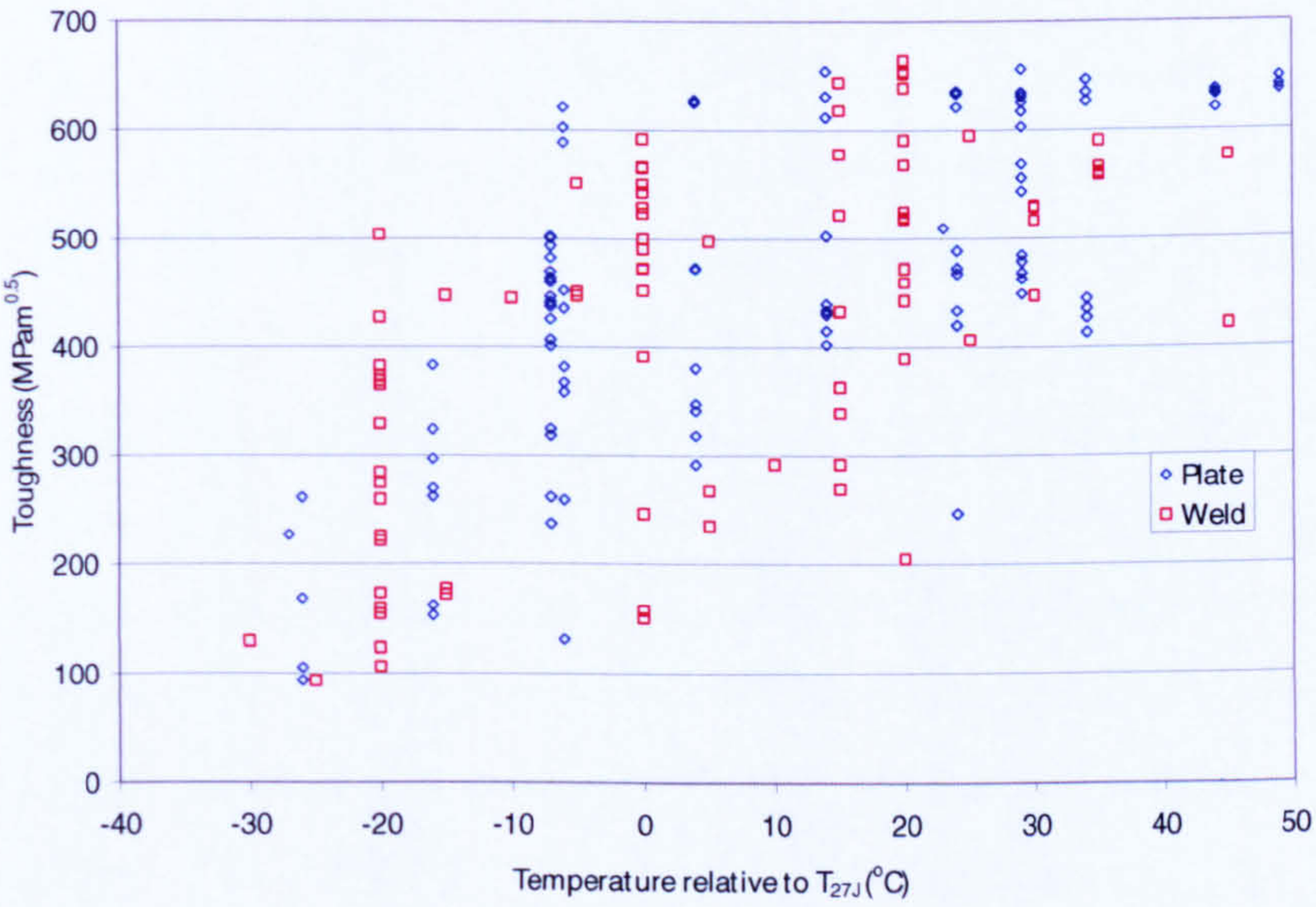

Figure 5-2 All toughness results plotted against test temperature relative to Charpy 27J temperature

It can be seen that the scatter in the results has been reduced and a more consistent trend is apparent in the data. Figure E-5 shows the test data plotted against temperature relative to Fracture Appearance Transition Temperature (FATT). The FATT is the temperature at which the surface of the test specimen is 50% crystalline.

The FATT is a better method of indexing the results than the Charpy 27J temperature, as it is measured from the actual toughness specimens. However, at present ship steel has no minimum FATT requirement, although a number of values proposed in the literature were discussed in Chapter 2. Different grades of plate do have minimum required Charpy 27J temperatures. However, the Charpy test is carried out on a blunt notch at a high loading rate. This means that there is a high degree of plastic deformation prior to failure. Despite these drawbacks, indexing the results to temperature relative to Charpy 27J temperature allows the toughness distribution to be modified for different grades of steel and external temperature.

5.4 Fitting the toughness distribution

A number of fit methods are evaluated in this section for their suitability in describing the scatter in toughness across the brittle to ductile transition. The methods are all based on the original 'master curve' approach, developed principally by Wallin (Wallin, 1984 and Wallin, 1985) and subsequently adopted in engineering testing and design standards (BS7910, 2005 and ASTM, 2005).

The basic master curve approach uses a three parameter Weibull distribution to describe the scatter in toughness at a given temperature, combined with a mean line to describe the trend in toughness with temperature. Recently, a number of refinements have been proposed in the literature to refine the master curve approach (Wallin, 2004). In this section the following methods will be evaluated:

1. original master curve;
2. master curve with censored specimens;
3. bimodal master curve;
4. engineering lower bound approach;
5. bimodal master curve / engineering lower bound approach;
6. master curve with random inhomogeneities.

There are two options for fitting the data: considering it as homogeneous dataset; or attempting to fit to the individual plate results, termed a mixed-mode approach. The advantage of the first approach is that the scatter seen in individual plate results can be encompassed into a single distribution and the greater number of tests allows more complicated fit methods, with more parameters, to be evaluated. However, a criticism of this approach is that pooling a large amount of data from a variety of sources can increase the scatter in the data and disguise trends seen in the individual plate data. Consequently, both approaches will be evaluated in this chapter although, due to the reduced number of test results available for each fit, only the basic master curve approach will be evaluated for the mixed-mode approach.

The fitted distributions are compared with the measured data using two plots. The first plot shows the trend of the fitted distribution with the measured data as a

function of temperature relative to Charpy 27J. The second plot compares the scatter present in the data with the fitted distribution. The data are normalised to the number of standard deviations from the mean to allow it to be plotted in a single diagram. These figures can be found in Appendix E.

Prior to the fitting of the distributions the test results are converted to an equivalent 25mm toughness using Equation 5-1 (Wallin, 1985). This equation simply accounts for the variation in material at the crack tip, as opposed to any constraint effects. The test specimen is still assumed to remain in plane strain.

$$K_{mat(25mm)} = K_{\min} + (K_{mat} - K_{\min})\left(\frac{B}{25}\right)^{1/4} \qquad \textit{Equation 5-1}$$

This term can then used to scale the resultant fit to thicker or thinner plates.

5.4.1 Master curve approach

The master curve is fitted using a maximum likelihood estimate, which calculates the likelihood of obtaining the set of data given the assumed probability model. The best estimate is then obtained by maximising the likelihood of obtaining the given data set.

The master curve for a single temperature can be written as:

$$P(K_{mat}) = 1 - \exp\left[-\left(\frac{K_{mat} - K_{\min}}{K_0 - K_{\min}}\right)^4\right] \qquad \textit{Equation 5-2}$$

where K_0 is the fracture toughness corresponding to a 63.2% probability of exceedance of K_{mat}, and K_{min} is the assumed lower bound of fracture toughness.

Experimental data have led to the setting of the shape factor as 4 (Wallin, 1984). An attempt is also made to verify this theoretically by attempting to characterise the volume of material taking part in the fracture process (Wallin, 1984).

K_{min} is the threshold toughness. Setting K_{min}=0 would result in finite probabilities of near zero material fracture toughness values. Fracture toughness data exhibit an absolute minimum that is above zero. A possible reason for this is warm pre-stress effects at the crack tip (Anderson, 1990). Experimental results have estimated the finite lower bound at 20 MPa$\sqrt{m}$ (Wallin, 1984), which is based on an extrapolation

of the data towards the lower tail using an assumed distribution. The justification for the selection of 20 MPa√m is rather vague; simply that it is estimated to lie between 10 and 20 MPa√m. This is confirmed by Zerbst (Zerbst, 1998) who states that K_{min} is more a mathematical fitting parameter than a finite lower bound.

The trend of toughness with temperature is assumed to follow (Wallin, 1985):

$$K_0 = 31 + 77\exp[0.019(T - T_0)] \qquad \textit{Equation 5-3}$$

In this study this has been modified slightly, to be indexed to the temperature relative to Charpy 27J temperature, giving:

$$K_0 = 31 + 77\exp[0.019(T - T_{27J} - T_0)] \qquad \textit{Equation 5-4}$$

The maximum likelihood estimate, L, is given by iterating the fit parameter, T_0, to maximise Equation 5-5.

$$L = \prod_{i=1}^{n} p(K_{mat}) \qquad \textit{Equation 5-5}$$

Equation 5-5 can be simplified by taking logs of both sides, converting the product symbol to a summation.

$$\ln L = \sum_{i=1}^{N} \ln[p(K_{mat})] \qquad \textit{Equation 5-6}$$

The test data are plotted against the temperature relative to the Charpy 27J transition temperature in Figure 5-3 and indexed by the plate identifier given in Table 5-1.

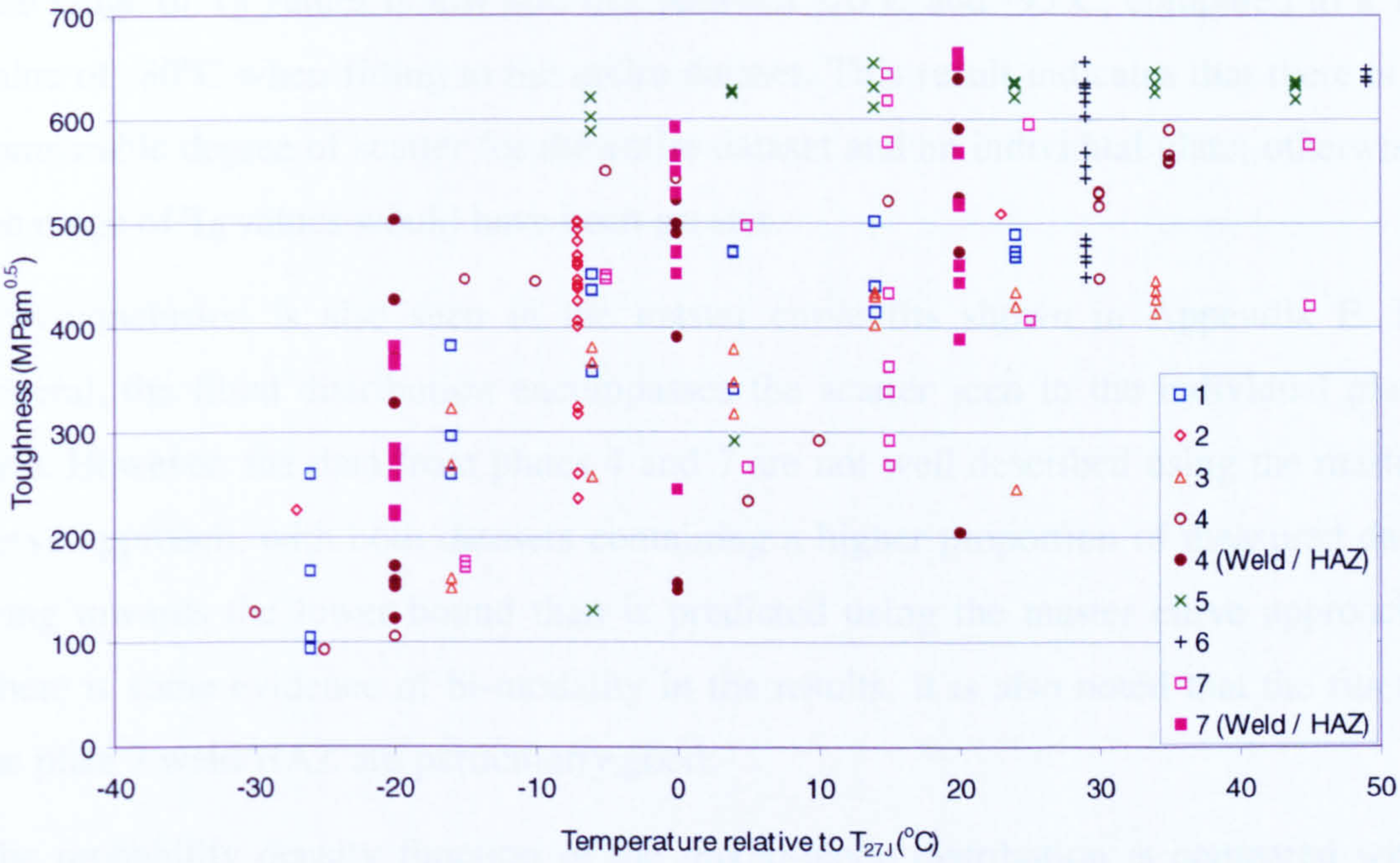

Figure 5-3 All toughness results plotted against temperature relative to Charpy 27J temperature indexed by plate identifier

Equation 5-6 is used to fit a distribution to the test data from each set of plate and weld/HAZ results, and to the entire dataset. The fits to each set of results are shown in Appendices E.3 to E.11 and to the entire dataset in Appendix E.12. The T_0 value for each distribution is given in Table 5-2.

Plate grade	Identifier	No. of samples	T_0 (°C)
A	1	19	-78.7
A	2	20	-93.5
D	3	20	-70.2
D	4	18	-84.4
D (weld/HAZ)	4 (weld/HAZ)	23	-90.6
D	5	20	-94.6
D	6	20	-71.7
DH	7	19	-79.3
DH (weld/HAZ)	7 (weld/HAZ)	24	-90.0
Entire dataset	-	183	-80.0

Table 5-2 Summary of T_0 parameters for master curve approach

The range of T_0 values is low and lies between -70°C and -95°C, compared to a T_0 value of -80°C when fitting to the entire dataset. This result indicates that there is a comparable degree of scatter for the entire dataset and an individual plate; otherwise the range of T_0 values would have been greater.

This conclusion is also seen in the master curve fits shown in Appendix E. In general, the fitted distribution encompasses the scatter seen in the individual plate data. However, the data from plates 4 and 7 are not well described using the master curve approach, with both datasets containing a higher proportion of measured data lying towards the lower bound than is predicted using the master curve approach. There is some evidence of bi-modality in the results. It is also noted that the fits to the plate 7 weld/HAZ are particularly good.

The probability density function of the mixed-mode distribution is compared with master curve fitted to all test data in Figure 5-4.

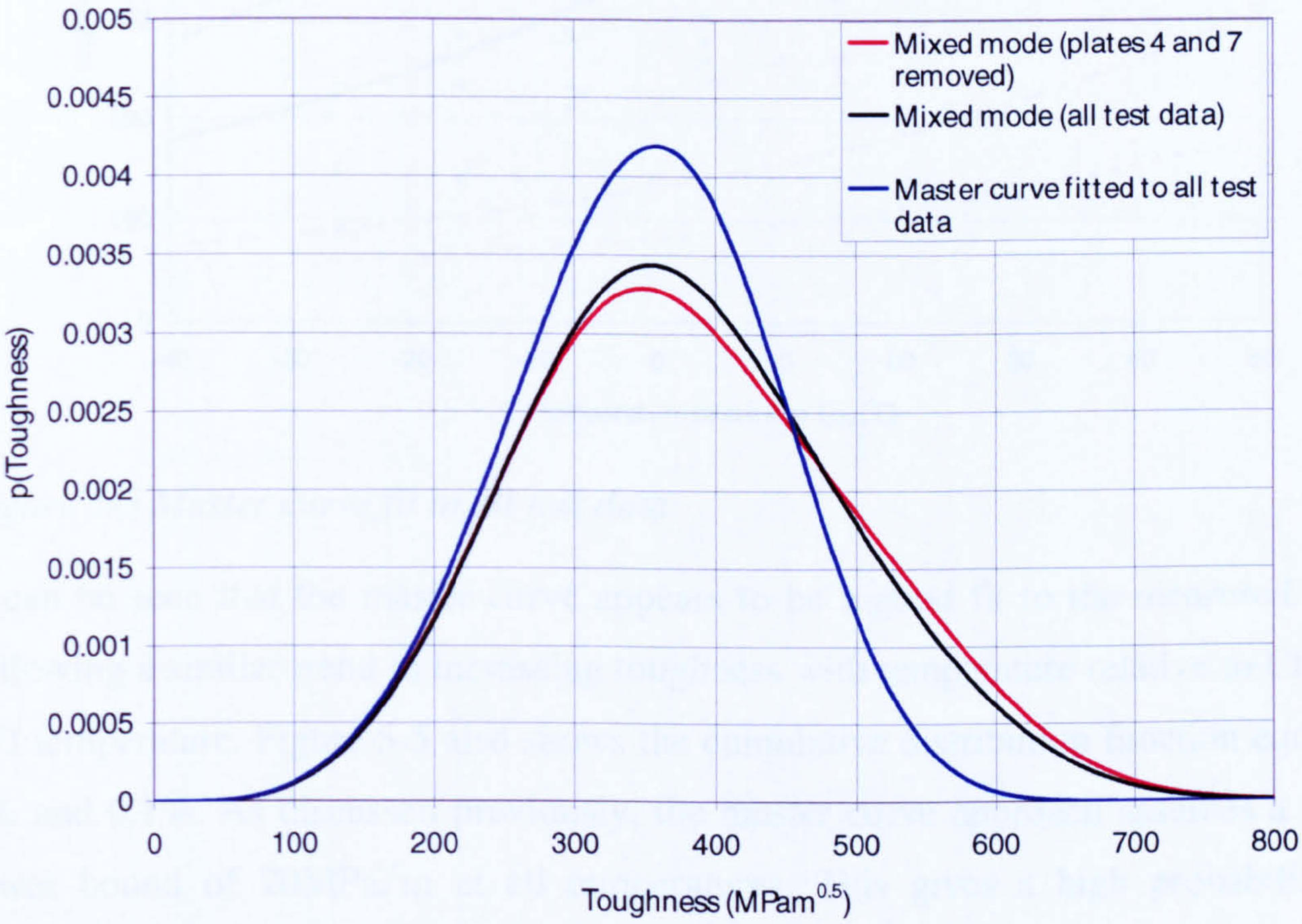

Figure 5-4 Comparison of mixed-mode distribution with basic master curve approach fitted to all test data

It can be seen that the mixed-mode distribution has encompasses a slightly wider range of toughness values, as would be expected due to the range of T_0 values. The

inclusion of the poor fits to plates 4 and 7 has only a minor effect on the distribution. However, at toughness values below 200MPa√m the mixed-mode distribution has a near identical shape to the master curve fitted to all the test data. The shape of the toughness distribution in this region is critical, as it will heavily influence the probability of brittle fracture. It is considered that the mixed-mode approach does not provide any benefits over treating the dataset as homogeneous, as a similar degree of scatter is seen in individual plate results and in the pooled test data. The master curve fit to all test data shown in Figure E-25 is repeated below.

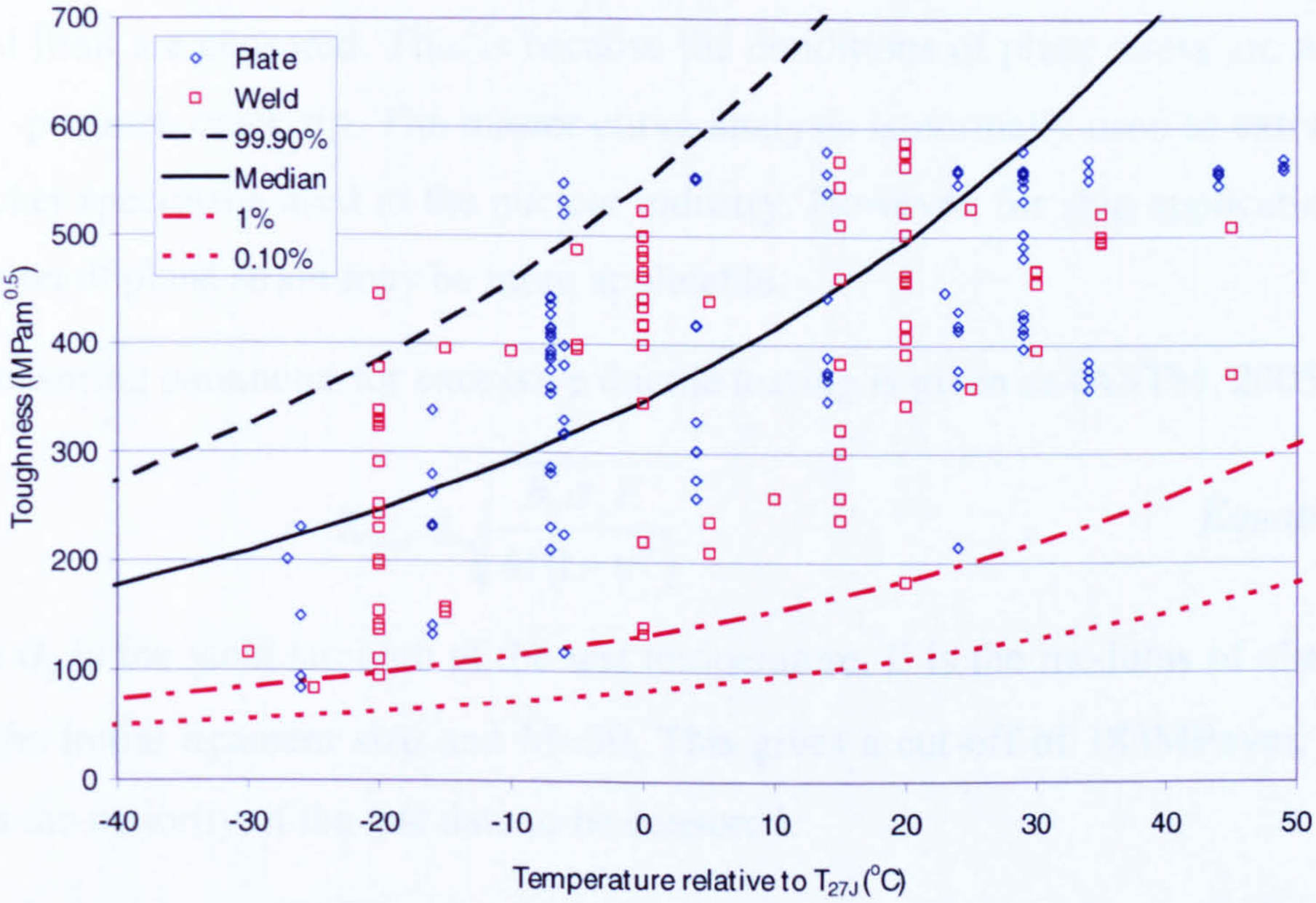

Figure 5-5 Master curve fit to all test data

It can be seen that the master curve appears to be a good fit to the measured data, following a similar trend in increasing toughness with temperature relative to Charpy 27J temperature. Figure 5-5 also shows the cumulative distribution function equal to 1% and 0.1%. As discussed previously, the master curve approach assumes a fixed lower bound of 20MPa√m at all temperatures. This gives a high probability of failure, even at relatively high temperatures. It is the author's opinion that this lower bound is over-pessimistic and does not model the true behaviour of ship steels. It can be seen that the data are bounded by a 1% lower bound. Consequently, it was decided to fix the lower bound at a cumulative probability of 0.1%, below which there is a 0% probability of a toughness value occurring. It is appreciated that this is

a somewhat empirical fit, but does appear valid when compared to the measured data. Without an unfeasible increase in the number of samples tested it would not be possible to validate this lower bound through material testing. Instead, it will be demonstrated in Chapter 7.3 that the inclusion of the lower bound givers results which correlate well with reference casualty statistics.

5.4.2 Master curve with censored specimens

It was assumed during the master curve fit that all test specimens were valid. It is recommended in test standards (ASTM, 2005) that toughness values higher than a critical limit are censored. This is because the conditions of plane stress are not met at the specimen crack tip. The master curve analysis is normally used to extrapolate to thicker specimens used in the nuclear industry. However, for ship applications the condition of plane strain may be more applicable.

The censoring parameter for excessive ductile tearing is given as (ASTM, 2005):

$$K_{mat} \leq \sqrt{\frac{b_0 \sigma_y E}{M\left(1-\nu^2\right)}} \qquad \textit{Equation 5-7}$$

where σ_y is the yield strength at the test temperature, E is the modulus of elasticity, b_0 is the initial ligament size and M=30. This gives a cut-off of 183MPa$\sqrt{m}$, which causes the majority of the test data to be censored.

Using the maximum likelihood technique gives T_0=-31.8°C. The fitted distribution is plotted against the measured data in Figure E-27 and Figure E-28. The fit is extremely over-conservative and does not provide a good representation of the shape of the measured data at low toughness values.

5.4.3 Bimodal master curve

The master curve can also be expressed in a bimodal form (Wallin, 2004), given in Equation 5-8.

$$P(K_{mat}) = 1 - p_a.\exp\left\{-\left(\frac{K_{mat} - K_{\min}}{K_{01} - K_{\min}}\right)^4\right\} - (1 - p_a).\exp\left\{-\left(\frac{K_{mat} - K_{\min}}{K_{02} - K_{\min}}\right)^4\right\}$$

Equation 5-8

where K_{01} and K_{02} are the characteristic toughness values for the two distributions and p_a is the probability of the toughness belonging to the first distribution. Equation 5-4 is then substituted into Equation 5-8 to index the toughness to temperature.

Using a maximum likelihood estimate this gives p_a=0.39, T_{01}=-59°C, and T_{02}=-85°C. The fitted distribution is plotted against the measured data in Figure E-29 and Figure E-30. It can be seen that the bimodal fit now gives a slightly better fit either side of the mean.

5.4.4 Engineering lower bound approach

The choice of K_{min} of is discussed in (Zerbst, 1998). It is stated that the choice of 20MPa$\sqrt{m}$ is seen as a mathematical fitting parameter but does not represent a physical lower bound to the toughness. Zerbst suggests a new model which uses a lower bound based on the measured toughness values. This removes the complication of using a shift parameter in the master curve approach. The original master curve equation is modified to:

$$P(J_c) = \begin{cases} \dfrac{\sqrt{\ln 2}}{J_0}(J_c - J_{LB}) & P_f \le 0.5 \\ 1 - \exp\left\{-\left(\dfrac{J_c}{J_0}\right)^2\right\} & P_f > 0.5 \end{cases}$$

Equation 5-9

where J_0 is the scale parameter and J_{LB} is the lower bound value. The same methodology has been used to derive a solution in terms of K.

The Weibull distribution is modified to a straight line between a cumulative probability of 0 to 0.5. The distribution starts at a lower bound of toughness, K_{LB}. This is shown in Figure 5-6.

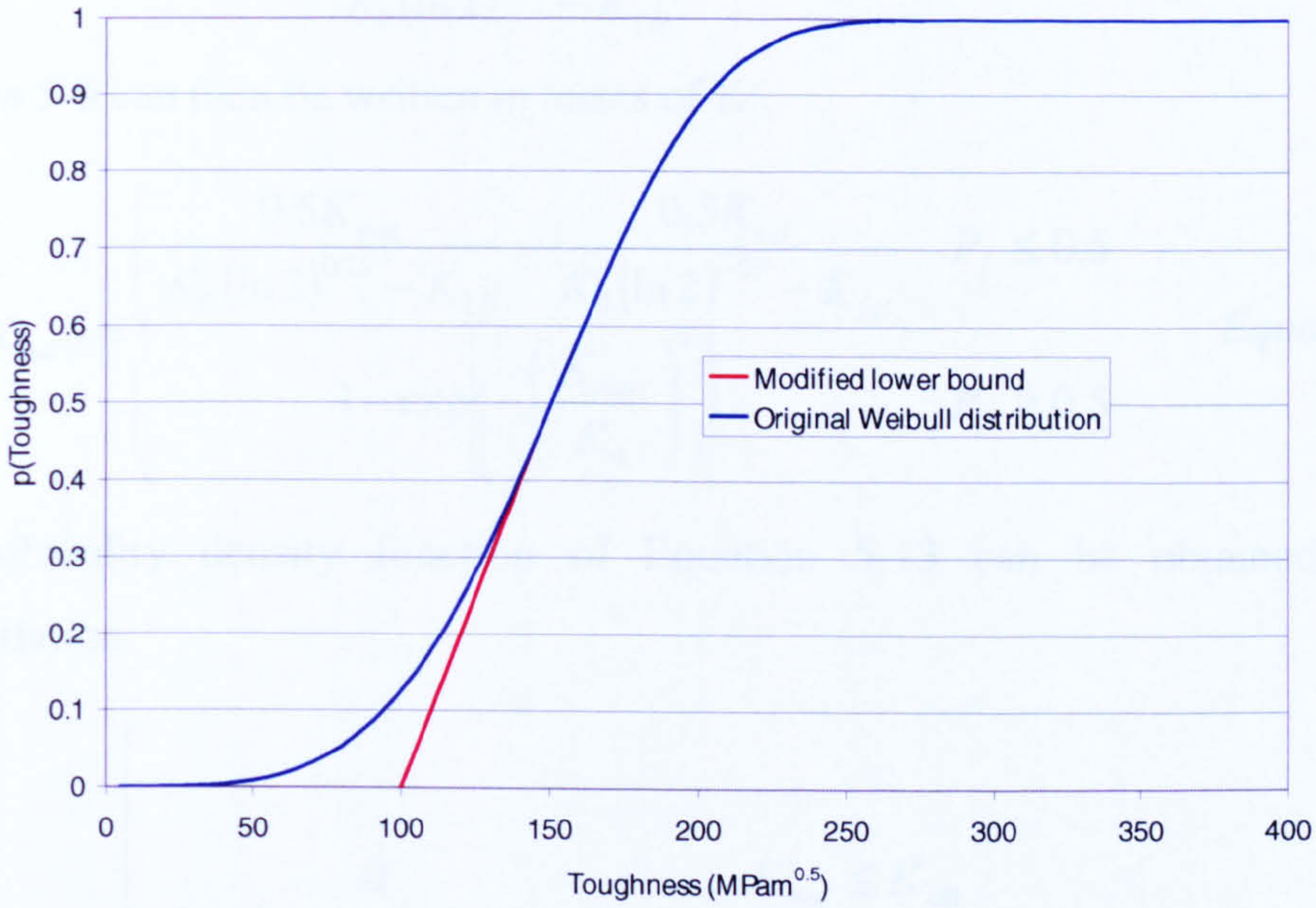

Figure 5-6 Plot of engineering lower bound approach

To calculate the equation of the line the locations of the start and end points must be known. The lower end of the line lies at (K_{LB}, 0). The x co-ordinate of the upper point is calculated from the master curve equation, in Equation 5-10.

$$0.5 = 1 - \exp\left\{-\left(\frac{K_{mat}}{K_0}\right)^4\right\}$$

Equation 5-10

$$\left(\frac{K_{mat}}{K_0}\right)^4 = \ln 2$$

$$K_{mat} = K_0 (\ln 2)^{0.25}$$

The gradient of the line can then be calculated as:

$$m = \frac{y_2 - y_1}{x_2 - x_1}$$

Equation 5-11

$$= \frac{0.5}{K_0 (\ln 2)^{0.25} - K_{LB}}$$

The intercept can then be calculated as:

$$y = mx + c$$

$$0 = \frac{0.5}{K_0(\ln 2)^{0.25} - K_{LB}} K_{LB} + c \qquad \textit{Equation 5-12}$$

$$c = -\frac{0.5K_{LB}}{K_0(\ln 2)^{0.25} - K_{LB}}$$

Equation 5-9 can then be written in terms of K:

$$P(K_{mat}) = \begin{cases} \dfrac{0.5K_{mat}}{K_0(\ln 2)^{0.25} - K_{LB}} - \dfrac{0.5K_{LB}}{K_0(\ln 2)^{0.25} - K_{LB}} & P_f \le 0.5 \\ 1 - \exp\left\{-\left(\dfrac{K_{mat}}{K_0}\right)^4\right\} & P_f \ge 0.5 \end{cases} \qquad \textit{Equation 5-13}$$

The probability density function of Equation 5-13 can be obtained through differentiation:

$$p(K_{mat}) = \begin{cases} 0 & K_{mat} \le K_{LB} \\ \dfrac{0.5}{(\ln 2)^{0.25} K_0 - K_{LB}} & K_{LB} \le K_{mat} \le 0.91K_0 \\ 4\dfrac{K_{mat}^3}{K_0^4} \exp\left\{-\left(\dfrac{K_{mat}}{K_0}\right)^4\right\} & K_{mat} \ge 0.91K_0 \end{cases} \qquad \textit{Equation 5-14}$$

K_0 and K_{LB} are indexed to temperature using Equation 5-4, giving equivalent T_0 and T_{LB} values, which are calculated using the maximum likelihood estimate. This gives T_0=-80°C and T_{LB}=-5°C. The distribution is plotted in Figure E-31 and Figure E-32. It can be seen that the lower bound fit is much less conservative. The cut-off occurs at the lowest measured toughness value. The probability density function is a horizontal line at low toughness values, indicating an equal probability of occurrence.

5.4.5 Bimodal engineering lower bound and master curve approach

The modified lower bound method shown in the previous section looked to be a reasonable approximation for the brittle region. However, it did not provide such a good fit to the more ductile values. It was decided to attempt to combine the advantages of the engineering lower bound approach with the bi-modal master curve

method. The probability density function becomes quite complicated and, for clarity, has been separated into two equations:

$$p(K_{mat}) = \begin{cases} 0 + Y & K_{jc} \le K_{LB} \\ \dfrac{p_a 0.5}{(\ln 2)^{0.25} K_0 - K_{LB}} + V & K_{LB} \le K_{jc} \le 0.91 K_0 \\ 4 p_a \dfrac{K_{mat}^3}{K_0^4} \exp\left\{ -\left(\dfrac{K_{mat}}{K_0} \right)^4 \right\} + V & K_{jc} \ge 0.91 K_0 \end{cases} \qquad \textit{Equation 5-15}$$

where:

$$V = 4(1 - p_a) \frac{(K_{mat} - 20)^3}{(K_{02} - 20)^4} \exp\left\{ -\left(\frac{K_{mat} - 20}{K_{02} - 20} \right)^4 \right\} \qquad \textit{Equation 5-16}$$

This gives four parameters to be calculated p_a, K_0, K_{LB}, and K_{02}. These are indexed to temperature using Equation 5-4 and calculated using the maximum likelihood estimate. The fitted values are summarised in Table 5-3 and the fitted distribution is plotted in Figure E-33 and Figure E-34.

P_a	T_0	T_{LB}	T_{02}
0.22	124	95	410

Table 5-3 Summary of fitted parameters for combined engineering lower bound and original master curve fit

5.4.6 Master curve with random inhomogeneities

The bimodal master curve is intended to account for small amounts of inhomogeneity in a dataset. As the degree of inhomogeneity increases K_0 becomes a random variable, with a mean value of μ_{K_0} and a standard deviation of σ_{K_0}, which can be described by the normal distribution (Wallin, 2004).

$$p(K_0) = \frac{1}{\sigma_{K_0}\sqrt{2\pi}} \exp\left[-\frac{(K_0 - \mu_{K_0})^2}{2\sigma_{K_0}^2} \right] \qquad \textit{Equation 5-17}$$

The probability density function of toughness at each value of characteristic toughness is given by:

$$p(K_{mat}) = 4\frac{(K_{mat} - K_{\min})^3}{(K_0 - K_{\min})^4}\exp\left\{-\left(\frac{K_{mat} - K_{\min}}{K_0 - K_{\min}}\right)^4\right\} \qquad \textit{Equation 5-18}$$

The maximum likelihood estimate is then given by:

$$\ln L = \sum_{i=1}^{N} \ln\left[\int_{-\infty}^{\infty} p\left(K_{mat_i}\right) p(K_0) dK_0\right] \qquad \textit{Equation 5-19}$$

Equation 5-19 is indexed to temperature by substituting Equation 5-4 into Equation 5-18 and assuming T_0 to be normally distributed. Solving Equation 5-19 gives μ_{T_0} =-74°C and σ_{T_0} =12°C. The fitted distribution is shown in Figure E-35 and Figure E-36. The high standard deviation means that there is an increased spread compared to a single master curve.

5.4.7 Evaluation of fit methods

The previous sections have fitted a variety of distributions to toughness tests data carried out on ship plate, weld and heat affected zone. The distributions are based on the master curve method, which uses a Weibull distribution to describe the scatter at a given temperature, combined with a mean line to describe the variation in toughness with temperature. The master curve method has been modified slightly to index the mean line to toughness relative to Charpy 27J transition temperature. This has been demonstrated to reduce the scatter in the test data, with the additional benefit that the Charpy 27J transition temperature is one of the parameters used by Classification Societies to index each grade of steel (Table A-1).

Two approaches have been adopted during the fit procedure: grouping all test data together and treating it as a homogeneous sample; and fitting a separate distribution to each set of plate or weld and heat affected zone data, termed a 'mixed-mode' approach. The advantage of treating all test data as homogenous is that is simplifies the fitting procedure and give a greater number of datum points. In addition, this approach does not require the position of the crack tip relative to a weld and heat-affected zone to be known. The drawback is that pooling the data can potentially

increase the scatter in the results and also requires that the sampled test data ars representative of the variation likely to be found in a typical ship.

It is found that the degree of scatter in an individual plate is comparable to that seen in the pooled data. This result is somewhat surprising, suggesting that even in the relatively high quality plates the toughness can vary quickly from regions of high toughness to very low values.

The probability of brittle fracture is very sensitive to the shape of the lower tail of the material fracture toughness distribution. It is demonstrated that in this region the mixed-mode distribution is very similar to the pooled data. Both methods give finite probabilities of low toughness values occurring, which are considered to be unrealistic. Consequently, a cut-off is proposed at a cumulative probability of 0.1%, below which it is assumed there is a 0% probability of a toughness value occurring. It is appreciated that this is somewhat crude but does appear to be reasonably valid when compared with test data.

A number of variations to the basic master curve approach which have been proposed in the published literature were then evaluated for the entire dataset. The quality of the fits can be compared using the maximum likelihood estimator, ln(L), with the highest estimate implying the best fit to the measured data.

Method	**ln(L)**
Master curve	-1161
Master curve with censoring	-89
Bimodal master curve	-1144
Engineering lower bound approach	-1156
Combined bimodal engineering lower bound and master curve	-1140
Master curve with random inhomogeneities	-1148

Table 5-4 Summary of maximum likelihood estimates for each fit method

It should be noted that the master curve with censoring has the highest estimate as it is only fitted to 19 results, as opposed to the 183 used in the other fits. It can be seen from the plots in Appendix E that the fit was extremely conservative. If we assume all results to be valid, the combined bimodal engineering lower bound and master

curve approach gives the lowest estimate. However, it can be seen from Figure E-31 that the lower bound cut-off lies at the lowest toughness result. This is extremely unconservative, assuming that the lowest possible toughness in a plate has been sampled during the material testing. This is extremely unlikely to be the case and this method is not considered to be a reliable method for calculating the material fracture toughness distribution.

The master curve with random inhomogeneities and the bimodal master curve both provide a good fit to the data; combining a realistic lower bound at a cumulative probability of 0.1% with a good fit to the scatter in the data. The bimodal master curve gives a slightly better fit as it is able to model the small second peak which lies approximately one standard deviation above the mean.

The effect of the toughness distribution on the calculated probability of failure is shown in Figure 5-7. The mixed-mode toughness distribution excludes the fits to plates 4 and 7. The input parameters used in the calculation are summarised in Appendix F; with the exception of the toughness distribution, which is based on the fits described in this section.

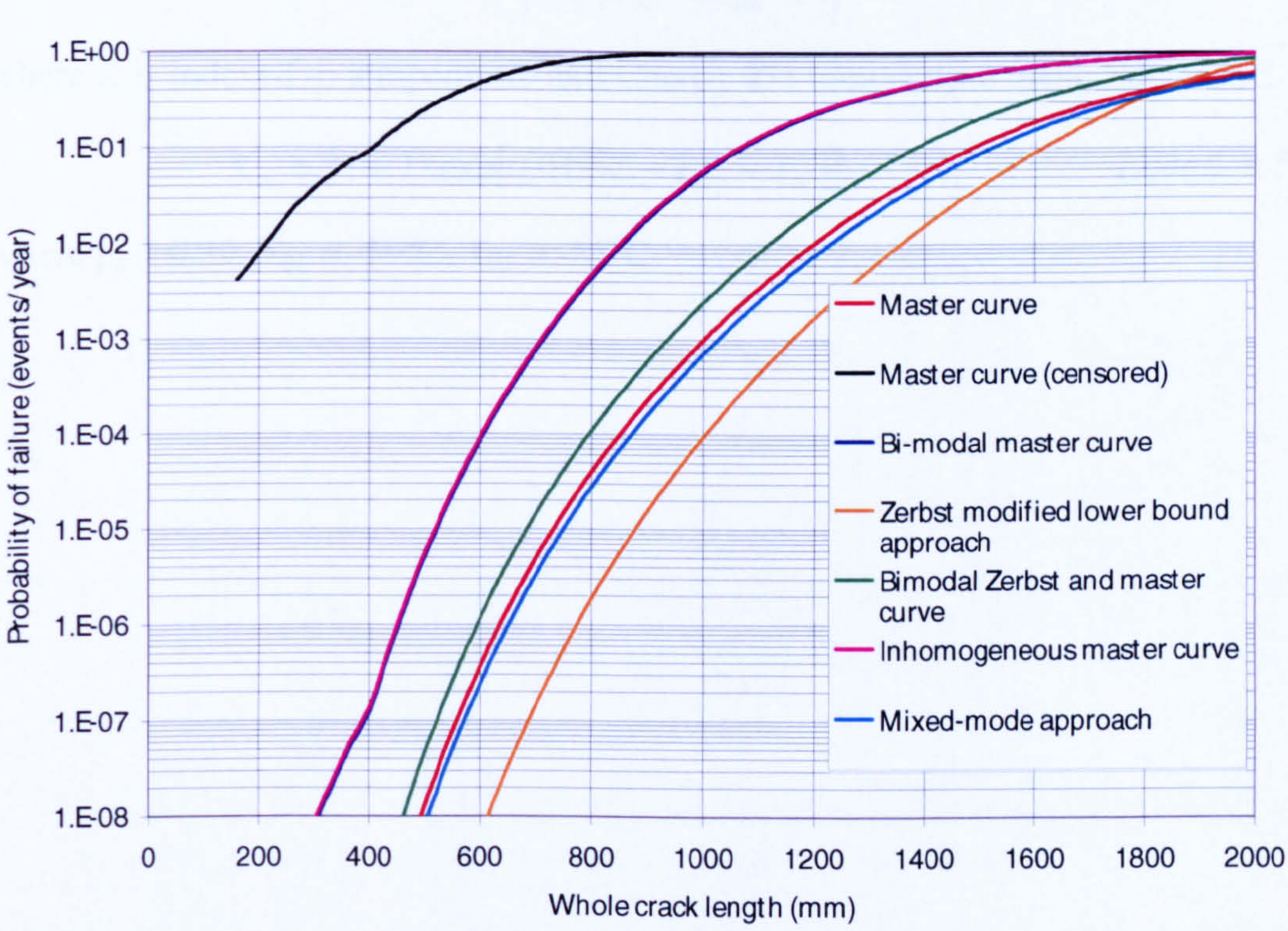

Figure 5-7 Effect of toughness model on probability of failure

As expected, the censored master curve gives the highest estimate of the probability of failure. The engineering lower bound approach gives the lowest estimate, as the lower bound is placed at the lowest measured toughness. The bimodal master curve and the master curve with random inhomogeneities give very similar results, and are slightly more conservative than the master curve, bimodal engineering lower bound and master curve fits, and mixed-mode fits. The mixed-mode approach gives very similar results to the master curve fitted to the entire dataset.

The random inhomogeneities method takes a considerable time to solve, as an extra loop is required to include the normal distribution on T_0. Consequently, it is felt that the bimodal master curve fit provides the most suitable method to describe the scatter in the material fracture toughness.

The equation used to describe the toughness is therefore:

$$P(K_{mat}) = 1 - p_a \exp\left[-\left(\frac{K_{mat} - K_{\min}}{K_{01} - K_{\min}}\right)^4\right] - (1 - p_a)\exp\left[-\left(\frac{K_{mat} - K_{\min}}{K_{02} - K_{\min}}\right)^4\right] \qquad \textit{Equation 5-20}$$

where K is indexed to temperature and Charpy 27J temperature using Equation 5-21:

$$K_{0i} = 31 + 77\exp[0.019(T - T_{27J} - T_{0i})] \qquad \textit{Equation 5-21}$$

where $p_a = 0.39$, $T_{01} = -59^{\circ}C$, $T_{02} = -85^{\circ}C$.

5.5 Defining a region of constant toughness

Cleavage fracture occurs at carbides or non-metallic inclusions that are distributed randomly throughout ship steel. The random location of these sites is shown as the variability of the associated material fracture toughness (ASTM, 2005). As the crack propagates there is then an associated probability of encountering a 'weak-link' which results in a cleavage failure.

The master curve approach describes the variability in toughness at a number of test sites that are taken from the plate. However, as the crack propagates through the steel each individual cycle could be thought of as a new fracture toughness test. If this were true, then the likelihood of sampling a toughness value from the lower shelf would quickly tend to one, resulting in a high probability of brittle fracture, even for short cracks.

To the best of the author's knowledge, no previous study has taken into account the variability of toughness. The studies described in the literature review appear to implicitly assume that the toughness remains constant as the crack propagates across a plate. These studies could then be considered unconservative as the toughness could be varying more quickly than has been modelled.

In this section some recent wide plates tests carried out at QinetiQ Rosyth will be used in an attempt to define empirically the distance over-which the toughness could be considered constant.

The specimen size for the tests was 800 mm wide and 15mm thick ship steel plate. In total, seven tests were carried out. The specimens were cycled at a load to give a tensile stress of between 10 MPa and 100 MPa, at a cycling frequency of 0.83 Hz.

During two of the tests the specimen was cooled to -50°C when the crack reached 300 mm. One of the cold temperature specimens was plain plate, while the second had both transverse and longitudinal welds. The plain specimen fractured at 650 mm, and the welded plate fractured at 528 mm. Crack growth in the welded specimen was uneven, with one tip propagating more quickly. The test set-up is shown in Figure 5-8. The bath of liquid nitrogen used to cool the test specimen to -50°C is shown in Figure 5-9.

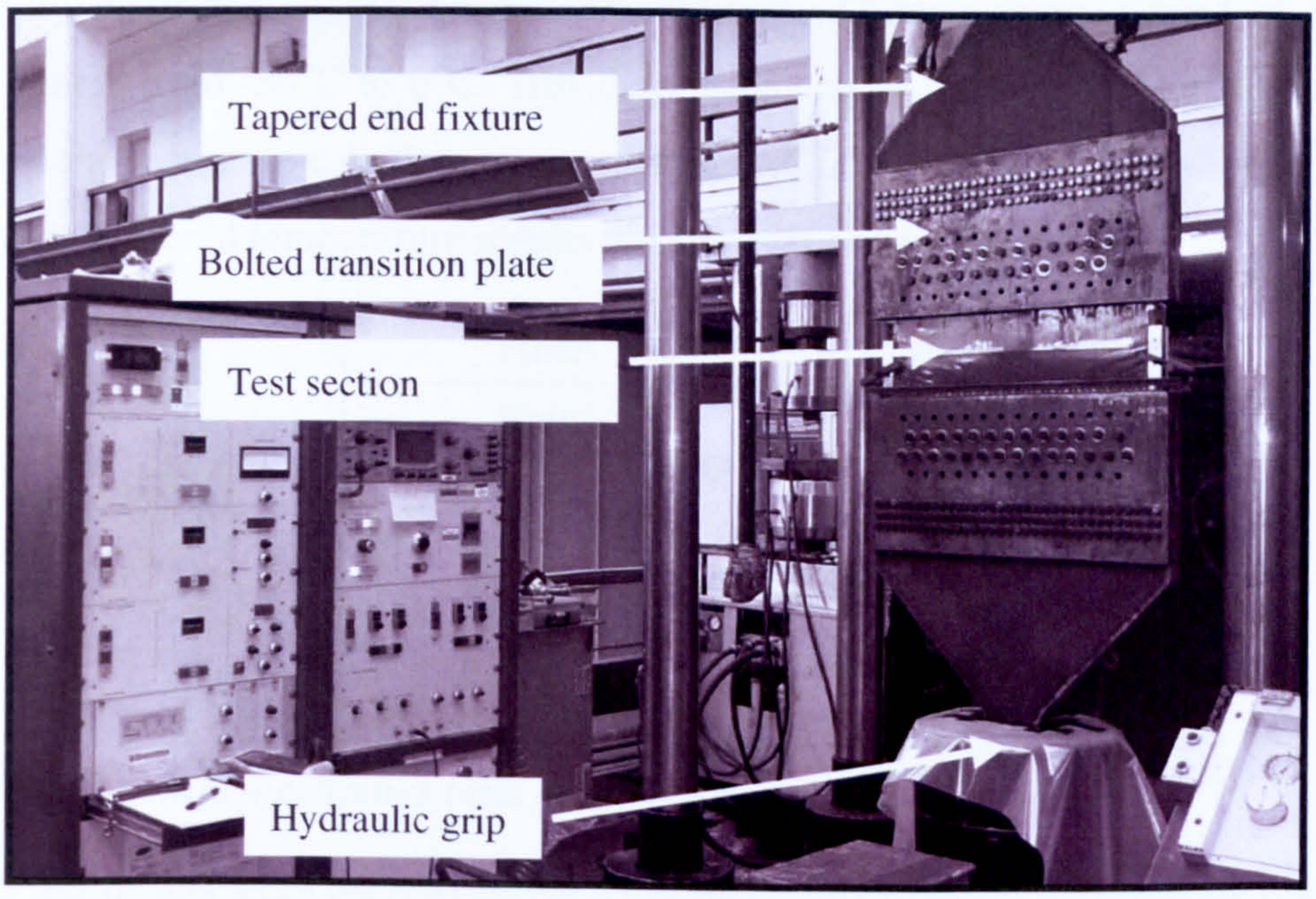

Figure 5-8 Wide plate test set-up

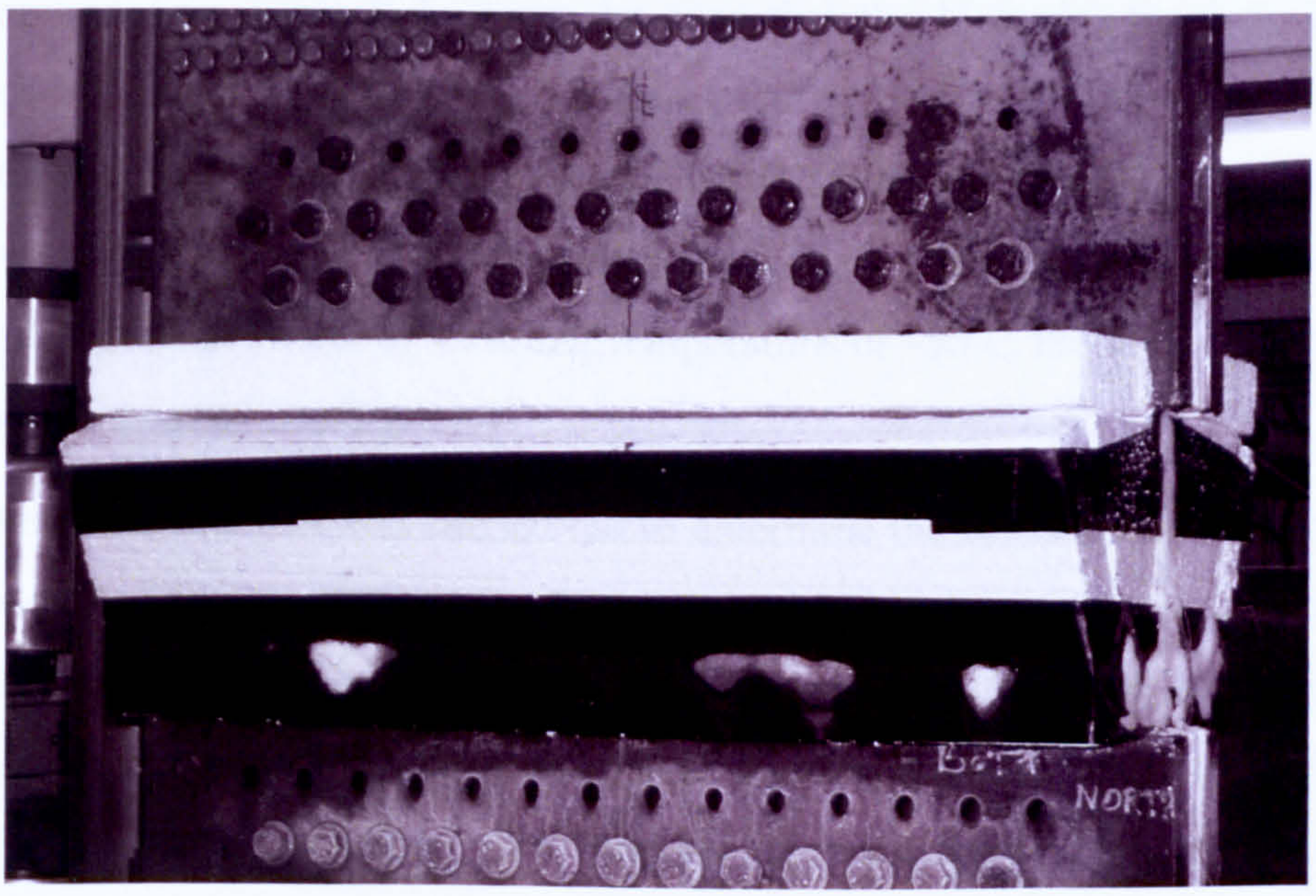

Figure 5-9 Close-up showing cold temperature tests

Following the tests, fracture mechanics samples were taken from the two cold temperature plates for analysis. Both plates were Lloyd's grade A, with a minimum required Charpy 27J transition temperature of +20°C. Charpy testing indicated that the plate had a Charpy 27J temperature of -23°C, just meeting the Lloyd's grade D requirement of -20°C. The plates could therefore be considered as a worst-case grade D plate. Five of the fracture mechanics tests were carried out at -50°C using the

procedure described in section 5.2. In addition, 34 tests were carried at higher temperatures from -30°C to 0°C. This data form part of the larger databank used in the previous section to calculate a general material fracture toughness distribution for ship steel. The cold temperature results are summarised in Table 5-5.

Plate	K_{mat} (MPa√m)
Plain	226
Welded	261
	168
	105
	94

Table 5-5 Fracture mechanics tests results from cold temperature test

The 39 test results were used to derive a toughness distribution for the wide plate test results. The co-efficients of the fits, together with the maximum likelihood indicator, are summarised in Table E-1. It can be seen that the bi-modal fit gives identical estimates of T_{01} and T_{02}, implying that there is no evidence of bi-modality in the test data. Consequently, it was decided to use a single master curve to describe the scatter in the test data. The fitted distribution is plotted against the measured data in Figure E-37 and Figure E-38. At an external temperature of -50°C the 0.1% lower bound lies at a toughness of 66MPa√m.

A finite element analysis was carried out to determine the stress intensity at the crack tip. It was found that the increased section thickness due to the transition plate constrained the crack tip. This lowers the stress intensity when compared to a standard solution for a centre cracked plate. The applied stress intensity calculated using the FE model is plotted as a function of crack length in Figure 5-10. The uneven crack growth in the welded plate results in a higher stress intensity at the more rapidly propagating tip.

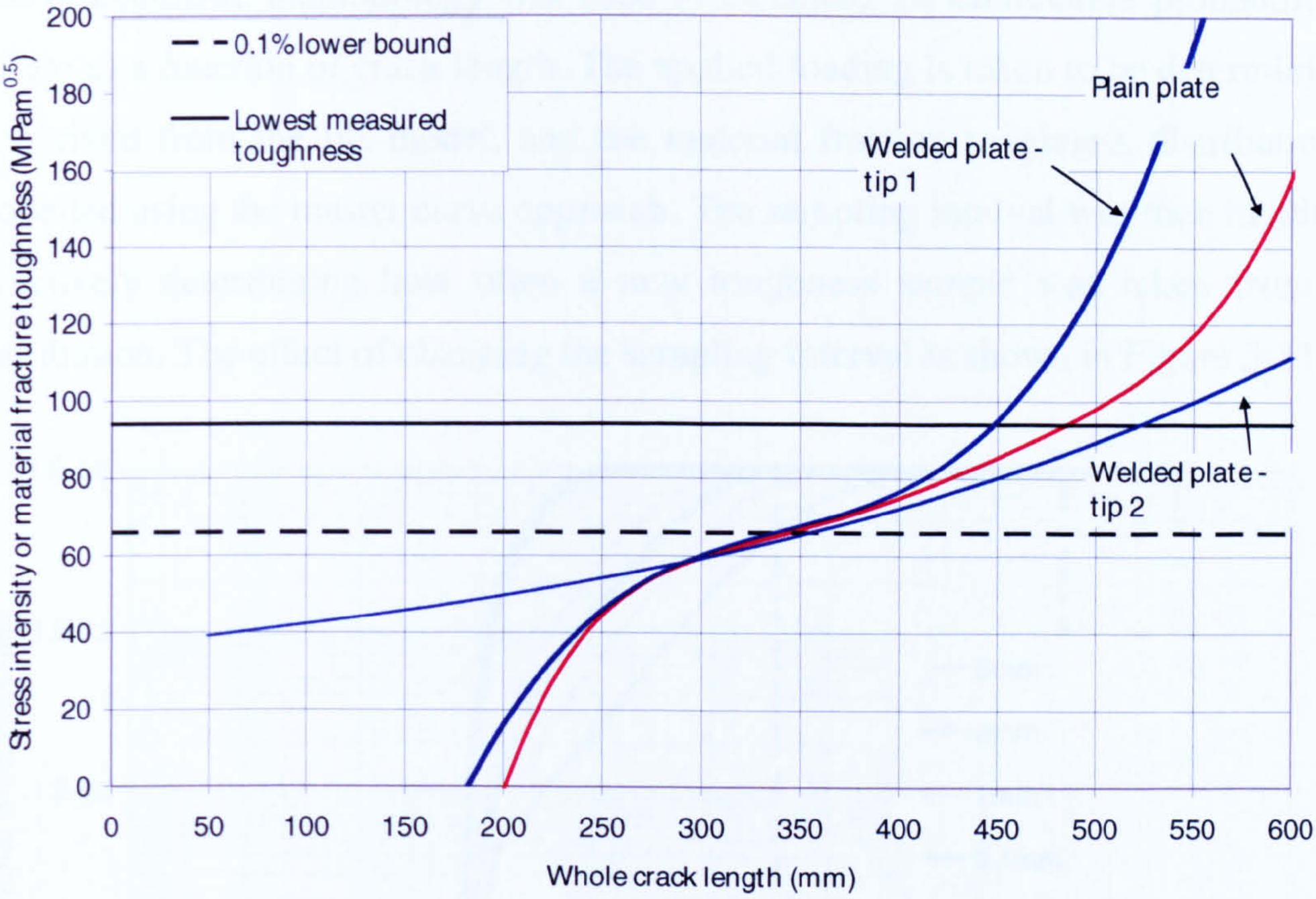

Figure 5-10 Applied stress intensity as a funciton of crack length plotted against material fracture toughness data

It can be seen that the applied stress intensity does not rise above the 0.1% lower bound until the crack length reaches approximately 350 mm. At this crack length the probability of failure is estimated to be 2×10^{-3} (1×10^{-3} for each crack tip). The cracked specimens did not fracture for an additional 178 mm (welded plate) and 300 mm (plain plate).

If it were true that the toughness was varying on every load cycle, then each load cycle would effectively act as a new fracture toughness test. The probability of failure of 2×10^{-3} on each load cycle would then tend to 1 in as little as 10 mm of crack growth. Clearly, this is not the case as the test specimens have propagated considerably beyond this without failure.

It is proposed in this thesis that the toughness does vary over some distance, termed the sampling interval. It is considered that it would be unconservative to ignore the cumulative effects of encountering varying material fracture toughness as a crack propagates across a plate. However, with only two tests it is not possible to calculate a definitive value of the sampling interval.

The probabilistic methodology was used to calculate the cumulative probability of failure as a function of crack length. The applied loading is taken to be deterministic, as derived from the FE model, and the material fracture toughness distribution is modelled using the master curve approach. The sampling interval was then modified, effectively determining how often a new toughness sample was taken from the distribution. The effect of changing the sampling interval is shown in Figure 5-11.

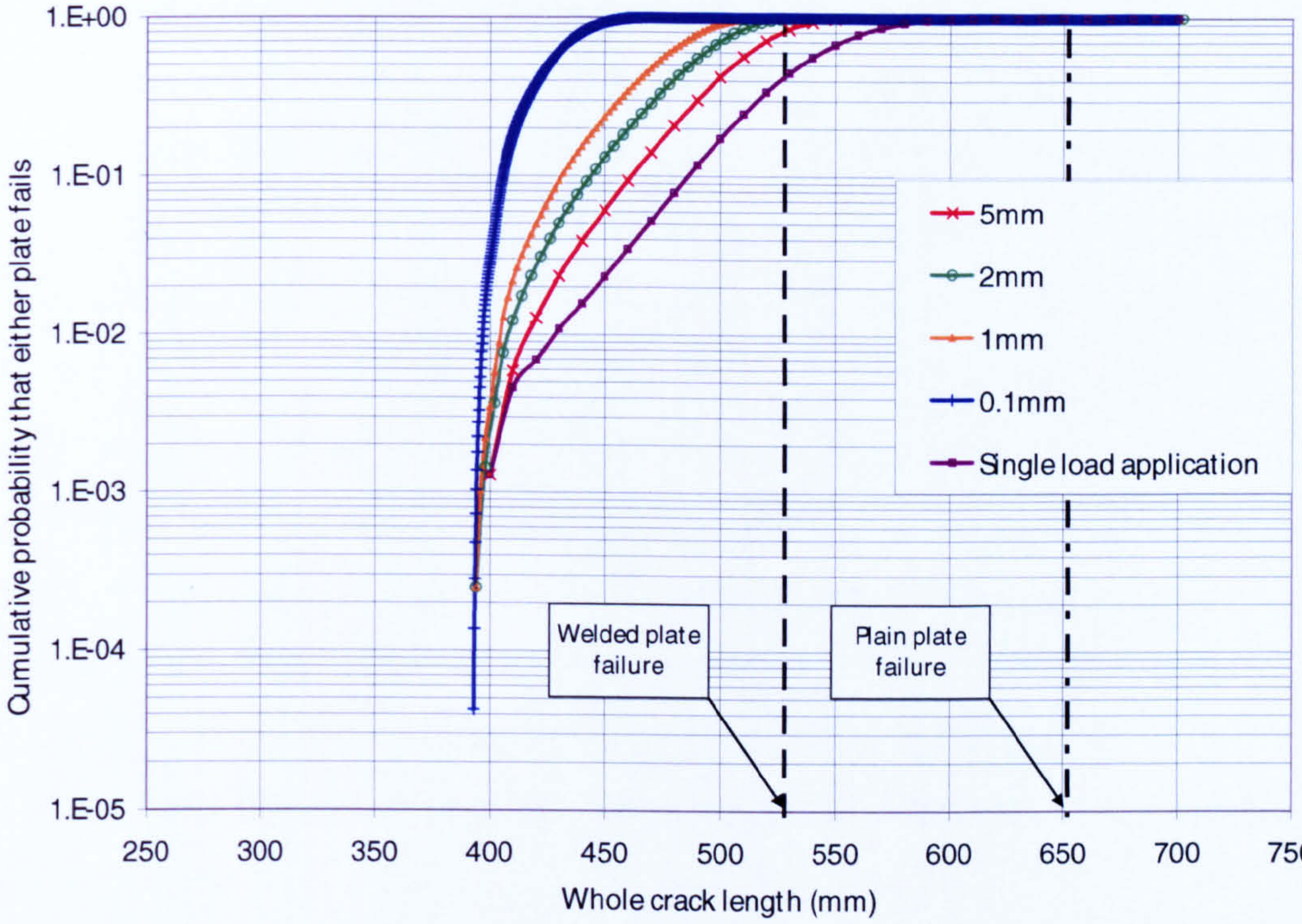

Figure 5-11 Effect of sampling interval on cumulative probability of failure

It can be seen that if the sampling interval is less than 1 mm the cumulative probability of failure quickly tends to 1. As the sampling interval is increased the slope is reduced. A sampling interval of 5mm gives a cumulative probability of 40% of either plate failing at 528mm and a 100% probability of failure at 650mm. By comparison, the results obtained using a single load application predict a probability of failure of 10% at 528 mm and 99.9% at 650mm.

It is not possible to make a definitive statement of the sampling interval with only two tests. It is likely that this distance could also be a random interval with 'good' plates containing regions of more homogeneous material. However, without a considerable number of repeat tests it would not be possible to quantify this variation. It is felt that the sampling interval of 5mm proposed here provides a

conservative estimate of the distance over-which the toughness could be considered to be constant.

The results of this chapter have been published in two summary papers: one covering the fitting of a toughness distribution (Sumpter, 2006a); and a second on the sampling interval (Sumpter, 2006b).

6 Structural reliability methods

6.1 Background

In recent years structural reliability methods have become increasingly prevalent in engineering analysis. Many of the partial safety factors applied in engineering standards have been derived using probabilistic methods.

The methods were introduced in the 1970s with the development of so-called 'first-order' methods through the work of Cornell (Cornell, 1969) and continued by Hasofer and Lind (Hasofer, 1974). During the 1990s these methods have moved from a research topic into more general usage. Commercial programs are now available, such as STRUREL and PROBAN, which allow complex problems to be quickly and easily evaluated.

Structural reliability methods are normally classified under three levels. Level III is the highest level of analysis and is often referred to as the fully probabilistic approach. It requires a high degree of information on the input variables and fully takes account of the nature of the failure domain. Level II is a 'semi-probabilistic' approach, which makes various approximations when calculating the probability of fracture. Level I involves the use of partial factors of safety, often calculated using a higher level analysis.

In this chapter four methods will be evaluated for a sample problem:

- Convolution integral;
- First-order reliability method;
- Monte Carlo simulation;
- Monte Carlo simulation with importance sampling.

The methods are classified as Level III methods with the exception of the first-order reliability method, which is a Level II method.

6.2 Example calculation

The example calculation used to evaluate the methods is based on a single time step for a half crack length of 255 mm. This should ensure a relatively high probability of failure, which will allow the Monte Carlo simulation to converge in a reasonable number of samples. The input parameters for the problem are summarised in Table 6-1.

Variable	Value
Half crack length at end of time period, a	255 mm
K_{res}	0.27 $MPam^{0.5}$
K_{SWBM}	31.3 $MPam^{0.5}$
Y	1.00
Wave induced loading	
Weibull scale, A	7.44
Weibull shape, B	1.23
Number of cycles, N	82349
Material toughness	
p_a	0.39
K_{01}	376.4 $MPam^{0.5}$
K_{02}	597.1 $MPam^{0.5}$

Table 6-1 Input parameters for sample problem

The extreme type-1 distribution, used to describe the distribution of maximum applied stress values during the time interval, is derived from the Weibull distribution parameters and the number of cycles using the equations given in Appendix C.5. For this example the still water bending moment is assumed to be deterministic. This simplifies the problem to two dimensions which allows the results to be plotted and discussed more easily.

The material fracture toughness variable is termed the strength variable, x_1, and the wave induced bending stress termed the load variable, x_2. The probability of a strength value occurring with a load value is given by the joint probability density function. For two independent variables this can be written as:

$$f_{x_1x_2}(x_1, x_2) = f_{x_1}(x_1) f_{x_2}(x_2) \qquad \textit{Equation 6-1}$$

where $f_{x_1x_2}(\ )$ is the joint probability density function and $f_{x_1}(\ )$ and $f_{x_2}(\ )$ are the probability density functions for the strength and load variables respectively. Two events can be said to be statistically independent if a change in the probability of one variable occurring does not change the probability of the second variable. It is assumed that the material fracture toughness is independent of the applied loading. This statement is reasonable for wave induced loading, which is applied over a relatively narrow frequency. However, slam and whipping induced loading occur at higher frequency which would increase the strain rate and reduce material fracture toughness. This effect is discussed in more detail in Section 8.2.1, but in this thesis the two variables are considered to be independent.

The joint probability distribution for the example problem, calculated using Equation 6-1, is shown in Figure 6-1.

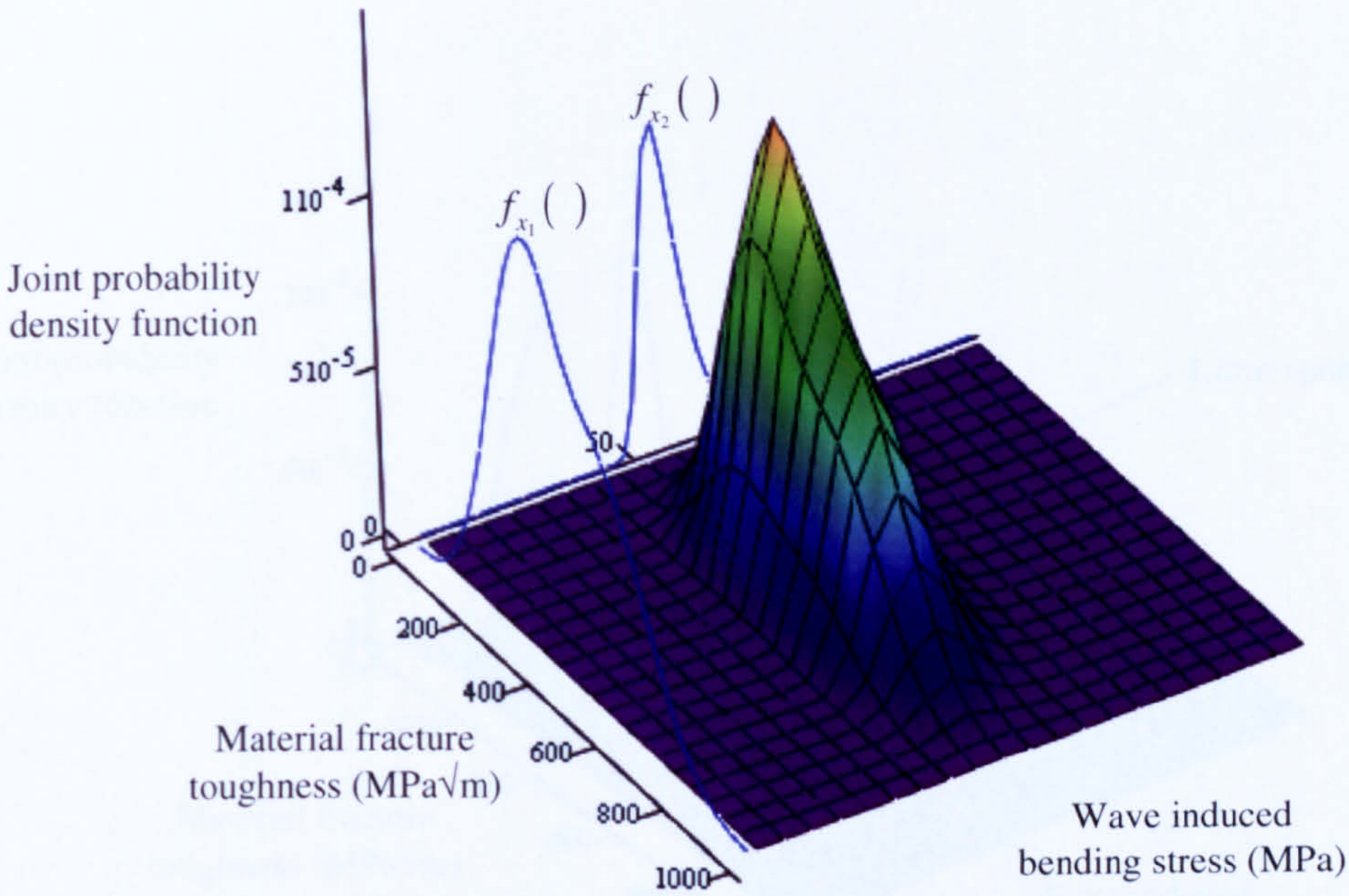

Figure 6-1 Joint probability density function of wave induced bending stress and material fracture toughness

6.3 Limit state function

The limit state function defining the boundary between the safe region and the failure region was defined in Section 3.4. This can be re-defined in terms of the variables x_1 and x_2 as:

$$G(\mathbf{X}) = X_1 - YX_2\sqrt{\pi a} - K_{res} - K_{SWBM} \qquad \textit{Equation 6-2}$$

where **X** is a random vector of material fracture toughness and wave induced bending stress and:

1. G(**X**) < 0 represents a failure condition;
2. G(**X**) = 0 represents the boundary between safe and failure conditions;
3. G(**X**) > 0 represents a safe condition.

The limit state function given by Equation 6-2 is plotted against the joint probability distribution in Figure 6-2.

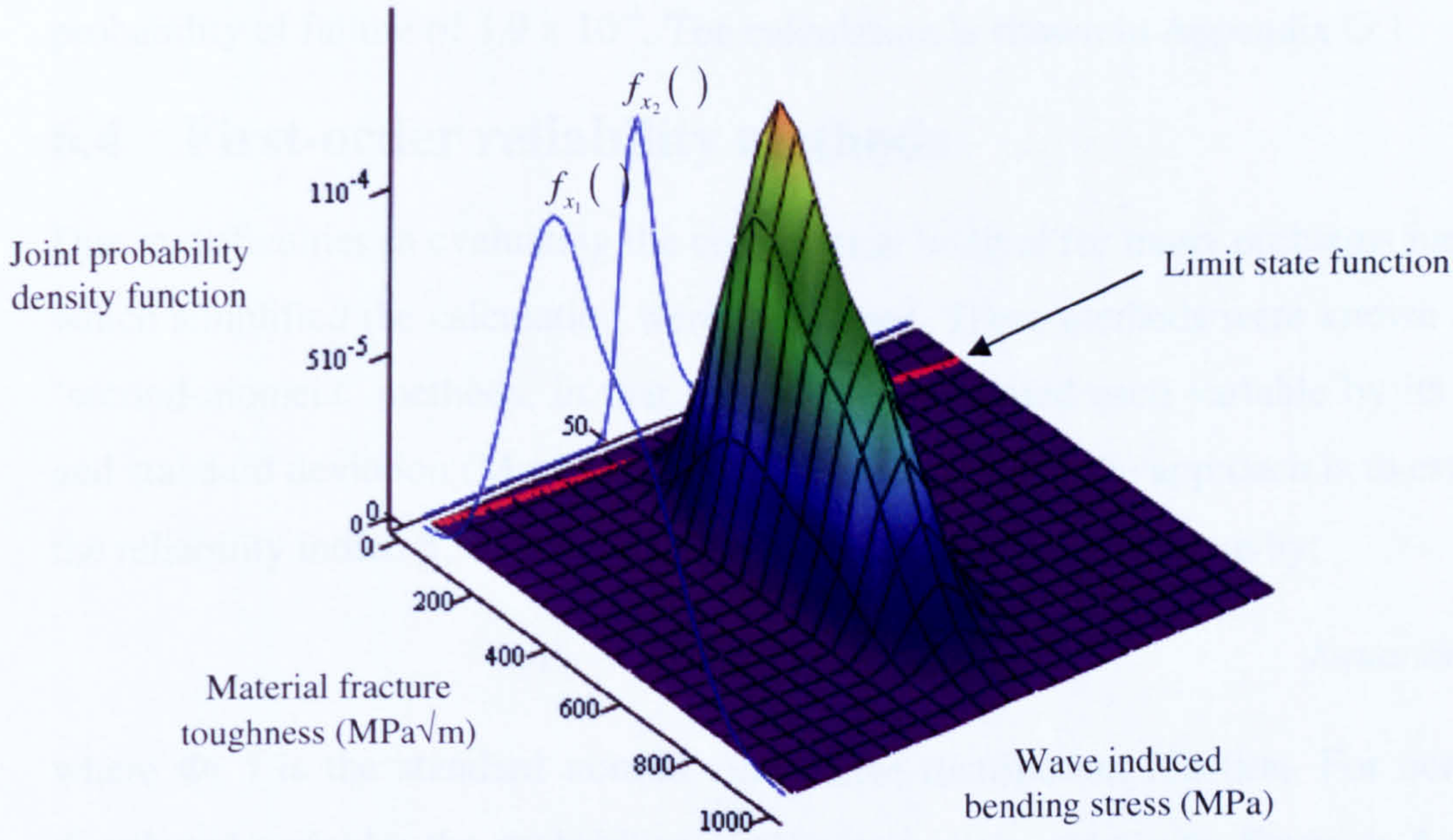

Figure 6-2 Joint probability density function showing limit state function

The probability of failure is given as the area of the joint probability distribution in the failure region. This can be written as:

$$p_f = P\left[X_1 - YX_2\sqrt{\pi a} - K_{res} - K_{SWBM} \leq 0\right] \qquad \textit{Equation 6-3}$$

or:

$$p_f = \int_{-\infty}^{\infty} \int_{-\infty}^{Yx_2\sqrt{\pi a}+K_{res}+K_{SWBM} \geq x_1} f_{x_1}(x_1) f_{x_2}(x_2) dx_1 dx_2 \qquad \textit{Equation 6-4}$$

For independent variables the order of integration can be reduced by one to give:

$$p_f = \int_{-\infty}^{\infty} F_{x_1}(x) f_{x_2}(x) dx \qquad \textit{Equation 6-5}$$

where $F_{x_1}(\,)$ is the cumulative distribution function of the material fracture toughness. Equation 6-5 is known as the convolution integral. The convolution integral calculates the exact probability of failure but for many examples can be difficult to evaluate. However, for the simple limit state function given in Equation 6-2 the convolution integral can be evaluated.

For the example distributions shown in Figure 6-2 the convolution integral gives a probability of failure of 3.9×10^{-4}. The calculation is shown in Appendix G.1.

6.4 First-order reliability methods

Due to difficulties in evaluating the convolution integral for many problems methods which simplified the calculation were developed. These methods were known as the 'second-moment' methods, in that they only represented each variable by its mean and standard deviation (Mansour, 1990). The objective of the approach is to estimate the reliability index, β, where β is linked to the probability of failure by:

$$p_f = \Phi(-\beta) \qquad \textit{Equation 6-6}$$

where $\Phi(\,)$ is the standard normal cumulative distribution function. For normally distributed variables the probability of failure is given exactly by Equation 6-6. For non-normally distributed variables Equation 6-6 gives a nominal estimate of the probability of failure.

For non-linear limit states the first two moments of G(X) are not easily obtainable. To find these values the limit state function is linearised about some point **x***. This is shown in Figure 6-3 for the limit state function given by Equation 6-2.

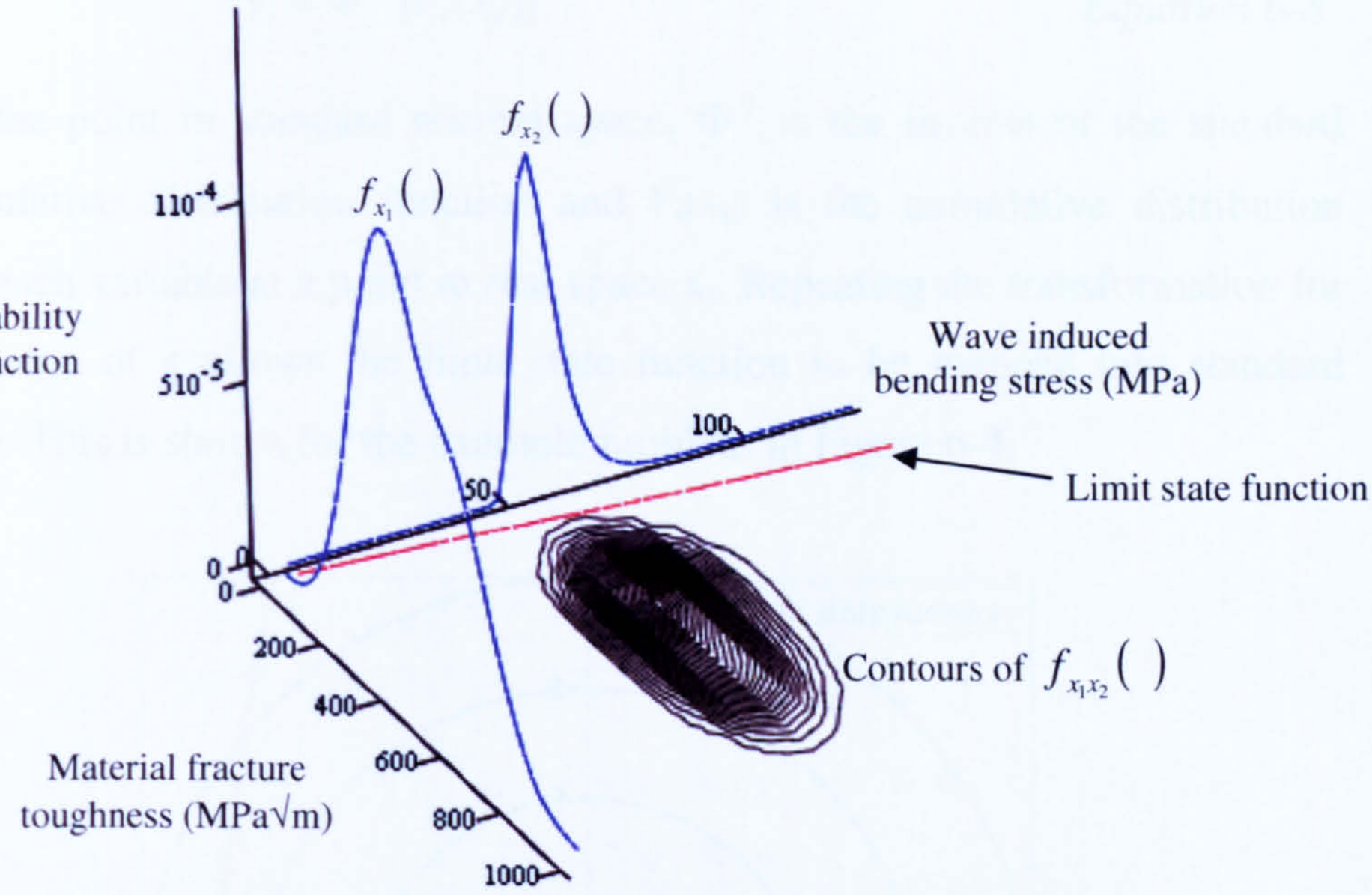

Figure 6-3 Joint probability density function showing limit state function

Note that as the limit state function given by Equation 6-2 is linear the choice of **x*** makes no difference to the linearization of the limit state function.

The linearization of the limit state function gave rise to name of 'First-Order Second Moment' method, or FOSM. A major drawback to the method was that it failed to account for the shape of the joint probability distribution in the failure region. While giving the exact probability of failure for normally distributed variables the method can give erroneous results for non-normally distributed variables, often by several orders of magnitude.

To overcome these problems a methodology was developed to transform the variables into so-called 'normal space'. For normal variables this transformation can be written as (Hasofer and Lind, 1974):

$$Y_i = \frac{X_i - \mu_i}{\sigma_i} \qquad \textit{Equation 6-7}$$

where Y has a mean of 0 and standard deviation of 1 (standard normal distribution), and the subscript i refers to the variable. For non-normally distributed variables the Rosenblatt transformation can be used (Melchers, 1999):

$$y_i = \Phi^{-1}[F_i(x_i)] \qquad \textit{Equation 6-8}$$

where y_i is the point in standard normal space, Φ^{-1} is the inverse of the standard normal cumulative distribution function and $F_i(x_i)$ is the cumulative distribution function for each variable at a point in real space x_i. Repeating the transformation for a range of value of x allows the limit state function to be mapped into standard normal space. This is shown for the example problem in Figure 6-4.

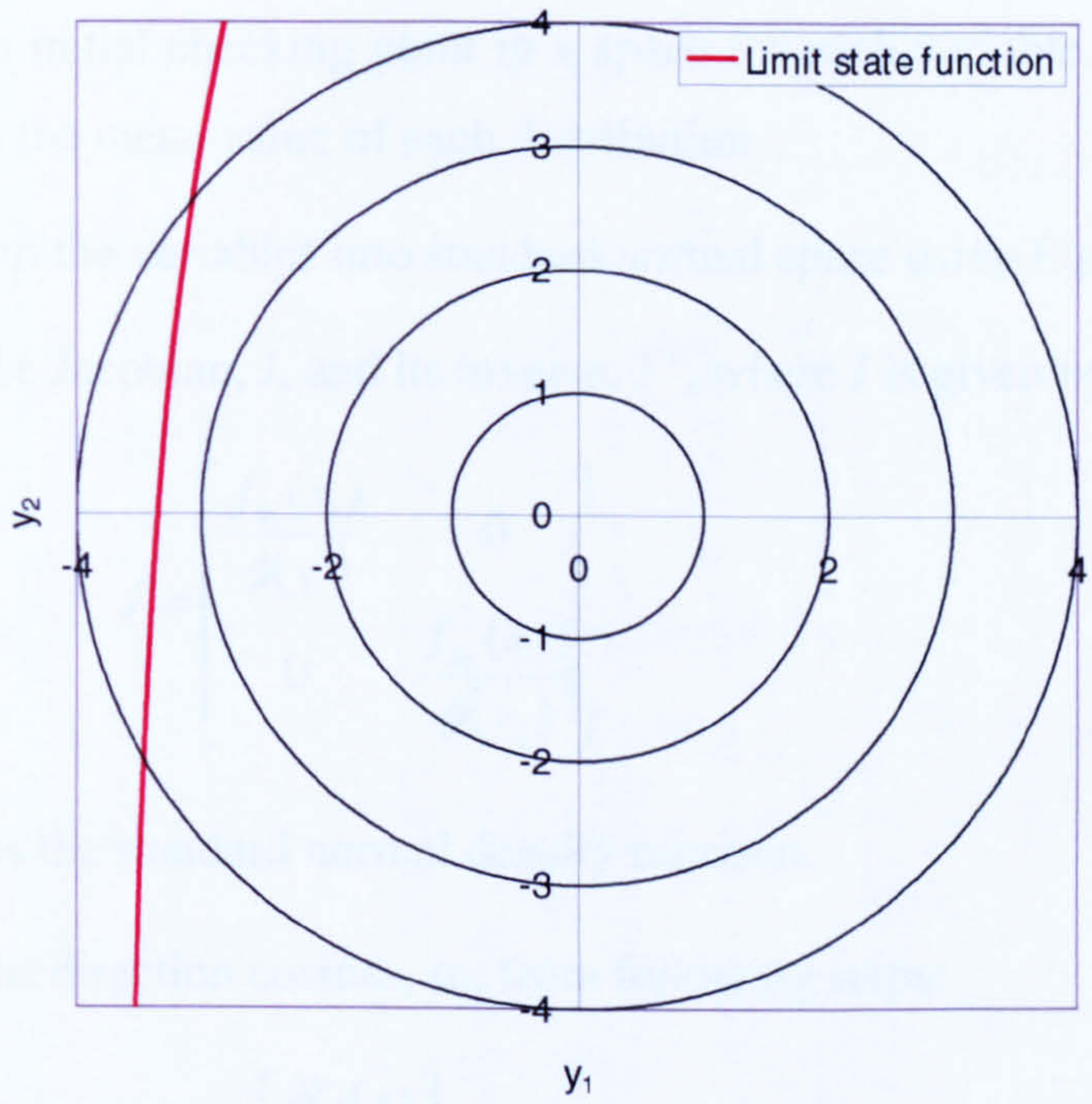

Figure 6-4 Limit state function mapped into standard normal space

Note that the non-normal distribution assumed for each variable means that the limit state function is no longer linear in standard normal space. The contours shown in Figure 6-4 represent equal values of the standard normal cumulative distribution function, and thus equal probabilities of failure. The closest point between the limit state function and the origin represents the highest probability of failure, or the point of maximum likelihood of the failure region. This point is commonly referred to as the checking or design point, $\mathbf{y}^*$ (which can be mapped into real space using Equation 6-8 to give $\mathbf{x}^*$).

In order to calculate the shortest distance between the limit state function in normal space and the origin the first order reliability (FOR) algorithm can be used (Melchers, 1999) . The algorithm satisfies the condition:

$$\beta = \min\left(\sum_{i=1}^{n} y_i^2\right)^{1/2} \quad \text{subject to } g(\mathbf{y}) = 0 \qquad \textit{Equation 6-9}$$

This is accomplished using an iterative algorithm, which refines the estimate of the checking point, **y***, until the condition of perpendicularity between the linearisation of the limit state function and the β direction is satisfied. The following steps are used in the algorithm (Melchers, 1999):

1. Select an initial checking point in x space for each variable. A suitable start point is the mean value of each distribution.

2. Transform the variables into standard normal space using Equation 6-9.

3. Derive the Jacobian, J, and its inverse, J^{-1}, where J is given by:

$$J = \begin{bmatrix} \dfrac{f_{x_1}(x_1)}{\phi(y_1)} & 0 \\ 0 & \dfrac{f_{x_2}(x_2)}{\phi(y_2)} \end{bmatrix} \qquad \textit{Equation 6-10}$$

and $\phi(\,)$ is the standard normal density function.

4. Obtain the direction cosines, α_i, from following steps:

$$\begin{bmatrix} c_1 \\ c_2 \end{bmatrix} = J^{-1} \begin{bmatrix} \dfrac{\delta G(x)}{x_1} \\ \dfrac{\delta G(x)}{x_2} \end{bmatrix} = J^{-1} \begin{bmatrix} 1 \\ -1 \end{bmatrix} \qquad \textit{Equation 6-11}$$

$$l = \left(\sum_i c_i^2\right)^{0.5} \qquad \textit{Equation 6-12}$$

$$\alpha_i = \frac{c_i}{l} \qquad \textit{Equation 6-13}$$

5. Obtain an estimate of β from:

$$\beta = \left(y_1^2 + y_2^2\right)^{0.5} \qquad \textit{Equation 6-14}$$

6. Obtain a new estimate of checking points from:

$$\begin{bmatrix} y_1 \\ y_2 \end{bmatrix} = -\begin{bmatrix} \alpha_1 \\ \alpha_2 \end{bmatrix}\left(\beta + \frac{g(y)}{l}\right) = -\begin{bmatrix} \alpha_1 \\ \alpha_2 \end{bmatrix}\left(\beta + \frac{\frac{g(x)}{|J|}}{l}\right) \qquad \textit{Equation 6-15}$$

7. Transform new checking points back into real space and repeat steps until x_i, y_i, and β converge.

The first iteration for the example calculation is shown in Appendix G.1. It can be seen that the new checking points in normal space have co-ordinates of $y_1 = 1779$ and $y_2 = 44.6$. These are clearly unrealistic and cannot be mapped back into real space as they correspond to extremely low probabilities. The large jump in the co-ordinates of the checking point is caused by the high value of the limit state function in real space at the mean values.

The probability of failure should be invariant to mechanical changes in the limit state function (Mansour, 1990). To 'damp' the effect of the limit state function in estimating the new checking point the limit state function is modified to:

$$G(\mathbf{X}) = \frac{X_1 - YX_2\sqrt{\pi a} - K_{res} - K_{SWBM}}{1000} \qquad \textit{Equation 6-16}$$

The 'damping' term slows the convergence algorithm, requiring 53 iterations to find the design point satisfying Equation 6-9. The co-ordinates of the design point are $y_1 = -3.33$ and $y_2 = 0.29$. This corresponds to a reliability index of 3.34 and an estimated probability of failure of 4.2×10^{-4}. The iteration steps are plotted in Figure 6-5.

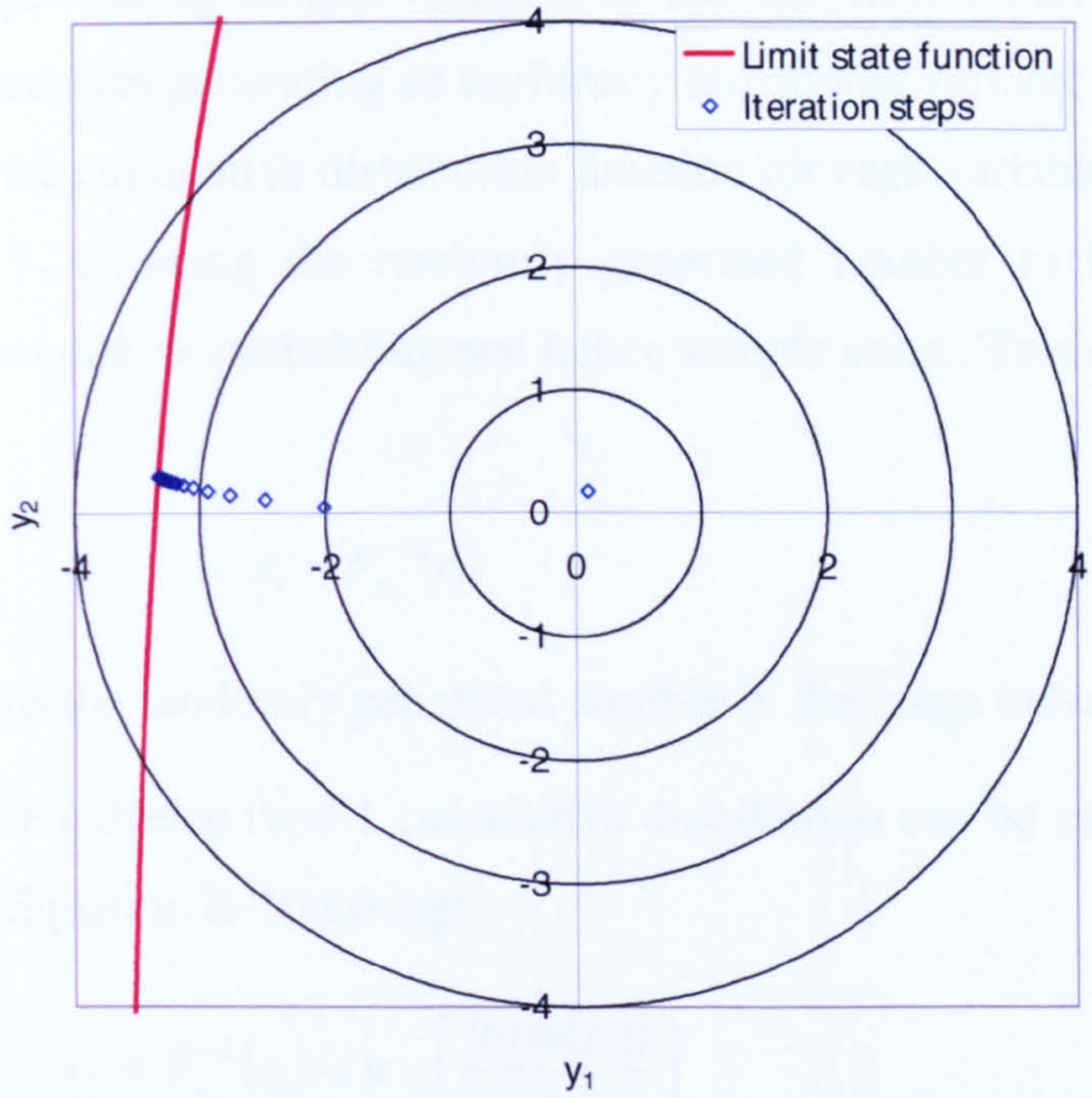

Figure 6-5 Limit state function showing design point in standard normal space

At the design point the direction cosines are $\alpha_1 = 0.996$ and $\alpha_2 = -0.088$. This result indicates that the probability of failure is very sensitive to changes in the material fracture toughness and much less affected by changes in the wave induced bending. This can also be seen in Figure 6-5, where a change in the y_1 co-ordinate will shift the checking point either side of the limit state function, while a change in y_2 co-ordinate has only a slight effect due to the near vertical limit state function.

6.5 Monte Carlo simulation

The Monte Carlo simulation involves sampling values of the basic variables to simulate possible results. By repeating the sampling procedure many times all possible outcomes can theoretically be simulated and the probability of failure can be estimated by dividing the number of failures by the sample size. This can be expressed as (Melchers, 1999):

$$p_f = \int \ldots \int I[G(\mathbf{x}) \leq 0] f_{\mathbf{x}}(\mathbf{x}) d\mathbf{x} = \frac{1}{N} \sum_{j=1}^{N} I[G(\mathbf{X}_j) \leq 0] \qquad \textit{Equation 6-17}$$

where I[ ] represents an indicator function which equals 1 if true and 0 if false and $\mathbf{X}_j$ represents the j-th vector of sampled values.

One method of generating sample values is to use the inverse-transform technique. This technique involves generating an uniformly distributed variable in the range 0 to 1. By definition the cumulative distribution function for each variable must also lie in the range 0 to 1, allowing the randomly generated number to be equated to a corresponding cumulative probability and hence sample value. This can be expressed as:

$$x_i = F_{x_i}^{-1}(r_i) \qquad \textit{Equation 6-18}$$

where r_i represents the randomly generated number in the range between 0 and 1.

The inverse of the extreme type-1 cumulative distribution can be calculated through manipulation of Equation B-10 giving:

$$x_2 = F_{x_2}^{-1}(r_i) = u - \left(\frac{\ln(\ln(r_i))}{\alpha}\right) \qquad \textit{Equation 6-19}$$

where u and α are the mode and location parameters as defined in Appendix C.5.

The bi-modal Weibull distribution used to model the scatter in material fracture toughness cannot be inverted in a closed form. Consequently, the cumulative probability is moved to the right-hand side of Equation 5-20 giving:

$$0 = -r_i + 1 - p_a \exp\left[-\left(\frac{K_{mat} - K_{\min}}{K_{01} - K_{\min}}\right)^4\right] - (1 - p_a)\exp\left[-\left(\frac{K_{mat} - K_{\min}}{K_{02} - K_{\min}}\right)^4\right] \qquad \textit{Equation 6-20}$$

The Newton-Rapson method is then used to find the root of Equation 6-20 using the iterative scheme:

$$x_{n+1} = x_n - \frac{P(r_i)}{p(r_i)} \qquad \textit{Equation 6-21}$$

where n is the number of iterations, $P(r_i)$ is the cumulative distribution function of the material toughness distribution evaluated at r_i, and $p(r_i)$ is the probability density function of the material toughness distribution evaluated at r_i. It is found that Equation 6-21 typically converges to 2 decimal places within four to five iterations.

The accuracy of the Monte Carlo simulation is heavily dependent on the number of sample values or simulations used. As the number of simulations increases the probability of failure will converge to the exact value. The required number of simulations can be estimated by carrying out a convergence study, increasing the number of simulations and viewing the effect on the probability of failure. The convergence of the probability of failure of the example problem is shown in Figure 6-6.

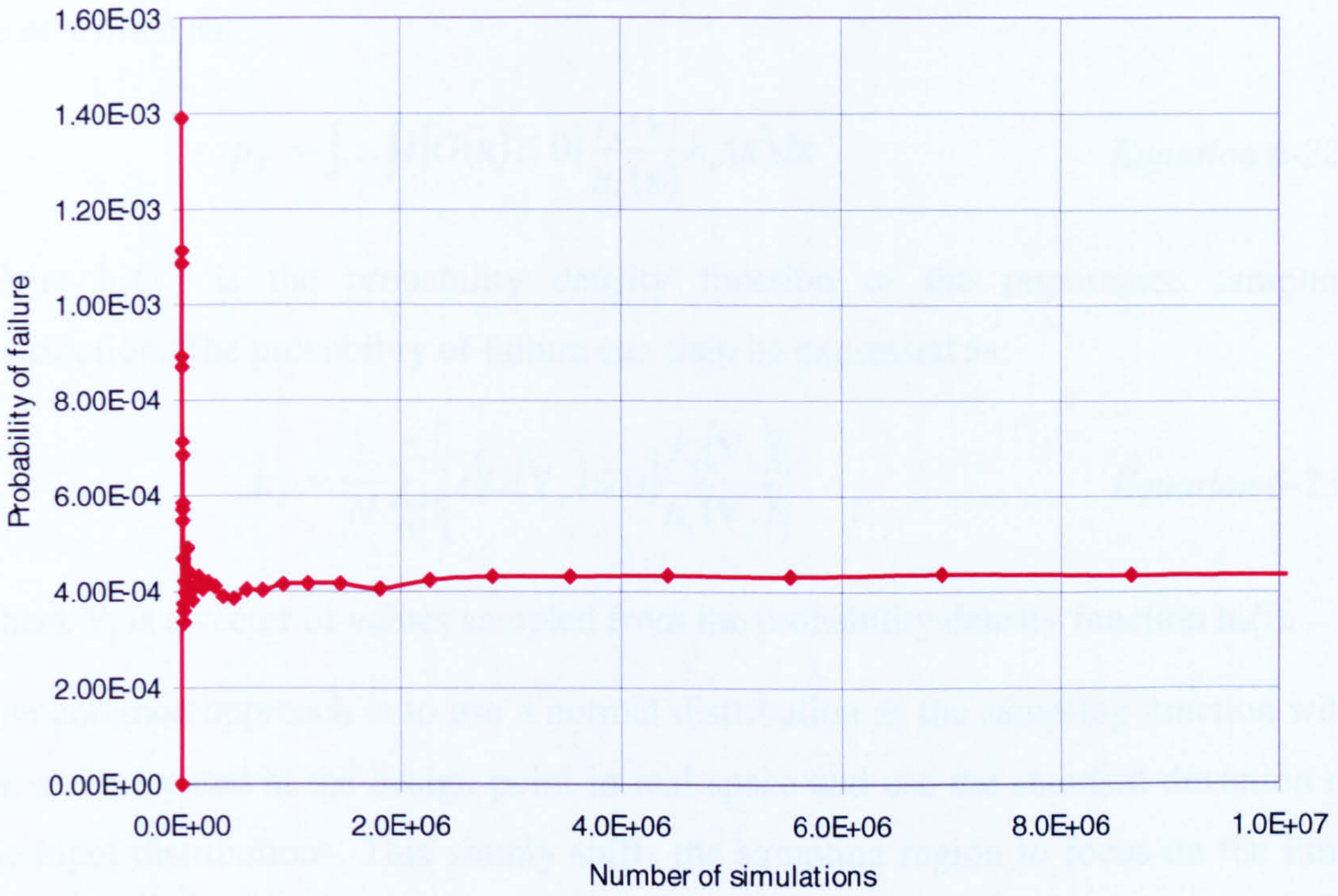

Figure 6-6 Convergence of Monte Carlo simulation

It can be seen that the probability of failure converges to a value of 4.3×10^{-4} after approximately 200,000 simulations.

6.6 Monte Carlo simulation with importance sampling

The Monte Carlo simulation is a computationally in-efficient technique as many of the samples generated do not result in a failure. The efficiency of the simulation could be improved if the sampling was focused around the area that contributes to the probability of failure, termed 'importance sampling'.

The importance sampling method assumes some prior information about the failure domain, the region in which the indicator function is less than 0. Equation 6-17 can be re-written as:

$$p_f = \int \dots \int I[G(\mathbf{x}) \le 0] \frac{f_{\mathbf{x}}(\mathbf{x})}{h_{\mathbf{v}}(\mathbf{x})} h_{\mathbf{v}}(\mathbf{x}) d\mathbf{x} \qquad \textit{Equation 6-22}$$

where $h_v(\ )$ is the probability density function of the importance sampling distribution. The probability of failure can then be expressed as:

$$p_f = \frac{1}{N} \sum_{j=1}^{N} \left\{ I[G(\mathbf{V}_j) \le 0] \frac{f_{\mathbf{x}}(\mathbf{V}_j)}{h_{\mathbf{v}}(\mathbf{V}_j)} \right\} \qquad \textit{Equation 6-23}$$

where $\mathbf{V_j}$ is a vector of values sampled from the probability density function $h_v(\ )$.

One common approach is to use a normal distribution as the sampling function with the mean located at the design point in real space and use the standard deviation of the input distributions. This simply shifts the sampling region to focus on the limit state function which, in this example, causes approximately 50% of sampled values to result in a failure. The design point can be calculated using a first-order reliability method, as described in Section 6.4.

As with the Monte Carlo simulation a convergence study was used to estimate the required number of samples and the probability of failure. The convergence of the probability of failure is plotted in Figure 6-7.

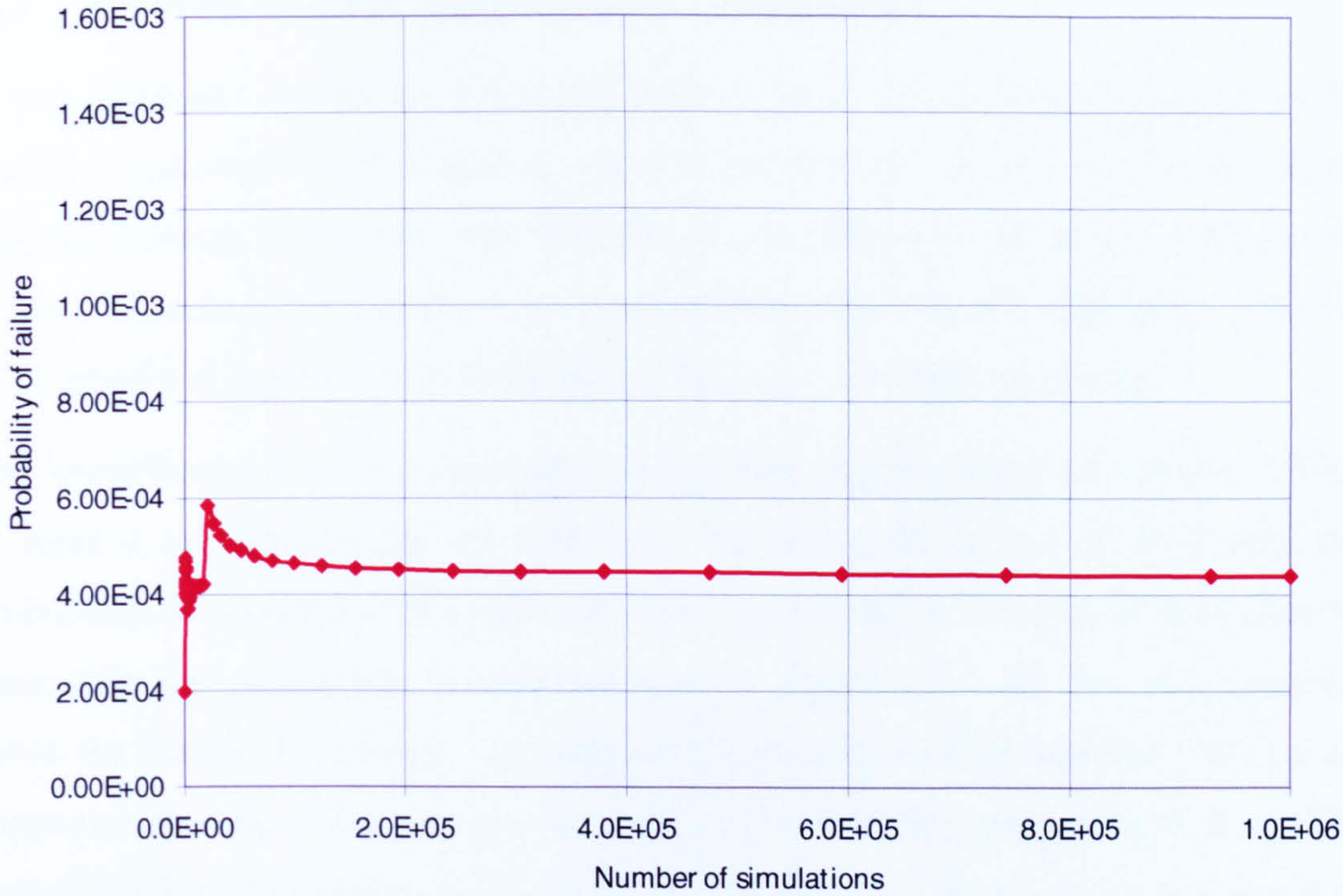

Figure 6-7 Convergence of Monte Carlo simulation with importance sampling

It can be seen that the probability of failure converges to a value of 4.4×10^{-4} after approximately 20,000 samples. The solution converges with 10 % of the samples required for the Monte Carlo simulation, reducing computational effort and processing time. This could be further reduced by improving the sampling routine to give more samples in the failure domain. However, the existing routine is considered sufficient to demonstrate the method.

6.7 Lower bound on fracture toughness

It was discussed in Chapter 5 that the master curve approach used to describe the scatter in material fracture toughness gave finite probabilities of very low toughness values occurring. These were felt to be unrealistic and would not occur in ship steels. A lower bound cut-off was fixed at a cumulative probability of 0.1 %, below which it is assumed that there is a 0 % probability of a toughness value occurring.

The lower bound cut-off is equivalent to a testing process where all samples failing to meet a set requirement are removed, which has the effect of increasing the probability of occurrence of values above the cut-off level. This can be modelled by increasing the probability density function in proportion with the area removed below the cut-off. The master curve approach uses a Weibull distribution with a scale parameter $A = K_0 - K_{min}$, shape factor $B = 4$, and a shift parameter of K_{min}. The probability density function of the bi-modal master curve including the lower bound then becomes:

$$p(K_{mat}) = \begin{cases} 0 & \text{if} \quad K_{mat} < K_{lb} \\ \left(\frac{1}{1-0.001} p_a \left(\frac{4}{K_{01} - K_{min}} \right) \left(\frac{K_{mat} - K_{min}}{K_{01} - K_{min}} \right)^3 \exp\left[-\left(\frac{K_{mat} - K_{min}}{K_{01} - K_{min}} \right)^4 \right] \right. & \\ \left. + \frac{1}{1-0.001} (1 - p_a) \left(\frac{4}{K_{02} - K_{min}} \right) \left(\frac{K_{mat} - K_{min}}{K_{02} - K_{min}} \right)^3 \exp\left[-\left(\frac{K_{mat} - K_{min}}{K_{02} - K_{min}} \right)^4 \right] \right) & \text{otherwise} \end{cases}$$

Equation 6-24

The effect of this on the probability density function is shown in Figure 6-8. Note that the re-distribution has been enhanced to show the increase in probability density above the cut-off level. The actual effect is minimal as only 0.001 is being added across the entire distribution.

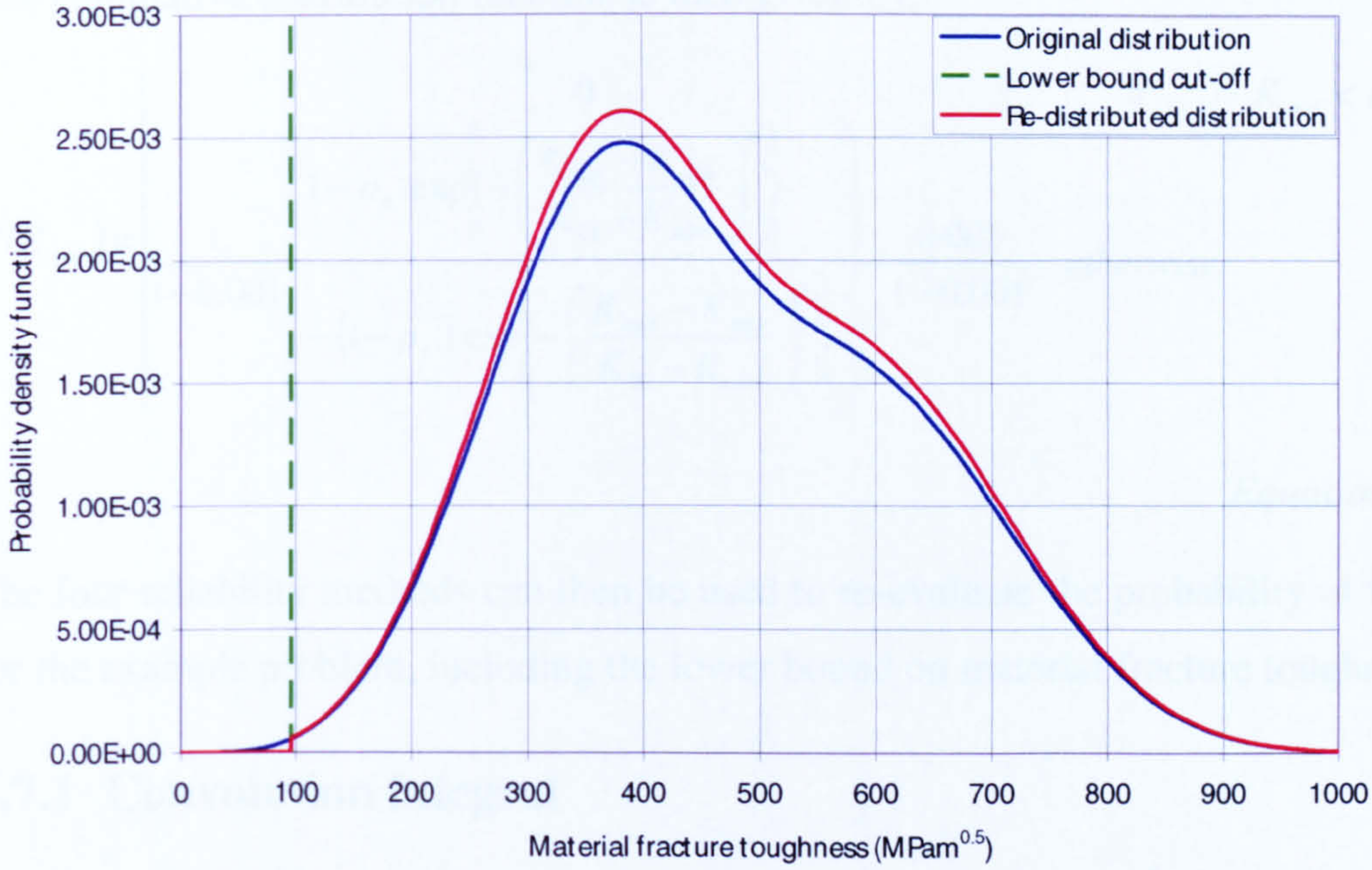

Figure 6-8 Probability density function of material fracture toughness modified to account for lower bound cut-off

The cumulative distribution function can then be derived through the integration of Equation 6-24:

$$P(K_{mat}) = \begin{cases} 0 & \text{if} \quad K_{mat} < K_{lb} \\ \dfrac{1}{1-0.001}\left(1 - p_a.\exp\left\{-\left(\dfrac{K_{mat}-K_{\min}}{K_{01}-K_{\min}}\right)^4\right\} - (1-p_a).\exp\left\{-\left(\dfrac{K_{mat}-K_{\min}}{K_{02}-K_{\min}}\right)^4\right\}\right) + C & \text{otherwise} \end{cases}$$

Equation 6-25

where C is a constant resulting from the indefinite integral and can be calculated by evaluating Equation 6-25 at a known point. It is known that the cumulative distribution function for the material fracture toughness with the lower bound will be zero at the lower bound. Consequently:

$$C = 0 - \frac{0.001}{1-0.001} = \frac{-0.001}{1-0.001} \qquad \textit{Equation 6-26}$$

The cumulative distribution function is then given by:

$$P(K_{mat}) = \begin{cases} 0 & \text{if} \quad K_{mat} < K_{lb} \\ \dfrac{1}{1-0.001}\left(\begin{array}{l} 1-p_a.\exp\left\{-\left(\dfrac{K_{mat}-K_{\min}}{K_{01}-K_{\min}}\right)^4\right\} \\ -(1-p_a).\exp\left\{-\left(\dfrac{K_{mat}-K_{\min}}{K_{02}-K_{\min}}\right)^4\right\} \end{array}\right) - \dfrac{0.001}{1-0.001} & \text{otherwise} \end{cases}$$

Equation 6-27

The four reliability methods can then be used to re-evaluate the probability of failure for the example problem, including the lower bound on material fracture toughness.

6.7.1 Convolution integral

The convolution integral gives a probability of failure of 1.4×10^{-6} for a single crack tip. This calculation is shown in Appendix G.2.

6.7.2 First-order reliability method

The effect of the lower bound cut-off on the material fracture toughness distribution on the limit state function in standard normal space is shown in Figure 6-9.

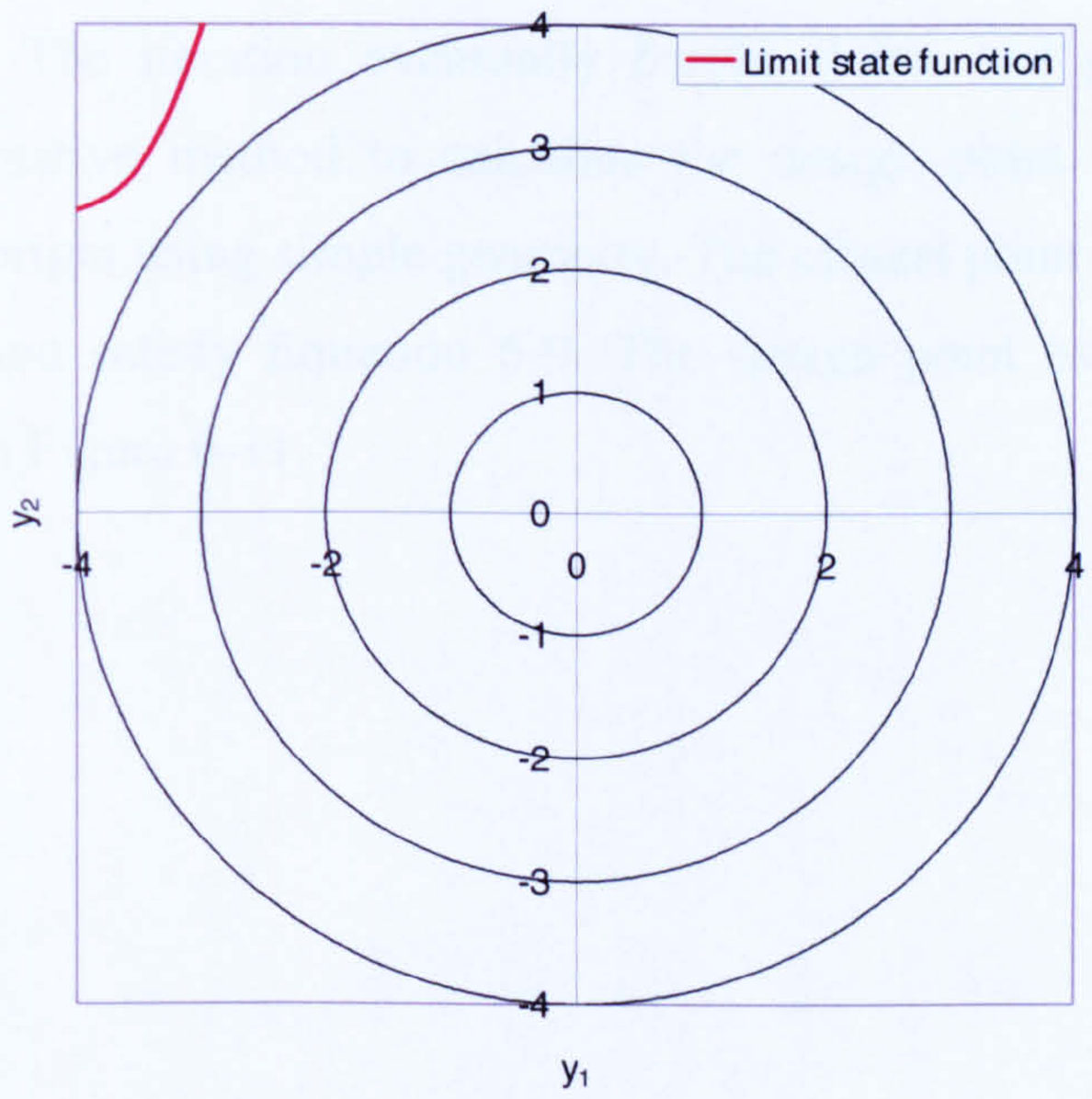

Figure 6-9 Effect of lower bound on material fracture toughness distribution on limit state function

The iteration scheme was then used to determine the design point. However, the solution failed to converge. This is shown in Figure 6-10.

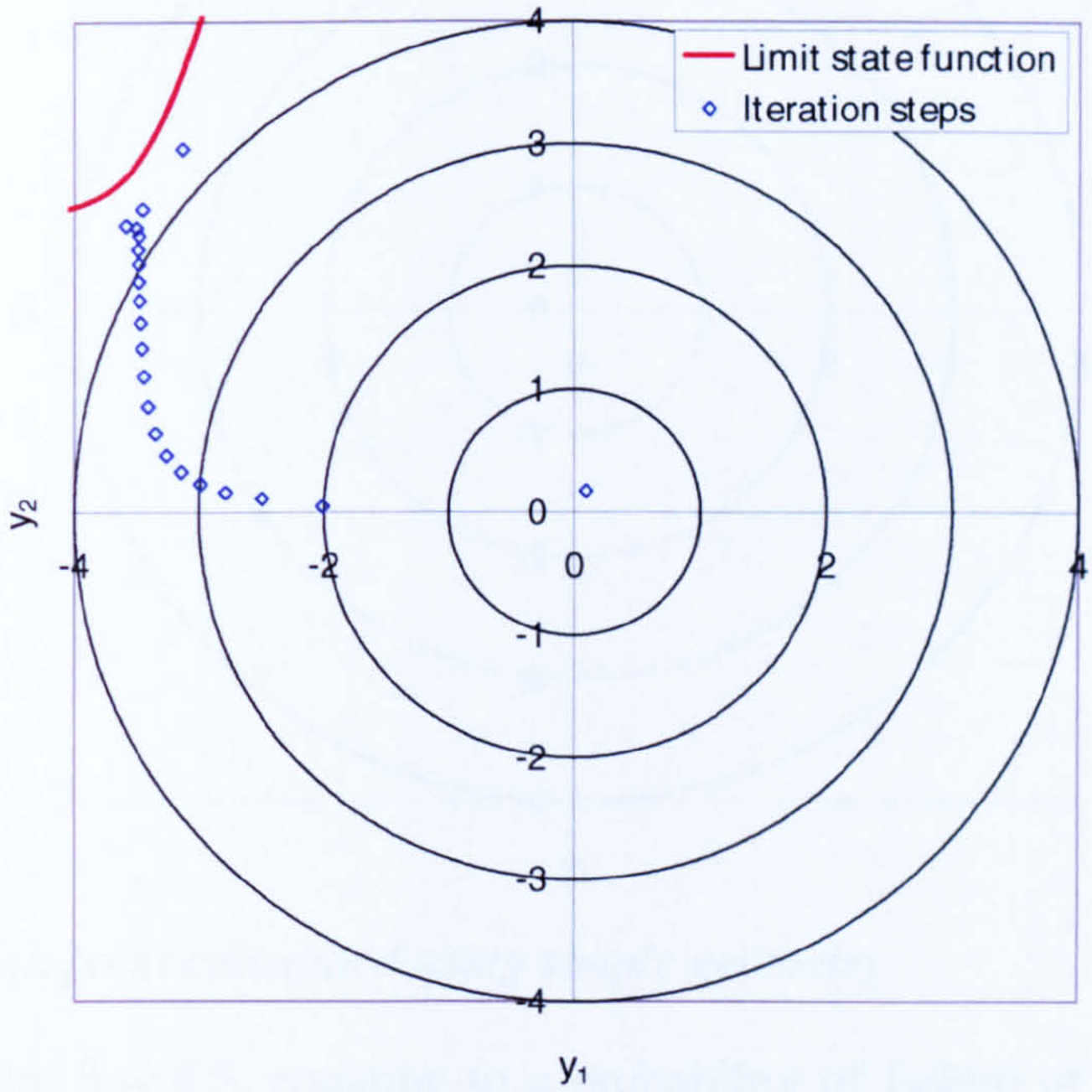

Figure 6-10 Convergence of FOR algorithm with lower bound on material fracture toughness distribution

It can be seen that the solution appears to approach the design point but then fails to find the solution. The iteration eventually breaks down and gives an incorrect estimate. An alternative method to calculate the design point is to evaluate the distance from the origin using simple geometry. The closest point will thus represent the design point and satisfy Equation 6-9. The design point estimated using this method is shown in Figure 6-11.

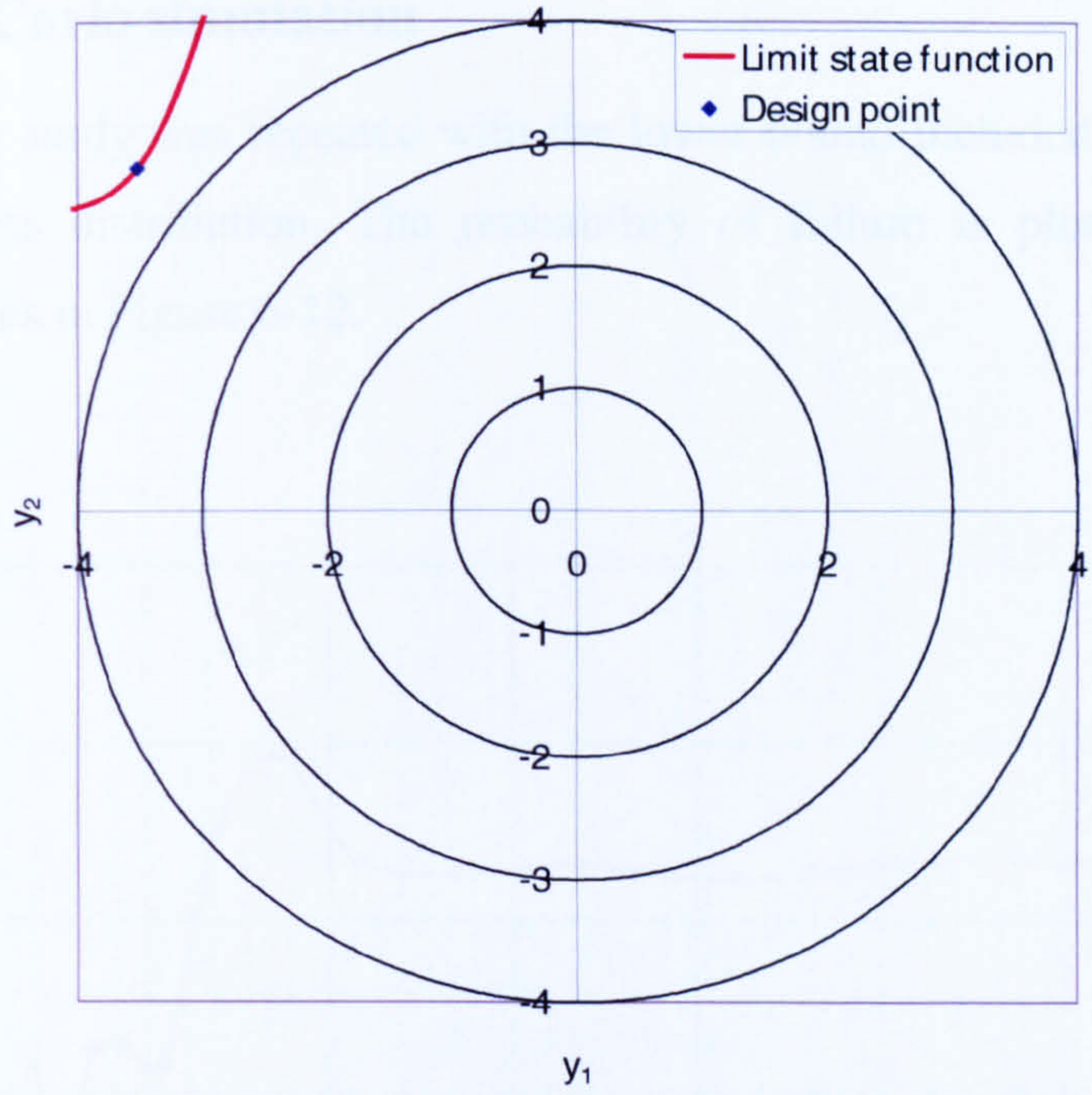

Figure 6-11 Design point calculated using simple geometry

At the design point $\beta = 4.5$, equating to a probability of failure of 3.4×10^{-6}. The design point lies in the curved region of the limit state function, caused by the introduction of the lower bound cut-off. This result indicates that the importance of the load component has increased.

6.7.3 Monte Carlo simulation

The convergence study was repeated with the lower bound included on the material fracture toughness distribution. The probability of failure is plotted against the number of samples in Figure 6-12.

Figure 6-12 Convergence of Monte Carlo simulation

It can be seen that the probability of failure converges to a value of 1.6×10^{-6} after approximately 1,000,000 samples. The increase in the required number of samples reflects the lower probability of failure when the lower bound cut-off is included on the material fracture toughness distribution.

6.7.4 Monte Carlo simulation with importance sampling

The convergence study for the Monte Carlo simulation with importance sampling was repeated with the lower bound included on the material fracture toughness distribution. This is shown in Figure 6-13.

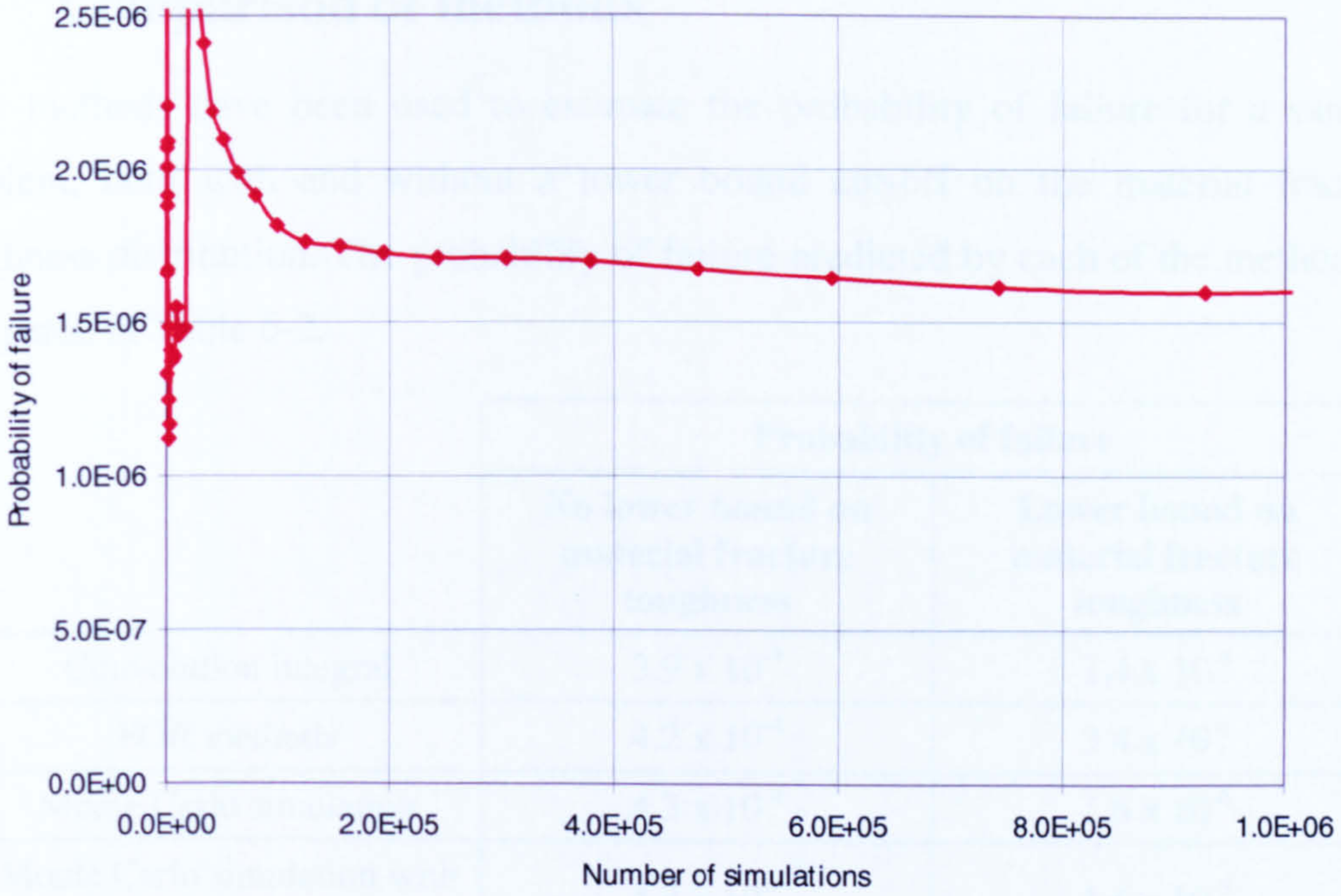

Figure 6-13 Convergence of Monte Carlo simulation with importance sampling

It can be seen that the probability of failure converges to a value of 1.6×10^{-6} after approximately 20,000 simulations. The result highlights the benefits of the importance sampling routine over 'crude' sampling, as it is not as sensitive to a reduction in the probability of failure.

6.8 Comparison of methods

Four methods have been used to estimate the probability of failure for a sample problem, both with and without a lower bound cut-off on the material fracture toughness distribution. The probability of failure predicted by each of the methods is compared in Table 6-2.

	Probability of failure	
	No lower bound on material fracture toughness	**Lower bound on material fracture toughness**
Convolution integral	3.9×10^{-4}	1.4×10^{-6}
FOR methods	4.2×10^{-4}	3.4×10^{-6}
Monte Carlo simulation	4.3×10^{-4}	1.6×10^{-6}
Monte Carlo simulation with importance sampling	4.4×10^{-4}	1.6×10^{-6}

Table 6-2 Comparison of predicted probabilities of failure estimated using a number of structural reliability methods

The convolution integral gives the lowest estimate of the probability of failure. This is an unexpected result. The convolution integral should agree with the results predicted by the Monte Carlo simulation methods, as they are all Level III methods and give an 'exact' estimate of the probability of failure. The numerical integration used in the evaluation of the convolution integral has been repeated with a range of integration steps and calculation methods but converges to the result given in the table. The convolution integral is the fastest of the methods, solving almost instantaneously.

The FOR algorithm gives a very good estimate of the probability of failure when no lower bound cut-off is included on material fracture toughness distribution. This is an expected result, due to the almost linear nature of the limit state function in normal space. The introduction of the lower bound reduces the accuracy of the estimate, which is caused by the concave nature of the limit state function at the design point. The failure of the FOR algorithm to converge when the lower bound is included is disappointing, as the method solves quickly, provides information on the influence of the basic variables, and provides a good estimate of the probability of failure. The

method used to calculate the design point from simple geometry would become increasingly difficult as the number of variables, or dimensions, increased.

The Monte Carlo simulation methods show very good agreement with the major difference being computational effort. The crude simulation takes several minutes to solve, even for a single time step. The importance sampling reduces the processing time to approximately 10 seconds.

The Monte Carlo simulation with importance sampling appears to be the most promising method, providing a good balance of accuracy and computational effort. Unfortunately, the method requires prior knowledge of the design point. While this can be calculated simply for two dimensions as the number of dimensions is increased it will become increasingly more difficult to calculate. The same criticism could be made of the convolution integral. However, this method solves extremely quickly and should give an accurate estimate of the probability of failure. Consequently, the convolution integral will be used in this thesis.

6.9 Discussion

An advantage of the FOR method is that the influence of the basic variables can be easily seen. It was shown in Figure 6-5 that with no lower bound on the distribution the material fracture toughness was by far the most important variable; with a change in the applied loading having a relatively small effect on the probability of failure. The introduction of the lower bound on the material fracture toughness increased the influence of the applied loading.

The effect of increasing the initial crack length on the shape of the limit state function is shown in Figure 6-14.

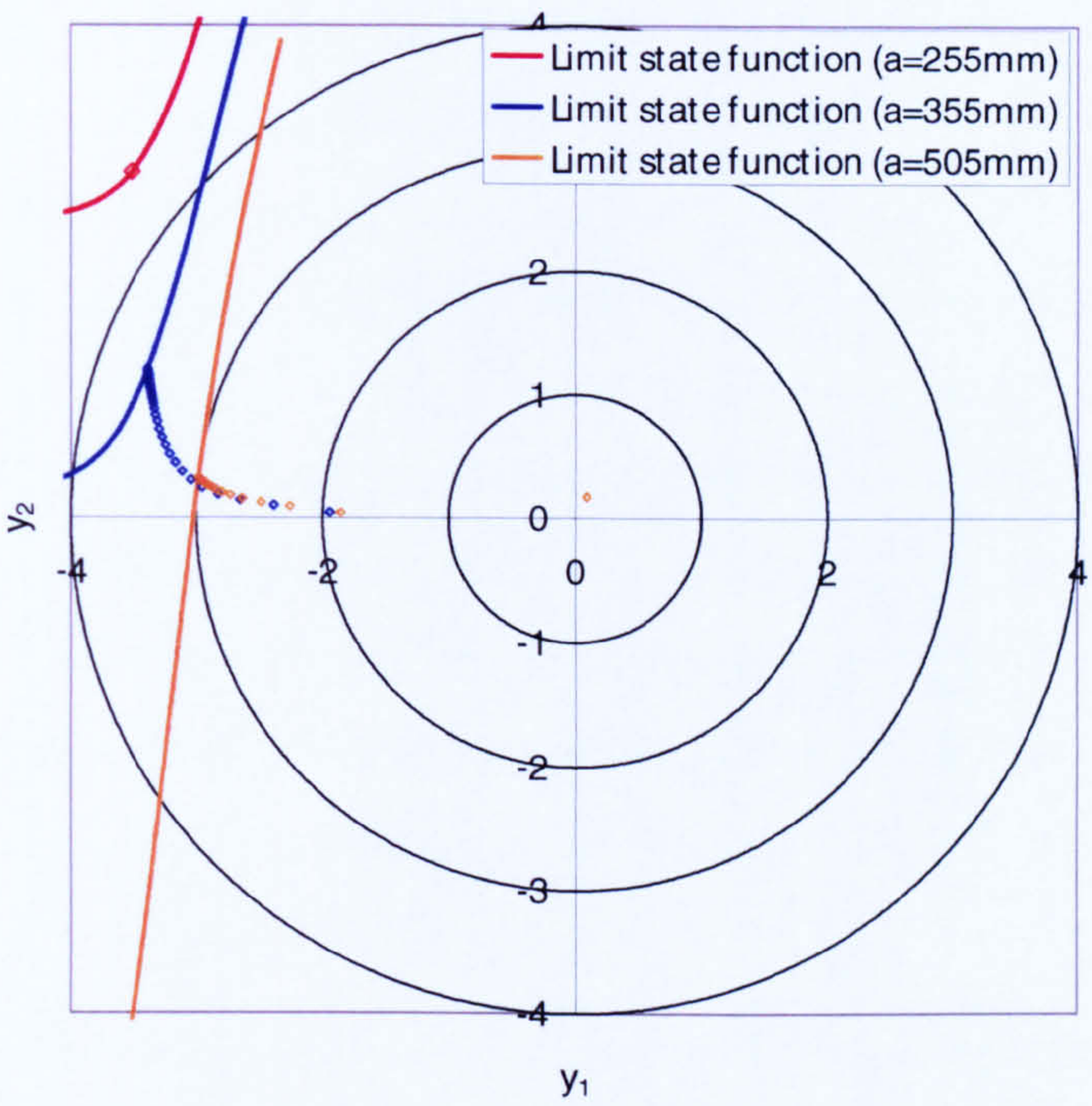

Figure 6-14 Effect of increasing crack length on shape of limit state function

It can be seen that as the crack length is increased the design point moves from the curved region around the lower bound area to the linear portion of the limit state function. In these regions the FOR algorithm is able to converge to a solution at the design point. As the probability of failure increases the sensitivity of the result to the material fracture toughness also increases. The reverse is also true: as the probability of failure reduces the solution becomes increasingly more sensitive to changes in the applied load distribution.

These results indicate that the material fracture toughness distribution should be considered to be the dominant parameter in the calculation procedure. The applied load distribution becomes important at very low probabilities of failure. Consequently, it is felt that further improvements in the material fracture toughness distribution would give greater benefit in improving confidence in the calculation methodology.

7 Results

7.1 Overview

The applicability of the fracture methodology will be evaluated in this chapter. The methodology is intended to provide advice on how long a crack can be safely left unrepaired. This requires an assessment of what level of risk an operator is willing to accept. There are various formulae available to the designer or operator of a structure to determine an acceptable level of risk, often based on the life of the structure and the number of people affected by the failure of the structure.

In this study the acceptable level of risk is determined through the use of reference casualty statistics. It is appreciated that there are drawbacks with this approach, namely that the methodology presented in this thesis is a prediction and often predictions do not match the observed failure rate (Melchers, 1999). This may be due to shortfalls in the recording of casualty rates, i.e. determining the type and cause of failure and the separation of in-service and construction incidents. The approach adopted in this thesis is felt to be justified as brittle fracture is not due to human error and occurs almost entirely during in-service operation. On the other hand, it is appreciated that brittle fracture may be under-reported as ships may simply be lost at sea due to unknown causes. The most important factor is that the predictions are felt to give reliable and consistent predictions of safe crack lengths from an engineering perspective.

Two target probabilities of failure have been extracted from the literature.

- $5x10^{-4}$ events/year is the value quoted in (Marspec, 1996) for possible incidence of brittle fracture (not necessarily catastrophic) in the merchant fleet.

- $4x10^{-3}$ events/year is the observed casualty rate in the merchant fleet for all causes of structural failure (Marspec, 1996). At this level of risk, the probability of brittle fracture would be the same as is accepted for other failure modes.

A traffic light approach has been adopted to allow a visual assessment to be made of the allowable crack lengths. These are defined below:

- Green – Safe;
- Amber – Repair as soon as possible;
- Red – Repair Immediately.

The boundary between the amber and red regions is defined as the crack length when the probability of failure in events/year reaches $4x10^{-3}$. The green to amber transition is defined by a probability of failure in events/year of $5x10^{-4}$. The crack growth in one day of operation in a storm (sea state 8) is then subtracted to allow for the growth that could occur before a repair can be made. A further 50mm is also removed to account for uncertainties in predicting the crack length and provides an additional safety factor.

The boundaries are shown in Figure 7-1.

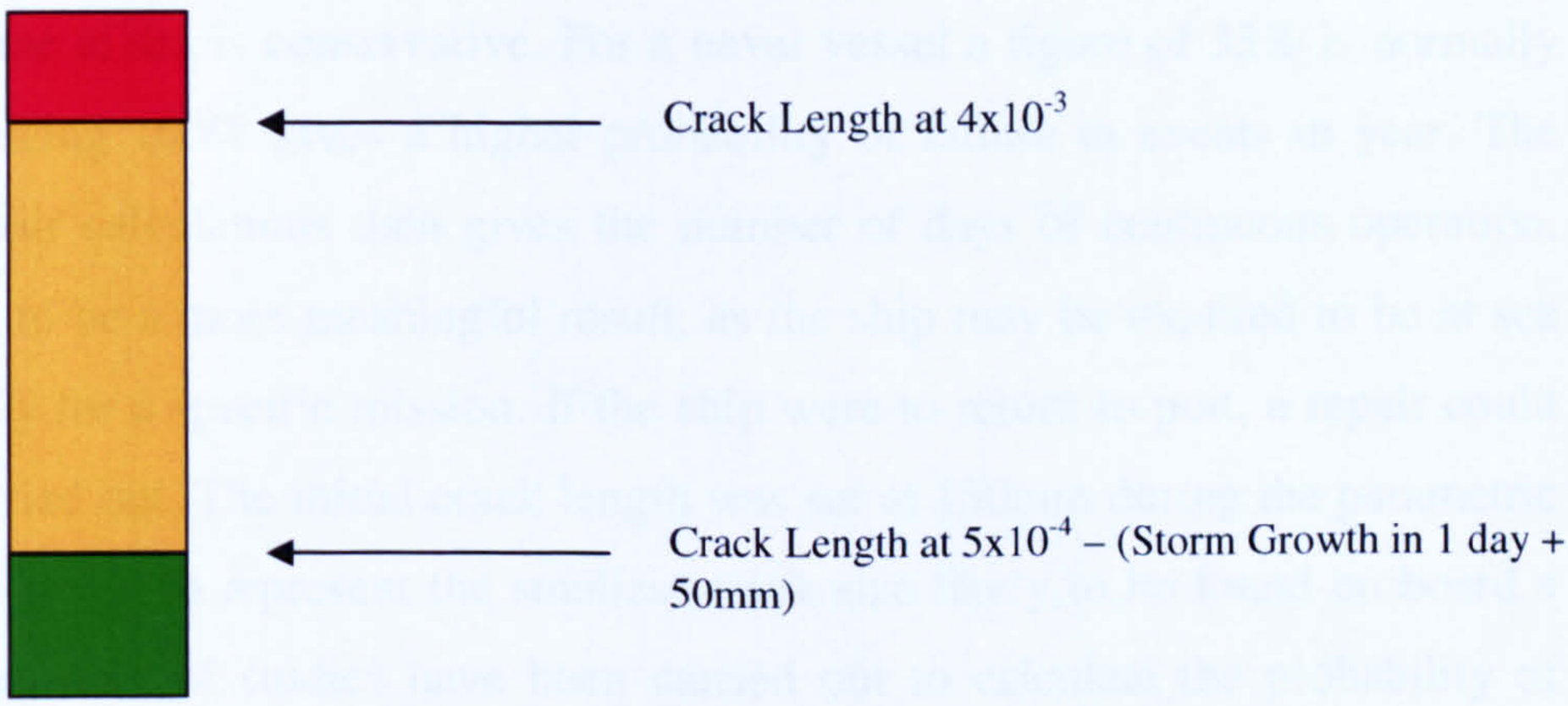

Figure 7-1 Construction of traffic light regions

The first stage of the analysis details the results of a parametric study which examines the effects of the input variables. An attempt has also been made to correlate the reducing incidence of brittle fracture since World War II with improvements in the Charpy 27J transition temperature. The final results of the study present the risk of brittle fracture as a function of steel grade.

7.2 Parametric Study

A parametric study was carried out to show the effect of the input variables. The variables analysed are shown in Table 7-1.

Variable	Values analysed
Temperature relative to T_{27J}	-20°C to + 60°C in 10°C increments
Residual stress	Included or not
Plate thickness	5 mm to 25 mm in 5mm increments
Operational profile*	Sea states: 2-8; 2-7; 2-6; 2-5; 2-4; 2-3; 2.
Crack type	Centre crack or crack growing from circular hole
Location of crack	Deck or keel

*Percentage of time spent in higher sea state added to next highest sea state based on Lloyd's Register operational profile (i.e. for sea states 2-7 1.16% is added to sea state 7)

Table 7-1 Input variables analysed in parametric study

The standard calculation parameters, as stated in Appendix F, are used in this study, with the values given in Table 7-1 substituted where applicable. The assumption of 100% of time at sea is conservative. For a naval vessel a figure of 33% is normally used. Assuming 100% gives a higher probability of failure in events in year. The time to repair calculations then gives the number of days of continuous operation. This is felt to be a more meaningful result, as the ship may be required to be at sea continuously for a specific mission. If the ship were to return to port, a repair could then be carried out. The initial crack length was set at 150mm during the parametric study. This is felt to represent the smallest crack size likely to be found on board a vessel. A number of studies have been carried out to calculate the probability of detection as a function of crack size. It is shown in SSC-389 (Demsetz, 1996) that even at a crack length of 200mm the probability of detection could be as low as 50%.

The results are presented as traffic light plots and time to repair graphs in Appendix H.1. The boundaries between the regions are described in Section 7.1. The time to repair is calculated as the number of days required to propagate the crack to the upper boundary of the safe region.

Figure H-1 shows the traffic light regions as a function of temperature relative to Charpy 27J temperature. The time to repair is plotted as a function of crack length in

Figure H-2. It can be seen for a grade D plate just meeting its Charpy 27J requirement at 0°C ($T-T_{27J} = +20°C$) the crack should ideally be repaired at 575mm but could be left until 770mm if there was an operational requirement. For a 150mm crack this would give approximately 470 days to repair.

Figure H-3 shows the effect of temperature relative to Charpy 27J temperature with no residual stress. Removing the residual stress only affects the low relative temperatures, which have a small acceptable crack length. The time to repair plot shown in Figure H-4 is near-identical to that shown in Figure H-2, with only a very slight change at a temperature relative to Charpy 27J temperature of 0°C.

The effect of thickness is shown in Figure H-5 and Figure H-6. Reducing the plate thickness increases the acceptable crack length and the time to repair.

The effect of operational profile is shown in Figure H-7 and Figure H-8. Limiting the operation to a maximum of sea state 6 increases the allowable crack length to 820mm. However, as the crack is propagating relatively quickly at this length the time to repair is only increased by 100 days.

The effect of the location of the crack is shown in Figure H-9 and Figure H-10. The still water bending stress reduces the peak stress intensity when the crack is located below the neutral axis. This gives an increase in acceptable crack length of 750mm and increases the time to repair to 700 days.

The effect of increasing the damage radius to the midships deck is shown in Figure H-11. Note that the limits are the acceptable probabilities of failure but do not include storm growth or an inspection margin. With a damaged area of 500mm in diameter (250mm in radius) the probability of failure rises very quickly and provides a very small margin against failure. This is because the radius of damage acts as part of the characteristic length, as shown in Figure 3-2. A large area of damage causes the crack to fail very quickly.

The effect of damage to the keel is shown in Figure H-12. The probabilities of failure rise more slowly than the deck due to the hogging still water bending stress. It can be seen that a damaged area of approximately 1.5m in diameter (750mm radius) causes the crack to enter the amber region at a very short length.

7.3 Comparison with reference casualty statistics

The examples of brittle fracture given in Chapter 1 demonstrated that brittle fracture often occurs from hidden defects. The ship appears to fracture without warning due to small initiating defects. These brittle fractures are caused by the localised effects of residual stress and stress concentrations. There has been a gradual reduction in these types of failures over time. The objective of this section is to attempt to correlate the reduction in failures of this type with improvements in steel quality.

A number of studies have attempted to estimate the incidence of brittle fracture at various dates:

- A study by Brown (Brown, 1952) estimated the number of brittle fractures as approximately 1 in 10 for all welded ships built before 1948 and under classification with the American Bureau of Shipping.

- A paper published by Hodgson and Boyd in 1958 (Hodgson, 1958) reviewed the Lloyd's Register database, excluding US ships. The results are based on a 12 year period during which there were 182 ship fractures, giving an estimated failure rate of 10^{-2} per year.

- The Lloyd's Register database was again reviewed by Buchanan in 1967 (Buchanan, 1969) which estimated that for new build ships the probability of brittle fracture had reduced slightly to $8x10^{-3}$ per year.

- An unpublished Ministry of Defence study of the Lloyd's Register database in 1996 recorded that there were only five incidences of brittle fracture among 40,000 ships during 1985-1995. This gives an estimated casualty rate of $1.25x10^{-4}$ events/year. This represents a marked decline in the frequency of brittle fracture since the 1945 to 1965 period, which is believed to be due to improvements in steel quality through control of carbon, sulphur and phosphorous content and increased manganese. It was seen in Chapter 5 that that the two modern grade A plates met the minimum grade D requirements.

The results from the studies are summarised in Table 7-2.

Date of study	Casualty rate (events/year)	Source
1948	0.08	Brown
1958	1.00×10^{-2}	Lloyd's database
1967	8.00×10^{-3}	Lloyd's database
1995	1.25×10^{-4}	Lloyd's database

Table 7-2 Reduction in incidence of brittle fracture

To carry out the study the program was extended to allow a distribution of both Charpy 27J temperatures and external temperatures to be input. The overall material fracture toughness distribution is then calculated by combining the material fracture toughness distribution for each Charpy 27J temperature and external temperature with their associated probability of occurrence.

The distribution of Charpy 27J temperatures as a function of the date of manufacture is taken from QinetiQ's in-house fracture toughness databank, shown in Figure 7-2.

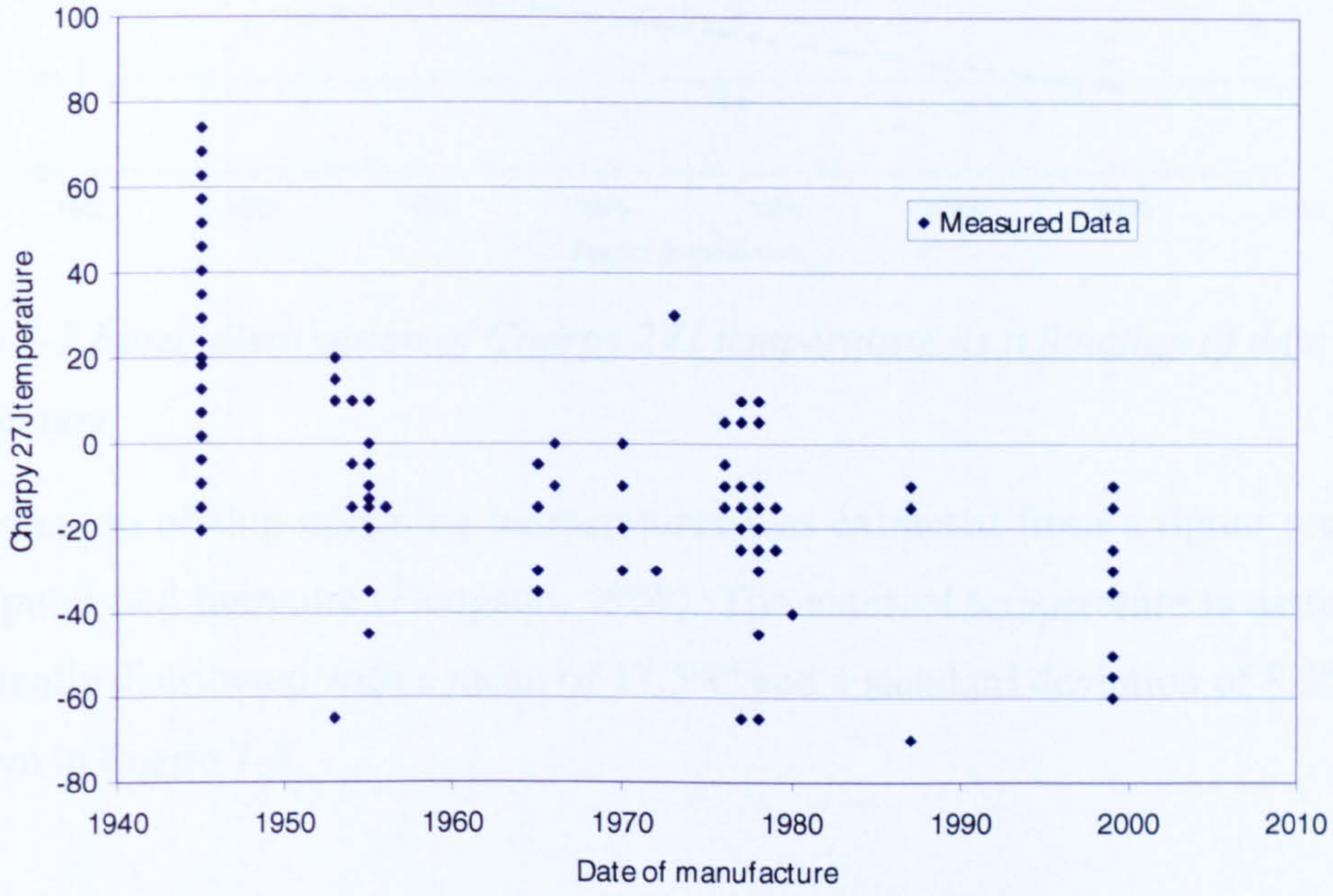

Figure 7-2 Spread of Charpy 27J temperature as a function of date of manufacture

It can be seen that the data from the period of the Liberty ships is markedly worse than the trend seen in the remaining data, which show a gradual reduction of Charpy 27J temperature with time. Consequently, it was decided to fit a distribution separately to these data. The Charpy 27J temperature was assumed to follow a normal distribution, with a mean 28°C and a standard deviation of 16.8°C.

A least squares mean line was fitted to the remainder of the data. The spread in Charpy 27J temperature was assumed to be normally distributed with a standard deviation of 15°C, which appears to encompass the scatter seen in the data.

The mean as a function of time is plotted against the measured data in Figure 7-3, together with the 5% and 95% levels.

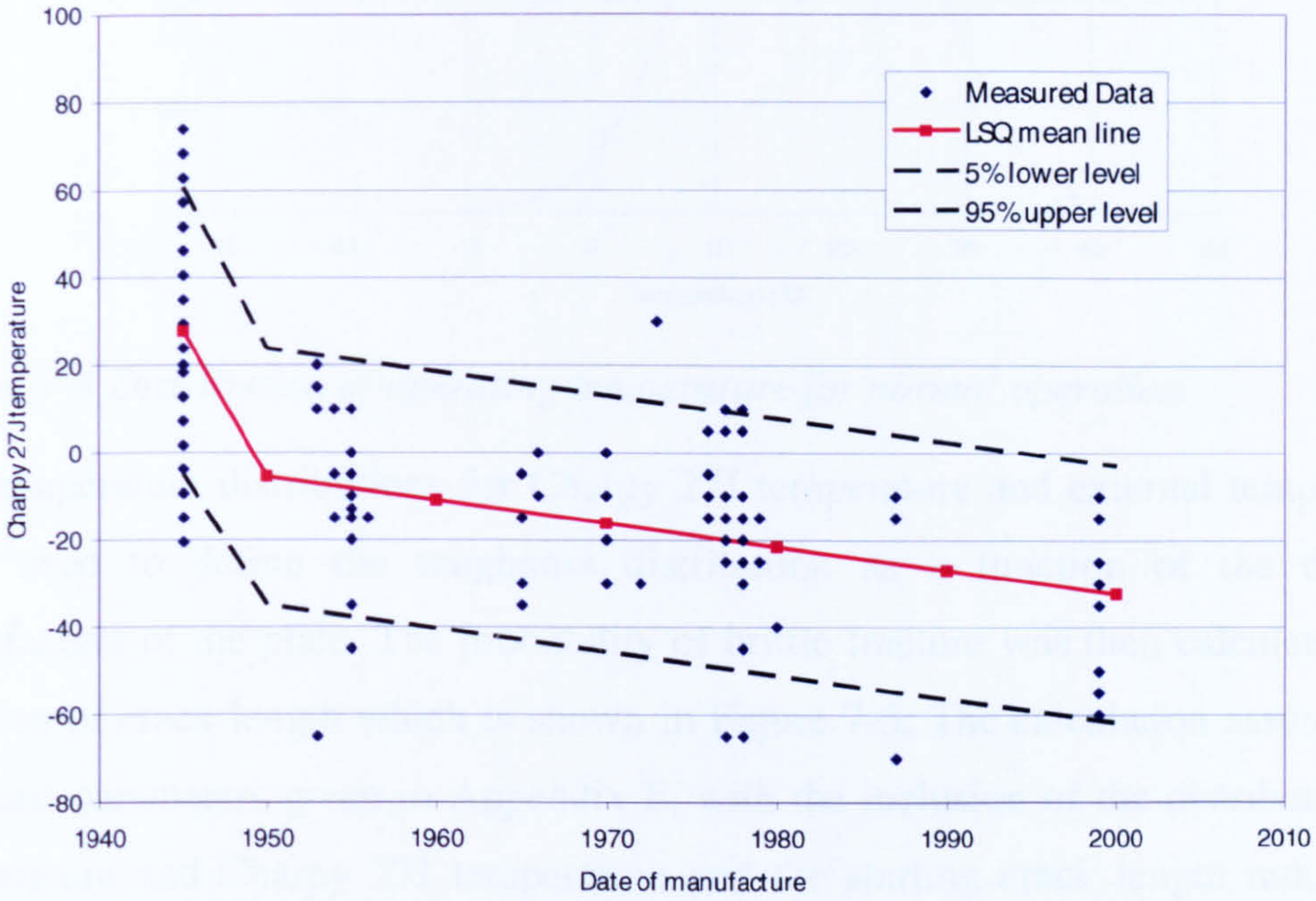

Figure 7-3 Fitted distribution of Charpy 27J temperature as a function of date of manufacture

A distribution of ship operating temperatures was extracted from a figure presented in the published literature (Hodgson, 1958). The external temperature is assumed to be normally distributed with a mean of 17.5°C and a standard deviation of 8.3°C, and is shown in Figure 7-4.

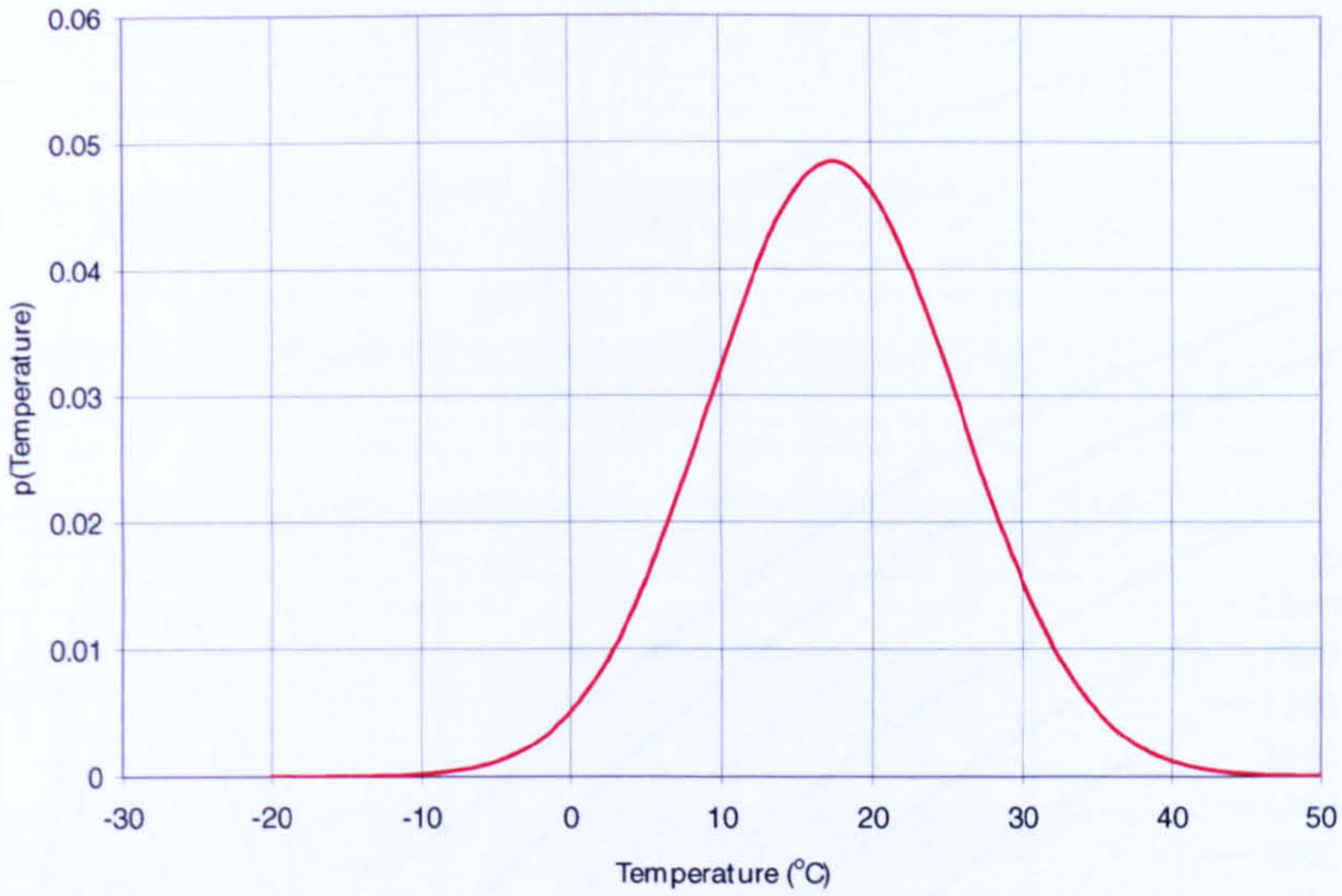

Figure 7-4 Distribution of operating temperature for normal operation

The temperature distributions for Charpy 27J temperature and external temperature were used to define the toughness distribution as a function of the date of manufacture of the plate. The probability of brittle fracture was then calculated as a function of crack length which is shown in Figure 7-5. The calculation assumes the standard parameters given in Appendix F, with the inclusion of the distributions of temperature and Charpy 27J temperature and the starting crack length reduced to 5 mm.

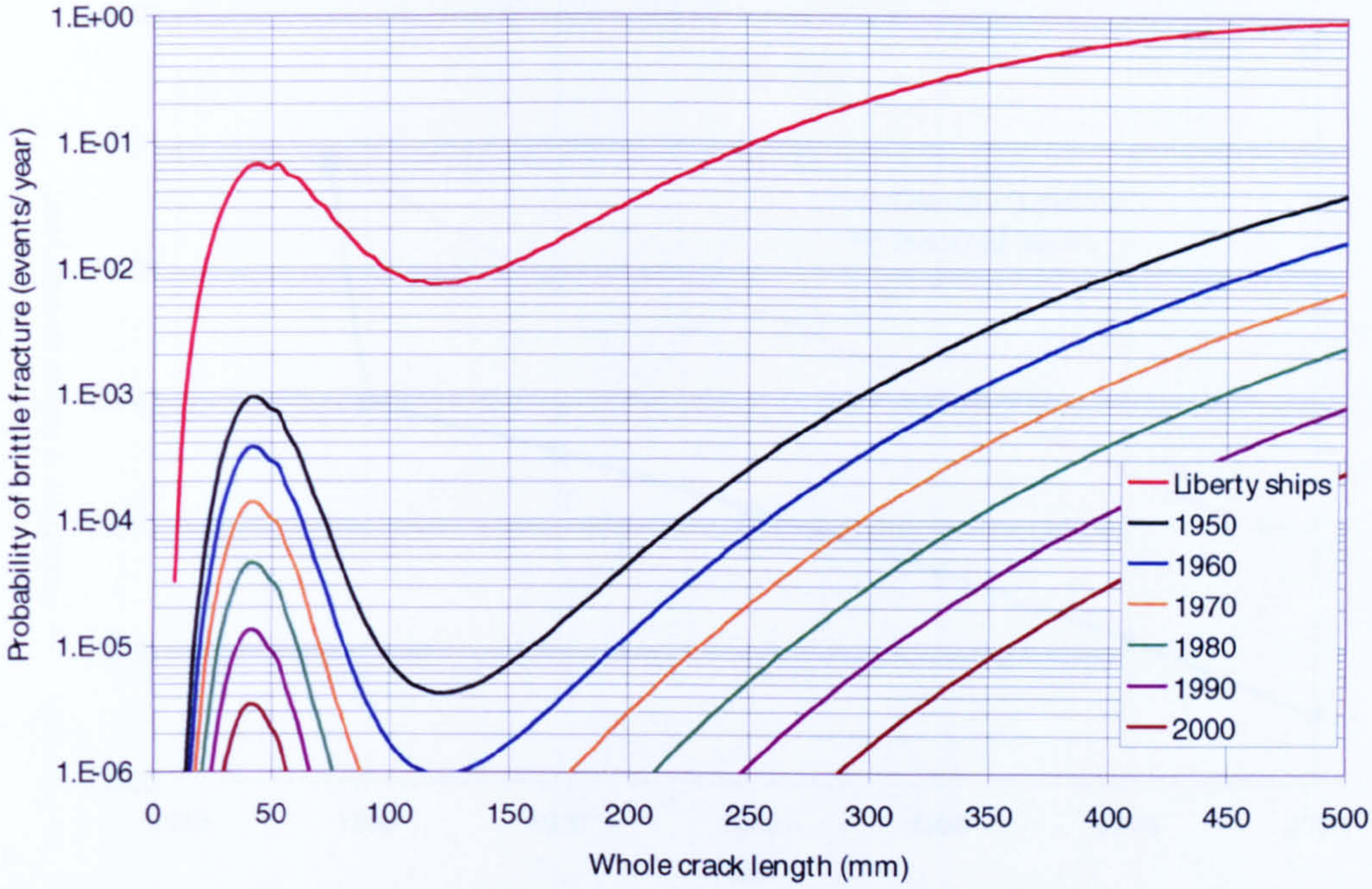

Figure 7-5 Probability of brittle fracture as a function of the date of manufacture of plate

It can be seen that the probability of brittle fracture rises quickly as the crack approaches 50mm and then reduces before rising again at longer crack lengths. The initial peak is caused by the effects of localised residual stress. It can be seen that the Liberty ship steel has an extremely high probability of failure in this region, and would thus be expected to have a high casualty rate. The probability of brittle fracture due to the initial peak at approximately 50mm was extracted and the results are plotted against the reference casualty statistics in Figure 7-6.

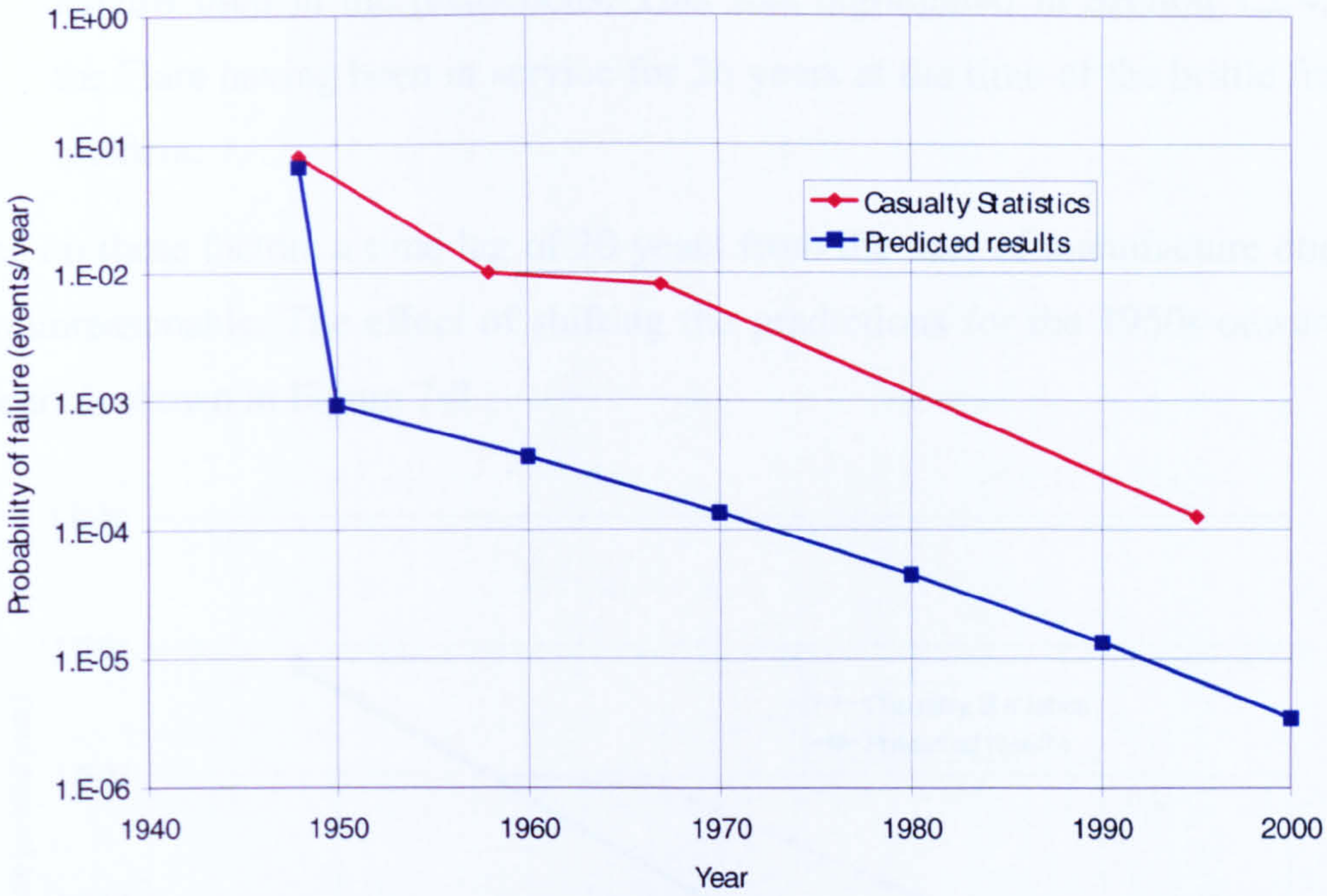

Figure 7-6 Comparison of reference casualty statistics with predicted risk of brittle fracture

It can be seen that there is an excellent agreement between the predicted risk of brittle fracture and the casualty statistics for the Liberty ships. Following 1945 the predicted probability of failure is approximately a factor of 10 lower than the actual casualty statistics. However, it is very encouraging to note that the gradients of both lines are similar.

There are a number of factors in the prediction which would bring the predicted incidence of brittle fracture in line with reference casualty statistics:

- Time lag before a ship enters service. The Charpy 27J temperatures are indexed to the date of manufacture of the plate. There is likely to be a delay of some years before a ship constructed from this steel actually enters service.

- Time lag before the brittle fracture incidence. There will a distribution of the age of the ship at the time of the brittle fracture incident. It is likely that this distribution would have an initial peak to account for construction defects such as incomplete welding which would cause a brittle fracture early in the ship's life. There is then likely to be a second peak some years later where small cracks have propagated from stress concentrations to the starting

lengths used in the predictions. This was highlighted in Section 1.2.4, with the Flare having been in service for 26 years at the time of the brittle fracture incident.

Based on these factors a time lag of 20 years from the date of manufacture does not seem unreasonable. The effect of shifting the predictions for the 1950s onwards by 20 years is shown in Figure 7-7 .

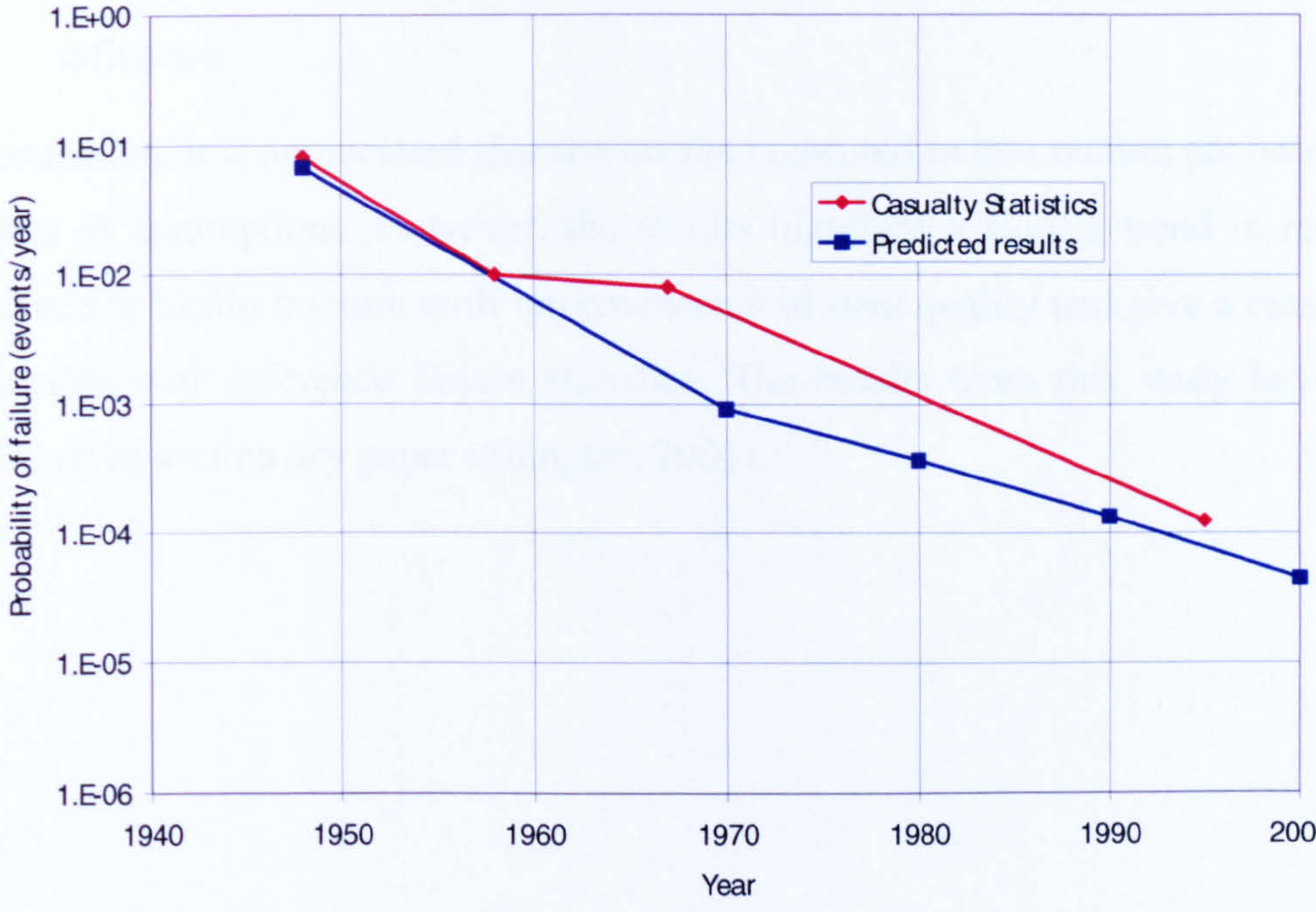

Figure 7-7 Comparison of reference casualty statistics with predicted risk of brittle fracture

It can be seen that shifting the predictions by 20 years brings them in line with the reference casualty statistics. Clearly, there have been a number of major assumptions made during these predictions, which are considered below:

- The results are based on the analysis of a single crack, while an in-service vessel is likely to contain numerous cracks. It was shown in Figure 7-5 that the probability of brittle fracture rises and falls quickly as a function of crack length. Consequently, the model assumes that only a single crack lies in the isolated peak at any one time.

- Shifting the predictions by 20 years is a rather large change. Steel is unlikely to be kept in stock for a number of years and failure due to short cracks would be likely to occur earlier in a ship's life.
- The results are based on a nominal ship operational profile. For merchant ships operating on specified routes the operational profile could be markedly different. However, the probability of failure is dominated by the effects of localised residual stress and the wave induced load has a relatively minor influence.

In conclusion, it is appreciated that the results presented in this section are based on a number of assumptions. However, the results highlight a similar trend in reducing incidence of brittle fracture with improvements in steel quality and give a reasonable correlation with reference failure statistics. The results from this study have been published in a summary paper (Sumpter, 2004).

7.4 Example safe crack lengths

The extension in the methodology to allow a distribution of Charpy 27J temperatures to be used, rather than a fixed value, can also be used to calculate the probability of brittle fracture for various grades of steel, rather than use the minimum Charpy 27J requirements specified in Table A-1.

The Charpy 27J temperature was assumed to be normally distributed with the mean 30°C below the minimum required value for each steel grade. The standard deviation was reduced slightly from that used in the previous section to 10°C. This gives a probability of 0.1% of exceeding the minimum required Charpy value. The assumed distributions are plotted in Figure 7-8.

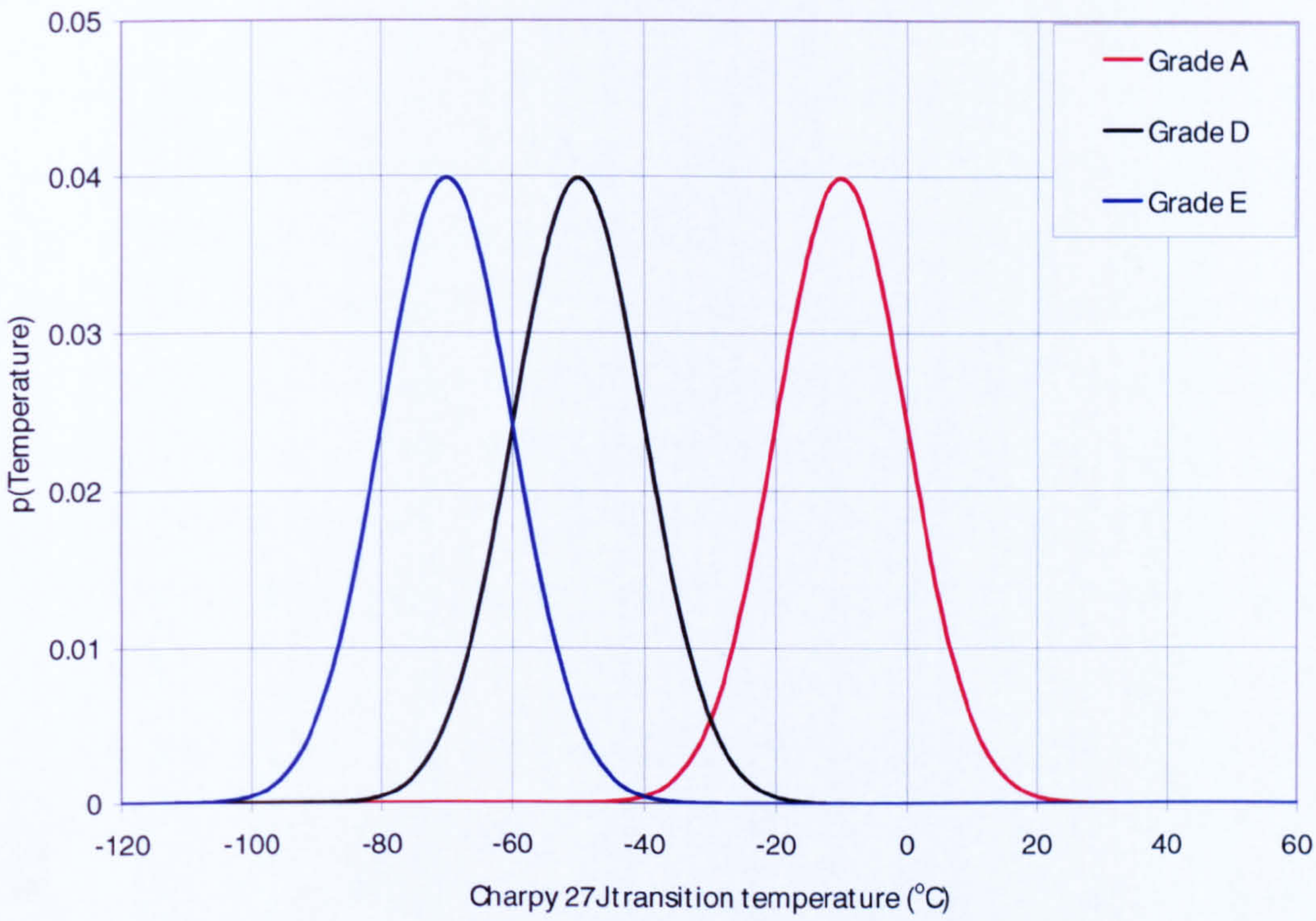

Figure 7-8 Assumed distribution of Charpy 27J transition temperature as a function of steel grade

Traffic light plots for each steel grade were calculated using the standard calculation parameters given in Appendix F, with the Charpy 27J temperature replaced by the distributions shown in Figure 7-8. The results are plotted in Figure H-13 to Figure H-15 for grades A, D and E respectively. If it is assumed that 0°C represents a realistic lower bound for normal ship operational temperature a crack in grade A

steel should be repaired before it reaches 300mm. This gives a very short window for repair if it is not discovered until 200mm. In contrast, a crack in a grade D plate would not require repair until over 1000mm in length. This compares with a repair length of 575mm if the Charpy 27J temperature is assumed to be the minimum for the steel grade (Figure H-1). Use of grade E steel would further increase the repair length to over 1500mm. These results highlight the considerable benefits of using improved steel grades in ship construction.

8 Conclusions and discussion

8.1 Summary

The number and complexity of welded connections in a ship structure make fatigue cracks an almost inevitable damage mechanism during the life of a vessel. In tough steels these cracks continue to propagate relatively slowly by fatigue until they reach lengths in excess of a number of metres, at which point the fatigue crack growth rate increases to such an extent as to make a plastic collapse of the cross section almost inevitable. In less tough steels under a sufficiently high loading, which can result from localised residual stresses or the wave action on the hull girder, a brittle fracture can occur. The consequences of this have been highlighted with some examples of the catastrophic failures that can occur in the event of a brittle fracture.

The initial development of the field of fracture mechanics was prompted by the dramatic failures of the Liberty ships during the Second World War. This led to a number of deterministic studies which attempt to control the problem through ensuring adequate material fracture toughness. These helped to reduce the problem but brittle fractures continued to occur. In recent years probabilistic methods have been increasingly prevalent. Some attempts have been made to apply these to ship structures but in the author's opinion these have poorly described the material fracture toughness distribution and failed to account for its variation as the crack propagates.

The nature of the problem analysed in this thesis is perhaps isolated to ship type structures. The study of cracks in pressure vessels deals with smaller surface flaws to prevent loss of containment. Pressure vessels are more suited to non-destructive testing methods which, in a ship structure, are only feasible for critical areas. Consequently, it is highly probable that cracks up to 200mm could remain undetected in ship structures.

This thesis has developed a methodology to calculate the risk of brittle fracture principally for cracks growing across the deck of a naval frigate, which has been incorporated into a software tool. This area is subject to cracking due to continual removal and re-welding of soft patches, and the stress concentrations caused by the

connection of superstructures blocks with the main deck. In addition, the distance from the neutral axis increases the vertical bending stresses which dominate the overall loading for slender-type structures. The methodology is generally applicable to any area of a ship if the geometry factor and applied loading are known.

In the methodology a brittle fracture has been assumed to occur when the applied stress intensity exceeds the material fracture toughness. The applied loading comprises three components: still water bending stresses; wave induced bending stress; and residual stress. The material fracture toughness distribution was fitted to a databank of material fracture toughness tests carried out on both grade D and grade A ship plate, weld and heat-affected zone. The distribution uses a mean line to describe the variation in toughness across the ductile to brittle transition combined with a bi-modal Weibull distribution to describe the scatter present at a given temperature. The Weibull distribution gives finite probabilities of low toughness values occurring. These are felt to be unrealistic and a fixed cut off has been applied at a cumulative probability of 0.1%, below which it is assumed there is a 0% probability of a toughness value occurring.

One of the major developments made in the thesis is to use time-dependent reliability to account for the variation in toughness as a crack propagates across a plate. It is proposed that the toughness be re-sampled at an interval of 5 mm. This distance was estimated using the results of recent wide plate tests at -50°C which failed in a brittle manner. It is felt that studies which have assumed that the toughness remains constant throughout the plate under-estimate the probability of brittle fracture.

The methodology aims to provide a fast and accurate analysis of a known defect. A number of methods of solving the limit state function have been compared. Three Level III (fully probabilistic) methods and one Level II (semi-probabilistic) method were evaluated. It was demonstrated that all methods showed good agreement with no lower bound included on the material fracture toughness distribution for a sample calculation. When the lower bound is introduced on the material fracture toughness distribution the algorithm used in the Level II method fails to converge. In the sample calculation with a reduced number of variables a solution can still be derived. However, this would prove increasingly difficult as the number of variables was

increased. The convolution integral is found to be the most suitable method, giving a good estimate of the probability of failure in an efficient manner.

The methodology has been used to predict example safe crack lengths for various grades of steel. A traffic light approach has been adopted to allow a visual assessment to be made of the allowable crack lengths. The boundaries between the regions are based on casualty statistics relating to the estimated risk of brittle fracture and overall structural failure.

An attempt has been made to correlate the predictions made using the methodology with the gradual reduction in incidence of brittle fracture since the failure of the Liberty ships. To carry out the study distributions of Charpy 27J temperature were fitted to historical test data and combined with an assumed distribution of ship operating temperature. The results given by the study indicated the same trend in reduction over time, but preceded the casualty statistics by approximately 20 years. The distribution of Charpy 27J temperature was based on new plates and it is felt that this could be attributed to a time lag before a ship enters service and a subsequent lag before cracks developed. Based on these factors a shift of 20 years does not seem unreasonable, and results in a good correlation between the predicted incidence of brittle fracture and the reference casualty statistics.

The results given by the study highlight the greatly reduced risk of brittle fracture by moving from grade A ship steel to grade D steel. At a temperature of 0°C (assumed to be the lowest temperature for normal ship operation) a crack in grade A steel should be repaired at or before 300mm. Given that cracks are unlikely to be found until they reach 200mm this provides a small margin of safety. For grade D steel the repair length is increased to over 1000mm potentially allowing the repair to be delayed to coincide with scheduled maintenance periods.

8.2 Areas of further work

The work presented in this thesis has developed a method to allow safe crack lengths to be calculated for a known defect. However, a number of potential areas which would increase understanding of the problem are discussed in the following sections under the headings of material fracture toughness and applied load components.

It was shown in Chapter 6 that the probability of failure was more sensitive to changes in the material fracture toughness distribution than the applied load. It is considered that applied loading components are also subject to a much greater degree of analysis in the published literature, in particular wave induced bending. It is therefore proposed that further studies into material fracture toughness would be of much greater benefit to the wider engineering community than further analysis of wave loading.

8.2.1 Material fracture toughness

The material fracture toughness distribution was fitted in Chapter 5 to a databank of tests carried out on grade A and D steel plate, weld and heat-affected zone. There exist a number of uncertainties both in the physical design and testing of the specimens, and in the statistical fitting of the data.

Specimen design

Tests were carried out using single edge notched bend specimens on plain plate, weld and heat affected zone. The test specimens are slightly non-standard having a ligament equal to plate thickness and the width fixed at 50 mm. This gives rise to a 'plane stress' condition at the crack tip, which is believed to model the constraint present in a ship structure, which has large in-plane dimension relative to the plate thickness.

It would be extremely desirable to validate these assumptions using a finite element model of both the test specimen and a real structure containing cracked elements. The stress conditions around the crack tip could then be compared to determine how closely the test specimen is modelling the real structure. Unfortunately, this will be a time-consuming process requiring a very dense mesh at the crack tip to give a smooth stress distribution.

Determination of a suitable loading rate

The material fracture toughness decreases as the strain rate is increased. This effect is caused by the increase in the yield stress due to the increased loading rate. This allows a greater stress to build up at the crack tip before local yielding occurs, increasing the likelihood of a cleavage failure.

The material fracture toughness tests used in this thesis were carried out at a loading rate of 300 MPa$\sqrt{m}$/s. This was based on the highest strain measured in the deck of a naval frigate during a severe storm and was thought to represent slamming loads. However, recent analysis has indicated that this strain rate is present in all sea states at all speeds and headings. This makes it unlikely to be slam and it is now believed to relate to the natural frequency of the hull girder, which is excited by some items of machinery. The value of 300 MPa$\sqrt{m}$/s is a factor of 100 lower than the $3x10^4$ MPa$\sqrt{m}$/s which was used up until the late 1990s by Sumpter (Sumpter, 1989). This was estimated to be representative of slamming pressure loading in a ship's bottom.

A number of recent studies in the literature have examined the effect of loading rate on material fracture toughness (Wallin, 1997) (Eurocode). Both methods model the effect of strain rate through a shift in the temperature. It can be seen in Figure 8-1 that both methods give very similar results.

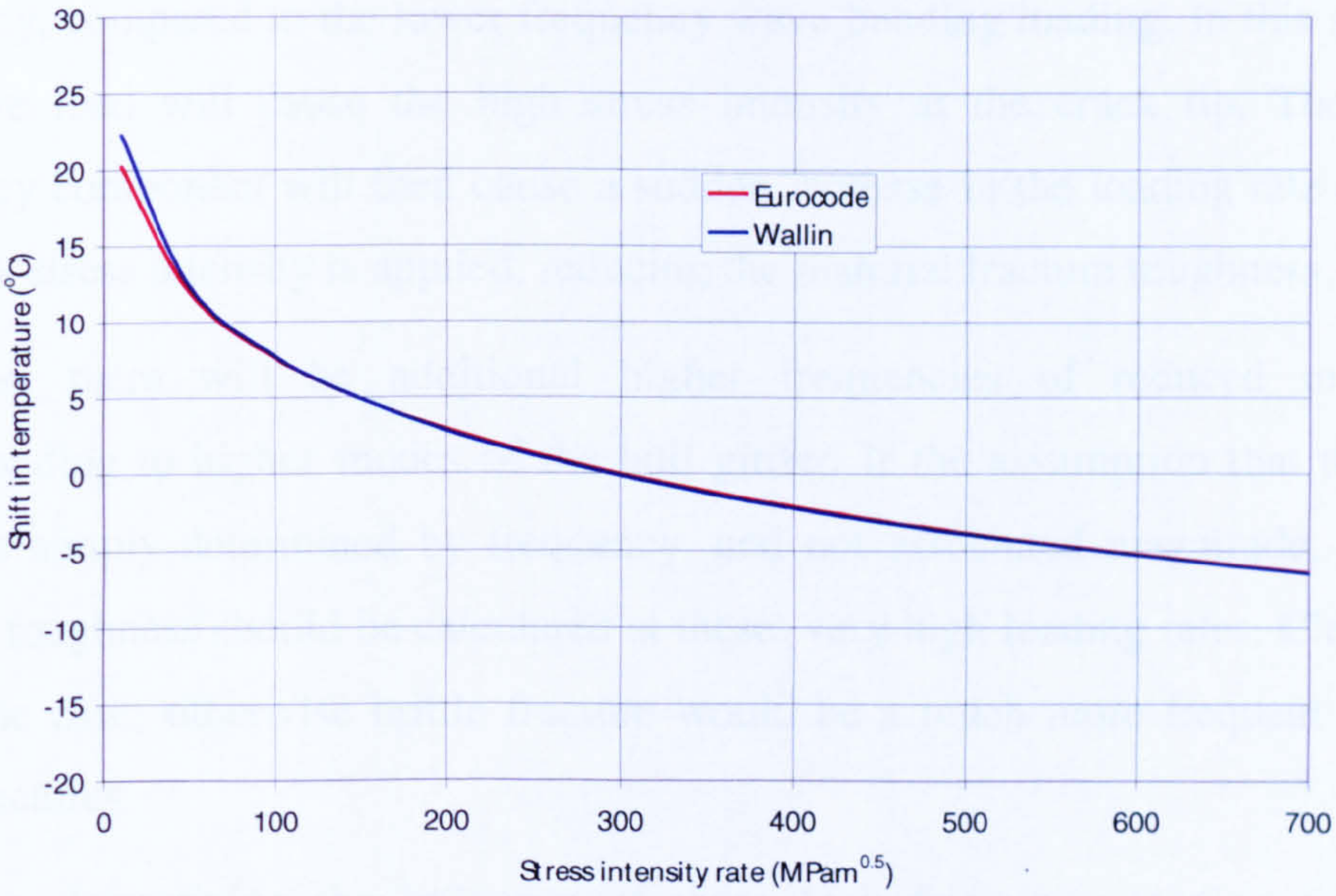

Figure 8-1 Shift in T_0 as a function of the stress intensity rate

These studies are based on a number of tests carried out at a variety of loading rates and temperatures. However, the determination of the applicable loading rate for ships is more complicated, due to the interaction of the hull vibration with the wave induced loading. This is shown in Figure 8-2.

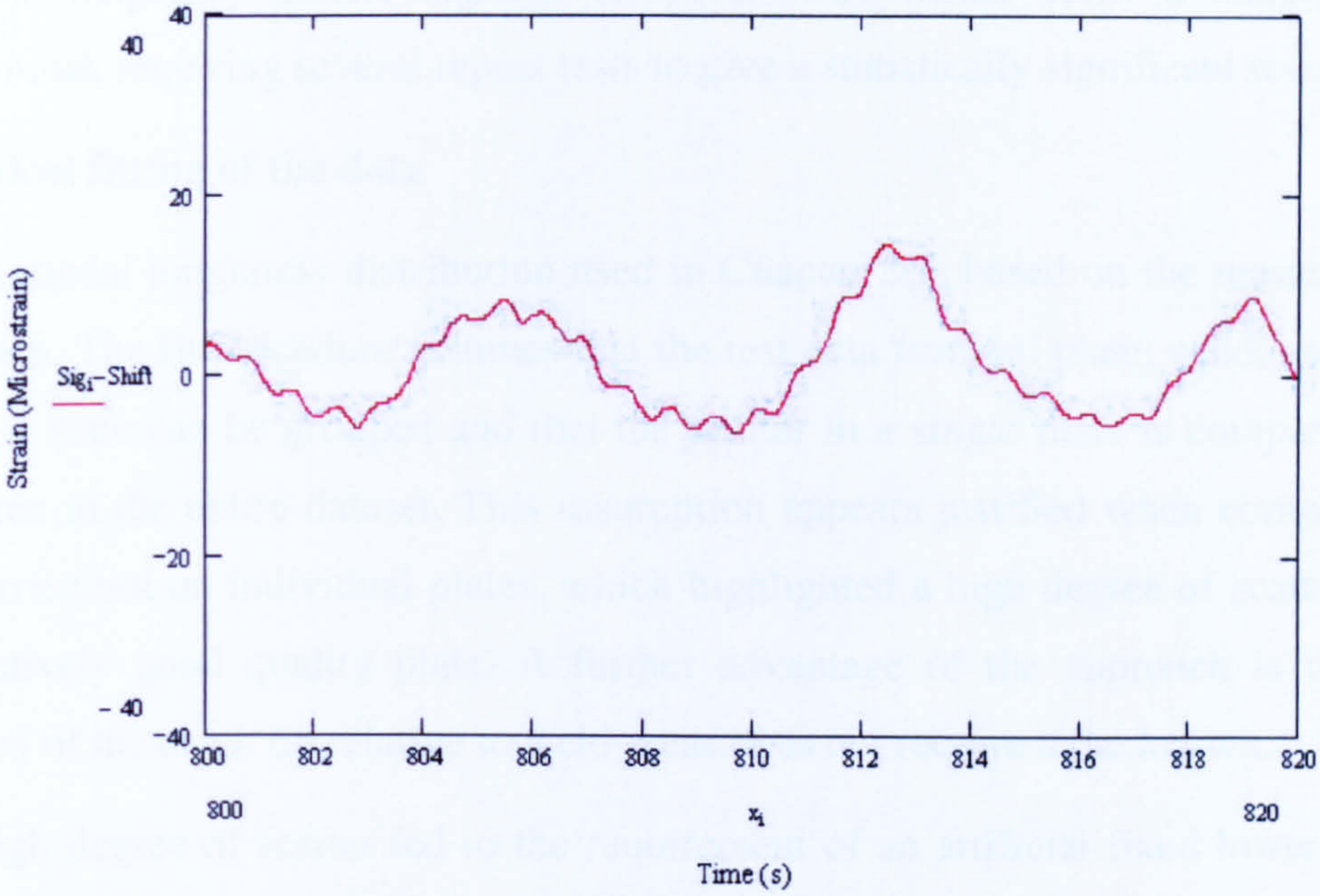

Figure 8-2 High frequency component of applied loading superimposed on low frequency wave bending

The value of 300 MPa√m/s represents a relatively small load applied at a high frequency, compared to the lower frequency wave bending loading. In this situation, the wave load will cause the high stress intensity at the crack tip. The natural frequency component will then cause a sudden increase in the loading rate at which this peak stress intensity is applied, reducing the material fracture toughness.

However, there will be additional higher frequencies of reduced magnitude corresponding to higher modes of the hull girder. If the assumption that the strain rate was simply determined by frequency, and not associated magnitude, then the fracture toughness should be calculated at these very high loading rates. Clearly this is not the case; otherwise brittle fracture would be a much more frequent event in ship structures.

However, determining the influence of these high frequency loading rates with reducing magnitude on material fracture toughness would not be easy. A suggested

method would be to carry out a set of toughness tests at various loading rates to determine the material fracture toughness distribution for a given plate. Fatigue tests could then be carried out at low temperature (to give a reasonable probability of fracture) with a series of time histories with high frequency components overlaid on the low frequency carrier signals. However, this would form a sizeable test programme, requiring several repeat tests to give a statistically significant result.

Statistical fitting of the data

The bi-modal toughness distribution used in Chapter 5 is based on the master curve approach. The fit procedure assumes that the test data from all plate, weld, and heat-affected zone can be grouped and that the scatter in a single plate is comparable to that seen in the entire dataset. This assumption appears justified when compared to fits carried out on individual plates, which highlighted a high degree of scatter even in relatively good quality plate. A further advantage of the approach is that the location of the crack tip relative to weld areas does not require to be known.

The high degree of scatter led to the requirement of an artificial fixed lower bound cut-off on the distribution. The inclusion of a cut-off is undesirable as the probability of failure is heavily dependent on the shape of the distribution in this region. However, the assumed distribution is felt to be a significant improvement over the extremely conservative distributions proposed in the literature, which led to high probabilities of failure for small defects.

It would be extremely desirable to carry out a further programme of toughness tests in an attempt to improve the shape of the toughness distribution in the lower tail. This could involve an increased number of tests on single plates to establish if the high degree of scatter found in the results used in this thesis is representative.

8.2.2 Applied loading

The applied loading used in this thesis is assumed to comprise of three components: wave induced bending stress; still water bending stress; and residual. These loading components are equated to an elastic stress intensity factor, by combining them with the defect size and a geometry factor.

The use of elastic stress intensities is considered to be valid, due to the relatively low stresses found in ship structures. However, a number of uncertainties still remain in the determination of the applied stress intensity. These are discussed below.

Geometry factor

The principal geometry factor used in this study is based on a finite element analysis of a superstructure detail. However, as the crack length increases this tends to the standard solution for a centre cracked plate. The geometry factor assumed for a damaged area is based on a published solution. As the complexity of the geometry in which the crack lies increases the only way to accurately determine the stress intensity factor is to use finite element analysis.

Many standard finite element solvers allow a crack to be modelled in a structure, either by using specialised crack elements, or by simply untying nodes to model the uncracked structure. More sophisticated tools, such as Zencrack (Chandwani, 2005) are able to automatically re-mesh the crack tip in a sub-model, which gives considerable time savings over manual meshing. In addition, the crack tip is free to take up the shape dictated by the local stress system. This is a valuable addition for complex stress geometries. It would be of great benefit to build up a databank of geometry factors for typical structural details.

Residual stress effects

The applied loading for short crack lengths (<200mm) is dominated by residual stress. The peak of residual stress has been assumed to remain at yield stress, taken to be a deterministic value of 265 MPa. A relatively simple extension to the program would allow this variable to be modelled using a distribution. A number of studies in the literature have modelled this using a normal or lognormal distribution (Hess, 2002).

In theory, residual stress is reduced in service due to shakedown effects. On application of a high load the material reaches its elastic limit so that plastic flow occurs. Load is then shed to adjacent material that is still elastic. When the load is removed the whole specimen unloads elastically and the peak residual stress is reduced. Incorporating shakedown effects would be of interest when using the methodology to assess shorter crack lengths.

Highest load coincides with lowest temperature

The predictions assume that the highest load coincides with the lowest temperature, and consequently minimum fracture toughness. At present, the temperature is sampled from the same distribution for every time interval, despite the time interval reducing as the crack length increases.

A more accurate method would be used to a daily distribution of temperature, perhaps specific to a desired area of location and current month or season. An extreme minimum could be used to determine the distribution of lowest temperatures over the time period. This would have the advantage of accounting for the changing time period as the crack propagates.

However, it would also assume that there was no correlation between the temperature and the sea state. It is the author's opinion that there does exist a correlation between these parameters. Low temperatures are normally associated with periods of low pressure, which can lead to calmer sea seas. Whether this assumption would be true for the entire globe would require investigation.

9 References

Ainsworth R A et al, *An overview of the European flaw assessment procedure SINTAP and its validation*, International Journal of Pressure Vessels and Piping, Vol. 77, pp 869-876, 2000.

Anderson T L, *Elastic-plastic fracture mechanics: a critical review*, Structural Committee Report No. 345, 1990.

Annual book of ASTM Standards, *Section Three: Metals test methods and analytical procedures*, volume 03.01, Designation: E 1921 – 05, ISBN 0-8031-3905-5, 2005.

Ayyub B M and White G J, *Life expectancy assessment of marine structures*, Marine Structures 3, pp 301-317, 1990.

Ayyub B M and Souza G F M, *Reliability-based methodology for life for prediction of ship structures*, SSC/SNAME/ASNE Ship Structure Symposium, June 13-14, 2000.

Baarholm G and Moan T, *Estimation of nonlinear long-term extremes of hull girder loads in ships*, Marine Structures 13, pp 495-516, 2000.

Bishop R E D et al, *A theory on the loss of the MV Derbyshire*, Royal Institute of Naval Architects, Vol. 133, pp 389-453, 1991.

British Standard 7910, *Guide to methods for assessing the acceptability of flaws in metallic structures*, ISBN 0-580-45965-9, 2005.

Brown D P, *Observations on experience with welded ships*, The Welding Journal, pp 765-782, 1952.

Buchanan G et al, *Lloyd's Register of Shipping's approach to the control of the incidence of brittle fracture in ship structures*, Paper presented at a colloquium on the properties and testing of weld metal in relation to structural failure from brittle fracture, IIW, Kyoto, July 1969.

Chandwani R et al, *An FE simulation tool for fracture mechanics*, International Seminar on Fatigue, Reliability and Performance Considerations in Design, Indian Institue of Science, Bangalore, India, 2005.

Clarke J D, *Prediction of fatigue cracking in warship hulls*, PRADS 1978, Trondheim, Norway, June 1987.

Corlett E C B et al, *Kurdistan – the anatomy of a marine disaster*, Paper presented at the spring meeting of the Royal Institute of Naval Architects (RINA), 1987.

Cornell C A, *A probability based structural code*, Journal of American Concrete Institute, Volume 66, No. 12, pp 974-985, 1969.

Det Norske Veritas (a), *Rules for the classification of ships*, Part 2, Chapter 2, Section 1, 1998.

Det Norske Veritas (b), *Rules for the classification of ships*, Part 3, Chapter 1, Section 2, 1998.

Demsetz L, Carlo R, and Schulte-Strathaus R, *Inspection of marine structures*, Ship Structural Committee Report No. 389, 1996.

Dillström P, ProSINTAP – *A probabilistic program implementing the SINTAP assessment procedure*, Engineering Fracture Mechanics, Vol. 67, pp 647-668, 2000.

Ditlevsen O and Madsen H O, *Structural reliability methods*, John Wiley and Sons, Chichester, England, 1996.

Dowling A R and Townley, *The effect of defects on structural failure: A two-criteria approach*, International Journal of Pressure Vessels and Piping, Volume 3, 1995.

Drucker D C, *An evaluation of current knowledge of the mechanics of brittle fracture*, Ship Structural Committee Report No. 69, 1954.

Eurocode 3: *European code for design of steel buildings*, Annex C: Material choice for avoidance of brittle fracture.

Ferry Borges J and Castanheta M, *Structural safety*, 2nd Edition, Laboratorio Nacional de Engenharia Civil, Lisbon Portugal, 1971.

Francis P H, Cook T S, and Nagy A, *Fracture criteria based on loading rates*, Ship Structural Committee Report No. 275, 1978.

Francis P H, Cook T S, and Nagy A, *Fracture behaviour characterization of ship steels and weldments*, Ship Structural Committee Report No. 276, 1978.

Garwood S J, *Failure investigation concerning MV Kurdistan casualty – final report*, The Welding Institute, 3642/1/80, April 1980.

Glen I F et al, *Sea operational profiles for structural reliability assessments*, Ship Structural Committee Report No. 406, 1998.

Glen I F et al, *Guide to damage tolerance analysis of marine structures*, Ship Structural Committee Report No. 409, 1999.

Hasofer A M and Lind N C, Exact and invariant second-moment code format, Journal of Engineering Mechanics Division, Volume 100, pp 111-121, 1974.

Hawthorne J R and Loss F J, *Fracture toughness characterization of shipbuilding steels*, Ship Structural Committee Report No. 248, 1974.

Hess P E et al, *Uncertainties in material strength, geometric and load variables*, ASNE Naval Engineers Journal, Vol. 114, pp 139-165, 2002.

Hinton P R, *Statistics Explained*, 2nd Edition, Routledge, 2004.

Hodgson J and Boyd G M, *Brittle fracture in welded ships – An empirical approach from recent experience*, The Institution of Naval Architects, Quarterly transactions, Vol. 100, no.3, July 1958.

International Association of Classification Societies (IACS), *Unified Requirements: Strength of ships*, Section S6, Revision 4, 2003.

International Association of Classification Societies (IACS), *Unified Requirements: Materials and welding*, Section W11, Revision 6, 2004.

Kappor S, *Fracture Properties of Grade A ship plate*, Offshore Technology Report – OTO 2000 01, Health and Safety Executive, January 2000.

Kent J S et al, *A probabilistic study into the effects of leaving fatigue cracks unrepaired while the ship is in service*, Offshore Mechanics and Artic Engineering Conference, OMAE 2002.

Kent J S and Sumpter J D G, *Probability of brittle fracture for a crack ship*, ASRANET, Barcelona, 2004.

Kent J S and Sumpter J D G, *An evaluation of methods to calculate the probability of brittle fracture of a cracked ship*, Proceedings of two part workshop at DTU, August 23-25, 2004.

Lloyd's Register (a), *Rules and Regulations for the Classification of Ships*, Part 3, Chapter 2, Section 2, 2000.

Lloyd's Register (b), *Rules and Regulations for the Classification of Ships*, Part 2, Chapter 3, Section 2, 2000.

Lloyd's Register, *Rules and Regulations for the Classification of Naval Ships*, Volume 1, Part 5, Chapter 2, 2003.

MaCallum J, *A case hstory – The World Concorde*, paper no. 2, RINA spring meeting 1981.

Mansour A, *An introduction to structural reliability theory*, Ship Structural Committee Report No. 351, 1990.

Mansour A et al, *Probability-based ship design (Phase 1): A demonstration*, Ship Structural Committee Report No. 368, 1992.

Marspec Report Castle Class offshore protection vessels, *Report on vessels' suitability for Antarctic operations*, Marspec C214/96, November 1996.

Melchers R E, *Structural reliability methods*, 2nd Edition, John Wiley and Sons, Chichester, England, 1999.

Murakami Y et al, *Stress Intensity Factors Handbook*, Volume 1, Pergamon Press, ISBN 0-08-034809-2, 1996.

North Atlantic Treaty Organisation (NATO), *Standardization agreement – Standardised wave and wind environments and shipboard reporting of sea conditions*, STANAG no. 4194, Edition 1, April 1983.

Paris P and Erdogan F, *A critical analysis of crack propagation laws*, Journal of Basic Engineering, Transactions of the American Society of Mechanical Engineers, pp. 528 – 534. 1963.

Pense A W, *Evaluation of fracture criteria for ship steels and weldments*, Ship Structural Committee Report No. 307, 1981.

Petinov S, *Fatigue analysis of ship structures*, Backbone Publishing Company, ISBN 0-9644311-8-1, 2003.

Proban user manual, DNV Software, Hovik, Norway.

Rolfe S T et al, *Fracture control guidelines for welded steel ship hulls*, Ship Structural Committee Report No. 244, 1974.

Rooke D P and Cartwright D J, *Compendium of stress intensity factors*, HMSO London, 1976.

SESAM user manual, WASIM Version 3.2, Det Norkse Veritas, Hovik, Norway, August 2004.

Soares C G and Ivanov L D, *Time-dependent reliability of the primary ship structure*, *Reliability*, Engineering and System Safety 26, pp 59-71, 1989.

Soares C G, *Combination of primary load effects in ship structures*, Probabilistic Engineering Mechanics, Vol. 7, pp 103-111, 1992.

Stone R F, *MV Kurdistan – Formal Investigation*, Report of Court No. 8069, ISBN 0-11-511664-8, 1981.

Strurel – A structural reliability analysis program, User manual, R C P GmbH, 2004.

Sumpter J D G et al, *Fracture toughness of ship steels*, Royal Institution of Naval Architects, Volume 131, 1989.

Sumpter J D G, *Fracture avoidance in submarines and ships*, Advances in Marine Structures, Volume 2, Ed Smith and Dow, Elsevier, 1991.

Sumpter J D G and Caudrey A J, *Recommended fracture toughness for ship hull steel and weld*, Marine Structures, Volume 8, 1995.

Sumpter J D G and Kent J S, *Prediction of ship brittle fracture casualty rates by a probabilistic method*, Marine Structures, Vol. 17, pp 575-589, 2004.

Sumpter J D G and Kent J S (a), *Fracture toughness of grade D ship steel*, Journal of Engineering Fracture Mechanics, Vol. 73, pp 1396-1413, July 2006.

Sumpter J D G and Kent J S (b), *Probability of cleavage fracture for a crack propagating by fatigue*, Journal of Engineering Fracture Mechanics, Vol. 73, pp 1414-1425, July 2006.

Sun H and Bai Y, *Time variant reliability assessment of FPSO hull girders*, Marine Structures 16, pp 219-253, 2003.

Tiku S, *In service non-destructive evaluation of fatigue and fracture properties for ship structures*, Ship Structural Committee Report No. 428, 2003.

Transportation Safety Board of Canada (TSBC), Marine Investigation Report, *Break-up and sinking - Bulk Carrier Flare*, Cabot Strait, *16th January 1998*, Report no. M98N0001, 1998.

Transportation Safety Board of Canada (TSBC), Marine Investigation Report, *Hull fracture – Bulk Carrier Lake Carling, Gulf of St Lawrence, Quebec, 19th March 2002*, Report no. M02L0021, 2003.

Wallin K, *The scatter in K_{IC} results*, Engineering Fracture Mechanics, Vol. 19, No. 6, pp 1085-1093, 1984.

Wallin K, *The size effect in K_{IC} results*, Engineering Fracture Mechanics, Vol. 22, No. 1, pp 149-163, 1985.

Wallin K, *The effect of strain rate on the fracture toughness reference temperature, T_0, for ferritic steels*, in Recent Advances in Fracture, edited by R K Mahidhara et al, 1997.

Wallin K, *Master curve analysis of ductile to brittle transition region fracture toughness round robin data – the EURO fracture toughness curve*, VTT publications, VTT Espoo Finland, 1998.

Wallin K, *A fracture mechanics interpretation of the DNV brittle fracture criteria for ships and mobile offshore units*, Journal of Fatigue and Fracture of Engineering Materials and Structures, Vol. 25, pp. 1033-1043, 2002.

Wallin K et al, *Master curve analysis of inhomogeneous ferritic steels*, Engineering Fracture Mechanics, Vol. 71, pp 2329-2346, 2004.

Yazdani N and Albrecht P, *Crack growth rates of steel in air and aqueous environments*, Engineering Fracture Mechanics, Vol.32, No. 6, pp 997-1007, 1989.

Zerbst U et al, *Engineering estimation of the lower bound toughness in the ductile to brittle transition regime*, Journal of Fatigue and Fracture of Engineering Materials and Structures, Vol. 21, pp 1273-1278, 1998.

10 Publications

Kent J S et al, *A probabilistic study into the effects of leaving fatigue cracks unrepaired while the ship is in service*, Offshore Mechanics and Artic Engineering Conference, OMAE 2002.

Kent J S and Sumpter J D G, *Probability of brittle fracture for a crack ship*, ASRANET, Barcelona, 2004.

Kent J S and Sumpter J D G, *An evaluation of methods to calculate the probability of brittle fracture of a cracked ship*, Proceedings of two part workshop at DTU, August 23-25, 2004.

Sumpter J D G and Kent J S, *Prediction of ship brittle fracture casualty rates by a probabilistic method*, Marine Structures, Vol. 17, pp 575-589, 2004.

Sumpter J D G and Kent J S (a), *Fracture toughness of grade D ship steel*, Journal of Engineering Fracture Mechanics, Vol. 73, pp 1396-1413, July 2006.

Sumpter J D G and Kent J S (b), *Probability of cleavage fracture for a crack propagating by fatigue*, Journal of Engineering Fracture Mechanics, Vol. 73, pp 1414-1425, July 2006.

A Selected Lloyd's Register material specifications

	Steel grade				
Requirement	**A**	**B**	**D**	**DH**	**E**
Minimum Yield Stress (MPa)	235	235	235	315	235
Ultimate Tensile strength (MPa)	400	400	400	440-590	400
Temperature (°C) at which minimum Charpy energy is 27J	20	0	-20	-20	-40
Maximum Carbon content (%)	0.21	0.21	0.21	0.18	0.21
Minimum manganese content (%)	2.5 x %C	0.8	0.6	0.19-1.6	0.7

*Specifications are for plate less than or equal to 50mm thick

Table A-1 Summary of material specifications (Lloyd's Register 2005b)

B Program flowchart

B.1 Overview

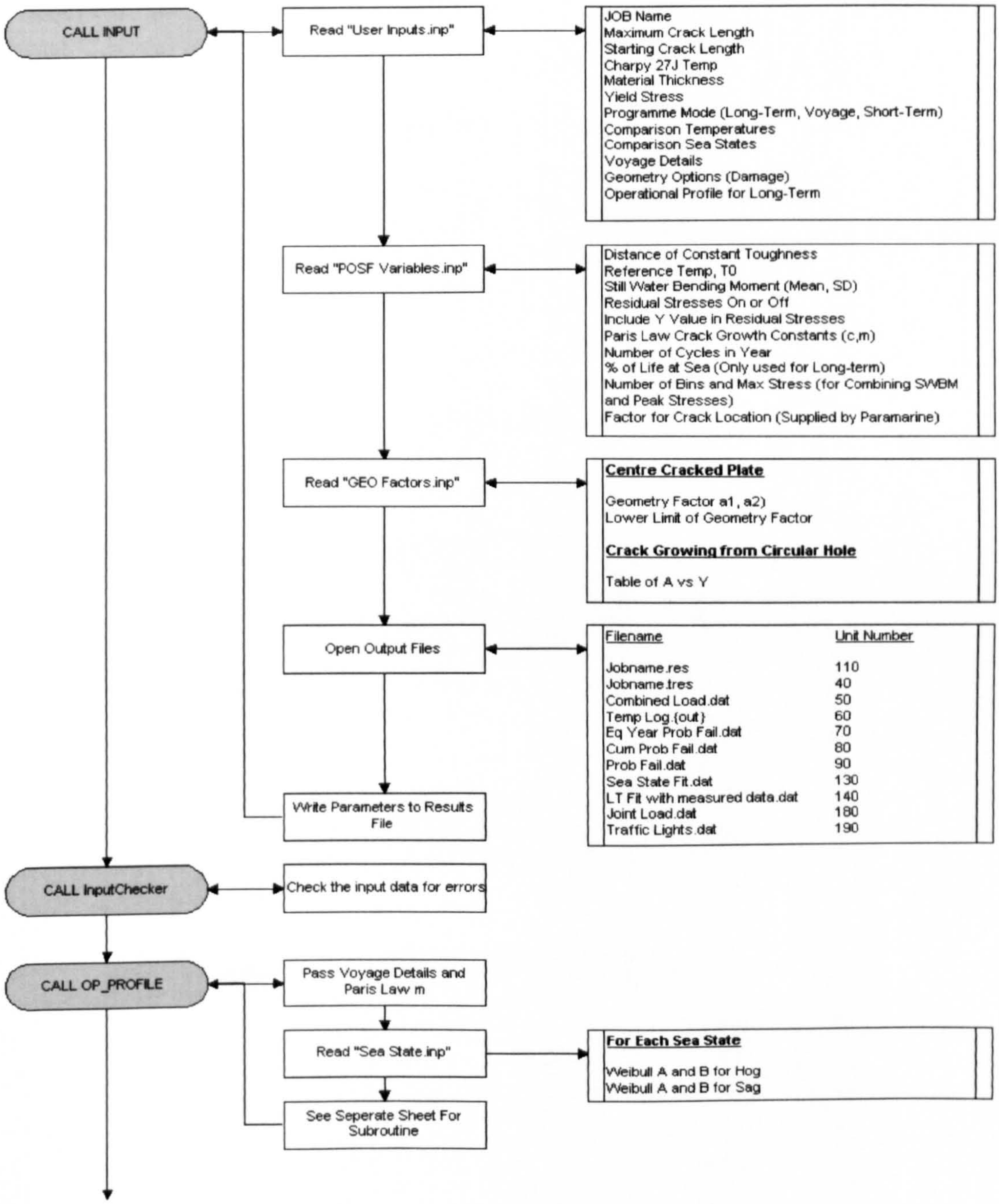

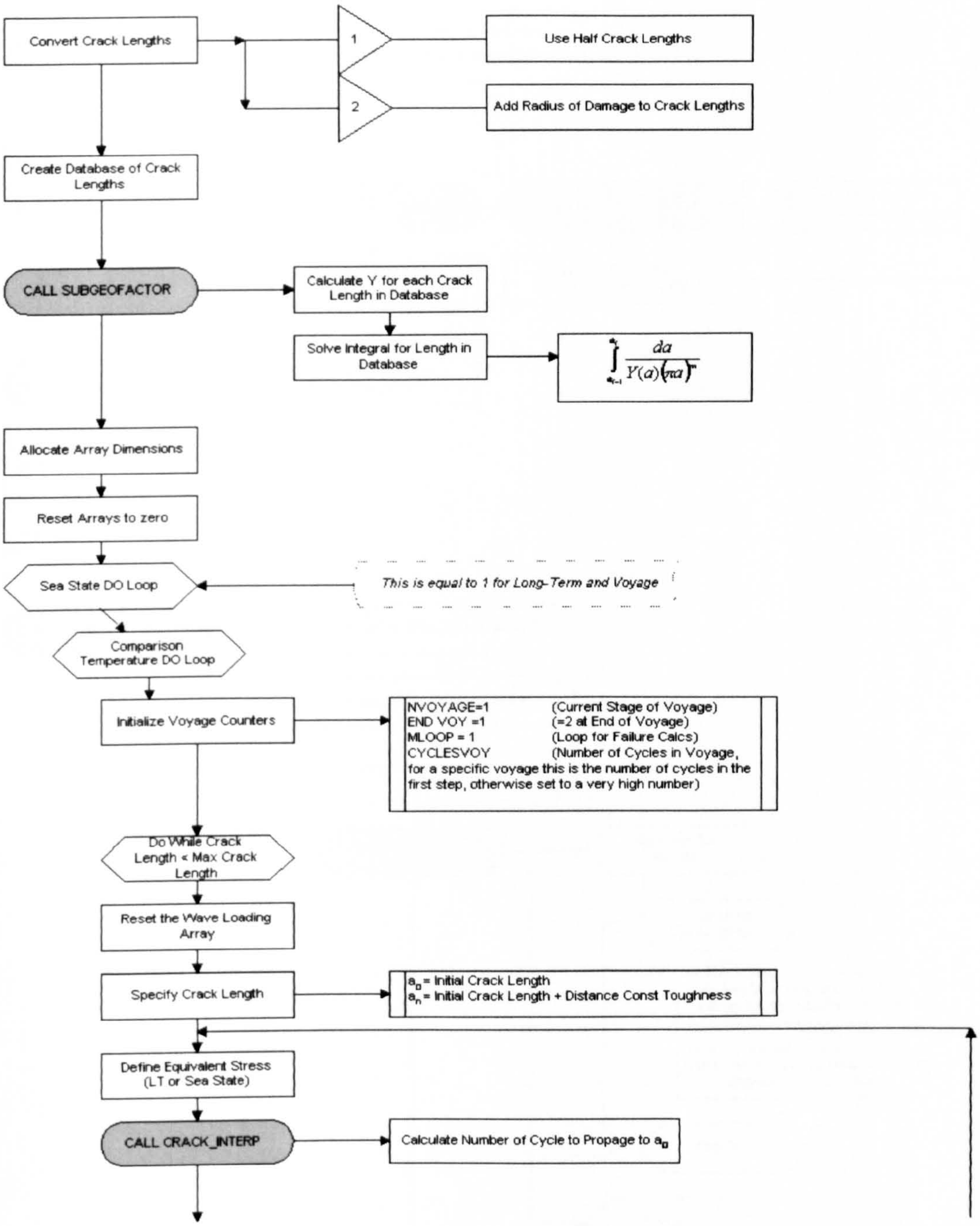
Convert Crack Lengths
1
Use Half Crack Lengths
2
Add Radius of Damage to Crack Lengths
Create Database of Crack Lengths
CALL SUBGEOFACTOR
Calculate Y for each Crack Length in Database
Solve Integral for Length in Database
$\int_{a_{i-1}}^{a_i} \frac{da}{Y(a)(\pi a)^m}$
Allocate Array Dimensions
Reset Arrays to zero
Sea State DO Loop
This is equal to 1 for Long-Term and Voyage
Comparison Temperature DO Loop
Initialize Voyage Counters
NVOYAGE=1 (Current Stage of Voyage)
END VOY =1 (=2 at End of Voyage)
MLOOP = 1 (Loop for Failure Calcs)
CYCLESVOY (Number of Cycles in Voyage, for a specific voyage this is the number of cycles in the first step, otherwise set to a very high number)
Do While Crack Length < Max Crack Length
Reset the Wave Loading Array
Specify Crack Length
a_0 = Initial Crack Length
a_n = Initial Crack Length + Distance Const Toughness
Define Equivalent Stress (LT or Sea State)
CALL CRACK_INTERP
Calculate Number of Cycle to Propage to a_0

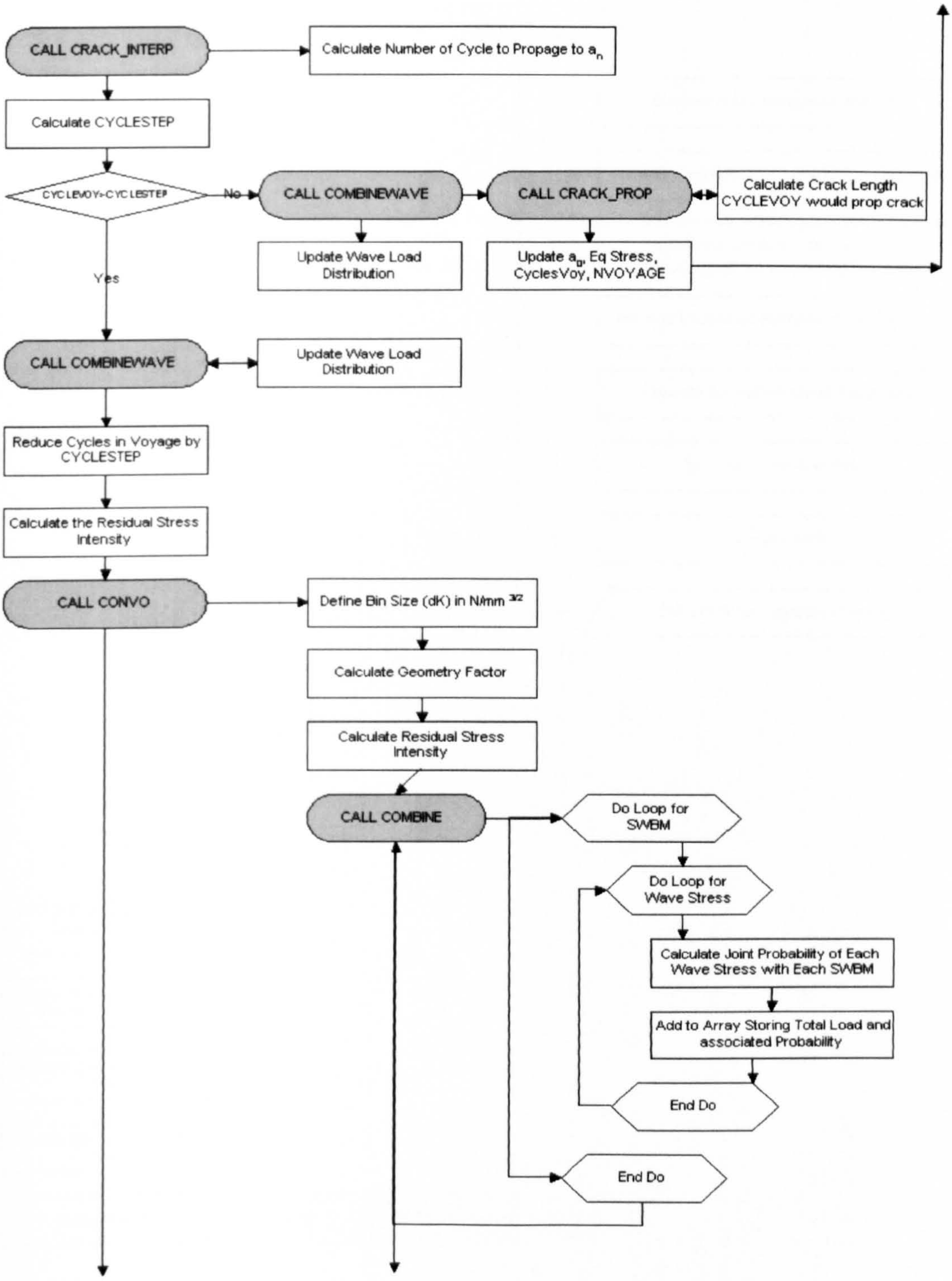
CALL CRACK_INTERP
Calculate Number of Cycle to Propage to a_n
Calculate CYCLESTEP
CYCLEVOY>CYCLESTEP
No
CALL COMBINEWAVE
CALL CRACK_PROP
Calculate Crack Length CYCLEVOY would prop crack
Update Wave Load Distribution
Update a_0, Eq Stress, CyclesVoy, NVOYAGE
Yes
CALL COMBINEWAVE
Update Wave Load Distribution
Reduce Cycles in Voyage by CYCLESTEP
Calculate the Residual Stress Intensity
CALL CONVO
Define Bin Size (dK) in N/mm $^{3/2}$
Calculate Geometry Factor
Calculate Residual Stress Intensity
CALL COMBINE
Do Loop for SWBM
Do Loop for Wave Stress
Calculate Joint Probability of Each Wave Stress with Each SWBM
Add to Array Storing Total Load and associated Probability
End Do
End Do

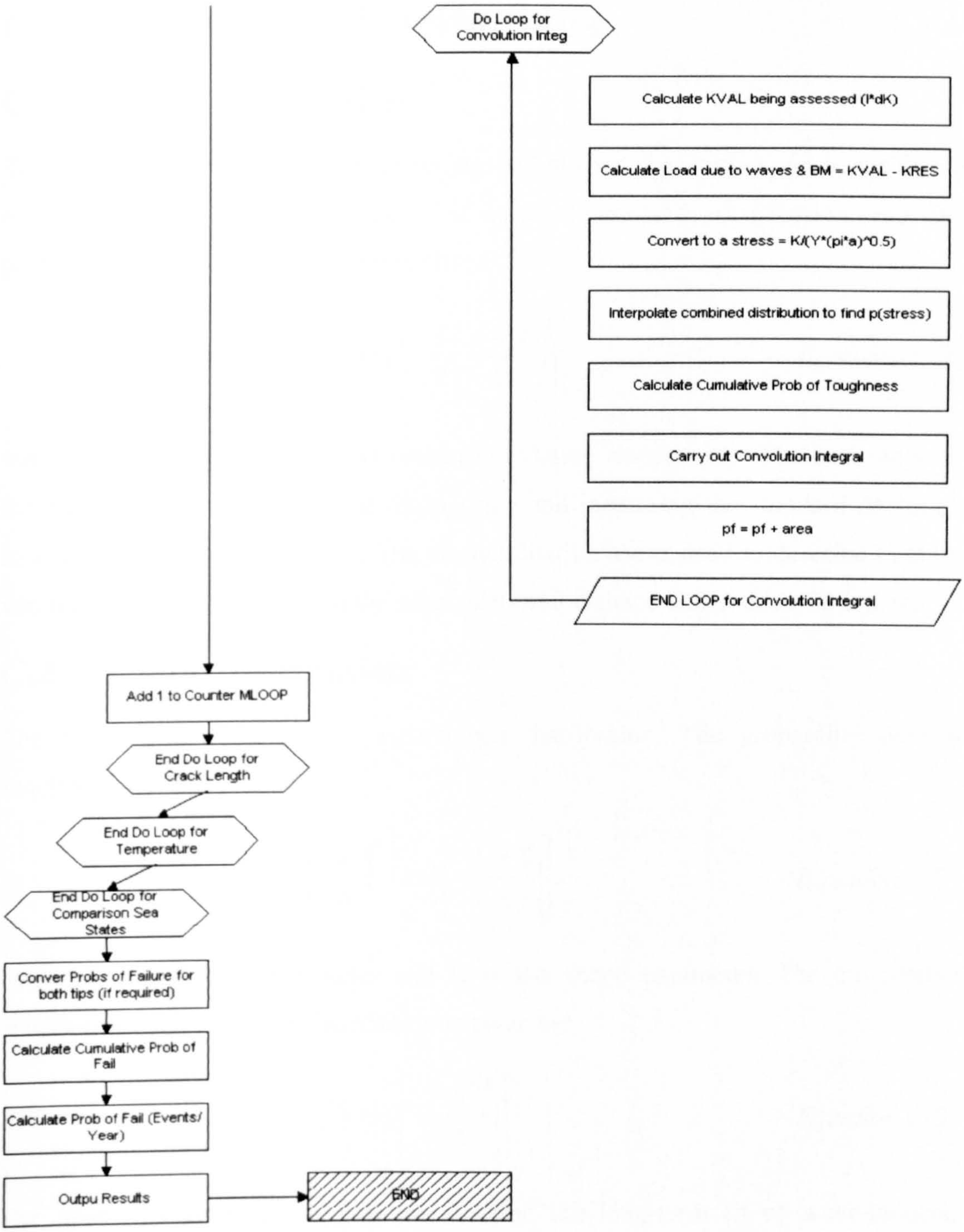
Do Loop for Convolution Integ
Calculate KVAL being assessed (I*dK)
Calculate Load due to waves & BM = KVAL - KRES
Convert to a stress = K/(Y*(pi*a)^0.5)
Interpolate combined distribution to find p(stress)
Calculate Cumulative Prob of Toughness
Carry out Convolution Integral
pf = pf + area
END LOOP for Convolution Integral
Add 1 to Counter MLOOP
End Do Loop for Crack Length
End Do Loop for Temperature
End Do Loop for Comparison Sea States
Conver Probs of Failure for both tips (if required)
Calculate Cumulative Prob of Fail
Calculate Prob of Fail (Events/ Year)
Outpu Results
END

C Summary of distributions

C.1 Normal distribution

The normal distribution has a characteristic bell shaped distribution and is one of the most commonly used distributions. It is a 2-parameter distribution and the probability density function is defined by:

$$p(x)=\frac{1}{\sigma\sqrt{2\pi}}\exp\left[-\frac{1}{2}\left(\frac{x-\mu}{\sigma}\right)^2\right] \qquad \textit{Equation C-1}$$

where μ and σ are the mean and standard deviation respectively. The bell shape of the distribution is centred on the mean value and increasing the standard deviation increases the spread of the data. The normal distribution is used to describe random variables whose values take on the same distribution shape either side of the mean.

C.2 Weibull distribution

The Weibull distribution is a 2-parameter distribution. The probability density function is given by:

$$p(x)=\frac{B}{A}\left(\frac{x}{A}\right)^{B-1}\exp\left[-\left(\frac{x}{A}\right)^{B}\right] \qquad \textit{Equation C-2}$$

where A is the scale parameter and B is the shape parameter. The cumulative distribution function of the distribution is given by:

$$P(x)=1-\exp\left[-\left(\frac{x}{A}\right)^{B}\right] \qquad \textit{Equation C-3}$$

The Weibull distribution is used to describe the long-term fit of wave-induced stresses for both peak and fatigue values. For fatigue analysis the m-th moment is input into Paris Law. This is calculated from:

$$E\left[\Delta\sigma^{m}\right]=A^{m}\Gamma\left(1+\frac{m}{B}\right) \qquad \textit{Equation C-4}$$

C.3 Rayleigh distribution

The Rayleigh distribution is a special case of the Weibull distribution with a scale parameter of $\sqrt{2}\sigma$ and a shape parameter of 2. It is a single parameter distribution, i.e. it is described by only one variable. The probability density function of the Rayleigh distribution is given by:

$$p(x)=\frac{x}{\sigma^2}\exp\left[-\frac{1}{2}\left(\frac{x}{\sigma}\right)^2\right] \qquad \textit{Equation C-5}$$

The m-th expected moment is given by:

$$E[\Delta\sigma^m]=\left(2\sqrt{2}\sigma_x\right)^m\Gamma\left(1+\frac{m}{2}\right) \qquad \textit{Equation C-6}$$

C.4 Exponential distribution

The exponential distribution is a special case of the Weibull distribution with a shape parameter of 1.0. This distribution plots as a straight line on a log scale. The probability density function of this distribution is given by:

$$p(x)=\frac{1}{A}\exp\left[-\left(\frac{x}{A}\right)\right] \qquad \textit{Equation C-7}$$

C.5 Extreme Type 1 distribution

The extreme Type 1 distribution describes the distribution of the largest values in N peaks. For example, if 1000 ships were to set sail in a sea state for 4 hours and the maximum stress they experienced was recorded the distribution would tend to the extreme value distribution. The probability density function of this distribution is given by:

$$p(x)=a.\exp\left(-a(x-u)-e^{-a(x-u)}\right) \qquad \textit{Equation C-8}$$

where u is the most probable value and can be found for the Weibull distribution from:

$$u=A[\ln(N)]^{1/B} \qquad \textit{Equation C-9}$$

where α is the measure of the dispersion. This is calculated by multiplying the number of cycles by the probability of the mode, u, in the parent distribution:

$$a = N.p_{Weibull}(u) \qquad \textit{Equation C-10}$$

The cumulative distribution function of this distribution is given by:

$$P(x) = \exp[-\exp(-\alpha(x-u))] \qquad \textit{Equation C-11}$$

D Sea state fits

D.1 Flowchart of fitting procedure

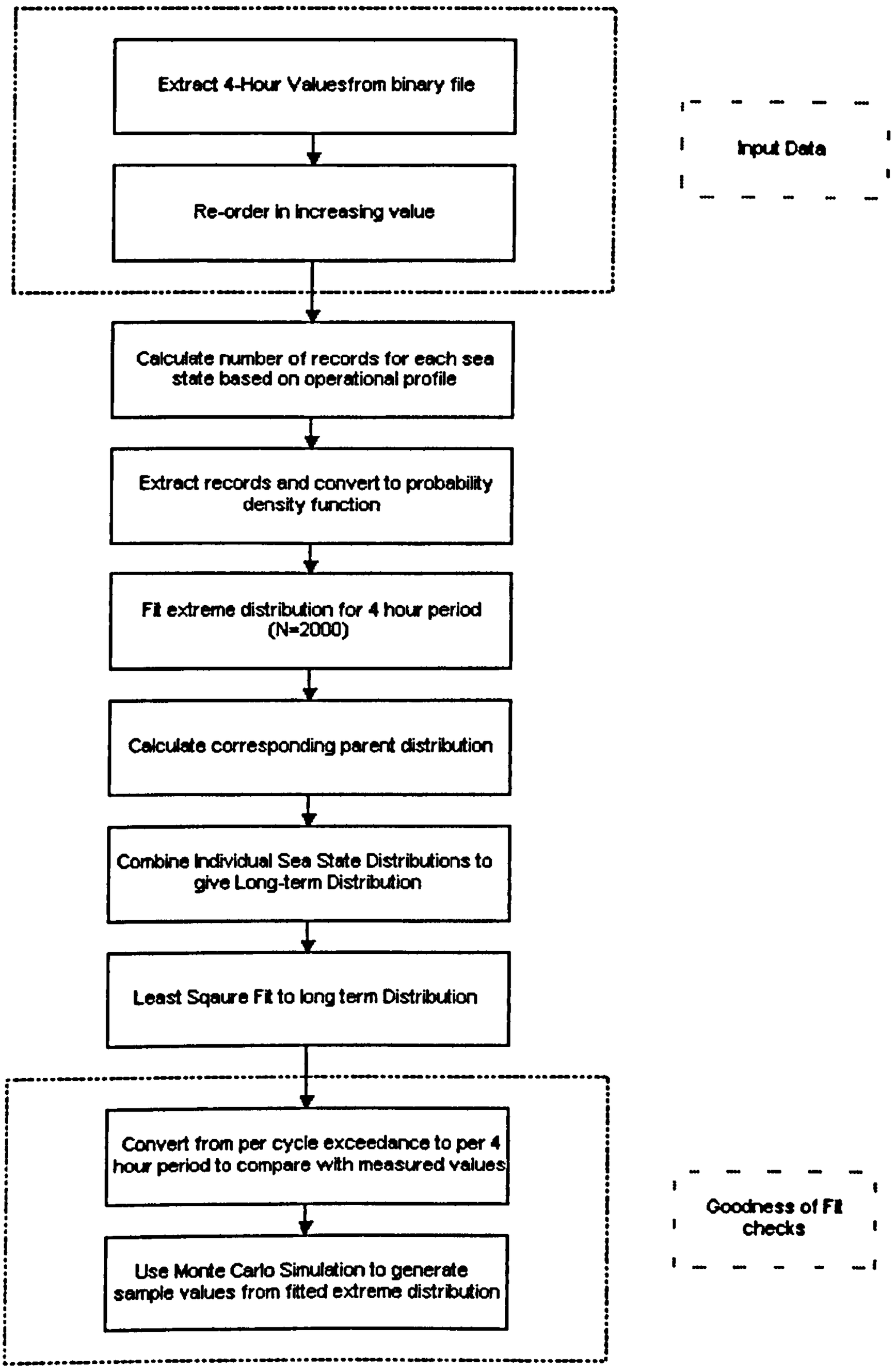

D.2 Sea state fit parameters

	Weibull co-efficients	
Sea state	**A**	**B**
8	16.90	1.72
7	11.50	1.64
6	10.00	1.88
5	7.84	1.95
4	5.56	1.85
3	4.65	2.02
2	3.65	2.02

Table D-1 Weibull co-efficients describing per cycle distribution of wave induced bending stress for hog response

	Weibull co-efficients	
Sea state	**A**	**B**
8	19.29	1.46
7	12.17	1.36
6	8.76	1.41
5	7.38	1.61
4	5.55	1.68
3	4.83	1.94
2	4.62	2.35

Table D-2 Weibull co-efficients describing per cycle distribution of wave induced bending stress for sag response

D.3 Least squares methodology

A regression analysis tries to predict the y-value for a given x-value. The y-value is called the dependent variable and the x-value called the independent variable, because a change in x-value leads directly to a change in the y-value.

A least squares linear regression analysis describes this change in the y-value as the x-value changes by a straight line. This is fitted by minimising the sum of the squares of the deviation of the data points from the straight line. The equation of the line of best fit is then given by:

Slope:

$$m = \frac{\sum (x - \bar{x})(y - \bar{y})}{\sum (x - \bar{x})^2} \qquad \textit{Equation D-1}$$

Intercept:

$$c = \frac{1}{n}\left(\sum y - m.\sum x\right) \qquad \textit{Equation D-2}$$

where: $\bar{x}$ is the mean value of the x data points.

$\bar{y}$ is the mean value of the y data points.

The Weibull function can then be manipulated to the form of a straight line, allowing an estimate of A and B to be made.

Probability of exceedance:

$$P(x) = \exp\left(-x/A\right)^B \qquad \textit{Equation D-3}$$

Convert to a form y=mx+c:

$$\begin{aligned} \ln(P(x)) &= \left(-x/A\right)^B \\ -\ln(P(x)) &= \left(x/A\right)^B \\ \ln[-\ln(P(x))] &= B\ln\left(x/A\right) \\ \ln[-\ln(P(x))] &= B\ln(x) - B\ln(A) \end{aligned} \qquad \textit{Equation D-4}$$

D.4 Least squares fits for long-term operation

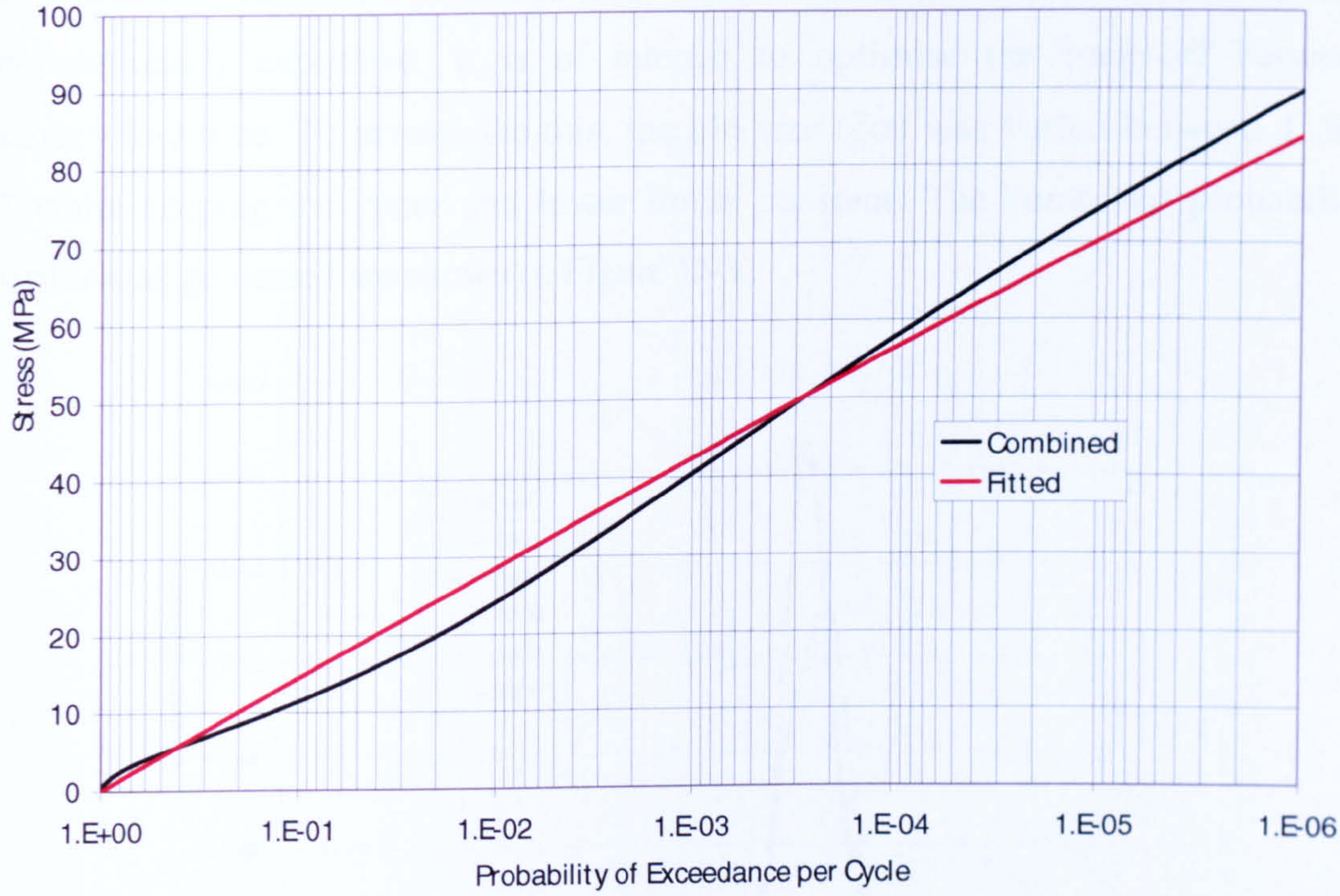

Figure D-1 Long term sagging fit to Lloyd's Register operational profile

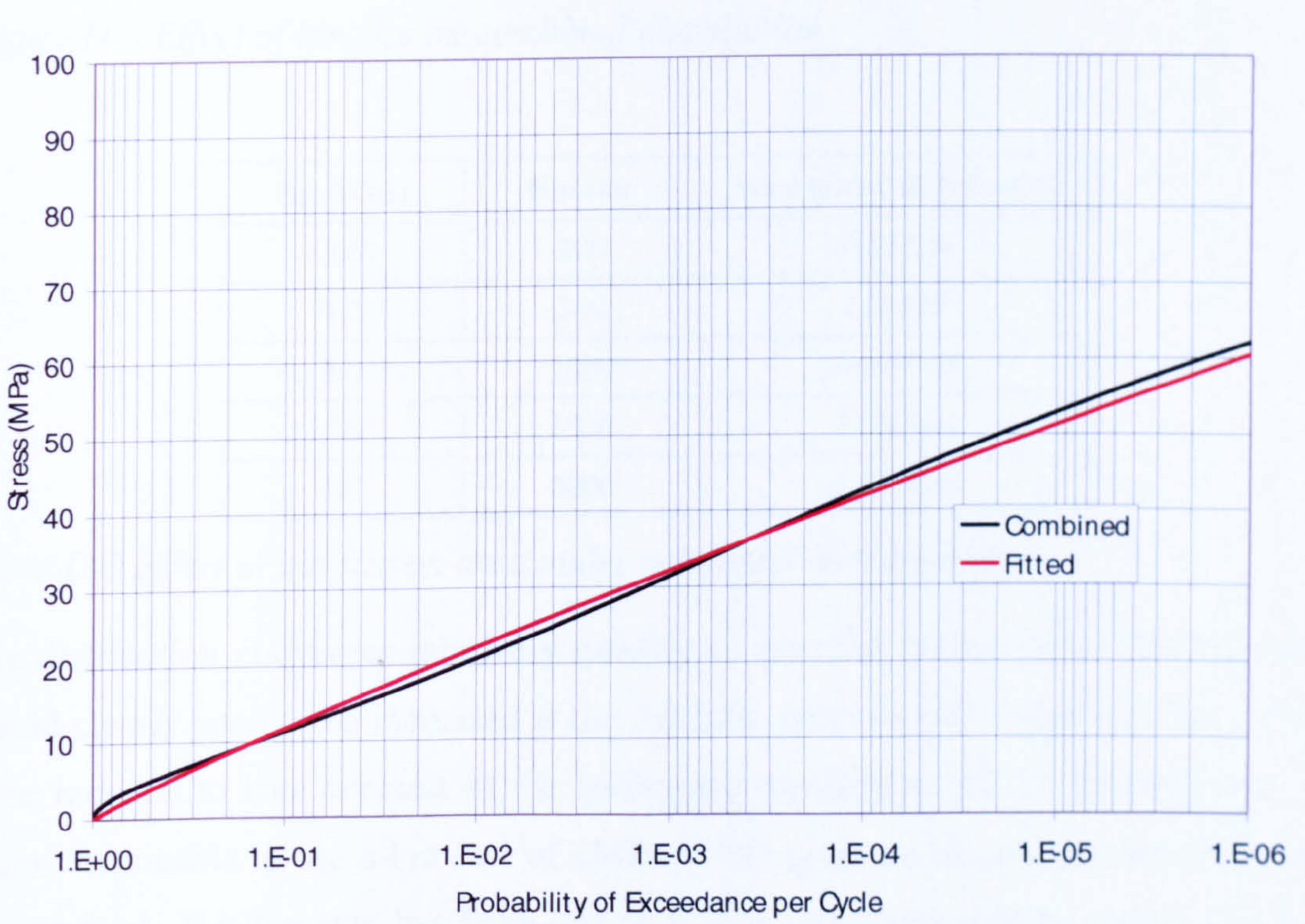

Figure D-2 Long term hogging fit to Lloyd's Register operational profile

D.5 Combined still water and bending stress distribution

The numerical integration described in Section 4.6 is 2-dimensional and as such is computationally expensive. It is of interest to optimise the trade-off between accuracy and time. To investigate this, the bin size ($\delta\sigma$) was varied between 1 and 6.7 while keeping the upper and lower limits constant. The combined probability distributions generated are shown in Figure D-3.

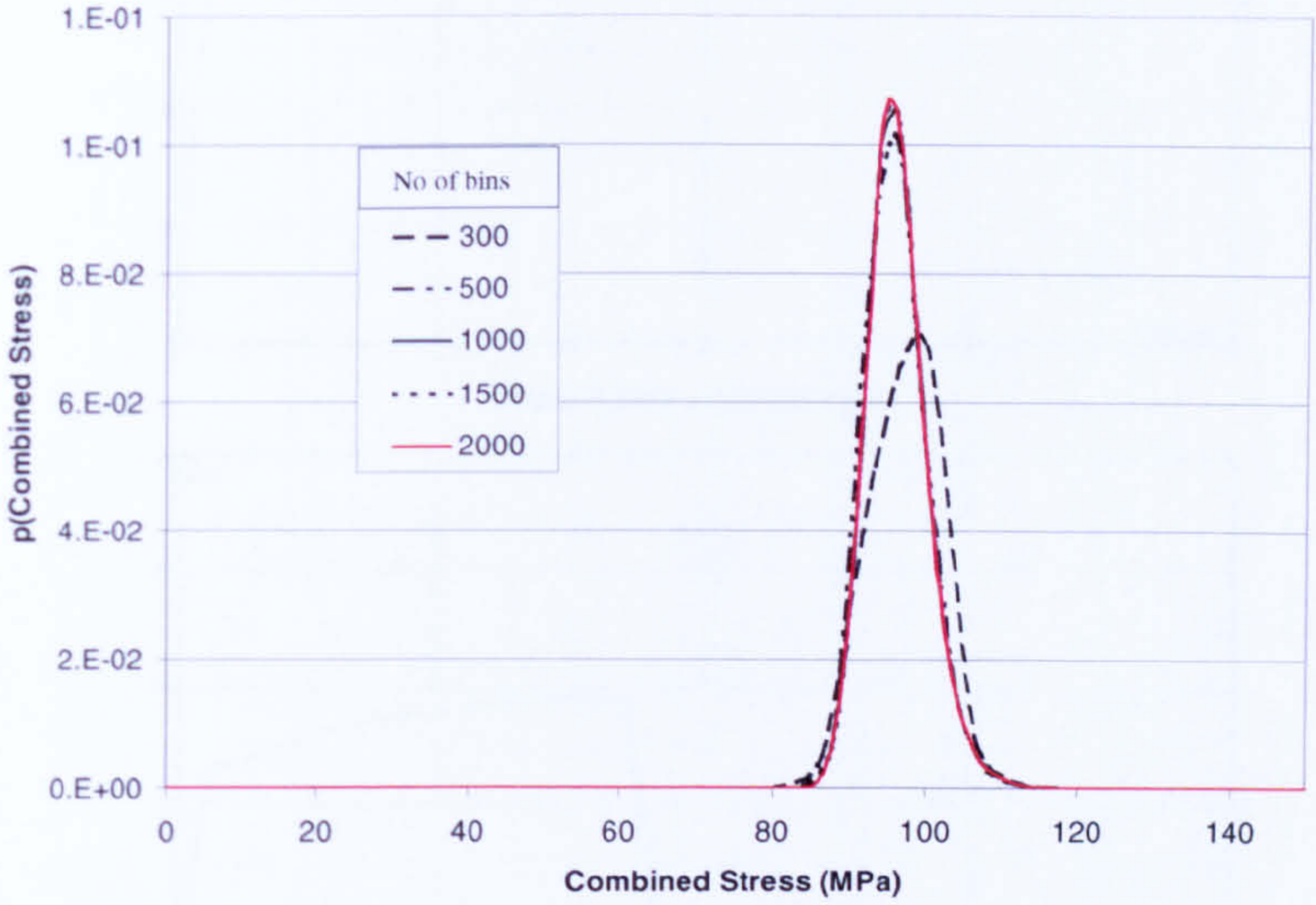

Figure D-3 Effect of bin size on combined distribution

$\delta\sigma$ (MPa)	Bin size	Area under distribution
6.667	300	0.87229
4.0	500	1.01548
2.0	1000	0.999983
1.333	1500	1.000000
1.0	2000	1.000000

Table D-3 Effect of bin size on area under combined distribution

The distribution converges relatively quickly to give the correct area. The bin size would clearly need to be increased if the extreme stress or still water bending stress were reduced to take account of the increasing slenderness of the distributions. It seems reasonable to use a bin size of 1MPa in the program to give the desired level of accuracy. The bin size has been left as a user input so could be reduced if the calculation time was felt to be prohibitive.

E Material fracture toughness

E.1 Example trace of toughness tests

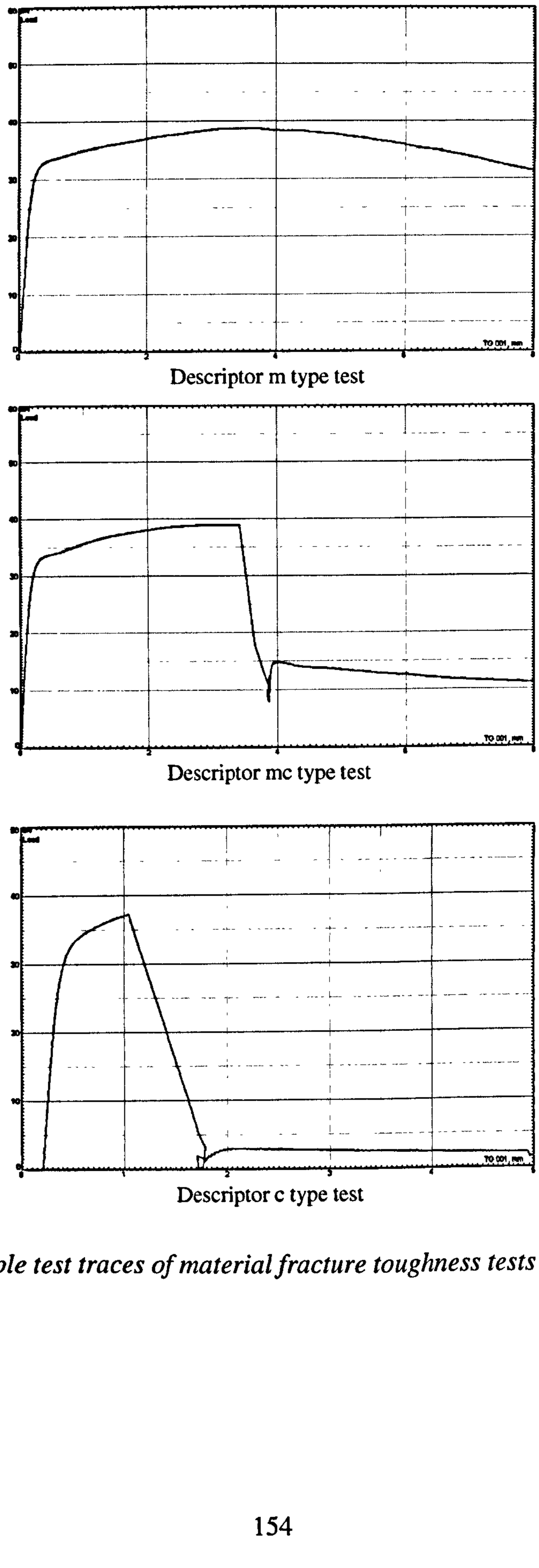

Descriptor m type test

Descriptor mc type test

Descriptor c type test

Figure E-1 Example test traces of material fracture toughness tests

E.2 Toughness data

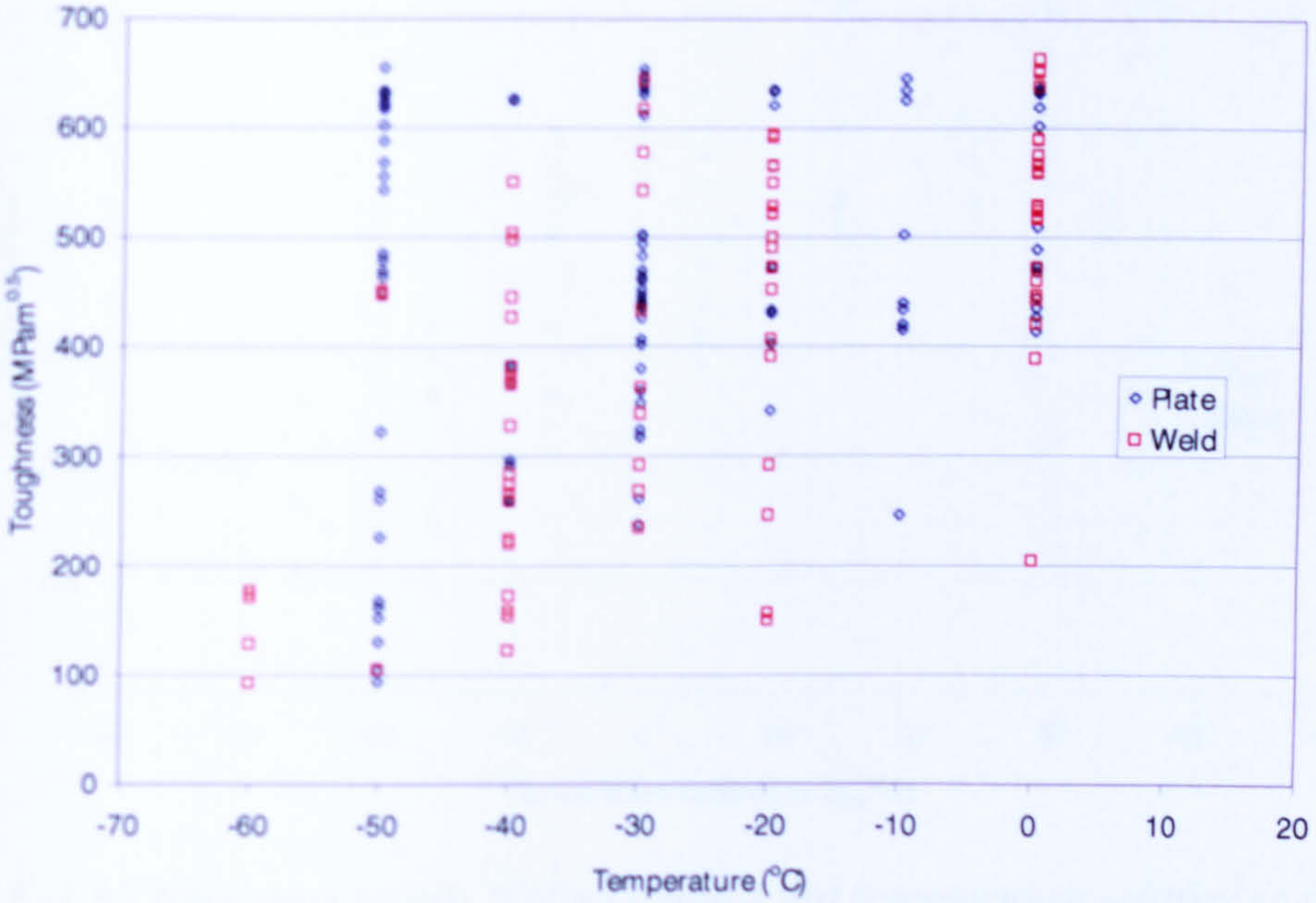

Figure E-2 All toughness results plotted against test temperature

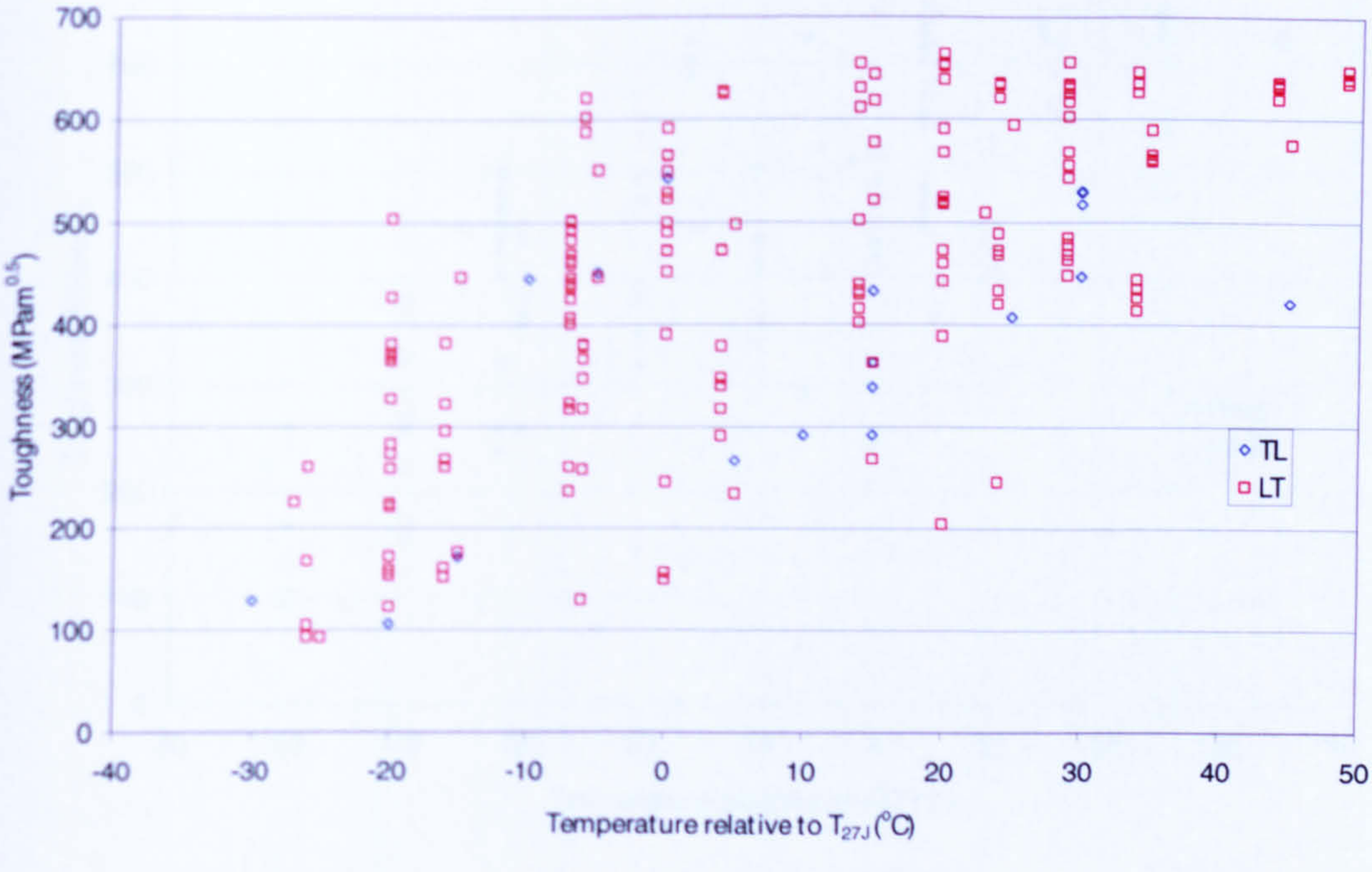

Figure E-3 All toughness results plotted against test temperature showing effects of rolling direction

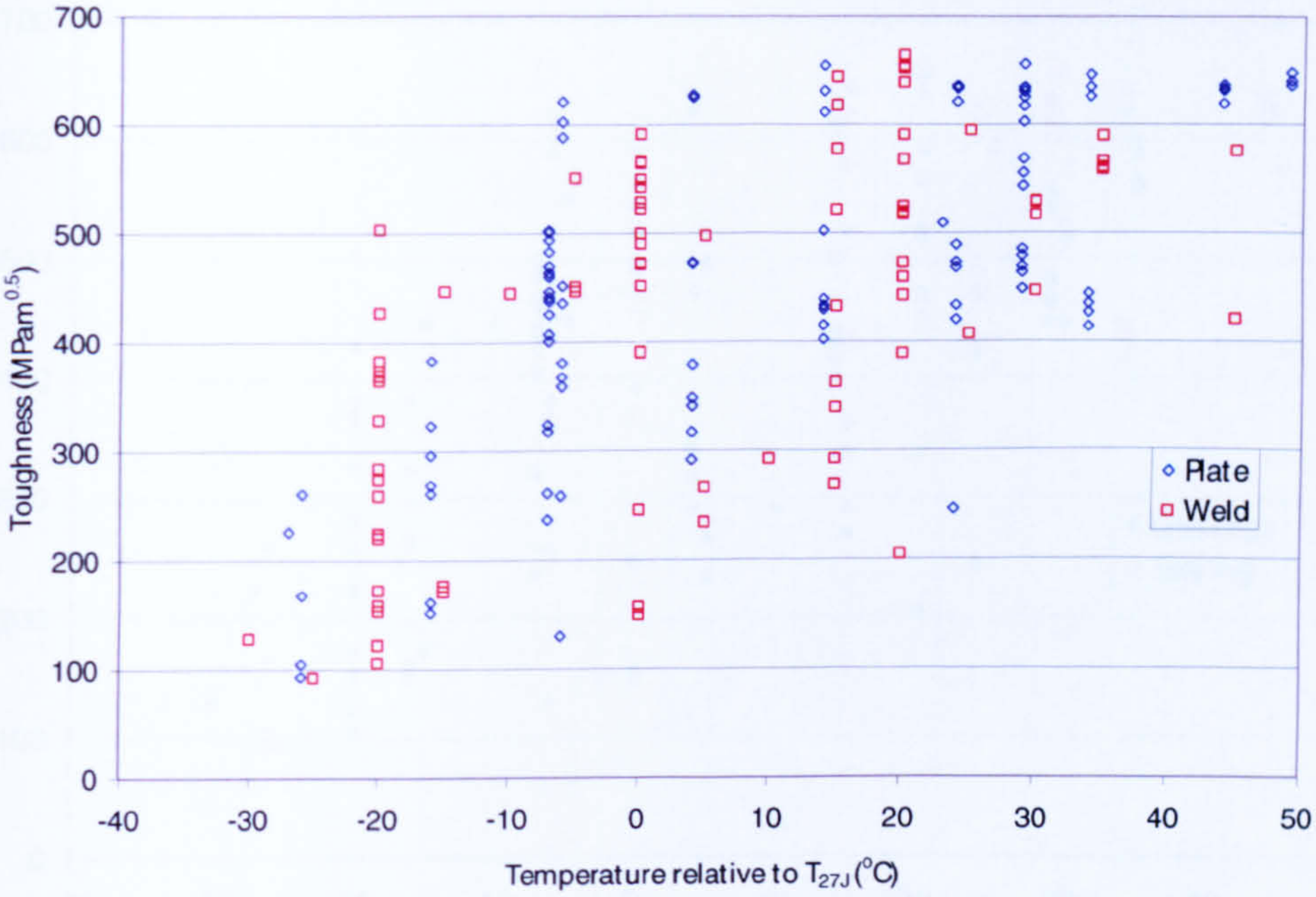

Figure E-4 All toughness results plotted against test temperature relative to Charpy 27J temperature

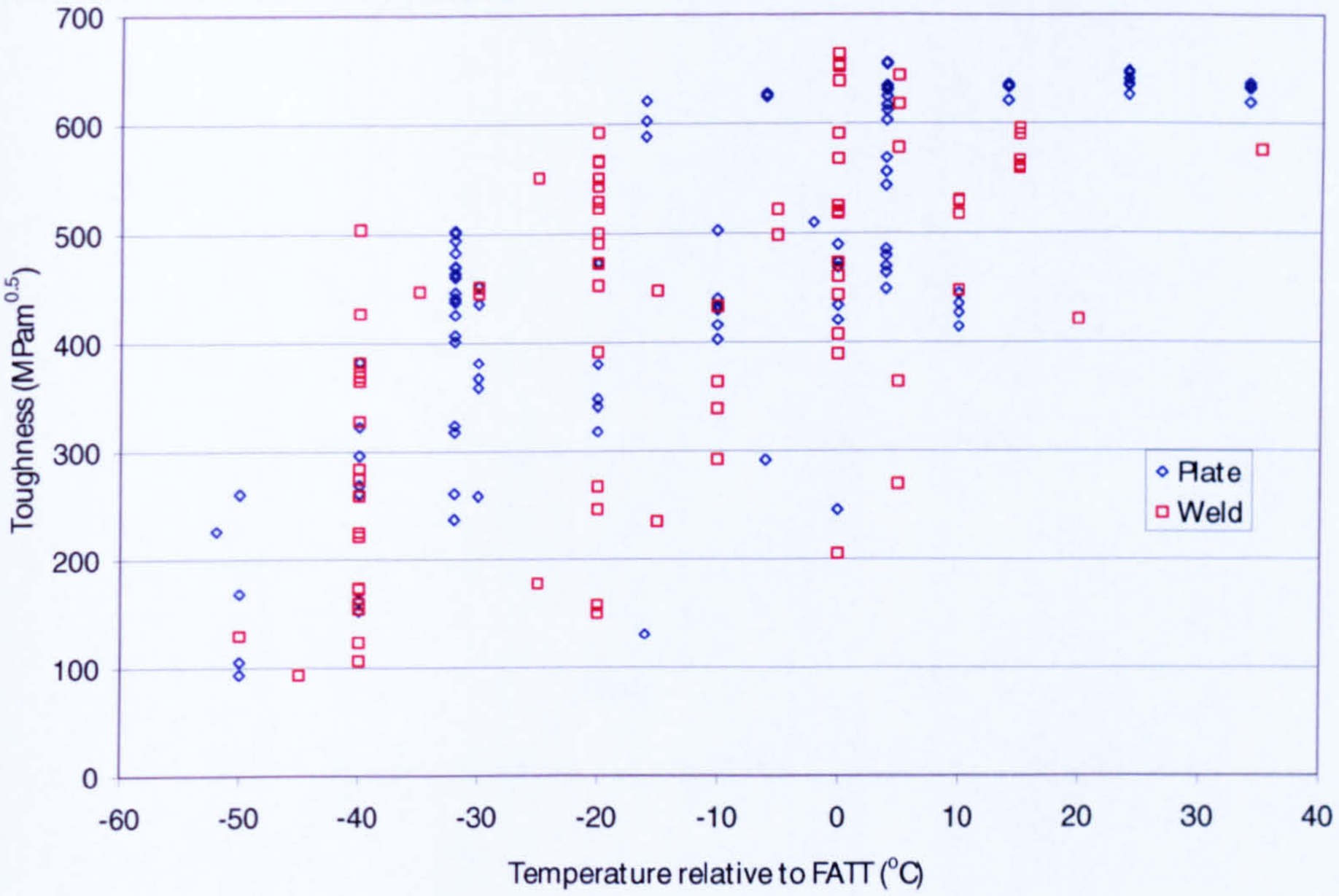

Figure E-5 All toughness results plotted against test temperature relative to FATT

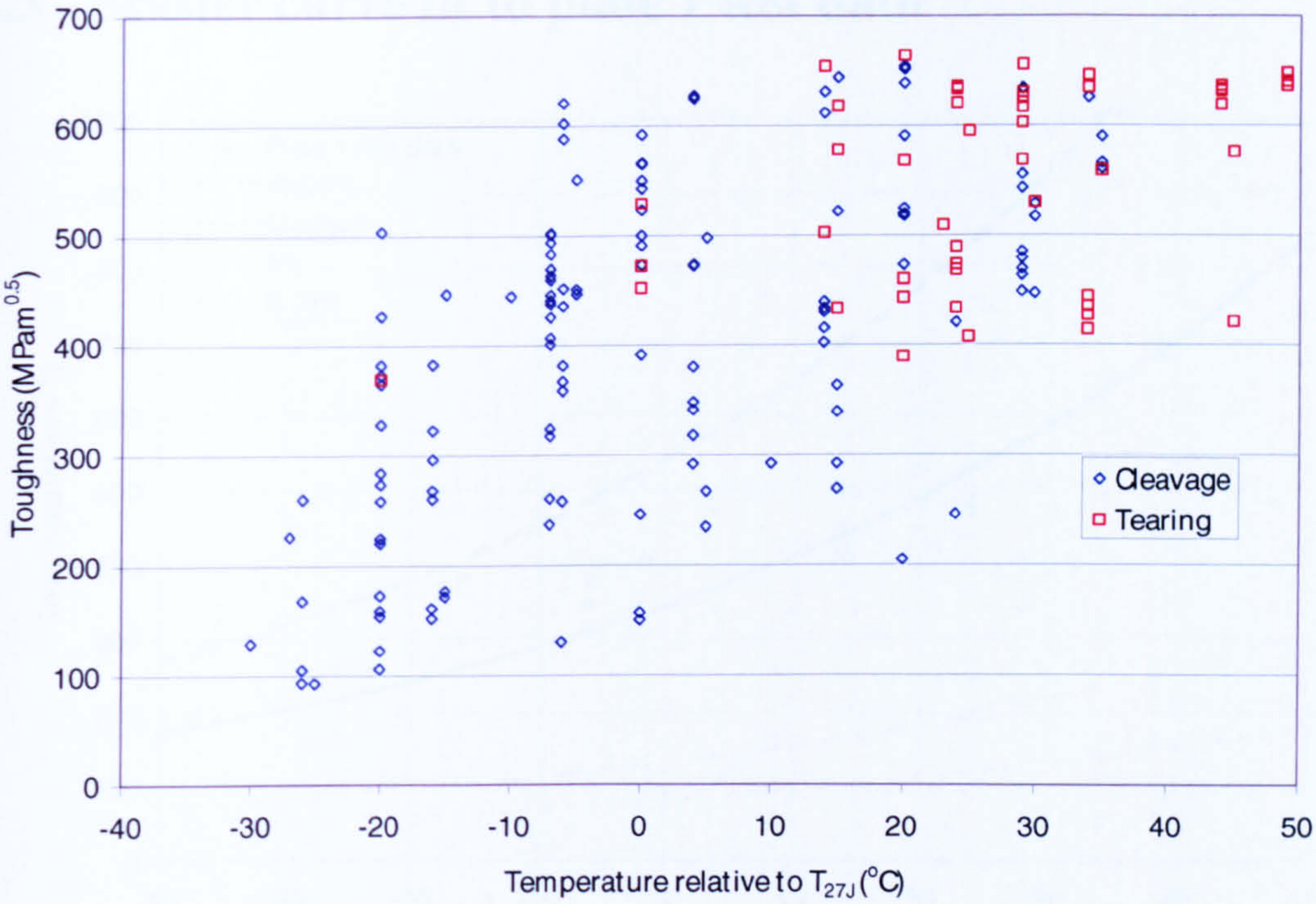

Figure E-6 All toughness results plotted against test temperature relative to Charpy 27J temperature – mode of failure

E.3 Master curve fit to plate 1 test data

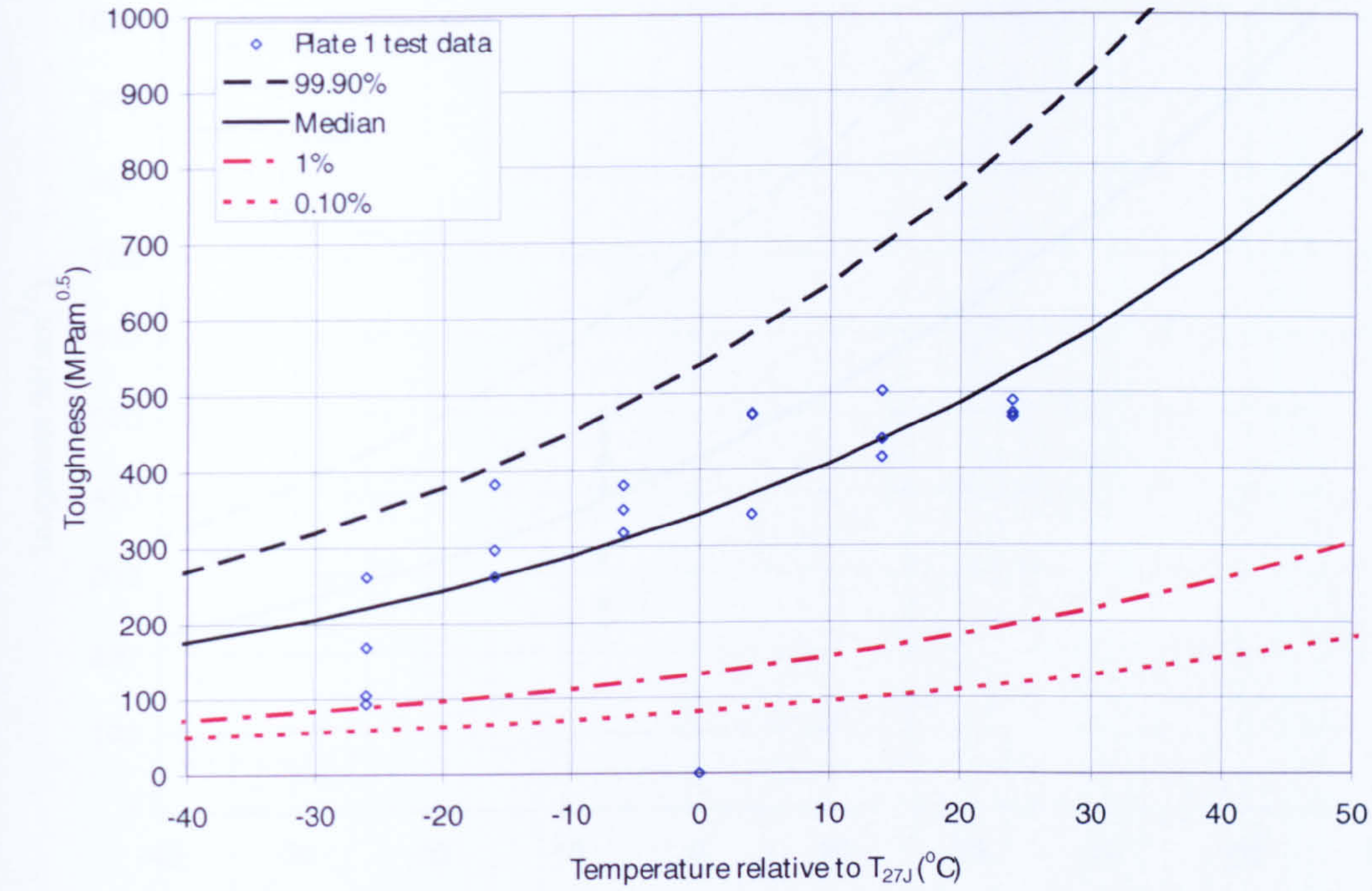

Figure E-7 Master curve fit to plate 1 test data

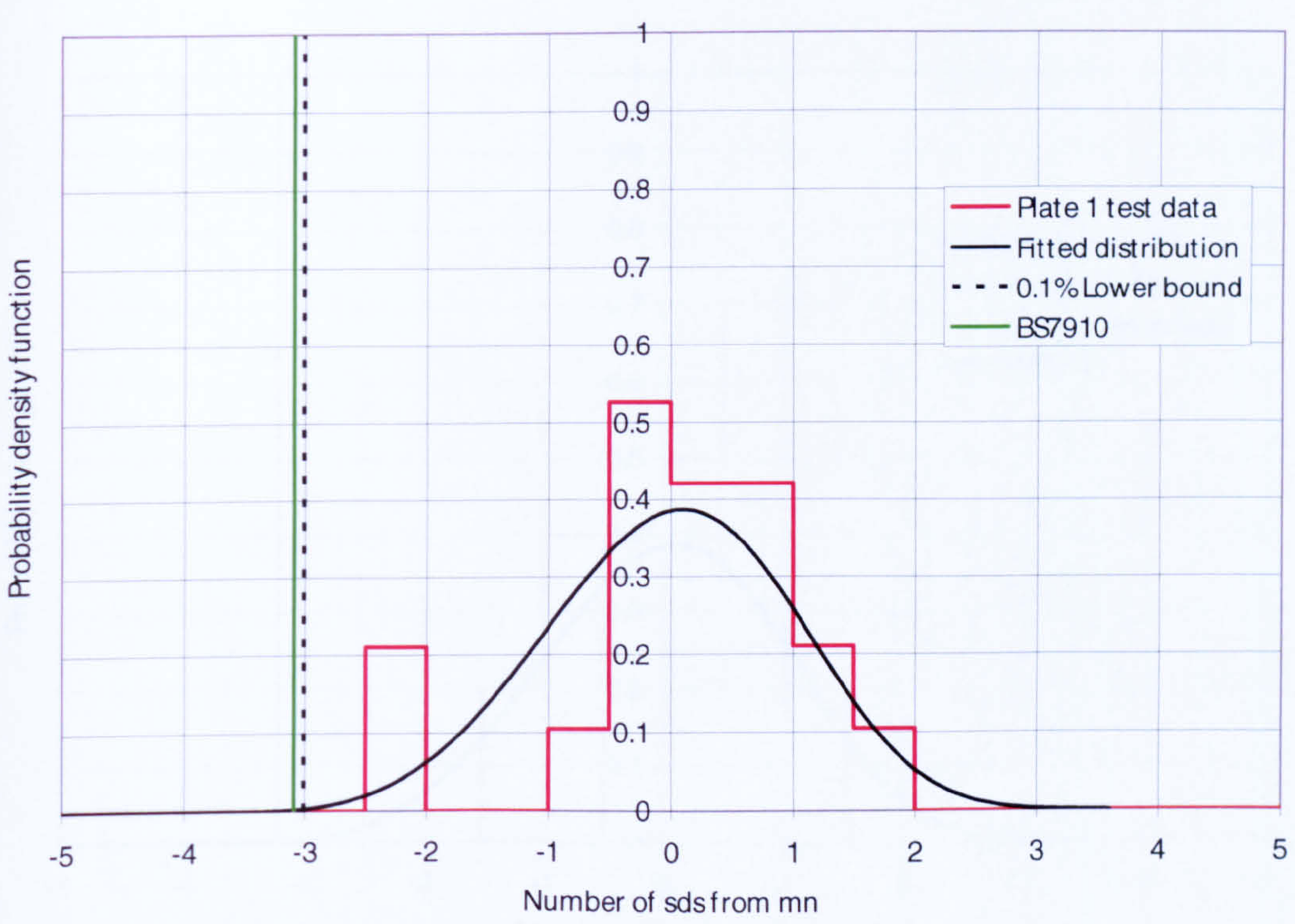

Figure E-8 Normalised scatter plot of master curve fit to plate 1 test data

E.4 Master curve fit to plate 2 test data

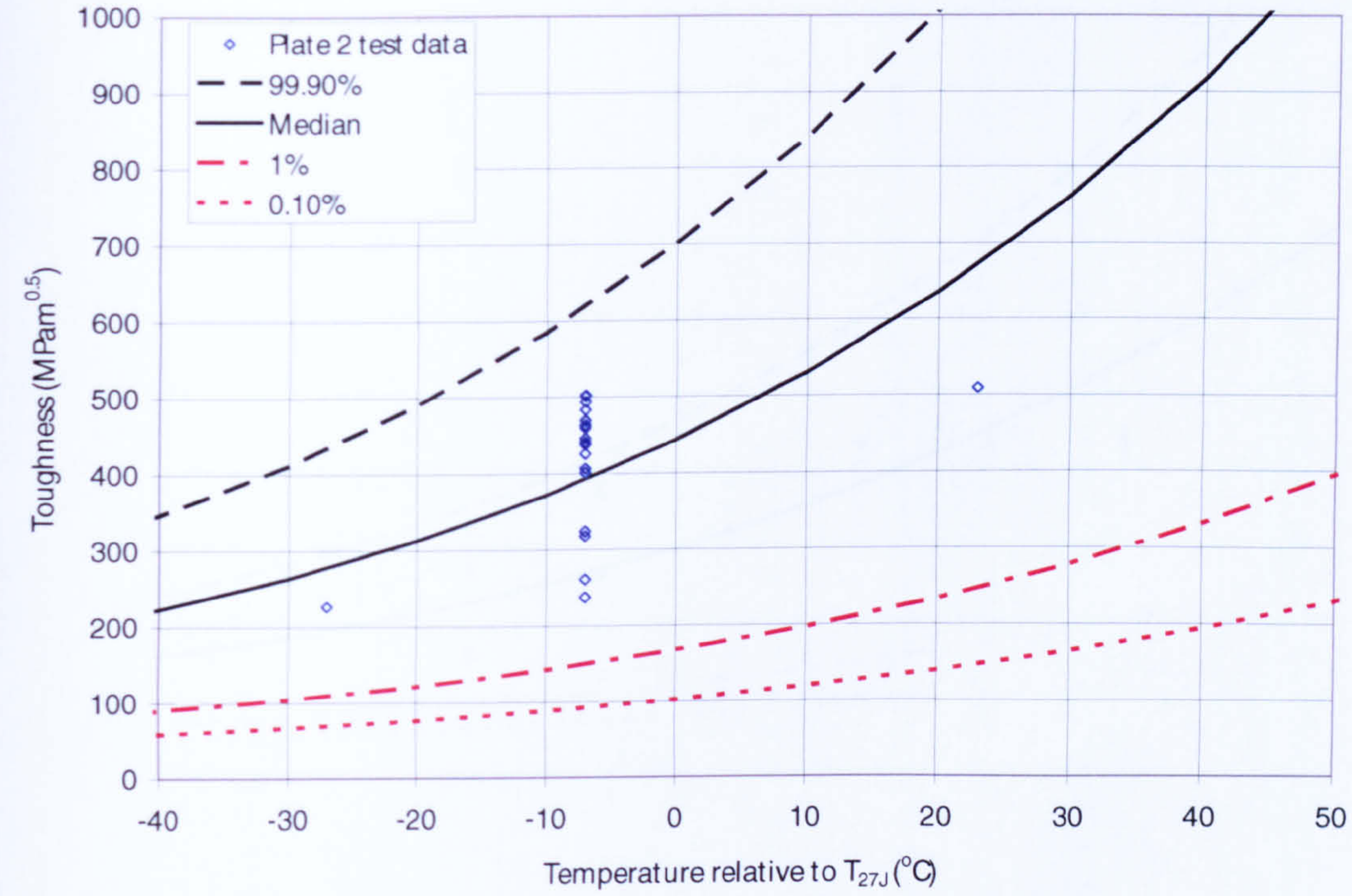

Figure E-9 Master curve fit to plate 2 test data

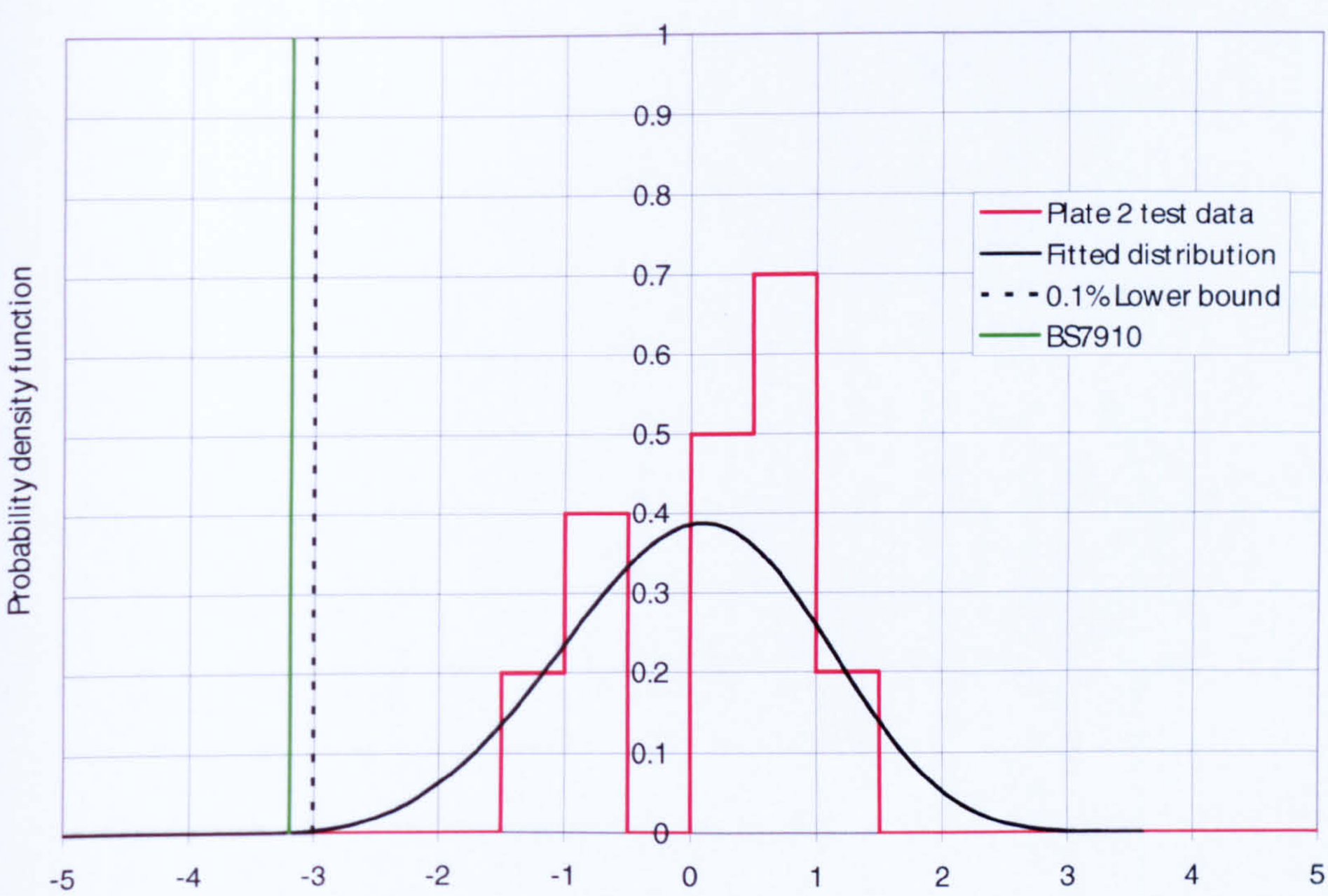

Figure E-10 Normalised scatter plot of master curve fit to plate 2 test data

E.5 Master curve fit to plate 3 test data

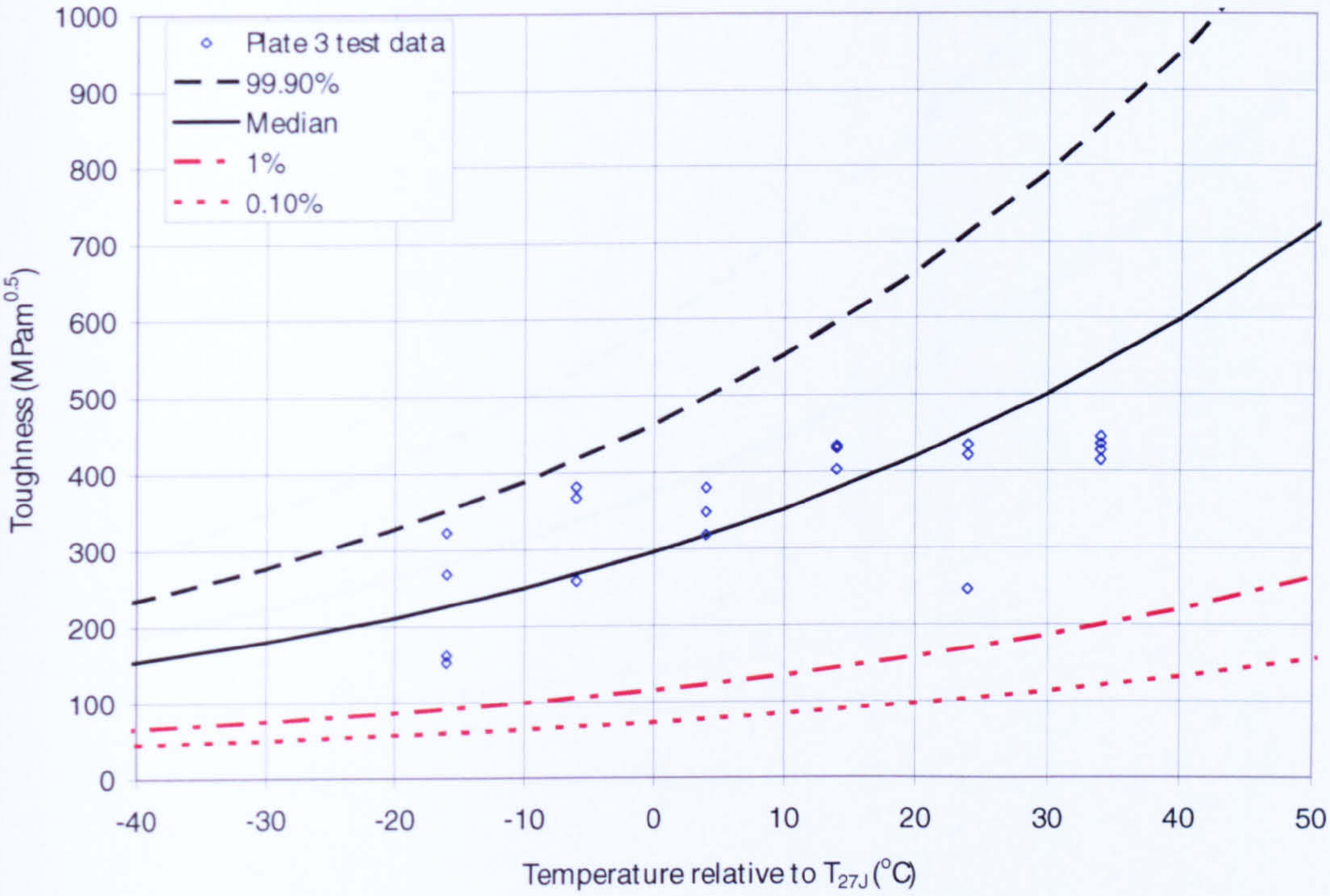

Figure E-11 Master curve fit to plate 3 test data

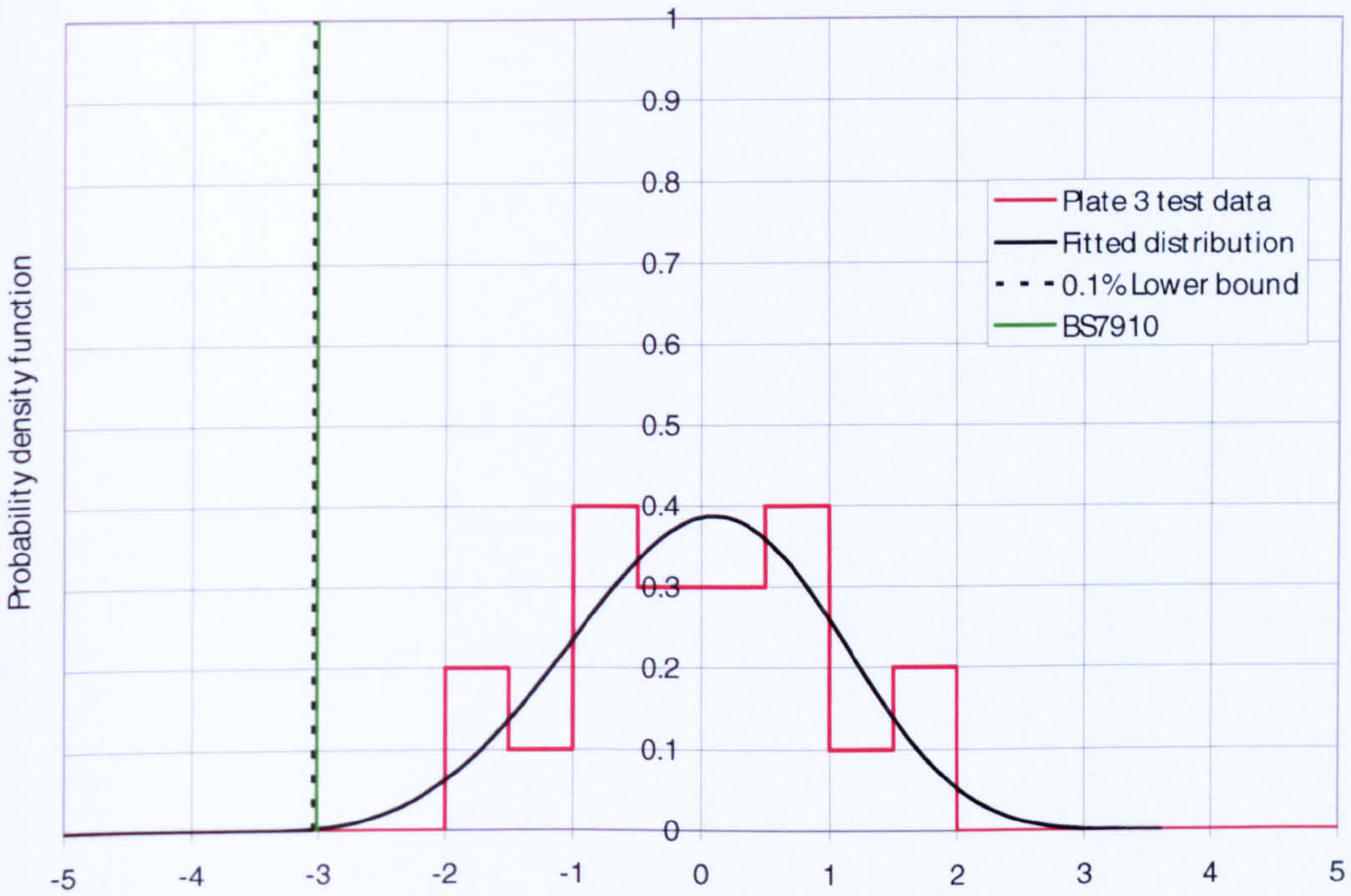

Figure E-12 Normalised scatter plot of master curve fit to plate 3 test data

E.6 Master curve fit to plate 4 test data

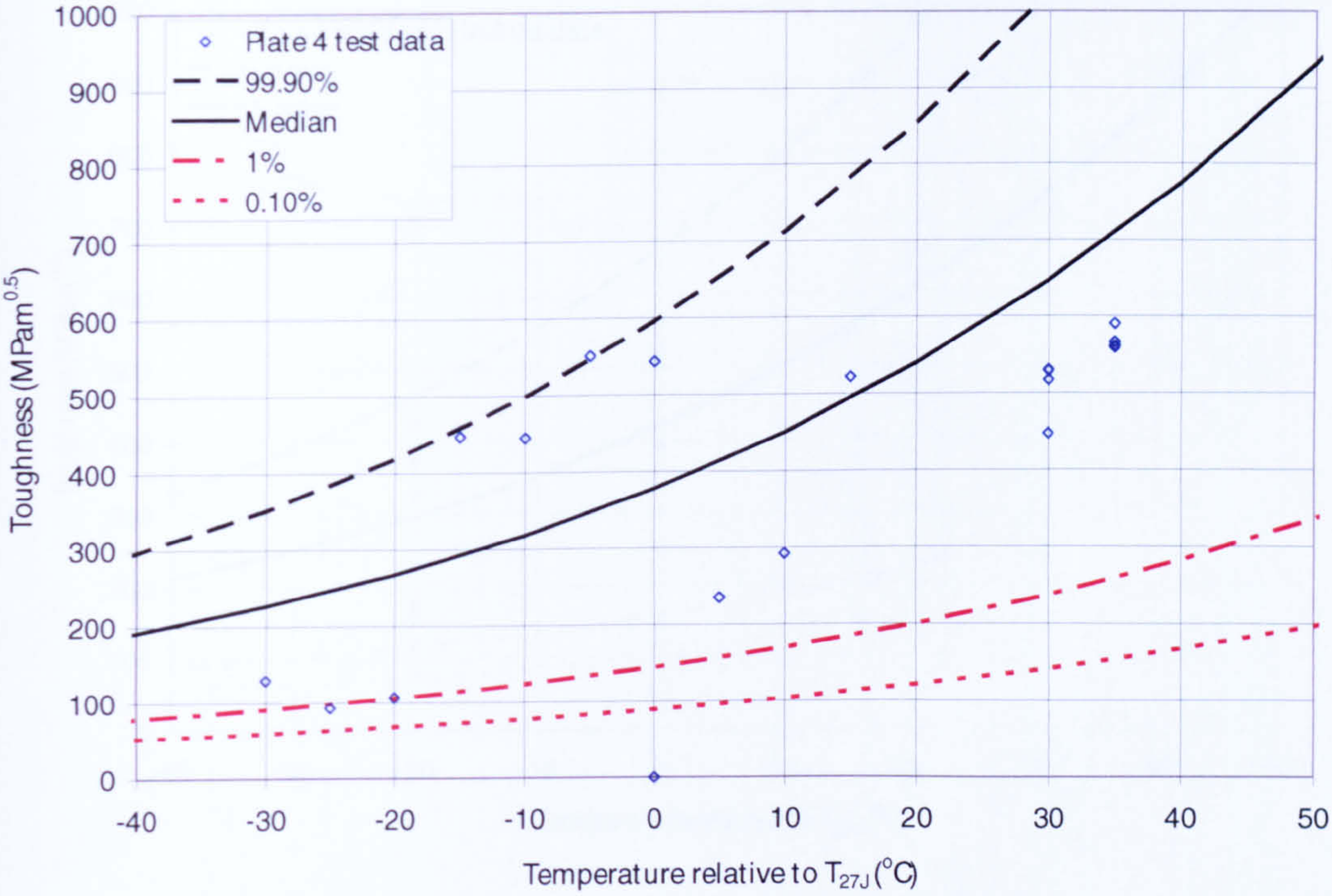

Figure E-13 Master curve fit to plate 4 test data

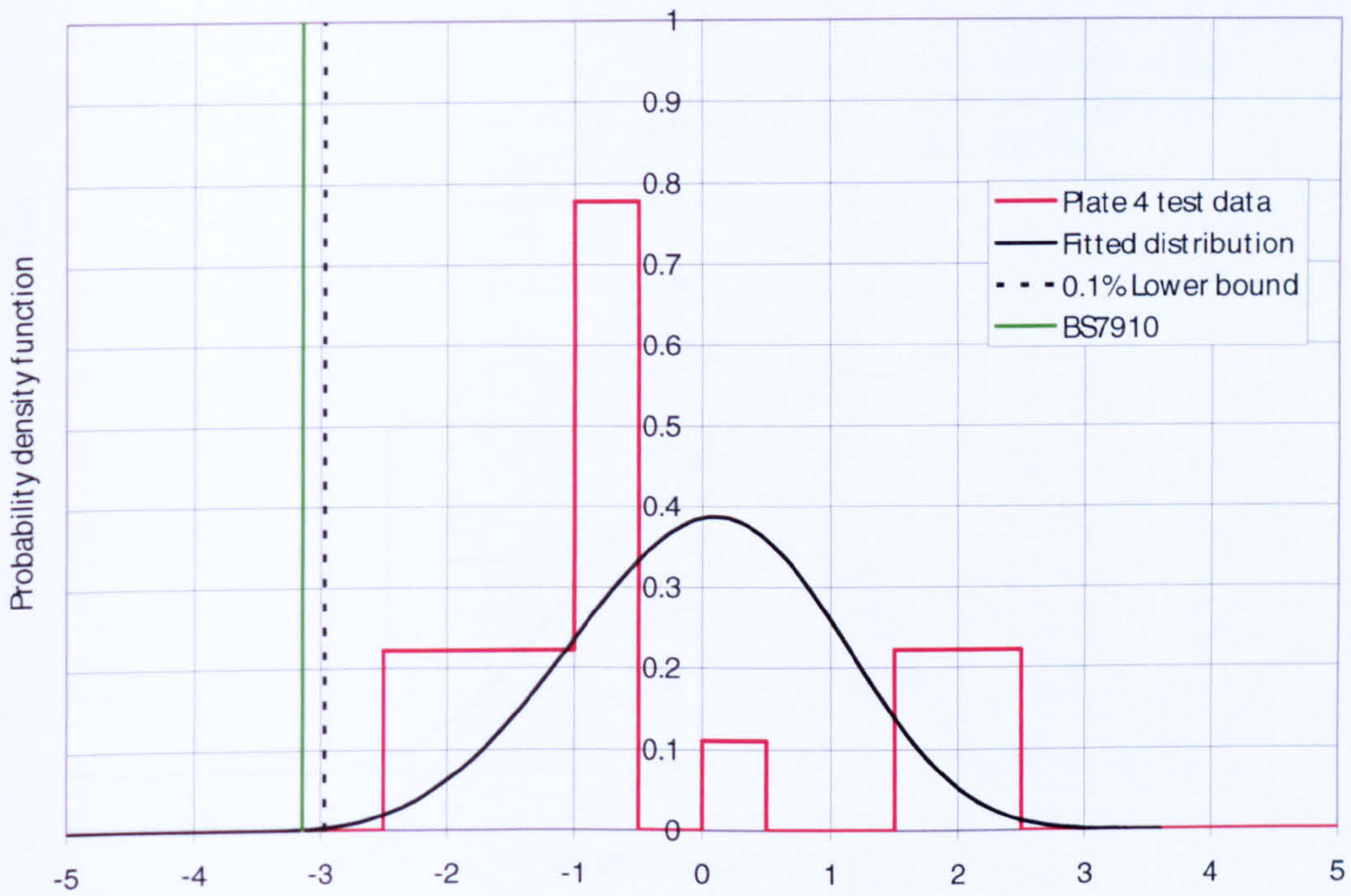

Figure E-14 Normalised scatter plot of master curve fit to plate 4 test data

E.7 Master curve fit to plate 4 weld and HAZ test data

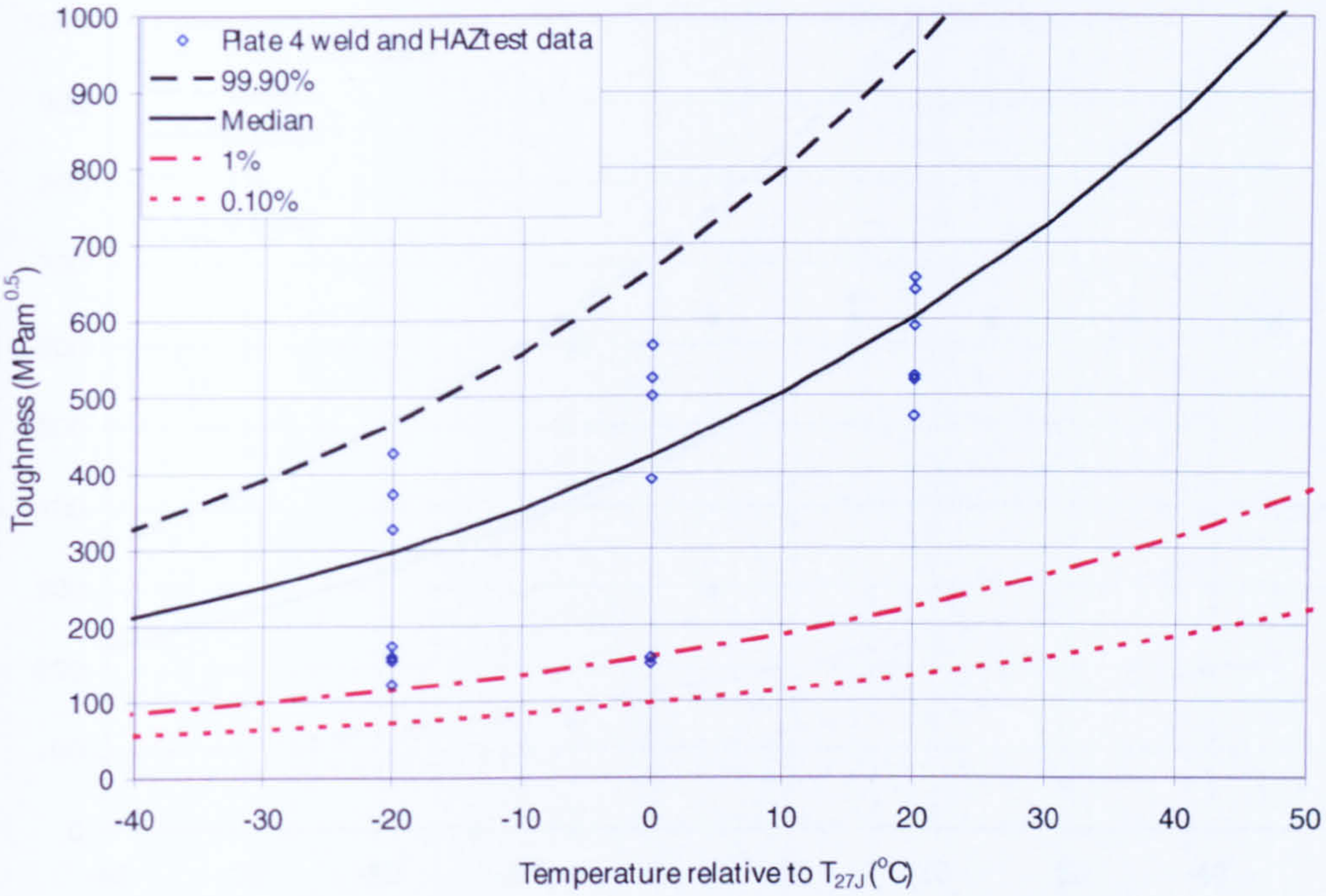

Figure E-15 Master curve fit to plate 4 weld and HAZ test data

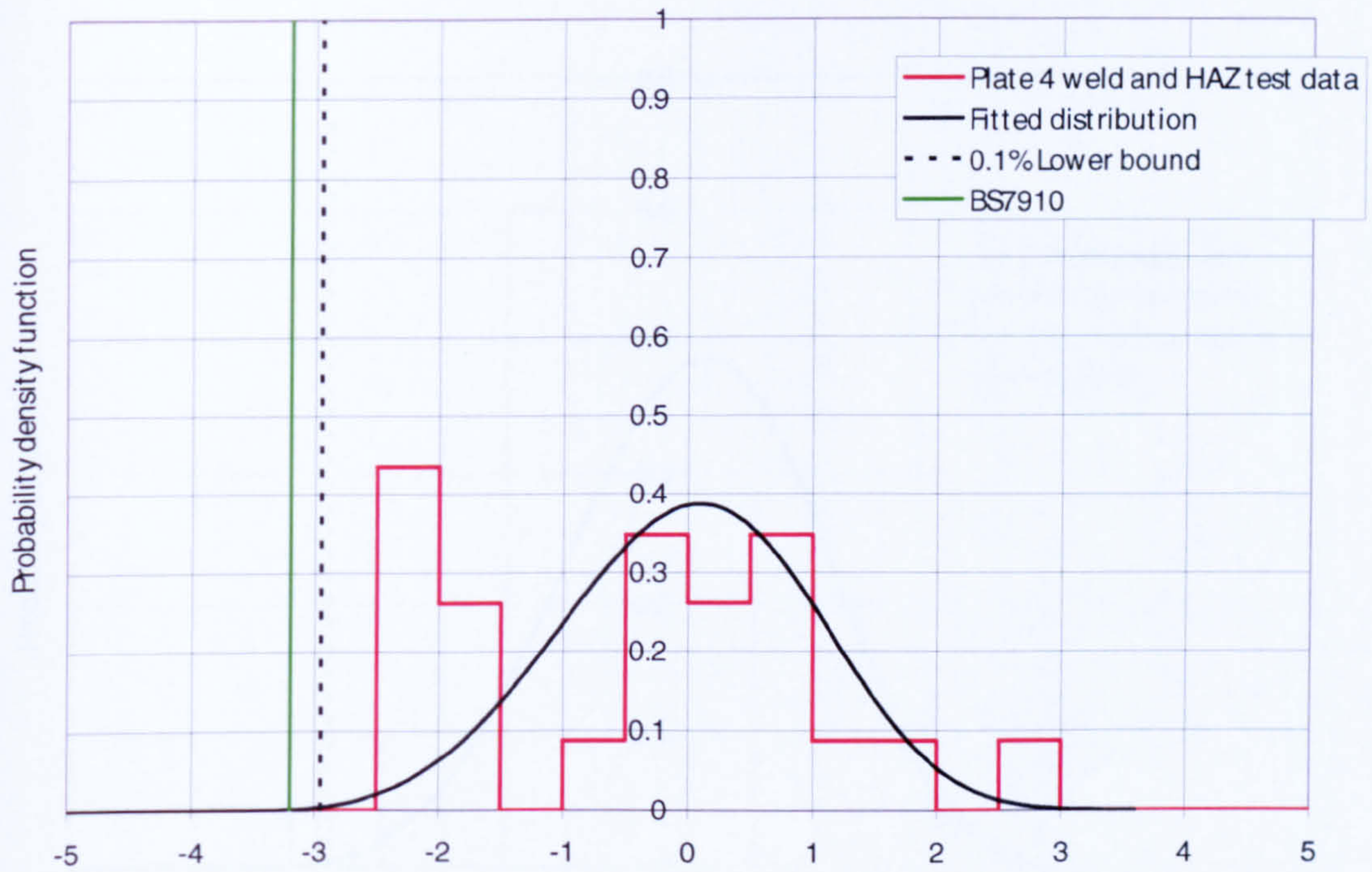

Figure E-16 Normalised scatter plot of master curve fit to plate 4 weld and HAZ test data

E.8 Master curve fit to plate 5 test data

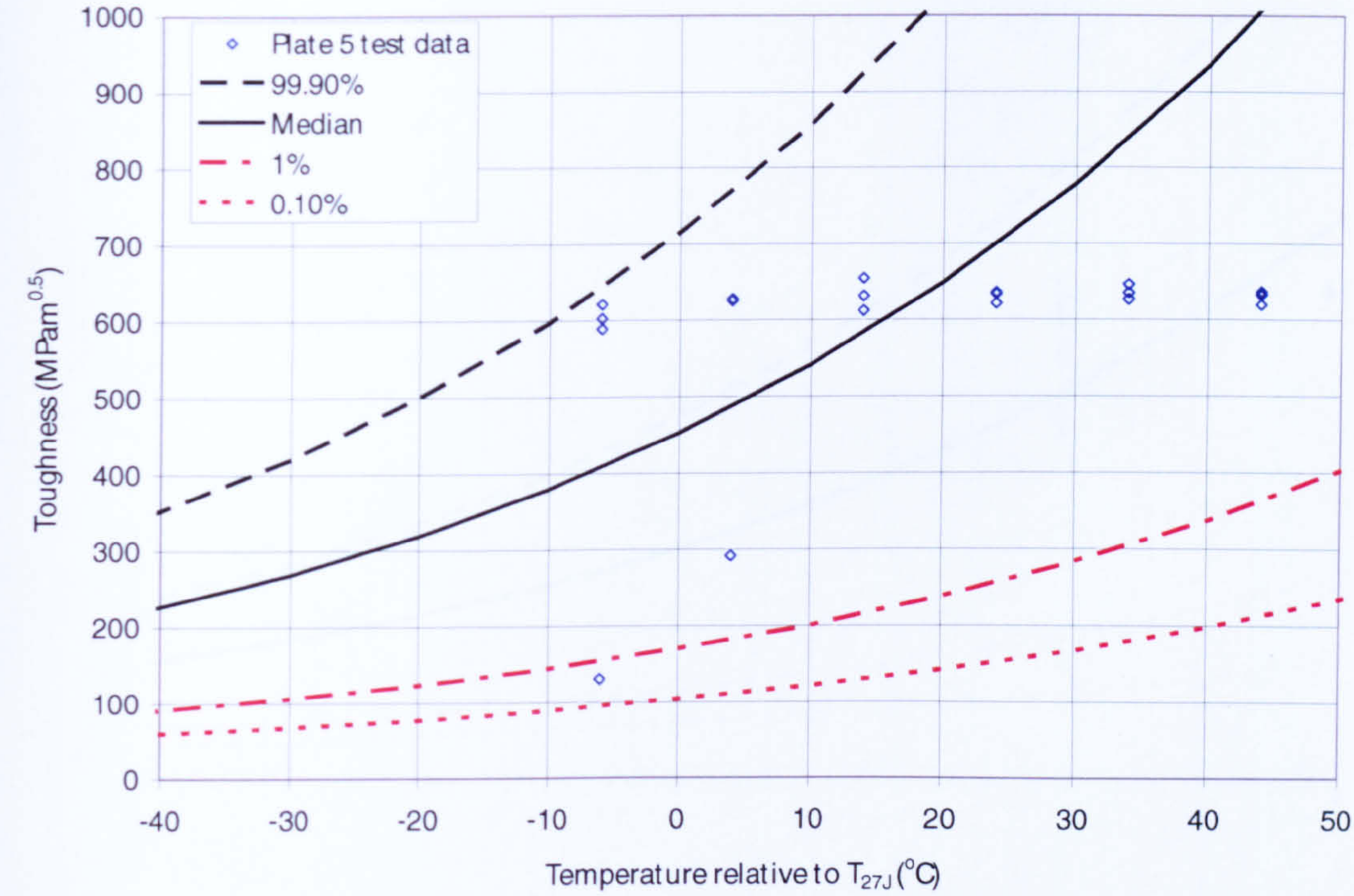

Figure E-17 Master curve fit to plate 5 test data

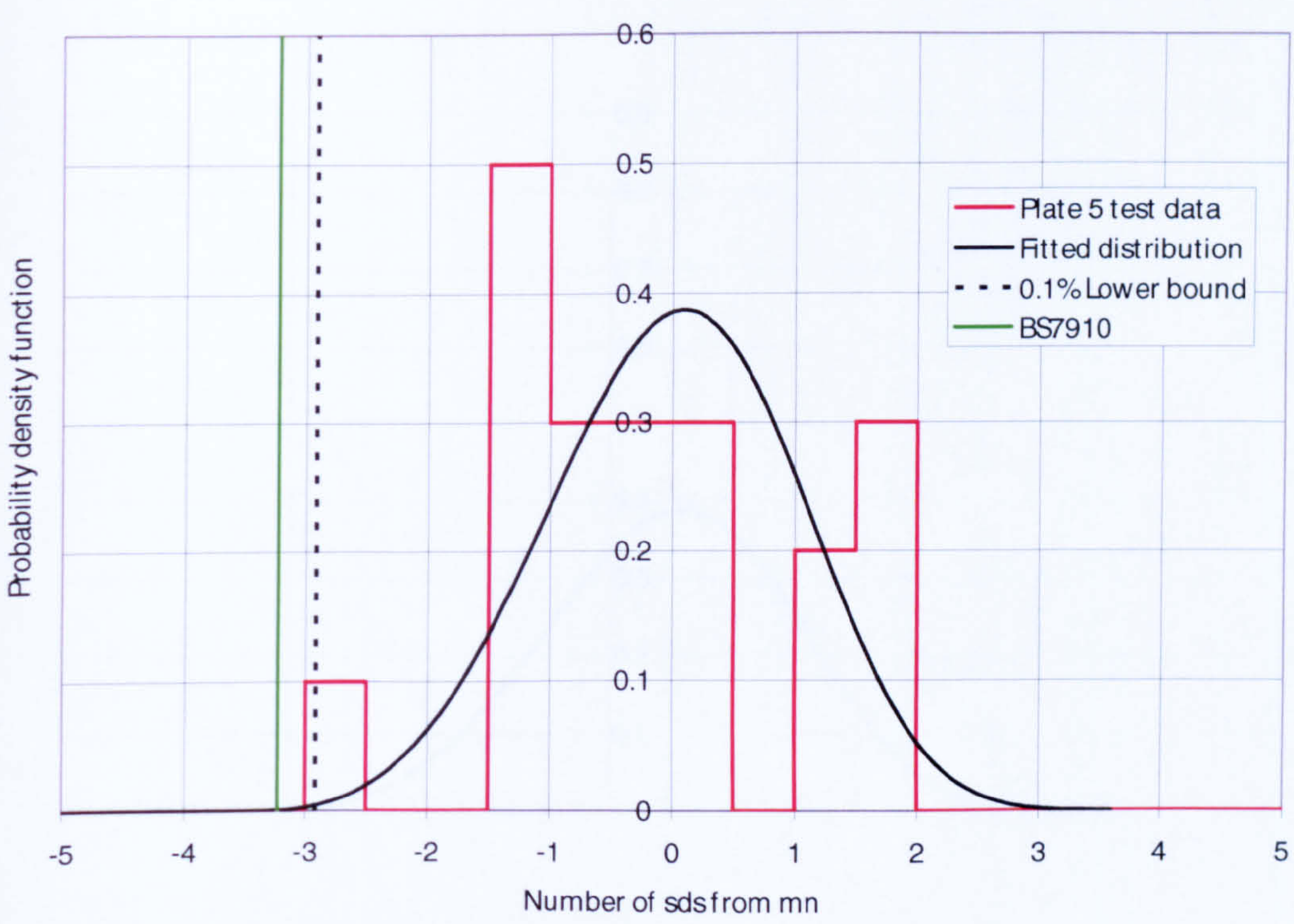

Figure E-18 Normalised scatter plot of master curve fit to plate 5 test data

E.9 Master curve fit to plate 6 test data

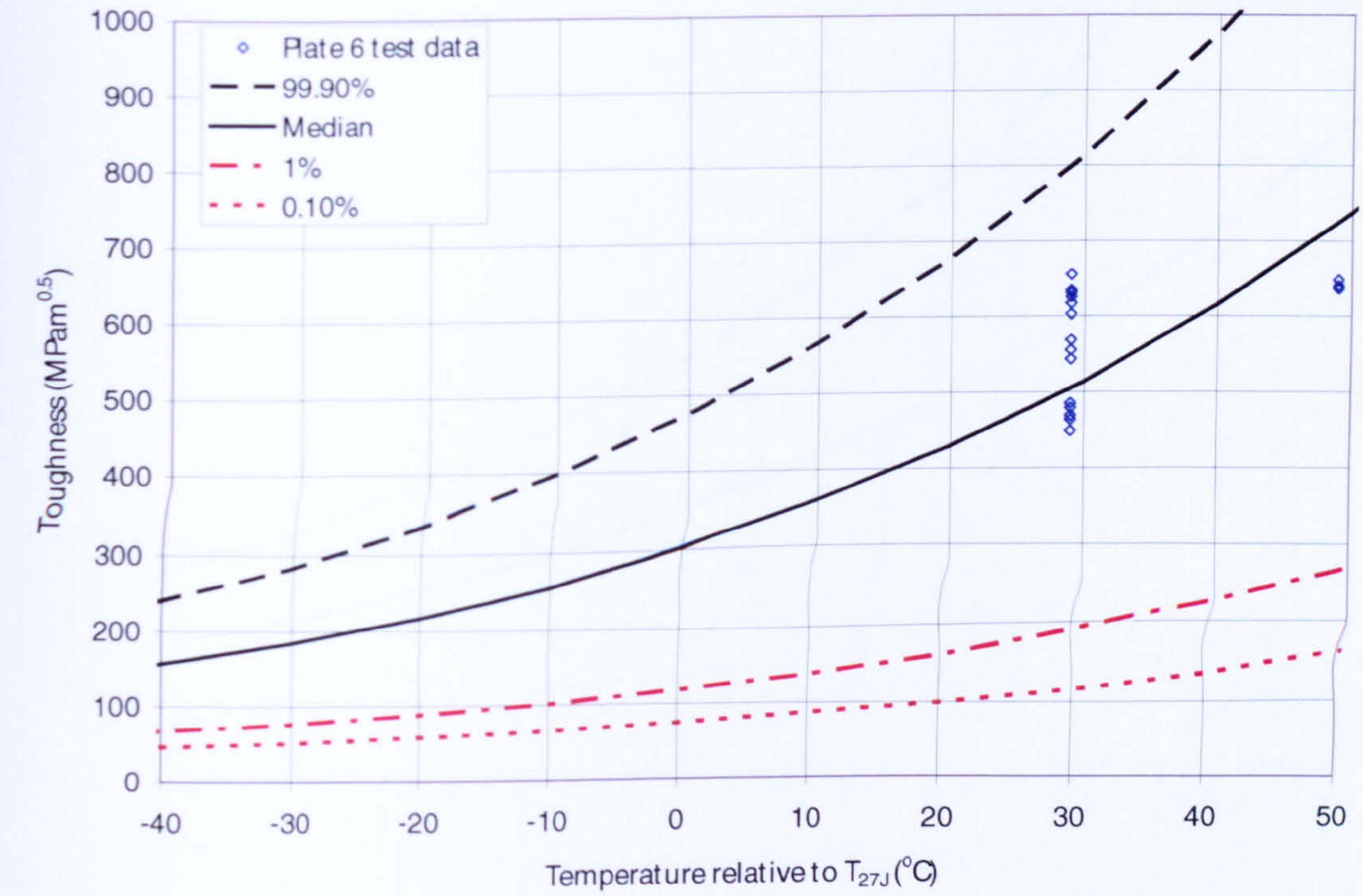

Figure E-19 Master curve fit to plate 6 test data

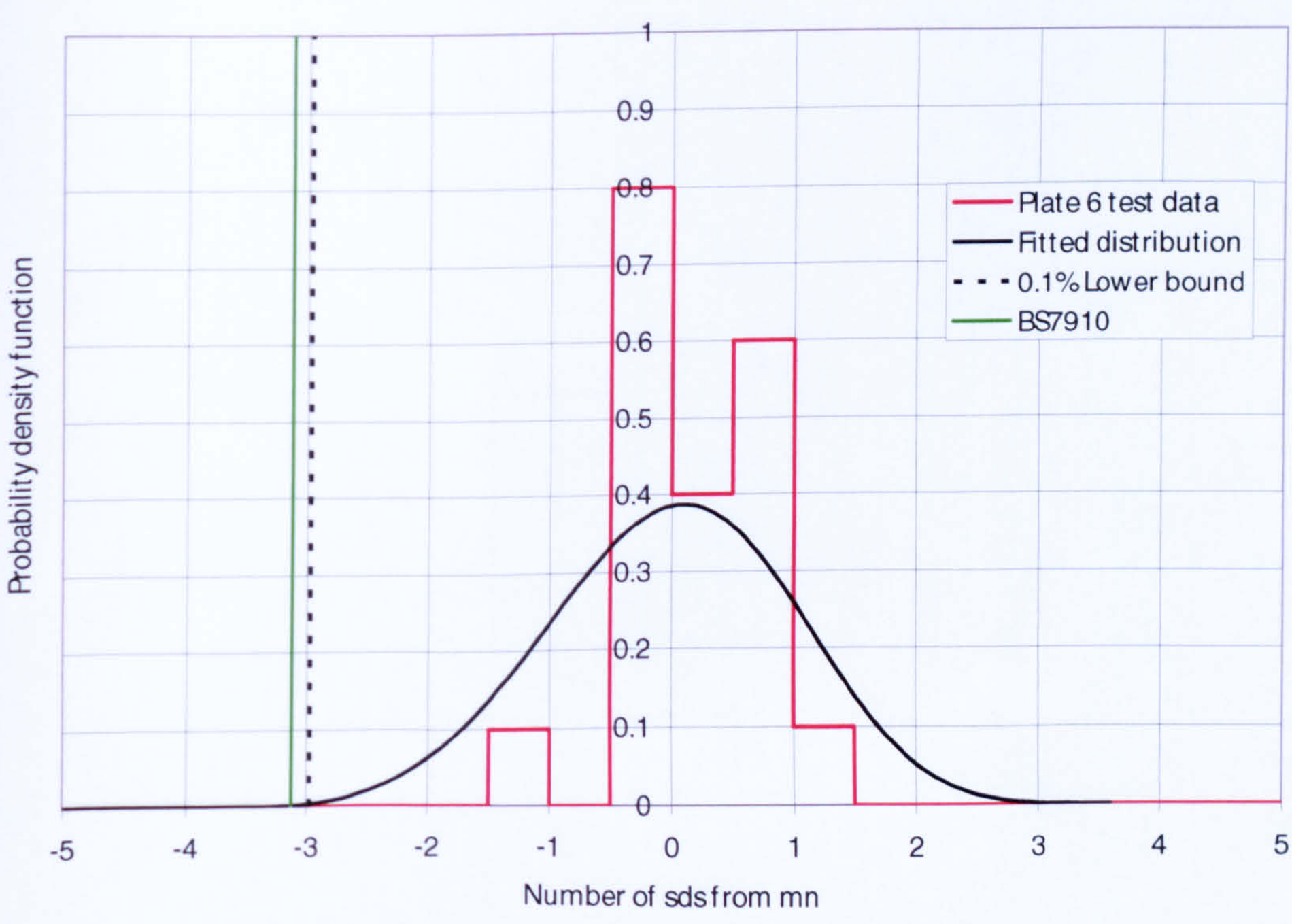

Figure E-20 Normalised scatter plot of master curve fit to plate 6 test data

E.10 Master curve fit to plate 7 test data

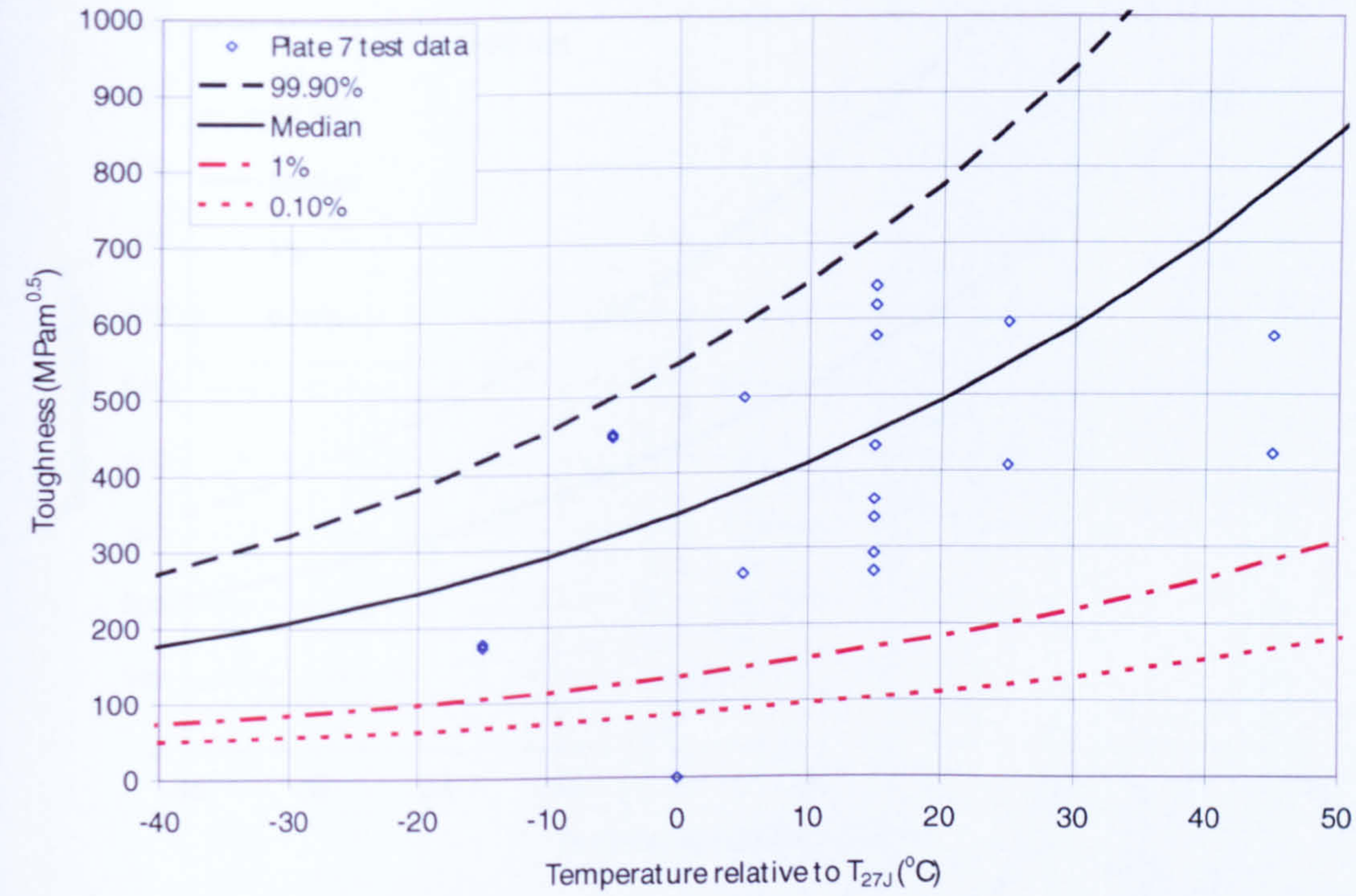

Figure E-21 Master curve fit to plate 7 test data

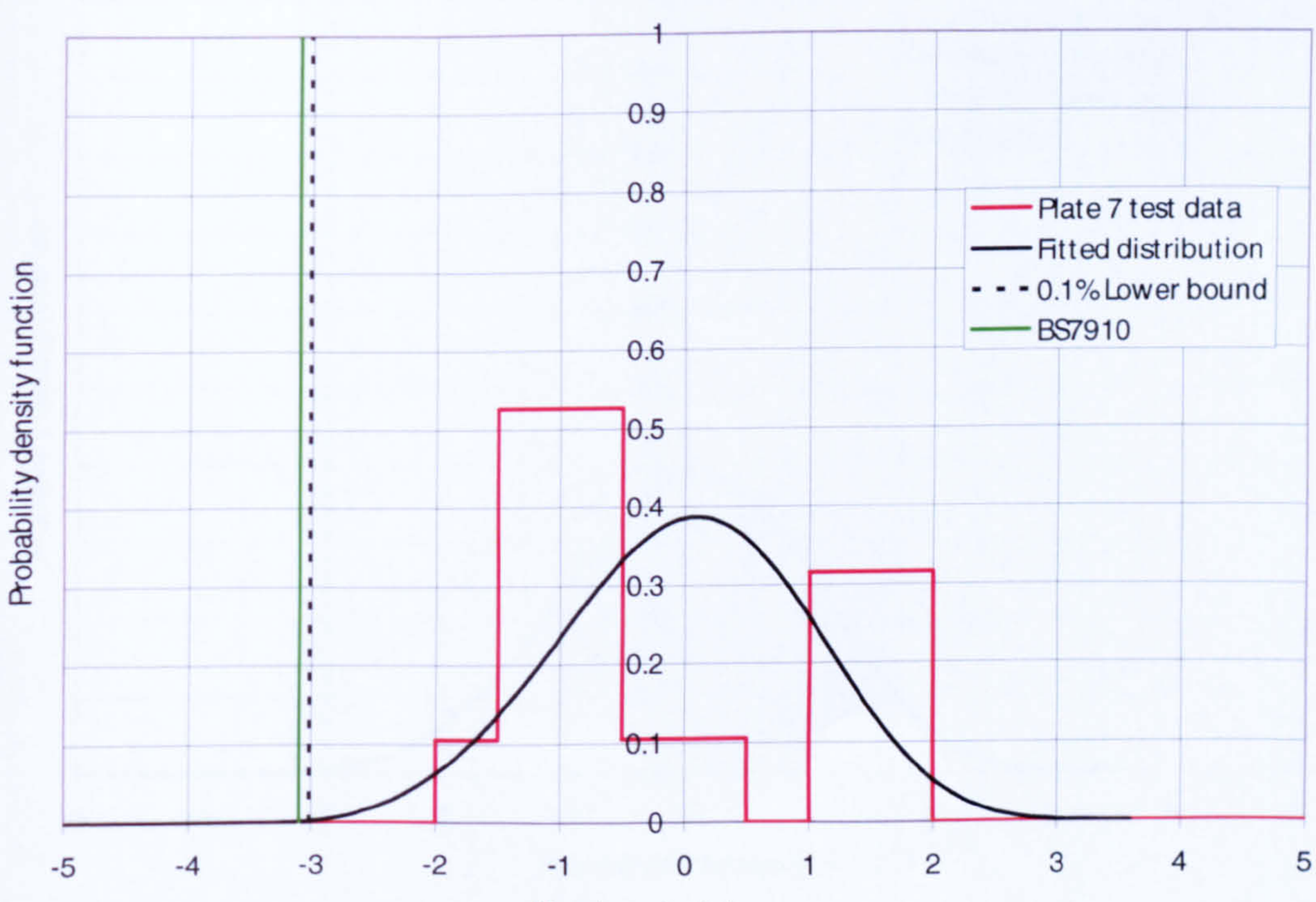

Figure E-22 Normalised scatter plot of master curve fit to plate 7 test data

E.11 Master curve fit to plate 7 weld and HAZ test data

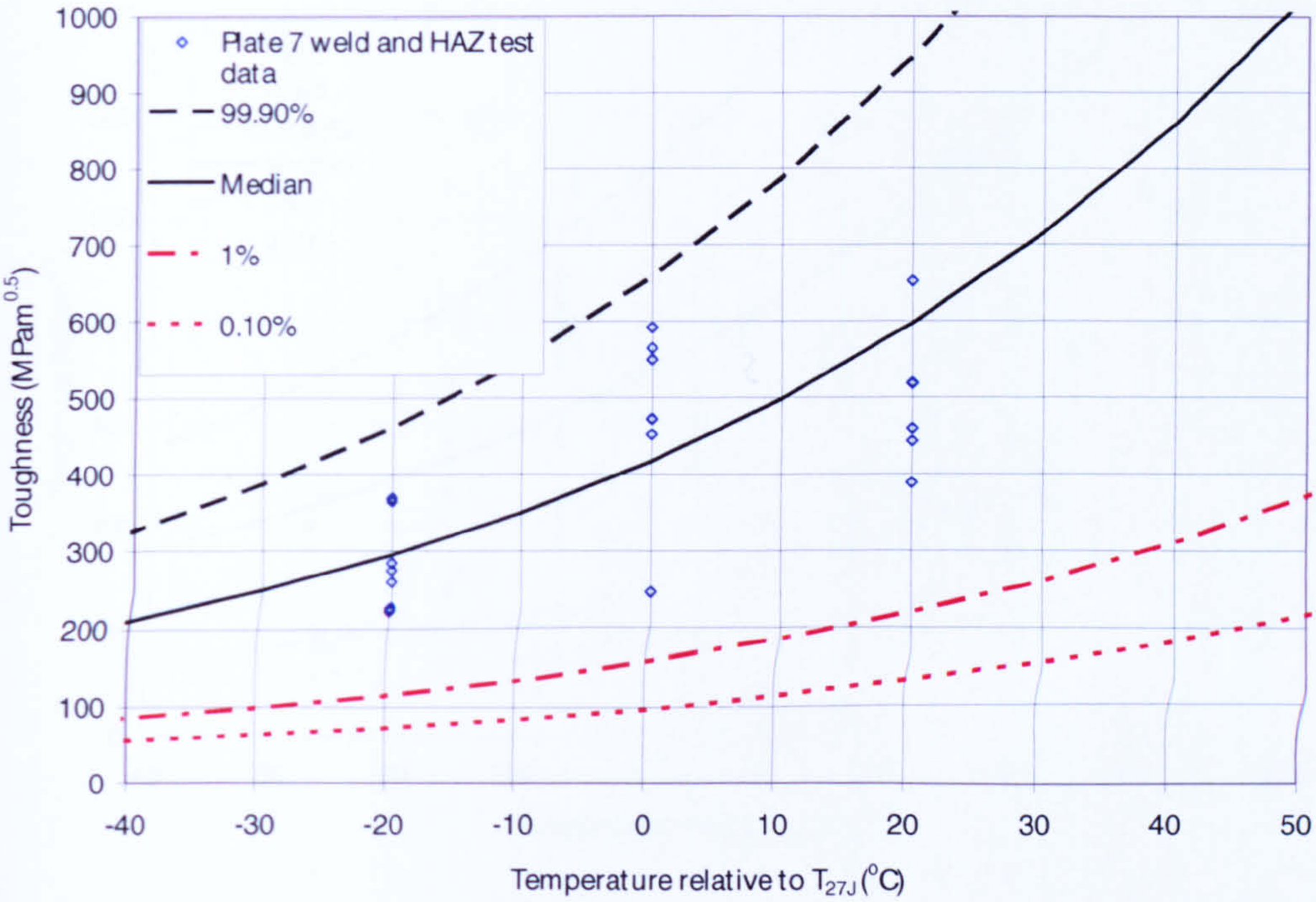

Figure E-23 Master curve fit to plate 7 weld and HAZ test data

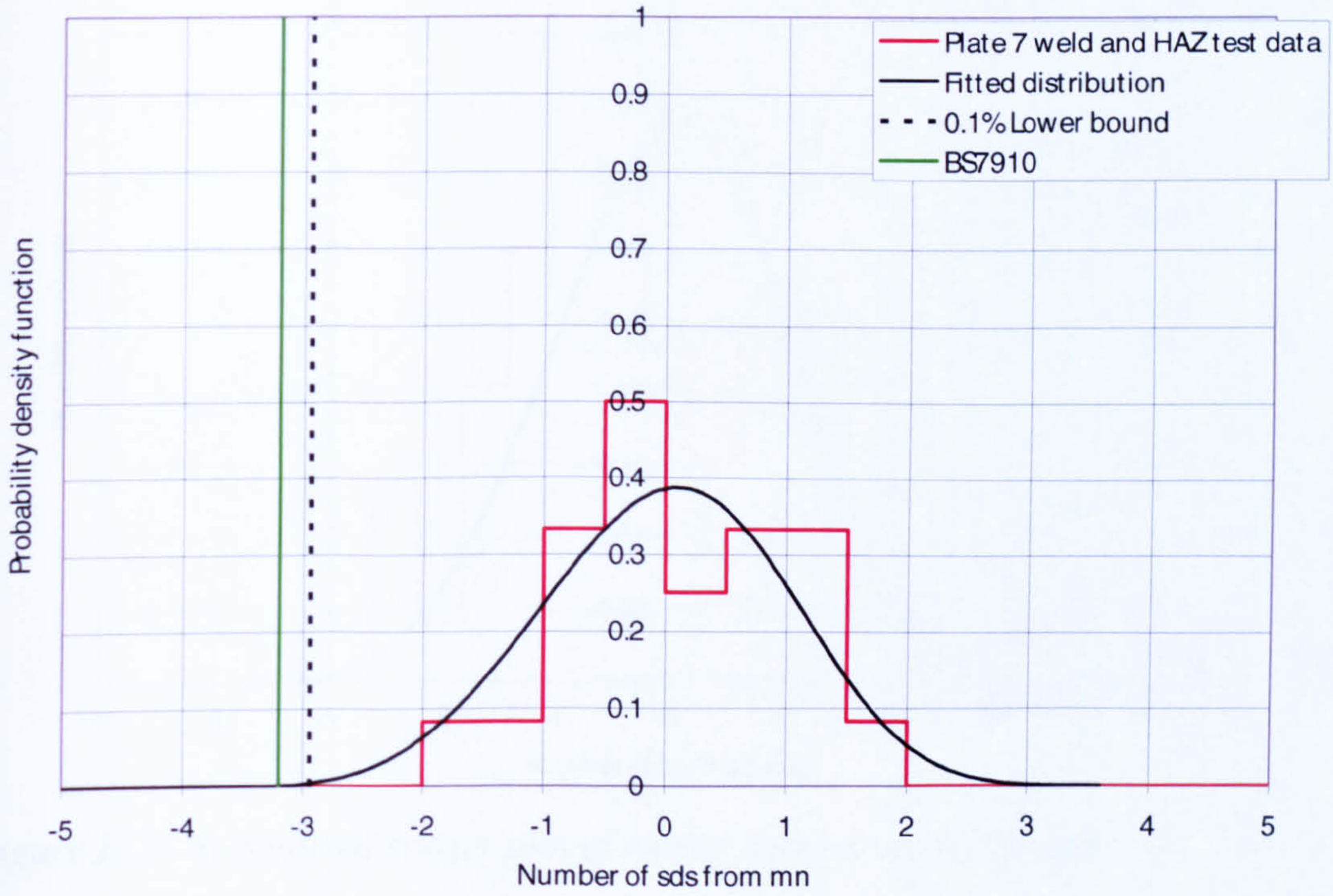

Figure E-24 Normalised scatter plot of master curve fit to plate 7 weld and HAZ test data

E.12 Master curve fit to all test data

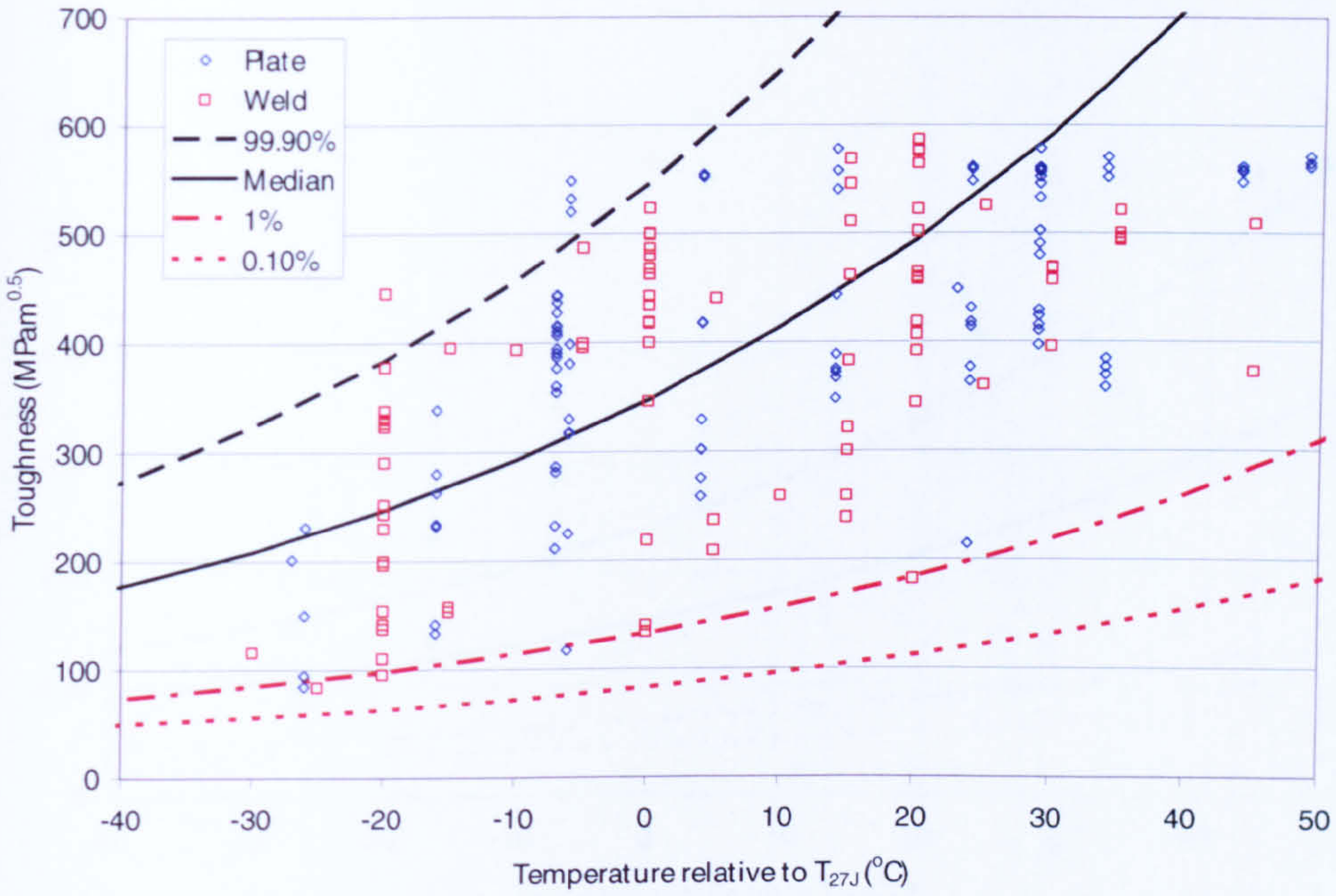

Figure E-25 Master curve fit to all test data

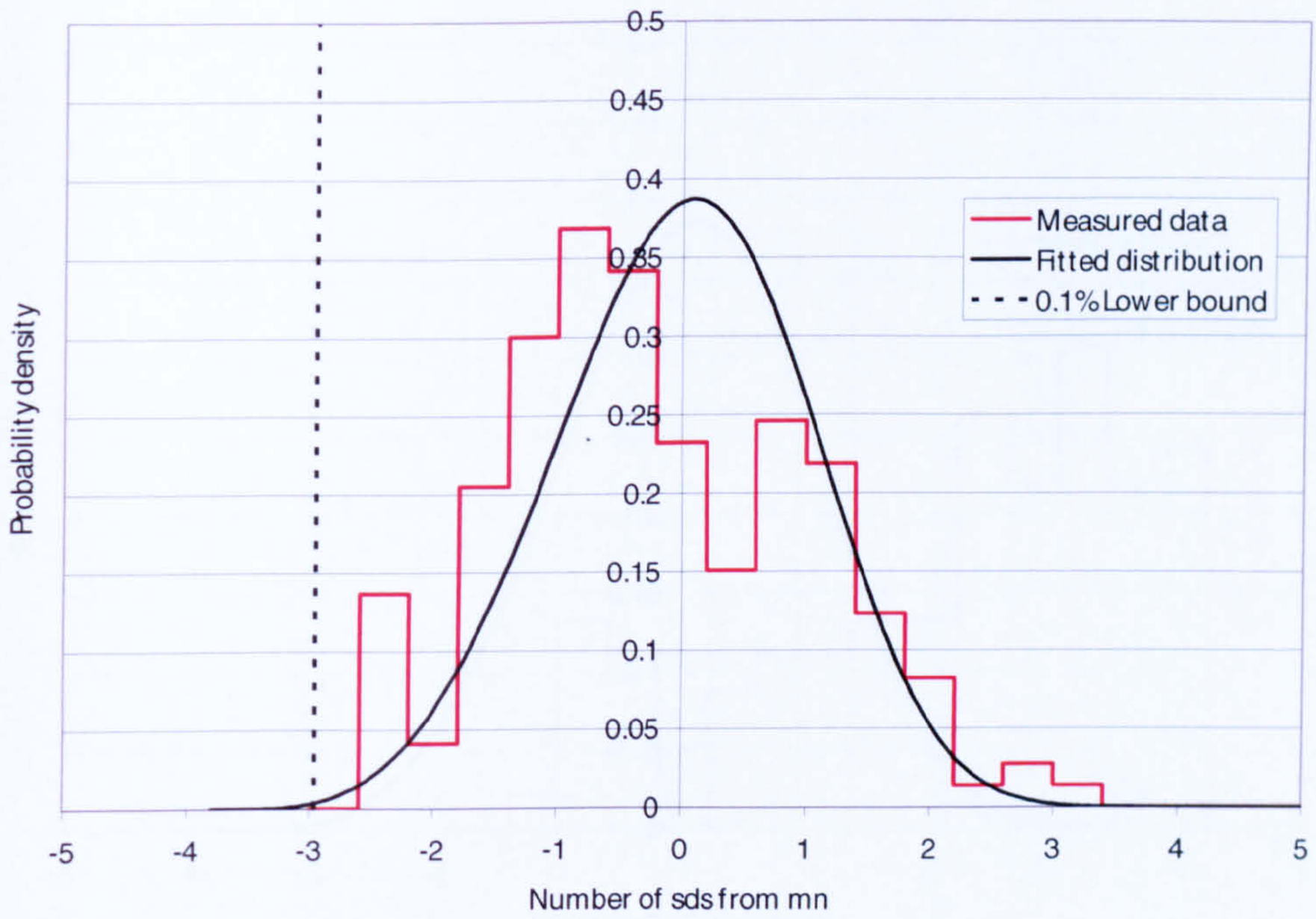

Figure E-26 Normalised scatter plot of master curve fit to all test data

E.13 Master curve with censored specimens

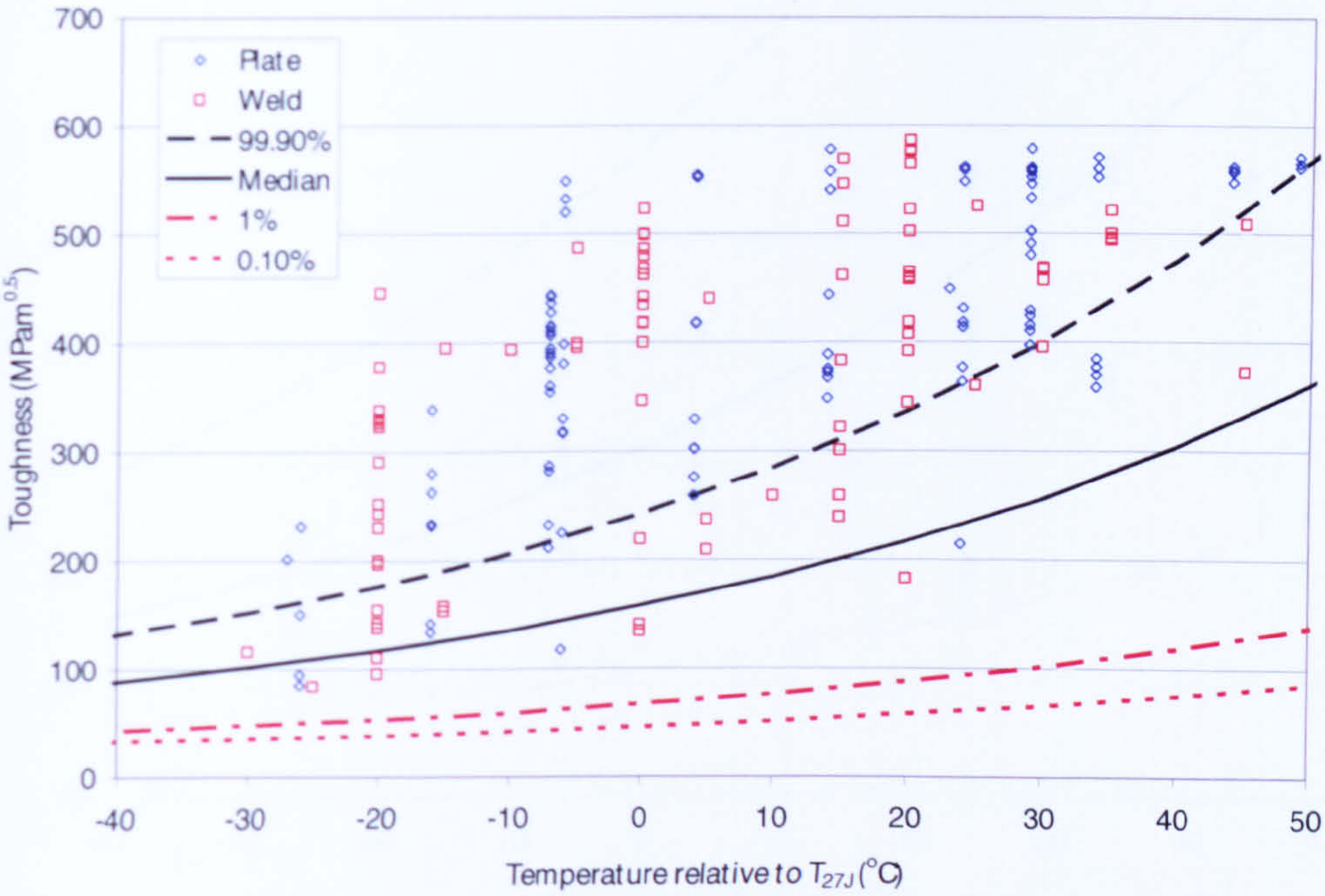

Figure E-27 Censored master curve fit to all test data

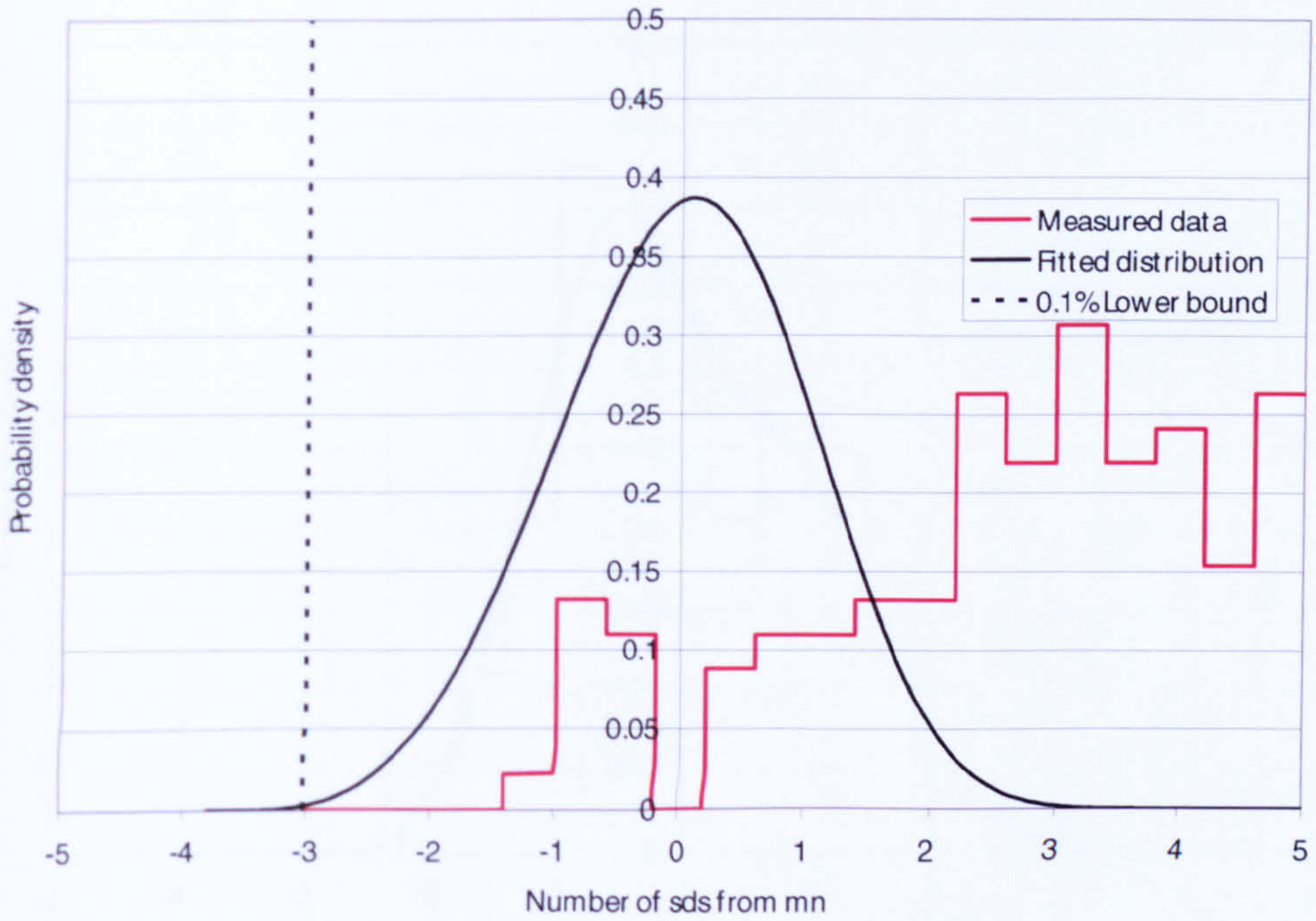

Figure E-28 Normalised scatter plot of censored master curve fit to all test data

E.14 Bimodal master curve

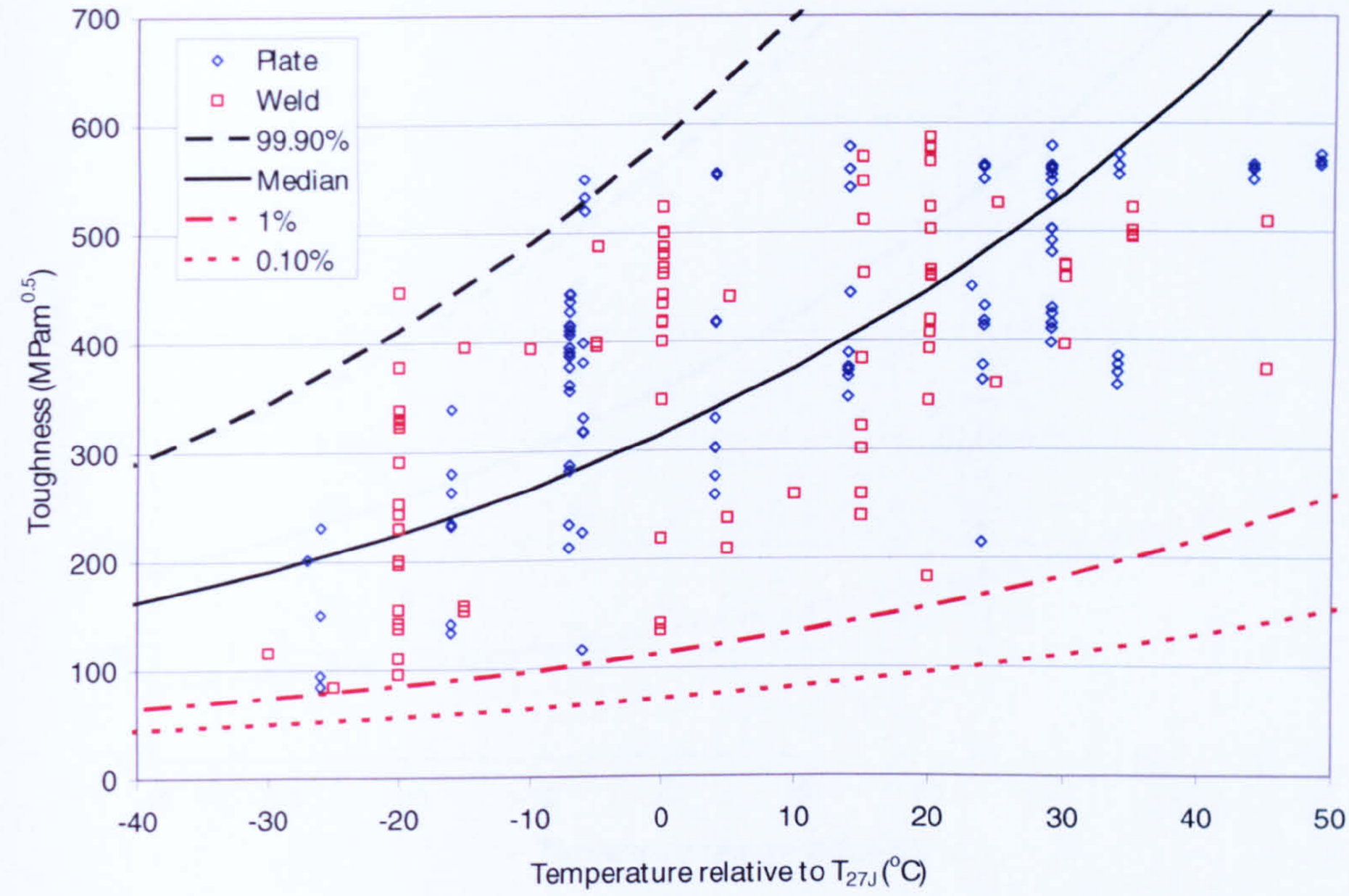

Figure E-29 Bimodal master curve fit to all test data

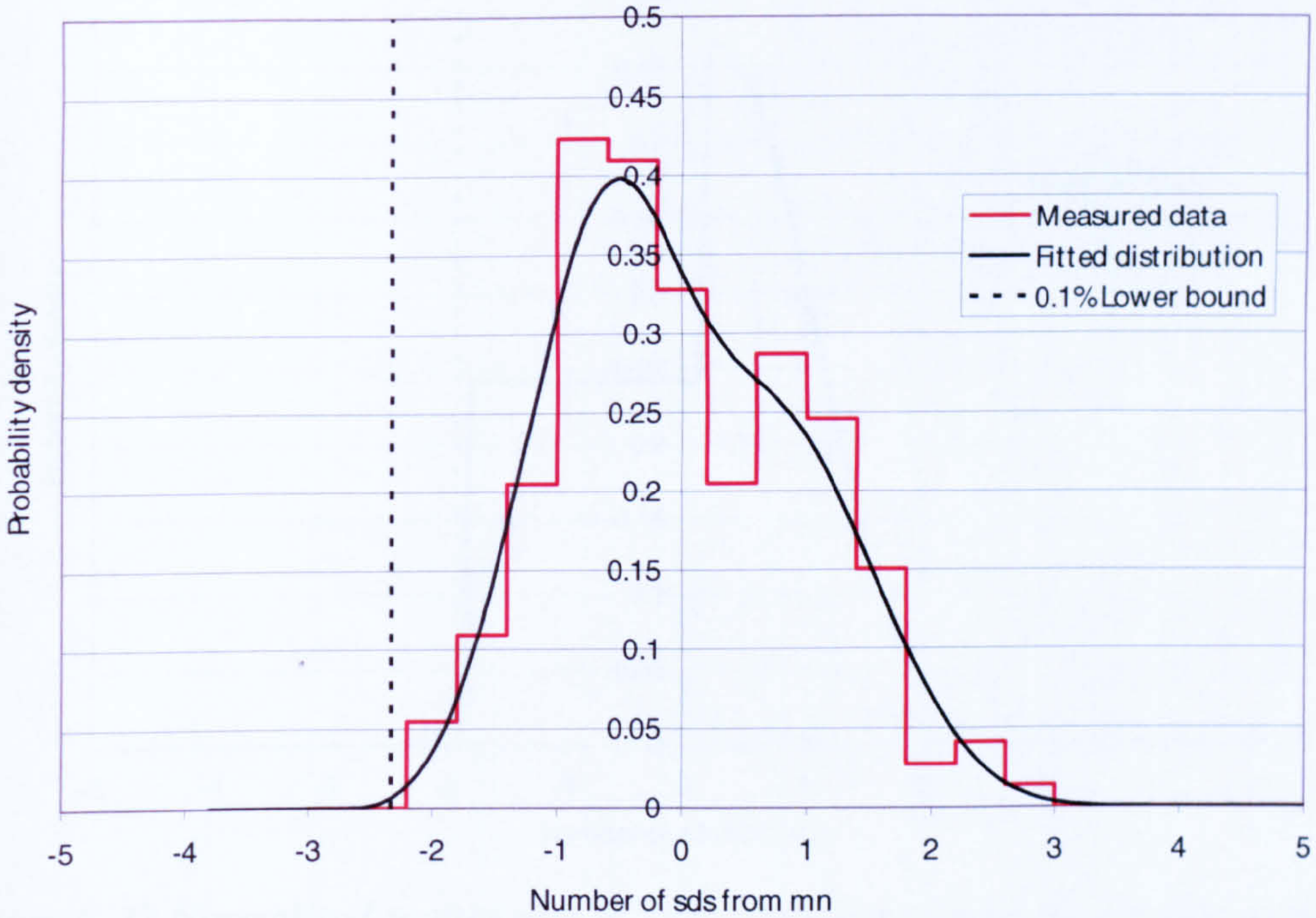

Figure E-30 Normalised scatter plot of bimodal master curve fit to all test data

E.15 Zerbst modified lower bound approach

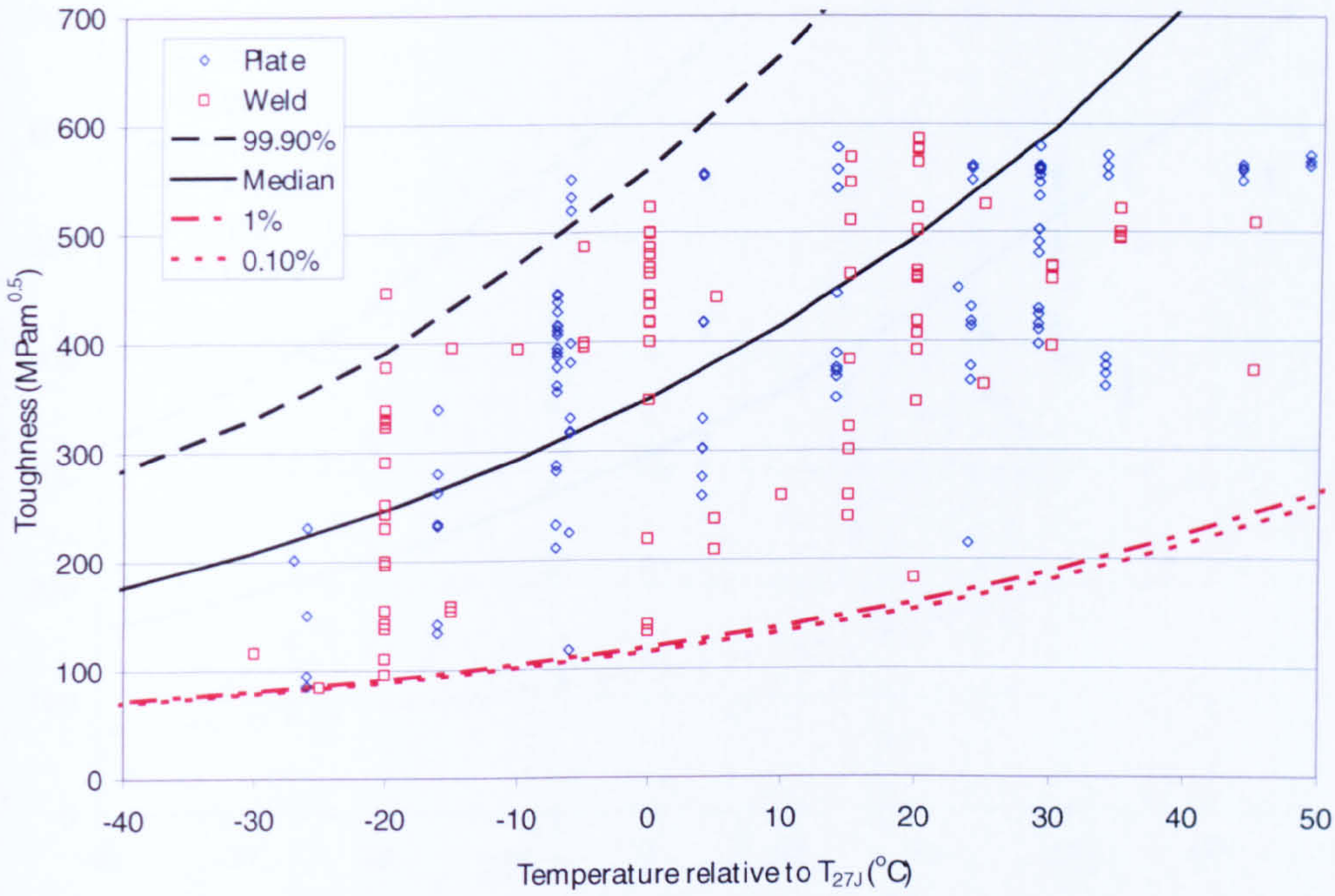

Figure E-31 Zerbst modified lower bound approach fit to all test data

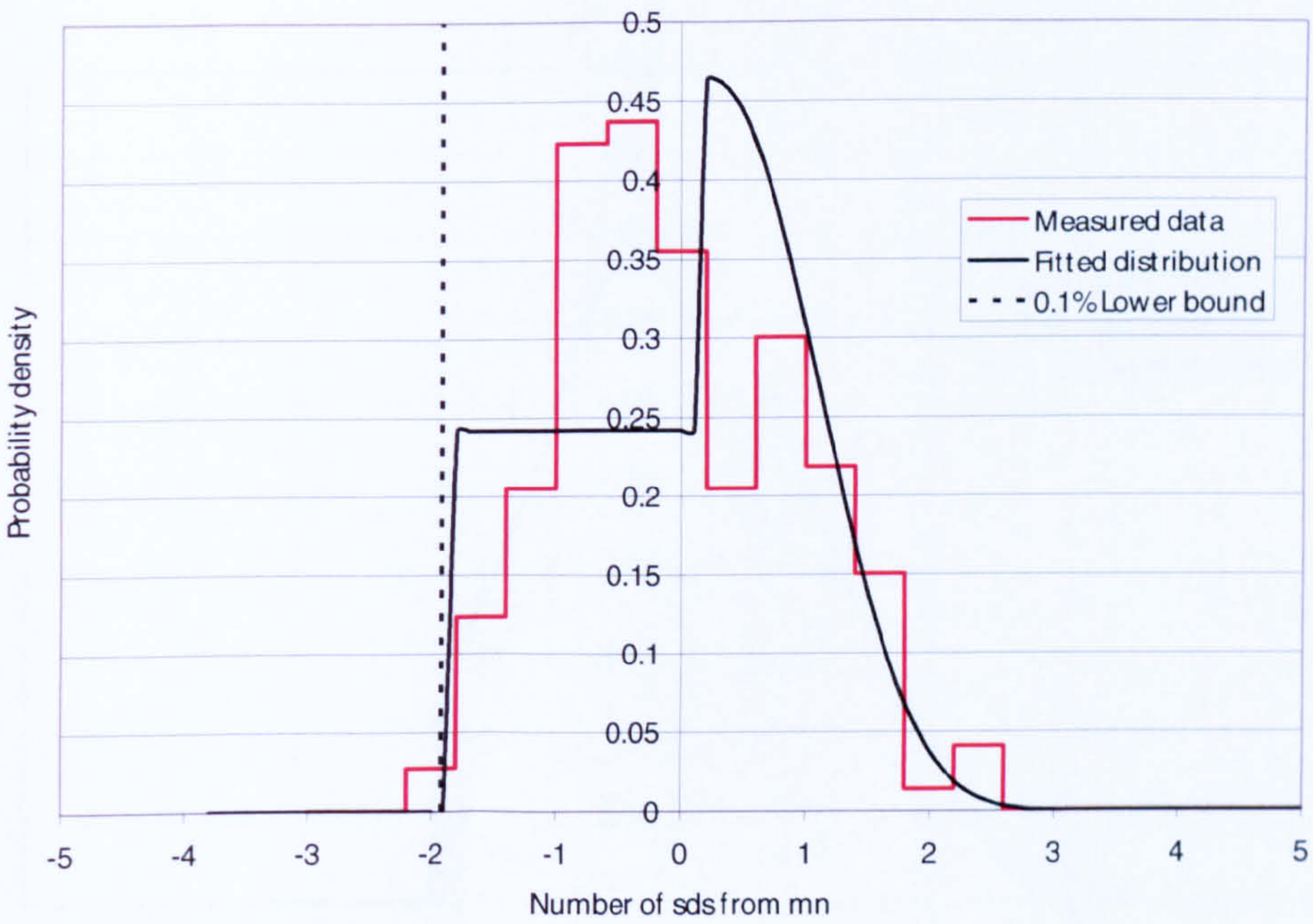

Figure E-32 Normalised scatter plot of Zerbst modified lower bound approach fit to all test data

E.16 Bimodal master curve and Zerbst approach

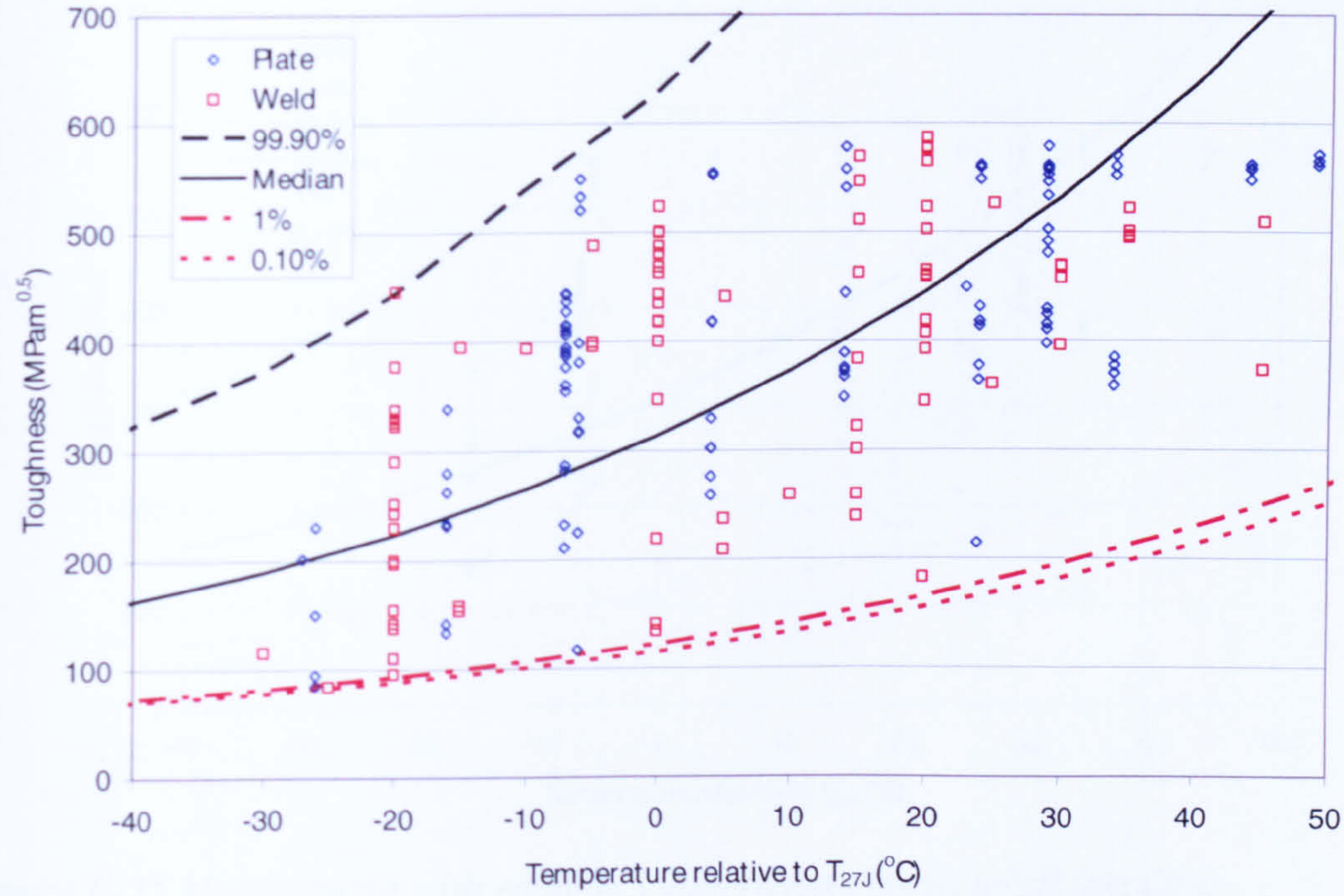

Figure E-33 Bimodal Zerbst and Master Curve fit to all test data

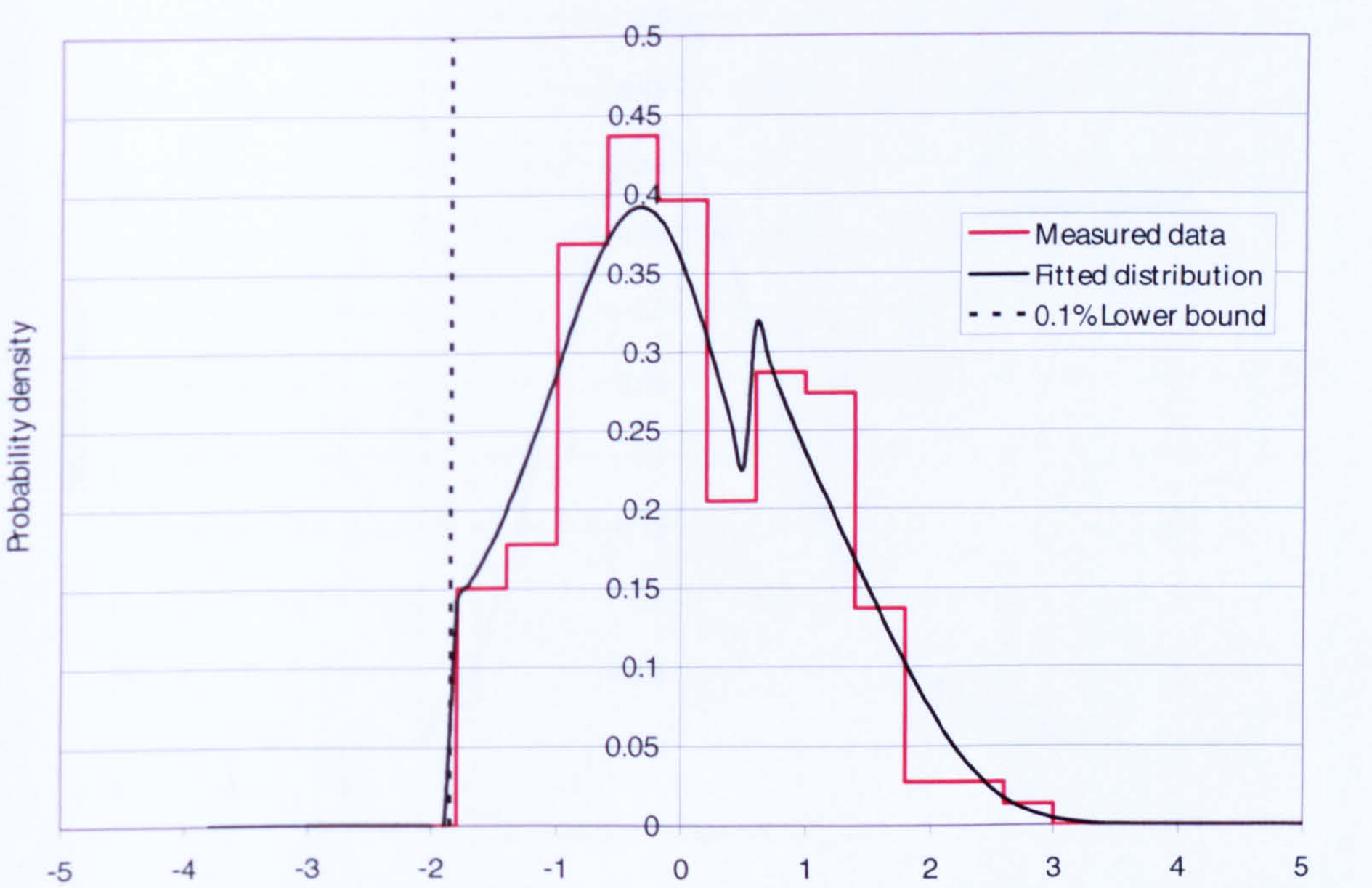

Figure E-34 Normalised scatter plot of bimodal Zerbst and master curve fit to all test data

E.17 Master curve with random inhomogeneities

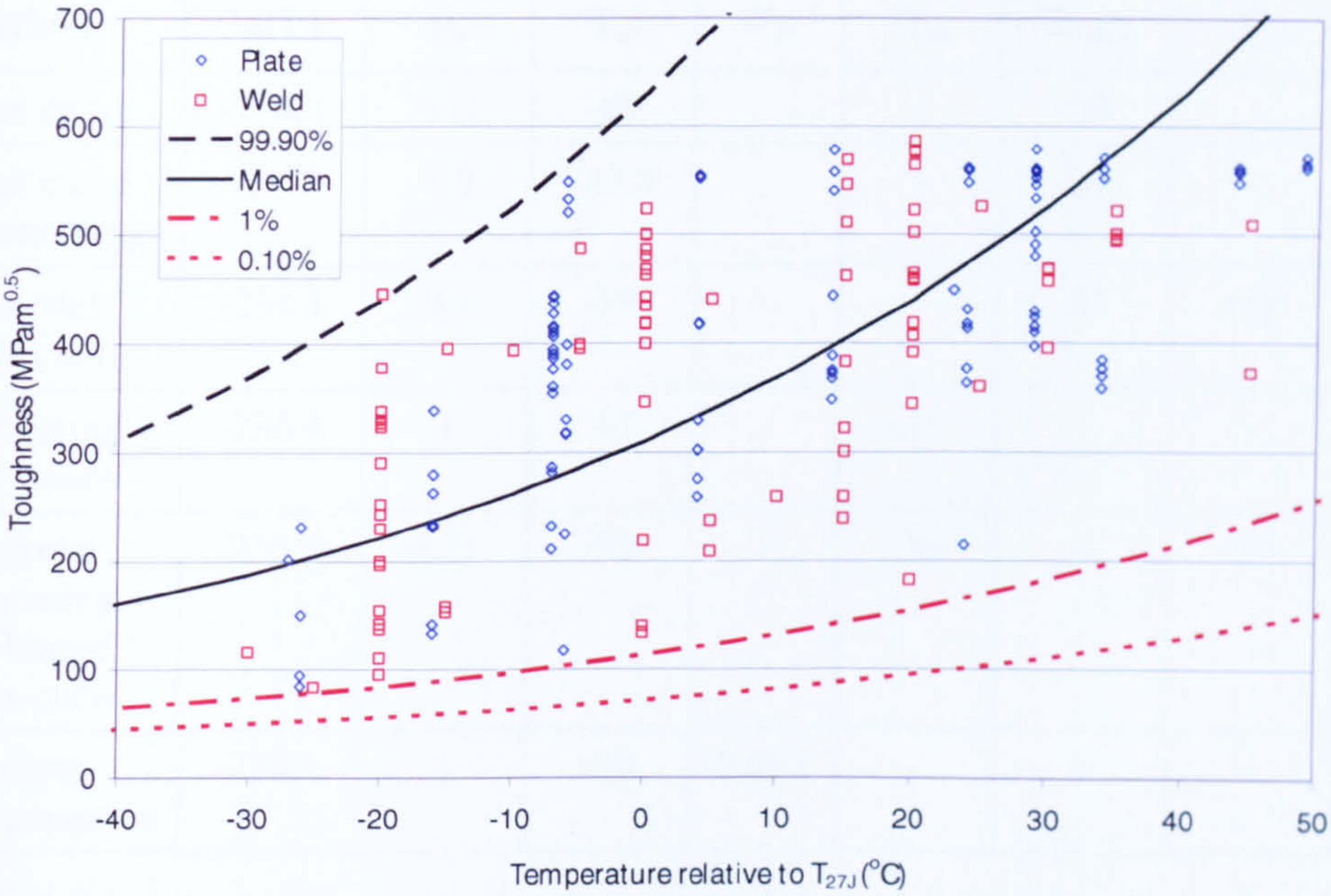

Figure E-35 Master curve with random inhomogeneities fit to all test data

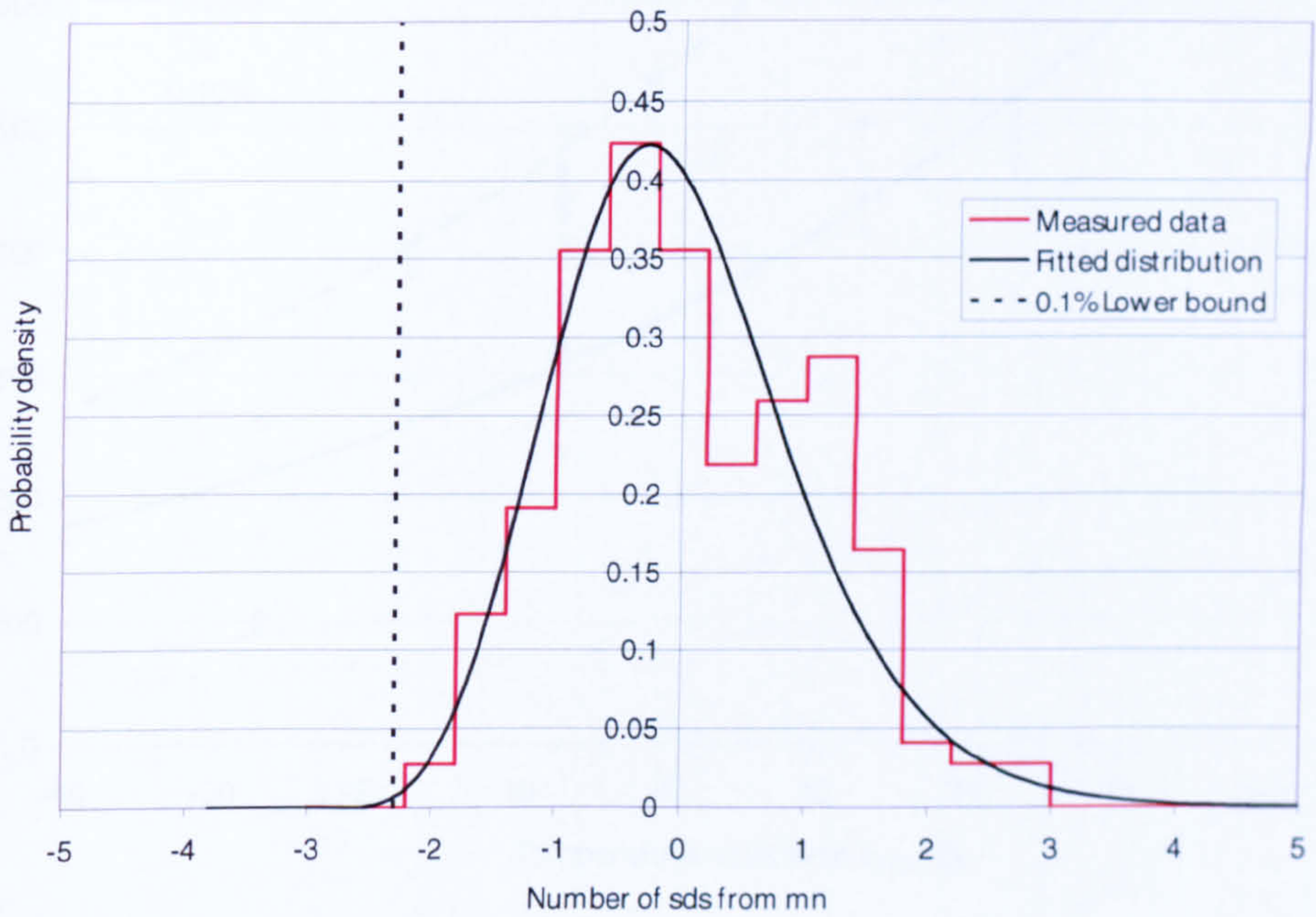

Figure E-36 Normalised scatter plot of master curve with random inhomogeneities fit to all test data

E.18 Wide plate analysis

Method	ln(L)	p_a	T_{01}	σ_{T_0}	T_{lb}	K_{min1}	T_{02}	K_{min2}
Master curve	-234.1	1.0	-89	-	-	20	-	-
Master curve with censoring	-14.7	1.0	-43.8	-	-	20	-	-
Bi-modal master curve	-234.1	0.5	-89	-	-	20	-89	20
Engineering lower bound	-236.4	1	-87	-	-16	-	-	-
Bi-modal engineering lower bound / master curve	-233.5	0.21	-93	-	-16	-	-89	20
Random inhomogeneities	-234.1	1	-89	0.001	-	-	-	-

Table E-1 Summary of fit parameters for wide plate toughness results

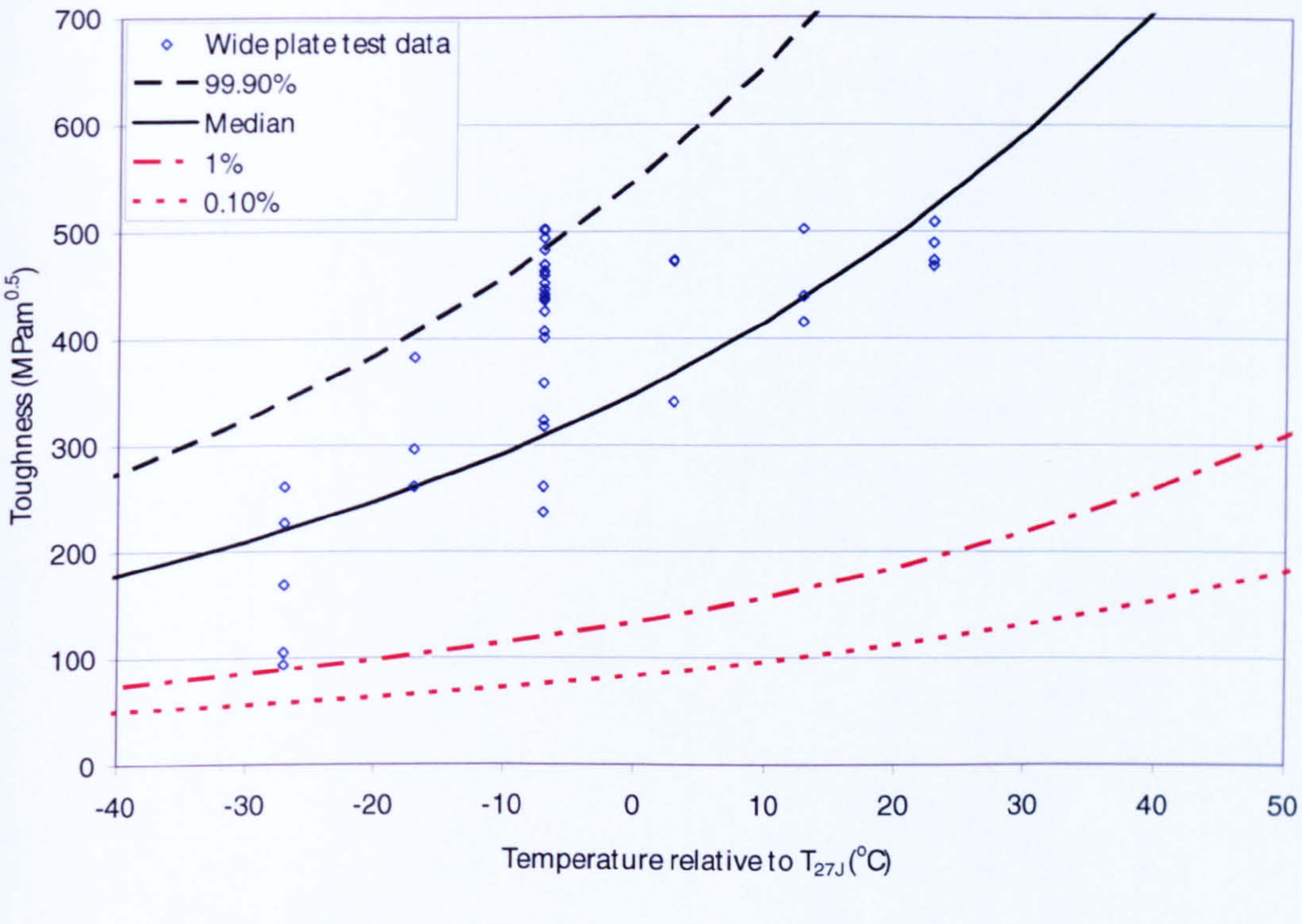

Figure E-37 Master curve fit to wide plate test results

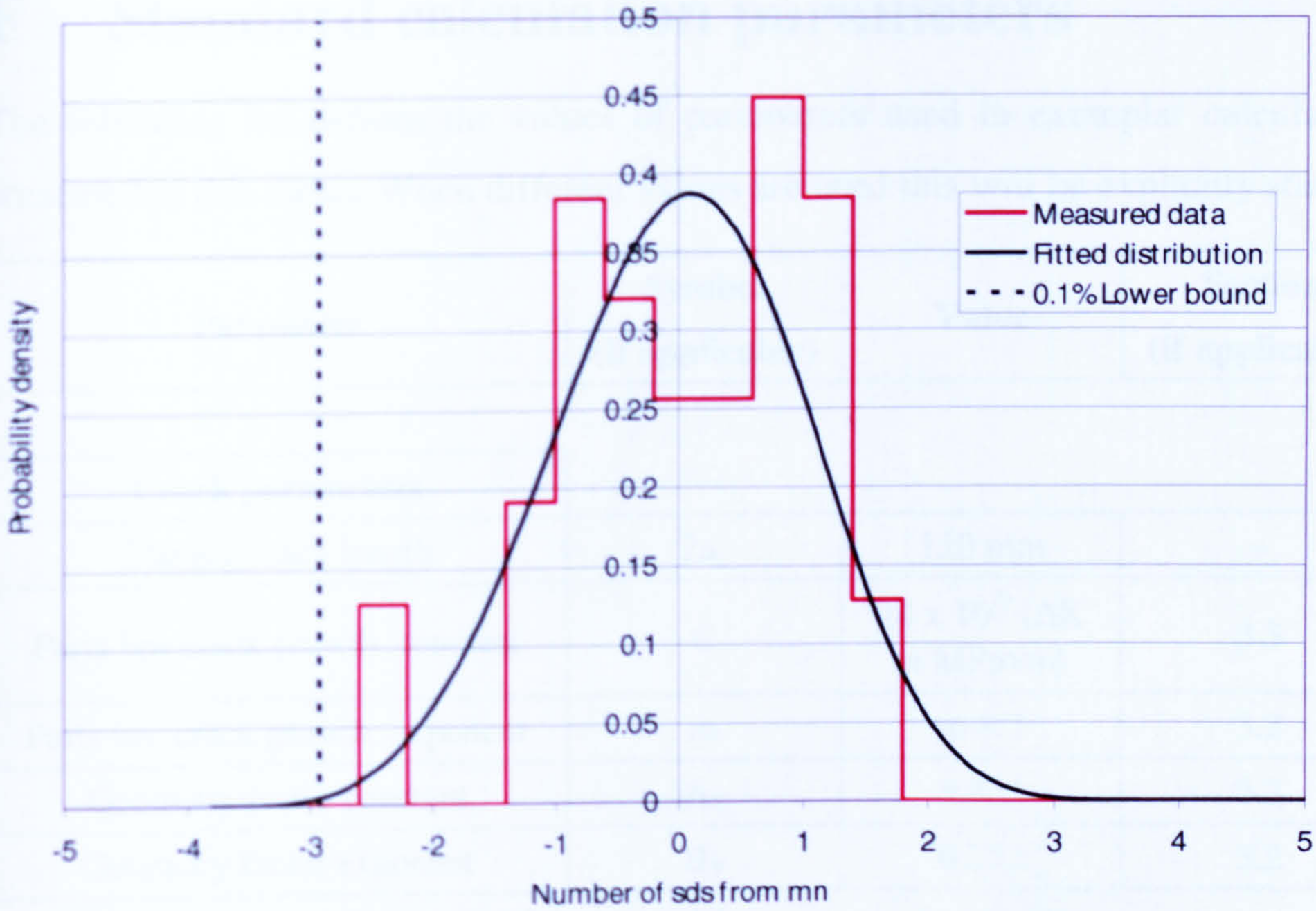

Figure E-38 Normalised scatter plot of Master Curve fit to wide plate test results

F Standard calculation parameters

The following list defines the values of parameters used in exemplar calculations presented in this thesis. When different values are used this will be explicitly stated.

Parameter	Symbol (if applicable)	Value	Section (if applicable)
Crack parameters			
Starting crack length	$2a_o$	150 mm	-
Paris law crack growth constant	C	24×10^{-9} (ΔK in MPa$\sqrt{m}$)	3.3
Paris law crack growth exponent	m	m = 3	3.3
Geometry factor constant	A_Y	3.425	3.2
Geometry factor exponent	B_Y	0.232	3.2
Lower limit of 1 assumed for geometry factor, Y.			
Applied loading parameters			
Long-term Weibull scale component	A	7.44	4.3.5
Long-term Weibull shape component	B	1.23	4.3.5
Long-term equivalent fatigue stress	$\Delta\sigma_{eq}$	15.3 MPa	4.4.4
Number of cycles per hour	N_H	500 cycles / hour	4.3.4
Percentage of life at sea	-	100.0 %	-
Still water bending stress mean	-	35 MPa	4.5
Still water bending stress standard deviation	-	3.5 MPa	4.5
Material parameters			
Yield stress assumed for residual stress model	σ_y	265 MPa	-
Plate thickness	t	15 mm	-
Bi-modal toughness distribution pa	p_a	0.39	5.4.3
Reference temperature for distribution 1	T_{01}	-59°C	5.4.3

Reference temperature for distribution 2	T_{02}	-85°C	5.4.3
Sampling interval	Δ	5 mm	5.5
Charpy 27 J transition temperature	T_{27J}	-20°C	-
External temperature	T	0°C	-
Bi-modal distribution cut-off at a cumulative probability of 0.1 %, below which there is assumed to be a 0 % probability of a toughness value occurring.			

Table F-1 Summary of standard calculation parameters

G Structural reliability methods

G.1 Example calculation at first time step

Define input variables

Half crack length $a := \frac{255}{1000}$

Residual stress intensity $K_{res} := 0.27$

Still water bending stress intensity $K_{swbm} := 31.3$

Geometry factor $Y := 1$

Applied loading

Weibull scale factor $A := 7.44$

Weibull shape factor $B := 1.23$

Number of cycles $N := 82349.949$

Material fracture toughness

Probability of first distribution $p_a := 0.39$

EXternal temperature $T := 0$

Charpy 27J temperature $T_{27J} := -20$

Reference temperature for first distribution $T_{01} := -59$

Reference temperature for second distribution $T_{02} := -85$

Assumed minimum fracture toughess $K_{min} := 20$

Define distributions

Weibull density function $p_{weib}(x) := \frac{B}{A} \cdot \left(\frac{x}{A}\right)^{B-1} \cdot \exp\left[-\left(\frac{x}{A}\right)^{B}\right]$

Mode for extreme type-1 $u := A \cdot \ln(N)^{\frac{1}{B}}$

Measure of dispersion for extreme type-1 $\alpha := N \cdot p_{weib}(u)$

Extreme Type-1 density function $p_{ext}(x) := \alpha \cdot \exp\left[-\alpha \cdot (x-u) - \exp\left[-\alpha \cdot (x-u)\right]\right]$

Extreme Type-1 distribution function $P_{ext}(x) := \exp\left[-\exp\left[-\alpha \cdot (x-u)\right]\right]$

Reference value for first distribution $K_{01} := 31 + 77 \cdot \exp\left[0.019 \cdot \left(T - T_{27J} - T_{01}\right)\right]$

Reference value for second distribution $K_{02} := 31 + 77 \cdot \exp\left[0.019 \cdot \left(T - T_{27J} - T_{02}\right)\right]$

Toughness distribution function

$$P_{mat}(K_{mat}) := 1 - p_a \cdot \exp\left[-\left(\frac{K_{mat} - K_{min}}{K_{01} - K_{min}}\right)^4\right] - (1 - p_a) \cdot \exp\left[-\left(\frac{K_{mat} - K_{min}}{K_{02} - K_{min}}\right)^4\right]$$

Toughness density function

$$p_{mat}(K_{mat}) := p_a \frac{4}{K_{01} - K_{min}} \cdot \left(\frac{K_{mat} - K_{min}}{K_{01} - K_{min}}\right)^{4-1} \cdot \exp\left[-\left(\frac{K_{mat} - K_{min}}{K_{01} - K_{min}}\right)^4\right] \ldots$$
$$+ (1 - p_a) \cdot \frac{4}{K_{02} - K_{min}} \cdot \left(\frac{K_{mat} - K_{min}}{K_{02} - K_{min}}\right)^{4-1} \cdot \exp\left[-\left(\frac{K_{mat} - K_{min}}{K_{02} - K_{min}}\right)^4\right]$$

Plot individual distributions

$i := 1 .. 100$

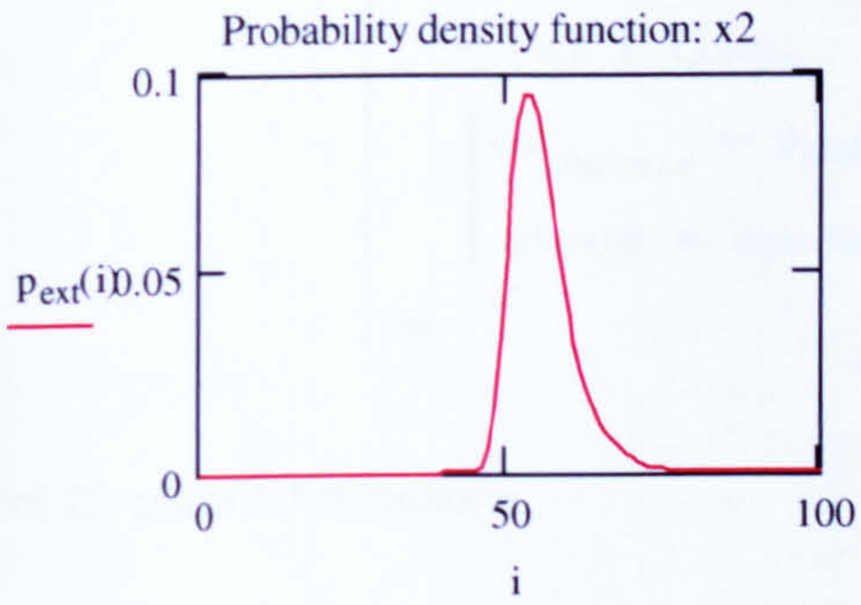

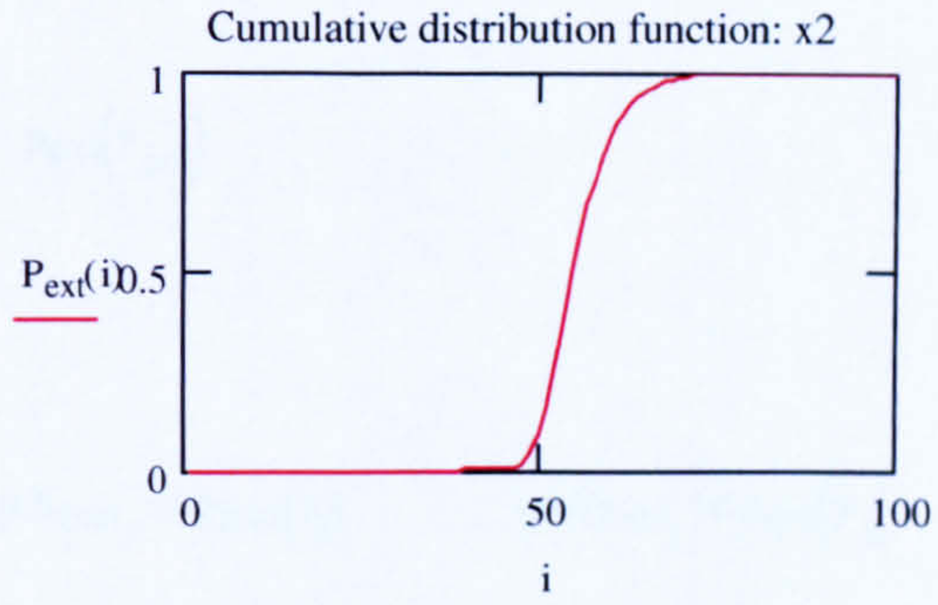

$j := 1 .. 1000$

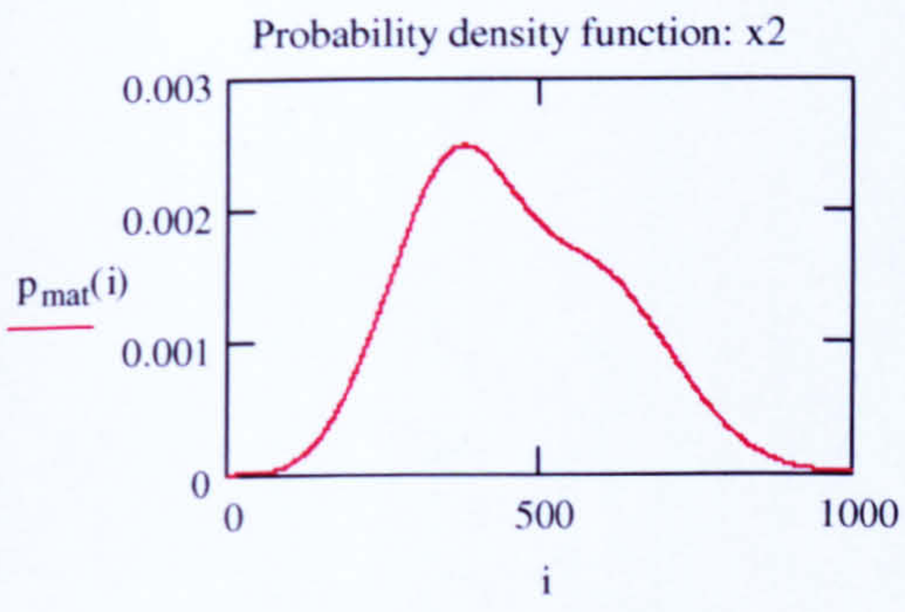

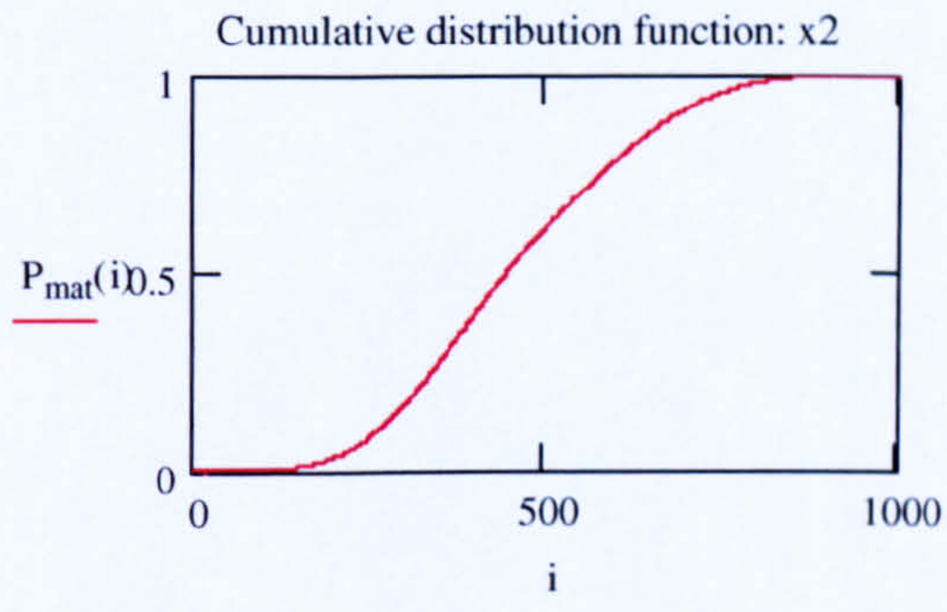

Plot joint probability distribution

Define counters

$i := 1..40$ $\quad x_i := i \cdot 25$ $\quad Count_x := rows(x)$

$j := 1..60$ $\quad y_j := j \cdot 2$ $\quad Count_y := rows(y)$

$$dens_x := \left| \begin{array}{l} outcount \leftarrow 1 \\ \text{for } row \in 1..Count_x \\ \quad \text{for } col \in 1..Count_y \\ \quad\quad out_{outcount} \leftarrow x_{row} \\ \quad\quad outcount \leftarrow outcount + 1 \\ out \end{array} \right.$$

$$dens_y := \left| \begin{array}{l} outcount \leftarrow 1 \\ \text{for } row \in 1..Count_x \\ \quad \text{for } col \in 1..Count_y \\ \quad\quad out_{outcount} \leftarrow y_{col} \\ \quad\quad outcount \leftarrow outcount + 1 \\ out \end{array} \right.$$

$$dens_z := \left| \begin{array}{l} outcount \leftarrow 1 \\ \text{for } row \in 1..Count_x \\ \quad \text{for } col \in 1..Count_y \\ \quad\quad out_{outcount} \leftarrow p_{mat}(x_{row}) \cdot p_{ext}(y_{col}) \\ \quad\quad outcount \leftarrow outcount + 1 \\ out \end{array} \right.$$

Plot 2D parent distributions

$pdf_{mat_i} := p_{mat}(x_i)$ $\quad pdf_{load_j} := p_{ext}(y_j)$

Define zero vectors

$Zero_{x_i} := 0$ $\quad Zero_{y_j} := 0$

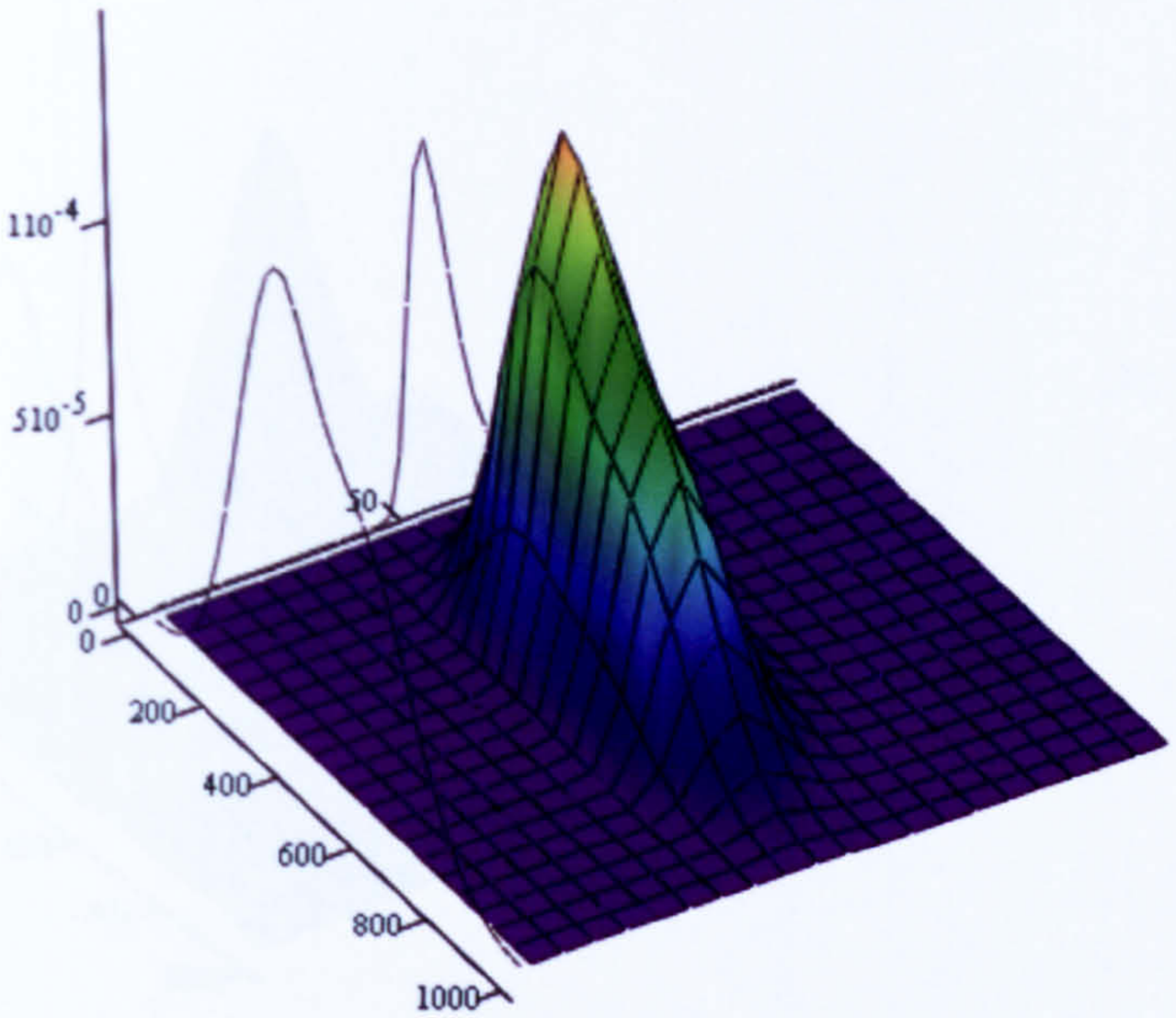

$$\left(x, \mathrm{Zero}_x, \frac{\mathrm{pdf}_{mat}}{20}\right), \left(\mathrm{dens}_x, \mathrm{dens}_y, \mathrm{dens}_z\right), \left(\mathrm{Zero}_y, y, \frac{\mathrm{pdf}_{load}}{1000}\right)$$

Plot limit state function

Define range of load values

$$x2_j := y_j$$

Calculate strength variables to satisfy limit state function

$$x1_j := Y \cdot x2_j \cdot \sqrt{\pi \cdot a} + K_{res} + K_{swbm}$$

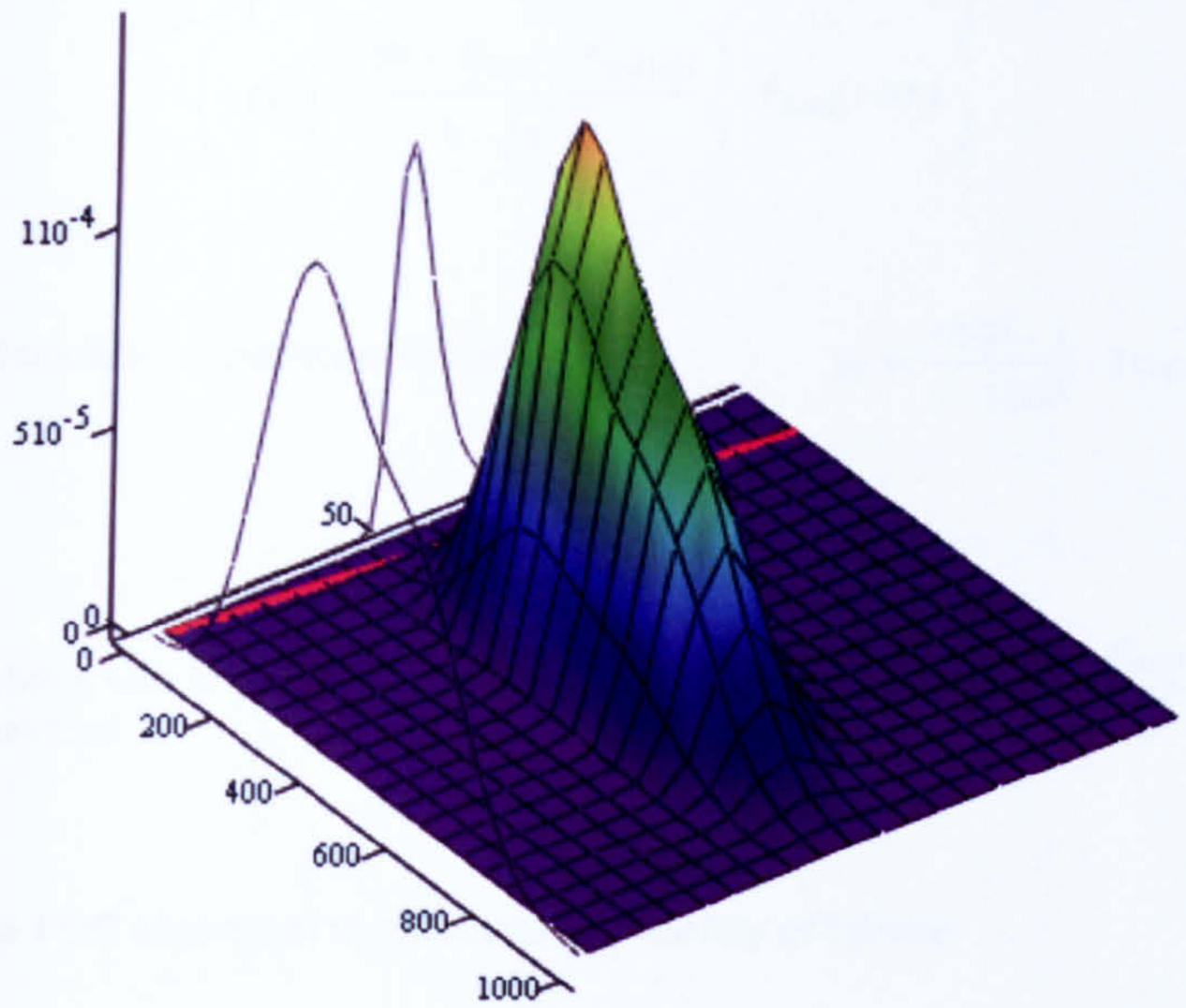

$$\left(x, \mathrm{Zero}_x, \frac{\mathrm{pdf}_{mat}}{20}\right), \left(\mathrm{dens}_x, \mathrm{dens}_y, \mathrm{dens}_z\right), \left(x_1, x_2, \mathrm{Zero}_y\right), \left(\mathrm{Zero}_y, y, \frac{\mathrm{pdf}_{load}}{1000}\right)$$

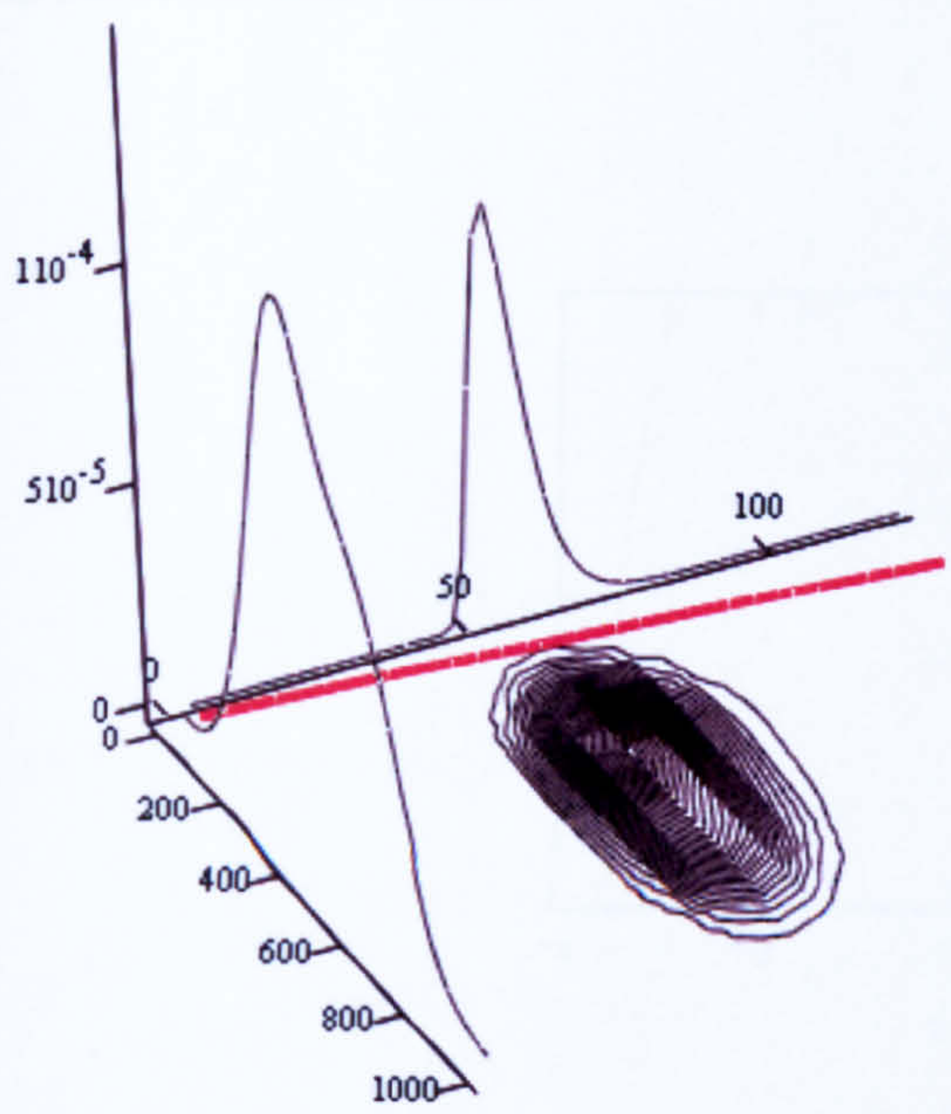

$$\left(x, \mathrm{Zero}_x, \frac{\mathrm{pdf}_{mat}}{20}\right), \left(\mathrm{dens}_x, \mathrm{dens}_y, \mathrm{dens}_z\right), \left(x_1, x_2, \mathrm{Zero}_y\right), \left(\mathrm{Zero}_y, y, \frac{\mathrm{pdf}_{load}}{1000}\right)$$

Calculate probability of failure using convolution integral (and trapezium rule)

$$\text{Trapsum} := \left[\sum_{x=1}^{1000}\left[2\left(p_{ext}\left(\frac{x - K_{res} - K_{swbm}}{Y\cdot\sqrt{\pi\cdot a}}\right)\cdot P_{mat}(x)\right)\right]\right] - \left(p_{ext}\left(\frac{1 - K_{res} - K_{swbm}}{Y\cdot\sqrt{\pi\cdot a}}\right)\cdot P_{mat}(1)\right)\ldots$$
$$+\left(-p_{ext}\left(\frac{1000 - K_{res} - K_{swbm}}{Y\cdot\sqrt{\pi\cdot a}}\right)\cdot P_{mat}(1000)\right)$$

Calculate probability of failure

$$p_f := \frac{1000-1}{2\cdot 1000}\cdot \text{Trapsum} \qquad p_f = 3.9\times 10^{-4}$$

Check with in-built function

$$\int_0^{600} p_{ext}\left(\frac{x - K_{res} - K_{swbm}}{Y\cdot\sqrt{\pi\cdot a}}\right)\cdot P_{mat}(x)\,dx = 3.904\times 10^{-4}$$

Use FOR algorithm to calculate probability of failure

Map limit state function into normal space

$$i := 1..500$$

Define range of load values

$$x2_i := i\cdot 0.1 + 40$$

Determine range of strength variables to meet limit state

$$x1_i := Y\cdot x2_i\cdot\sqrt{\pi\cdot a} + K_{res} + K_{swbm}$$

Map points into failure domain

$$y1_i := \text{qnorm}\left(P_{mat}\left(x1_i\right), 0, 1\right)$$

$$y2_i := \text{qnorm}\left(P_{ext}\left(x2_i\right), 0, 1\right)$$

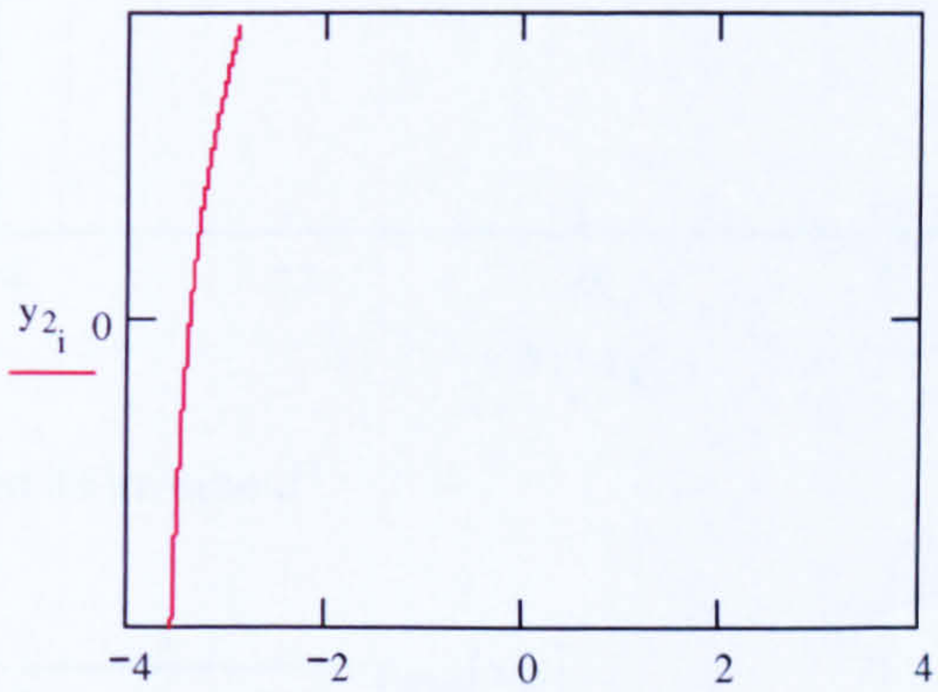

Calculate means of variables to determine suitable start points for algorithm

$$\mu_{x1} := \sum_{i=1}^{2000} \left[i \cdot \left(p_{mat}(i) \right) \right] \qquad \mu_{x1} = 465.091$$

$$\mu_{x2} := \sum_{i=1}^{1000} \left[i \cdot \left(p_{ext}(i) \right) \right] \qquad \mu_{x2} = 55.714$$

Set means as first checking point

$$x_{\chi 1} := \mu_{x1} \qquad x_{\chi 2} := \mu_{x2}$$

Transform into normal space

$$y_{\chi 1} := \text{qnorm}\left(P_{mat}\left(x_{\chi 1} \right), 0, 1 \right) \qquad y_{\chi 1} = 0.094$$

$$y_{\chi 2} := \text{qnorm}\left(P_{ext}\left(x_{\chi 2} \right), 0, 1 \right) \qquad y_{\chi 2} = 0.177$$

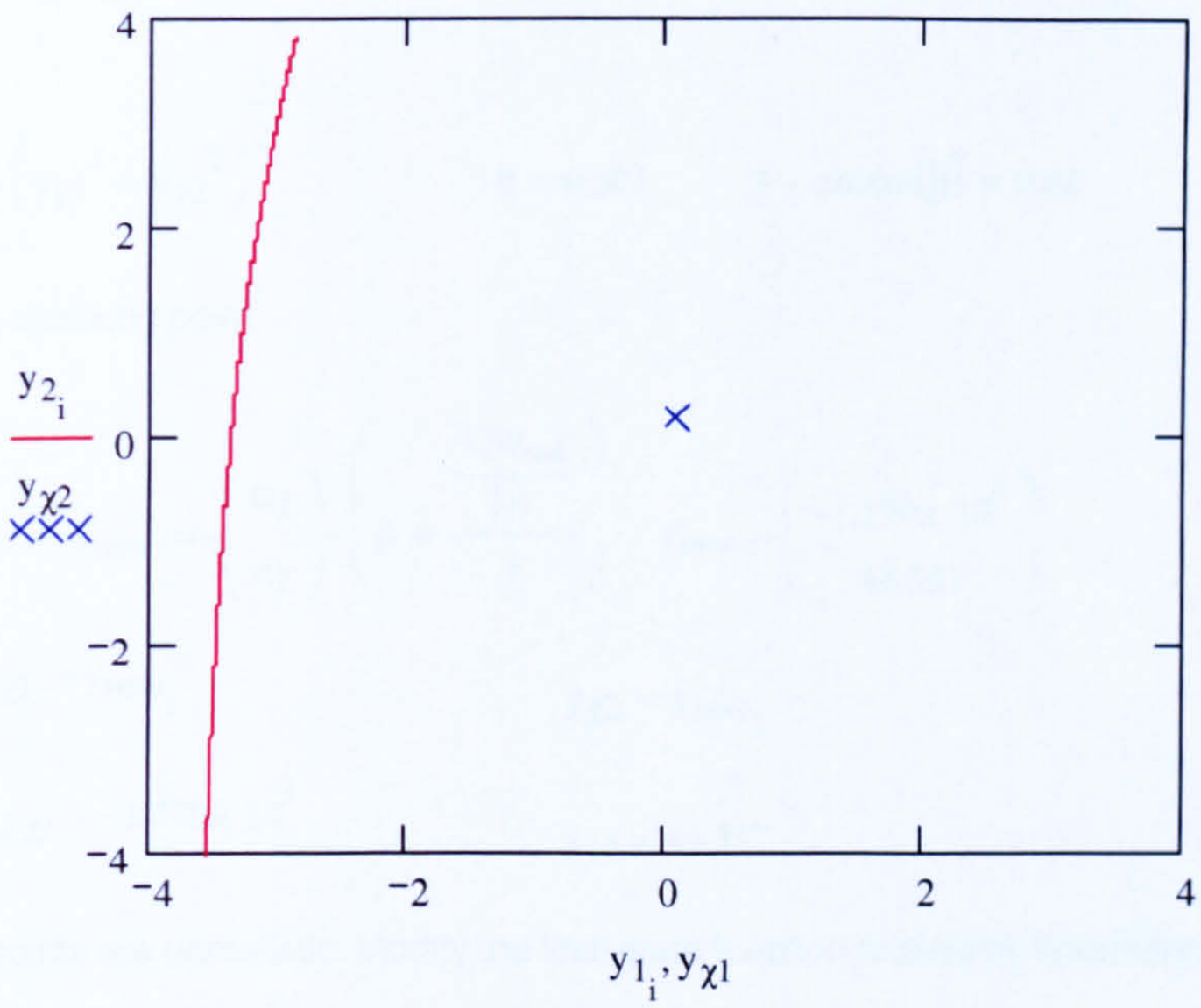

Obtain Jacobian J and its inverse J^{-1}

$$J := \begin{pmatrix} \frac{1}{\text{dnorm}\left(y_{\chi 1}, 0, 1 \right)} \cdot p_{mat}\left(x_{\chi 1} \right) & 0 \\ 0 & \frac{1}{\text{dnorm}\left(y_{\chi 2}, 0, 1 \right)} \cdot p_{ext}\left(x_{\chi 2} \right) \end{pmatrix}$$

$$J = \begin{pmatrix} 5.314\times 10^{-3} & 0 \\ 0 & 0.212 \end{pmatrix} \qquad J^{-1} = \begin{pmatrix} 188.177 & 0 \\ 0 & 4.712 \end{pmatrix}$$

Calculate direction cosines

$$c := J^{-1} \cdot \begin{pmatrix} 1 \\ -1 \end{pmatrix} \qquad c = \begin{pmatrix} 188.177 \\ -4.712 \end{pmatrix}$$

$$l := \left[\sum_{i=1}^{2} \left[(c_i)^2 \right] \right]^{\frac{1}{2}} \qquad l = 188.236$$

$$\alpha_1 := \frac{c_1}{l} \qquad \alpha_1 = 1 \qquad \alpha_2 := \frac{c_2}{l} \qquad \alpha_2 = -0.025$$

Evaluate limit state

$$LSF_{real} := x_{\chi 1} - (x_{\chi 2} + K_{swbm} + K_{res}) \qquad LSF_{real} = 377.808$$

Calculate reliability index

$$\beta := \left(y_{\chi 1}{}^2 + y_{\chi 2}{}^2 \right)^{\frac{1}{2}} \qquad \beta = 0.201 \qquad 1 - \text{cnorm}(\beta) = 0.42$$

Determine new checking point

$$y_{new} := -\begin{pmatrix} \alpha_1 \\ \alpha_2 \end{pmatrix} \cdot \begin{pmatrix} \beta + \dfrac{LSF_{real}}{|J|} \\ l \end{pmatrix} \qquad y_{new} = \begin{pmatrix} -1.779\times 10^{3} \\ 44.557 \end{pmatrix}$$

$$y_{\chi 1} := y_{new_1} \qquad y_{\chi 2} := y_{new_2}$$

$$y_{\chi 1} = -1.779\times 10^{3} \qquad y_{\chi 2} = 44.557$$

New checking points are unrealistic. Modify the limit state function to reduce increment and re-calculate the points.

Evaluate limit state

$$LSF_{real} := \frac{x_{\chi 1} - \left(x_{\chi 2} + K_{swbm} + K_{res}\right)}{1000}$$

$$LSF_{real} = 0.378$$

Determine new checking point

$$y_{new} := -\begin{pmatrix} \alpha_1 \\ \alpha_2 \end{pmatrix} \cdot \begin{pmatrix} \beta + \dfrac{LSF_{real}}{|J|} \\ 1 \end{pmatrix} \qquad y_{new} = \begin{pmatrix} -1.98 \\ 0.05 \end{pmatrix}$$

$$y_{\chi 1} := y_{new_1} \qquad y_{\chi 2} := y_{new_2}$$

$$y_{\chi 1} = -1.98 \qquad y_{\chi 2} = 0.05$$

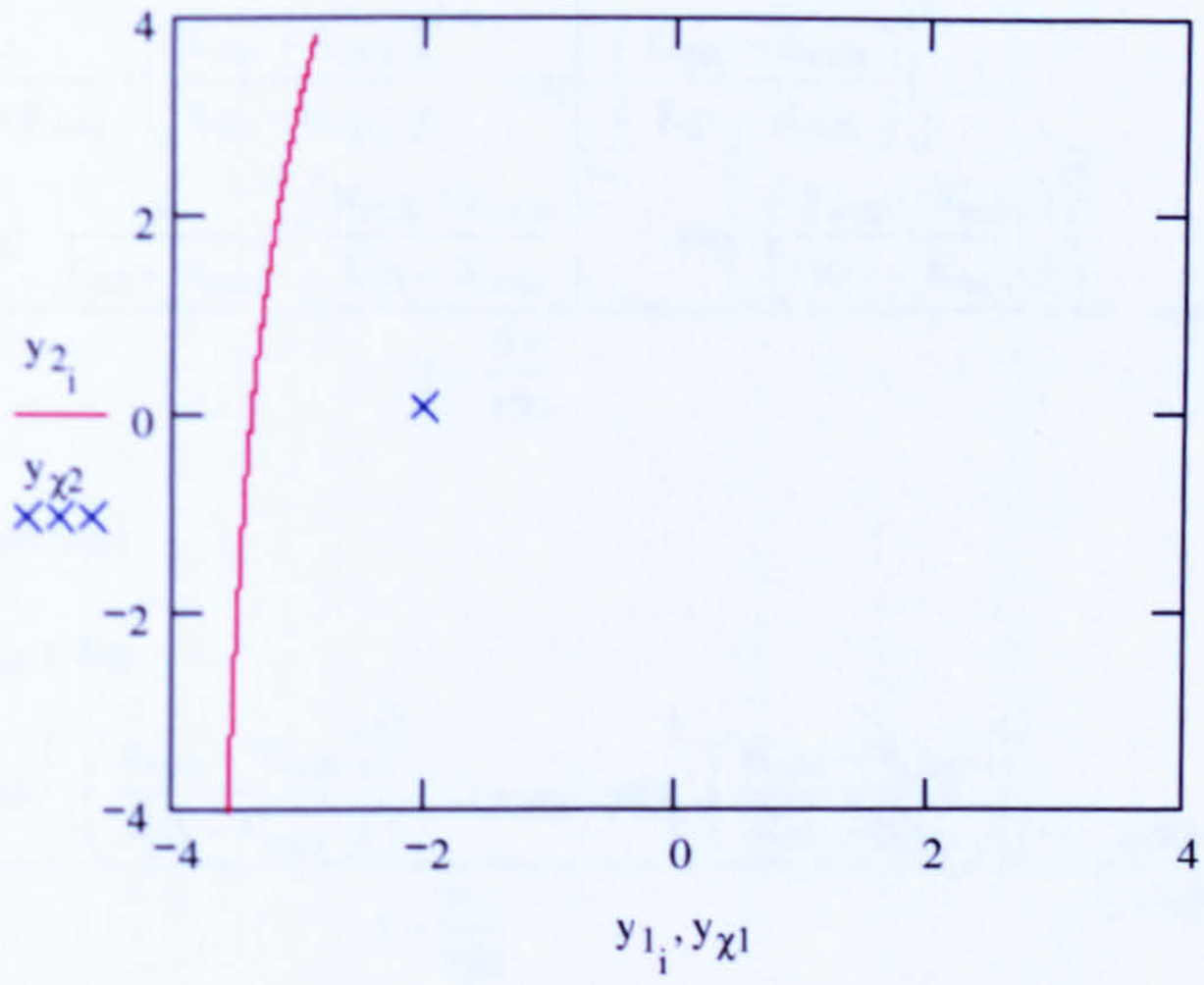

G.2 Inclusion of lower bound on fracture toughness

Calculate position of lower bound

$$K_{guess} := 100$$

Given

$$1 - p_a \cdot \exp\left[-\left(\frac{K_{guess} - K_{min}}{K_{01} - K_{min}}\right)^4\right] - (1 - p_a) \cdot \exp\left[-\left(\frac{K_{guess} - K_{min}}{K_{02} - K_{min}}\right)^4\right] = \frac{0.1}{100}$$

$$K_{lb} := \text{Find}(K_{guess}) \qquad K_{lb} = 96.216$$

Re-define density and cumulative functions in terms of lower bound

Toughness density function

$$p_{mat}(K_{mat}) := \begin{cases} 0 & \text{if } K_{mat} \le K_{lb} \\ \dfrac{p_a \dfrac{4}{K_{01} - K_{min}} \cdot \left(\dfrac{K_{mat} - K_{min}}{K_{01} - K_{min}}\right)^{4-1} \cdot \exp\left[-\left(\dfrac{K_{mat} - K_{min}}{K_{01} - K_{min}}\right)^4\right] \ldots}{1 - \frac{0.1}{100}} \\ \quad + (1 - p_a) \cdot \dfrac{4}{K_{02} - K_{min}} \cdot \left(\dfrac{K_{mat} - K_{min}}{K_{02} - K_{min}}\right)^{4-1} \cdot \exp\left[-\left(\dfrac{K_{mat} - K_{min}}{K_{02} - K_{min}}\right)^4\right] \\ \qquad\qquad 1 - \dfrac{0.1}{100} \end{cases} \quad \text{otherwise}$$

Toughness distribution function

$$P_{mat}(K_{mat}) := \begin{cases} 0 & \text{if } K_{mat} \le K_{lb} \\ \dfrac{1 - p_a \cdot \exp\left[-\left(\dfrac{K_{mat} - K_{min}}{K_{01} - K_{min}}\right)^4\right] - (1 - p_a) \cdot \exp\left[-\left(\dfrac{K_{mat} - K_{min}}{K_{02} - K_{min}}\right)^4\right]}{1 - \frac{0.1}{100}} - \dfrac{0.001}{1 - 0.001} & \text{otherwise} \end{cases}$$

$i := 1 .. 1000$

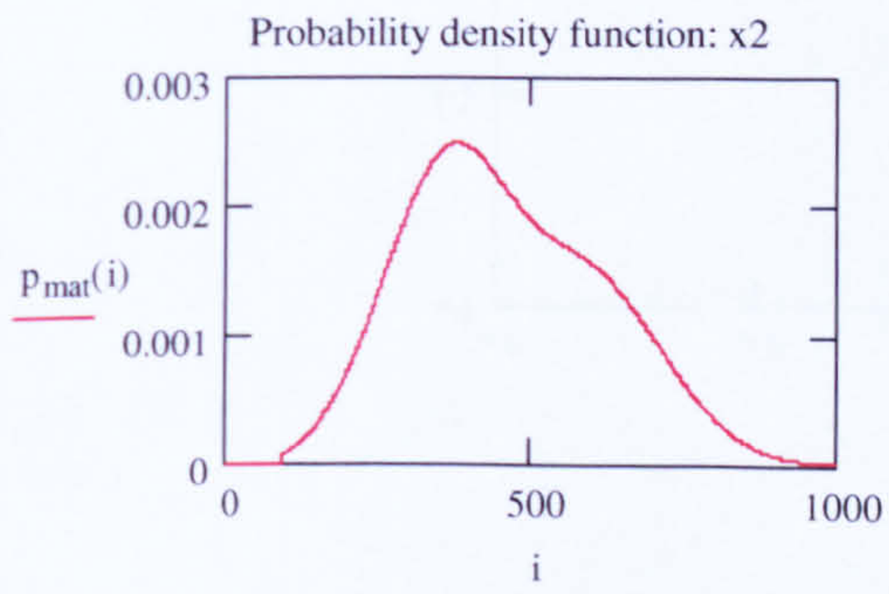

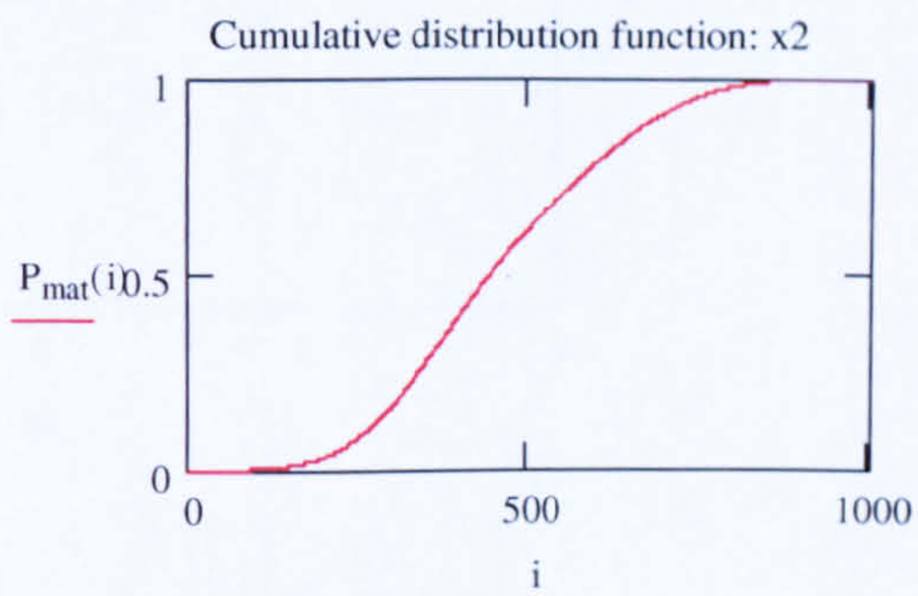

Calculate probability of failure using convolution integral (and trapezium rule)

$$Trapsum := \left[\sum_{x=1}^{1000} \left[2 \left(p_{ext}\left(\frac{x - K_{res} - K_{swbm}}{Y \cdot \sqrt{\pi \cdot a}} \right) \cdot P_{mat}(x) \right) \right] \right] - \left(p_{ext}\left(\frac{1 - K_{res} - K_{swbm}}{Y \cdot \sqrt{\pi \cdot a}} \right) \cdot P_{mat}(1) \right) \ldots + \left(-p_{ext}\left(\frac{1000 - K_{res} - K_{swbm}}{Y \cdot \sqrt{\pi \cdot a}} \right) \cdot P_{mat}(1000) \right)$$

Calculate probability of failure

$$p_f := \frac{1000 - 1}{2 \cdot 1000} \cdot Trapsum \qquad p_f = 1.412 \times 10^{-6}$$

Check with in-built function

$$\int_0^{200} p_{ext}\left(\frac{x - K_{res} - K_{swbm}}{Y \cdot \sqrt{\pi \cdot a}} \right) \cdot P_{mat}(x)\, dx = 1.4 \times 10^{-6}$$

Use FOR algorithm to calculate probability of failure

Map limit state function into normal space

$$i := 1 .. 50$$

Define range of load values

$$x2_i := i + \frac{K_{lb} - K_{res} - K_{swbm}}{Y \cdot \sqrt{\pi a}}$$

Determine range of strength variables to meet limit state

$$x1_i := Y \cdot x2_i \cdot \sqrt{\pi \cdot a} + K_{res} + K_{swbm}$$

Map points into failure domain

$$y1_i := qnorm\left(P_{mat}\left(x1_i\right), 0, 1\right)$$

$$y2_i := qnorm\left(P_{ext}\left(x2_i\right), 0, 1\right)$$

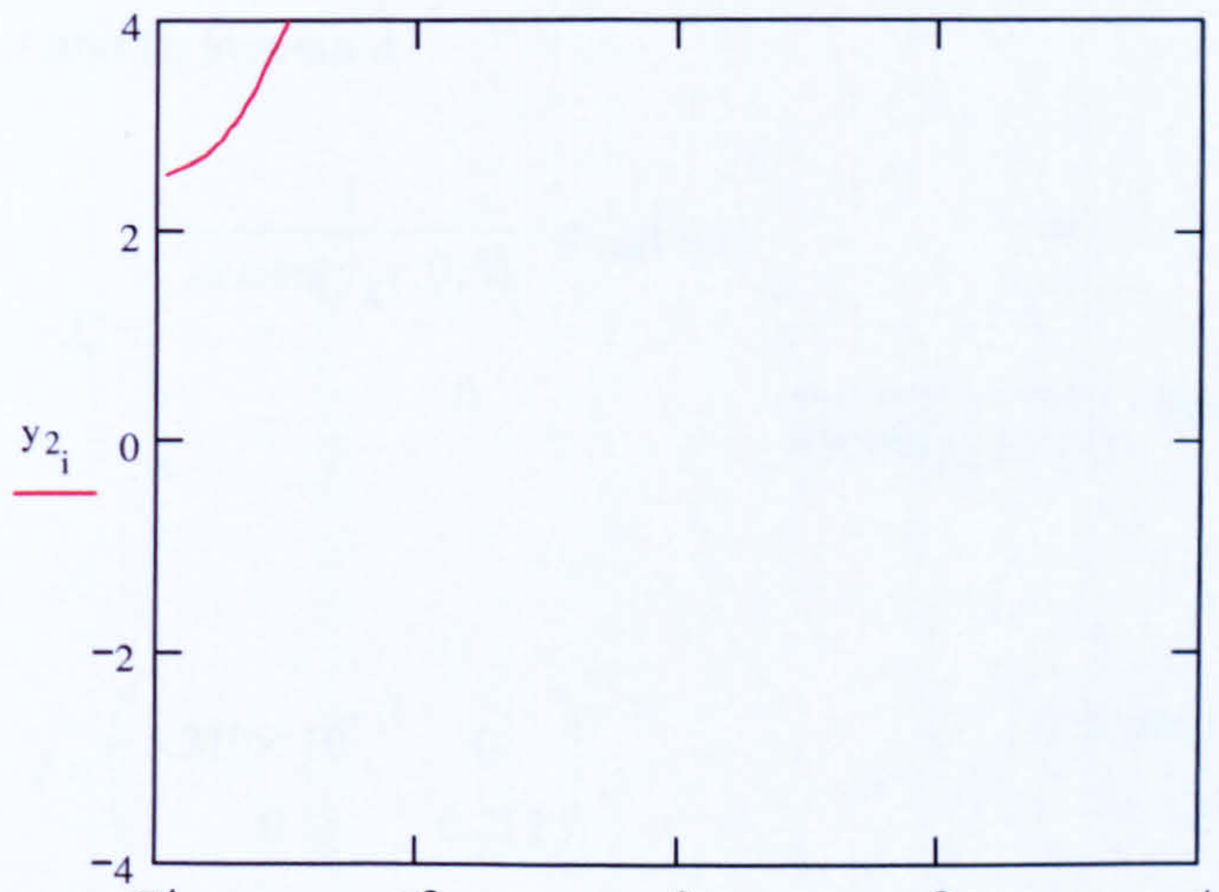

Set means as first checking point

$x_{\chi 1} := \mu_{x1}$ $x_{\chi 2} := \mu_{x2}$

Transform into normal space

$y_{\chi 1} := \text{qnorm}\left(P_{mat}\left(x_{\chi 1}\right), 0, 1\right)$ $y_{\chi 1} = 0.093$

$y_{\chi 2} := \text{qnorm}\left(P_{ext}\left(x_{\chi 2}\right), 0, 1\right)$ $y_{\chi 2} = 0.177$

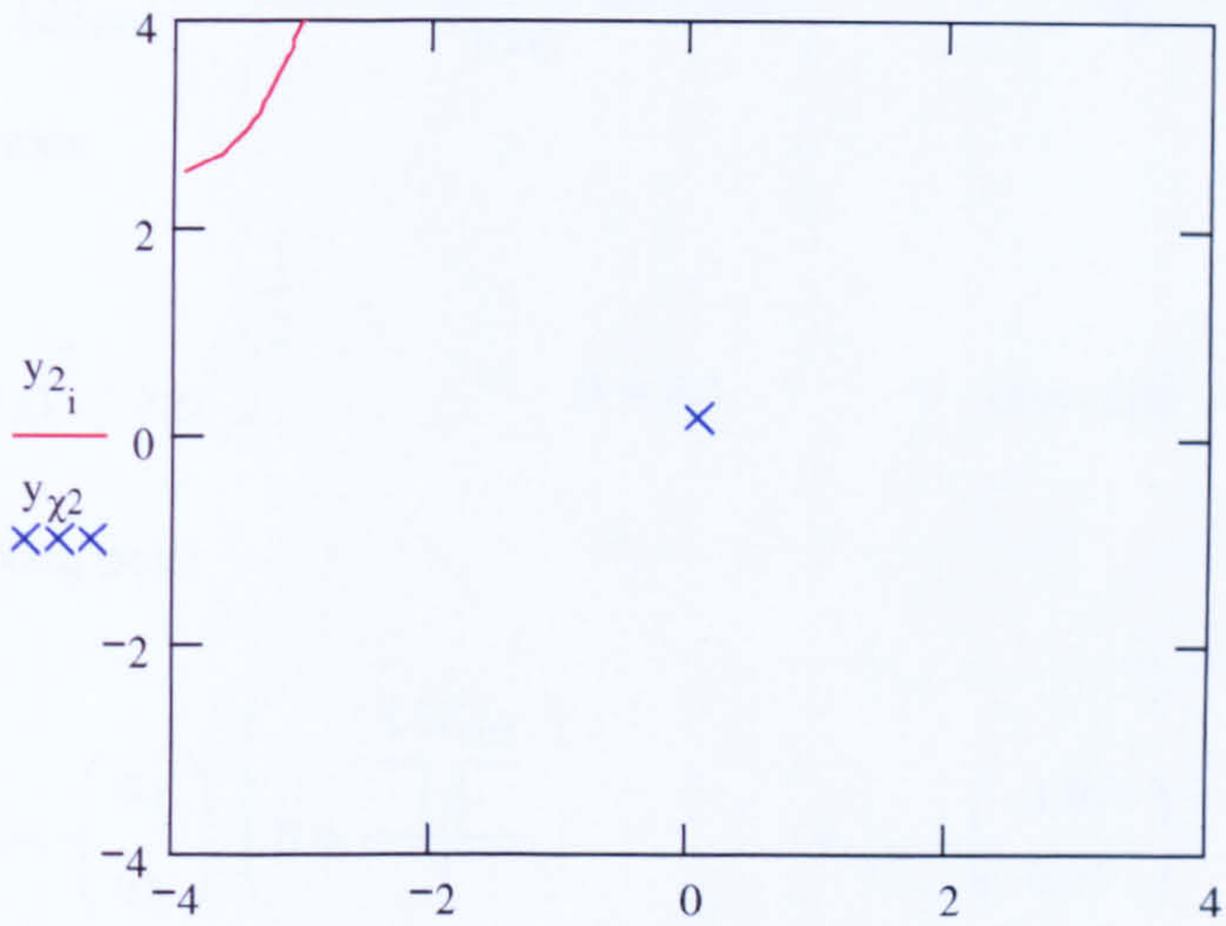

Obtain Jacobian J and its inverse J^{-1}

$$J := \begin{pmatrix} \frac{1}{\text{dnorm}\left(y_{\chi 1}, 0, 1\right)} \cdot p_{mat}\left(x_{\chi 1}\right) & 0 \\ 0 & \frac{1}{\text{dnorm}\left(y_{\chi 2}, 0, 1\right)} \cdot p_{ext}\left(x_{\chi 2}\right) \end{pmatrix}$$

$$J = \begin{pmatrix} 5.319 \times 10^{-3} & 0 \\ 0 & 0.212 \end{pmatrix} \qquad J^{-1} = \begin{pmatrix} 188.009 & 0 \\ 0 & 4.712 \end{pmatrix}$$

Calculate direction cosines

$$c := J^{-1} \cdot \begin{pmatrix} 1 \\ -1 \end{pmatrix} \qquad c = \begin{pmatrix} 188.009 \\ -4.712 \end{pmatrix}$$

$$l := \left[\sum_{i=1}^{2} \left[\left(c_i\right)^2\right]\right]^{\frac{1}{2}} \qquad l = 188.068$$

$$\alpha_1 := \frac{c_1}{l} \qquad \alpha_1 = 1 \qquad \alpha_2 := \frac{c_2}{l} \qquad \alpha_2 = -0.025$$

Evaluate limit state

$$LSF_{real} := \frac{x_{\chi 1} - \left(x_{\chi 2} + K_{swbm} + K_{res}\right)}{1000} \qquad LSF_{real} = 0.378$$

Calculate reliability index

$$\beta := \left(y_{\chi 1}{}^2 + y_{\chi 2}{}^2\right)^{\frac{1}{2}} \qquad \beta = 0.2 \qquad 1 - cnorm(\beta) = 0.421$$

Determine new checking point

$$y_{new} := -\begin{pmatrix} \alpha_1 \\ \alpha_2 \end{pmatrix} \cdot \left(\beta + \frac{LSF_{real}}{\frac{|J|}{l}}\right) \qquad y_{new} = \begin{pmatrix} -1.979 \\ 0.05 \end{pmatrix}$$

$y_{\chi 1} := y_{new_1}$ $\qquad$ $y_{\chi 2} := y_{new_2}$

$y_{\chi 1} = -1.979$ $\qquad$ $y_{\chi 2} = 0.05$

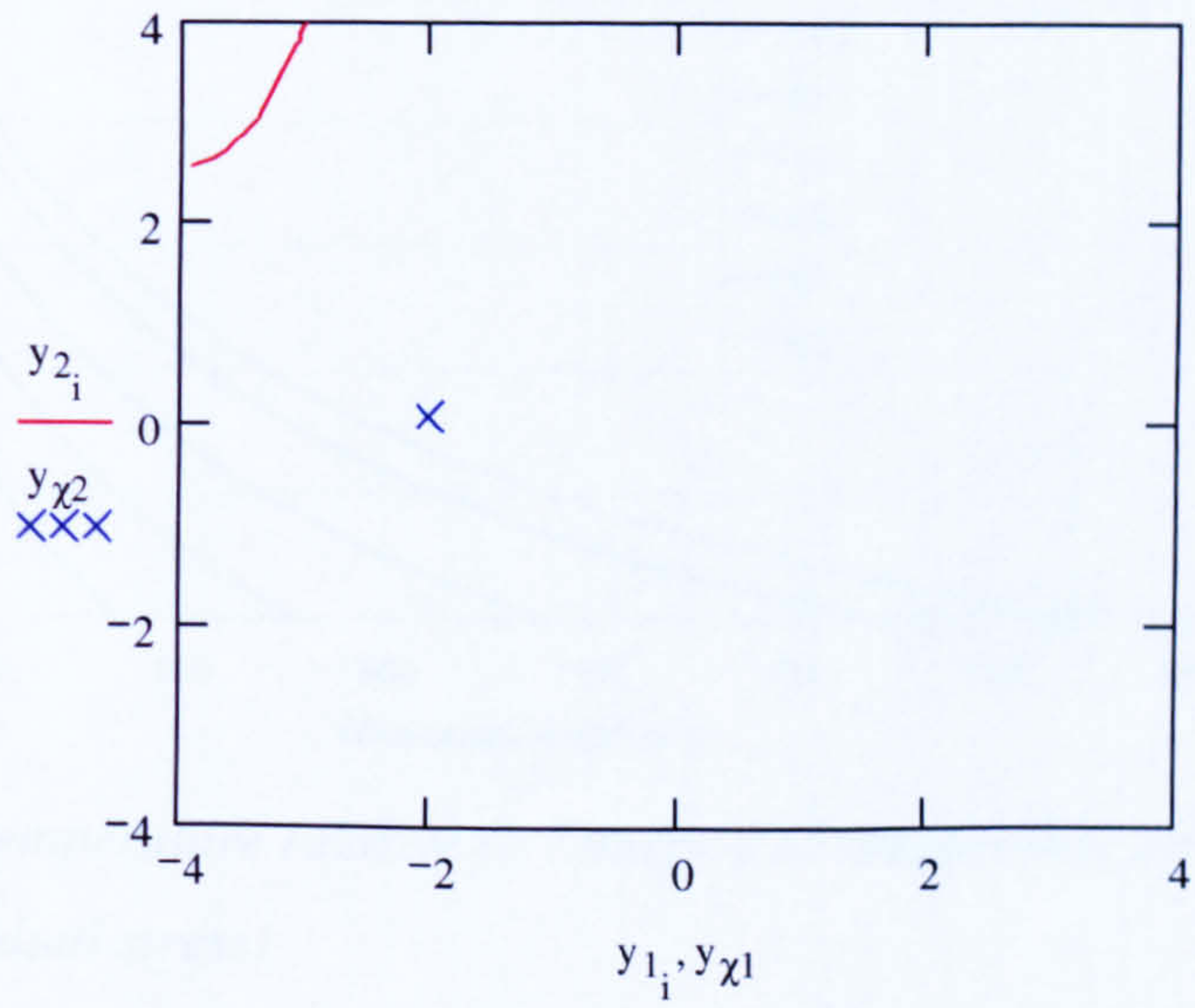

H Results

H.1 Parametric study

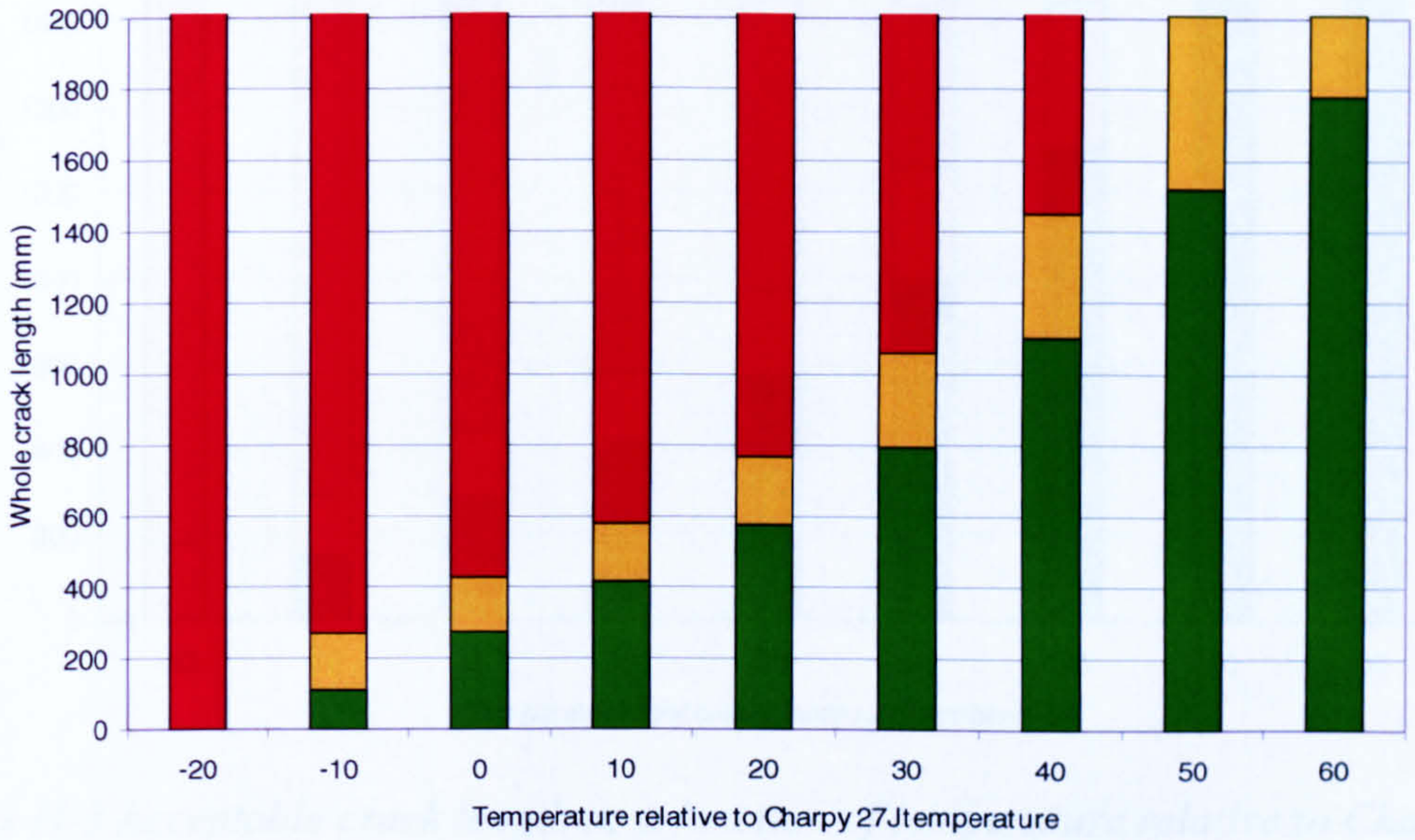

Figure H-1 Acceptable crack length as a function of temperature relative to Charpy 27J temperature (residual stress)

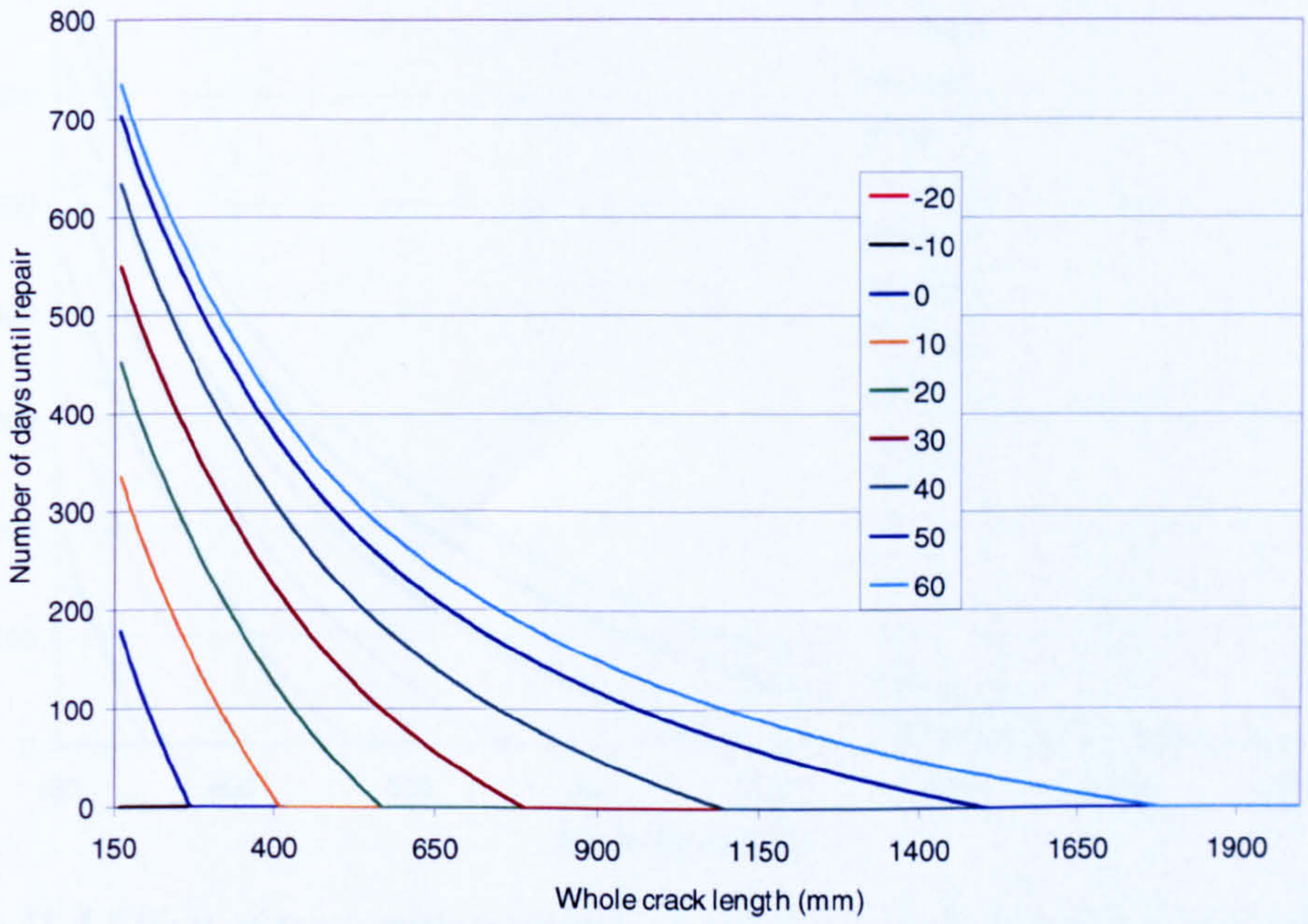

Figure H-2 Effect of temperature relative to Charpy 27J temperature on number of days until repair (residual stress)

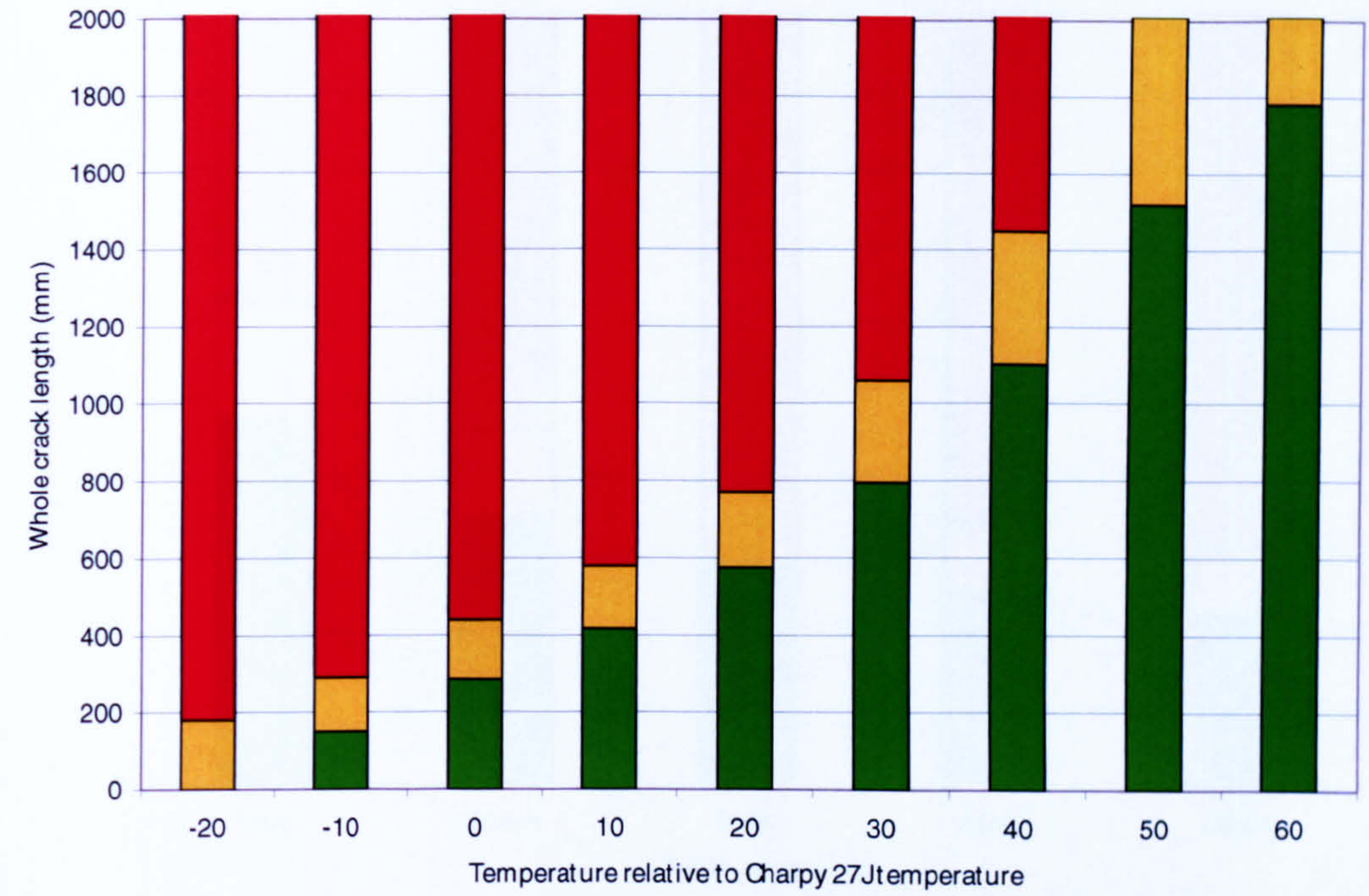

Figure H-3 Acceptable crack length as a function of temperature relative to Charpy 27J temperature (no residual stress)

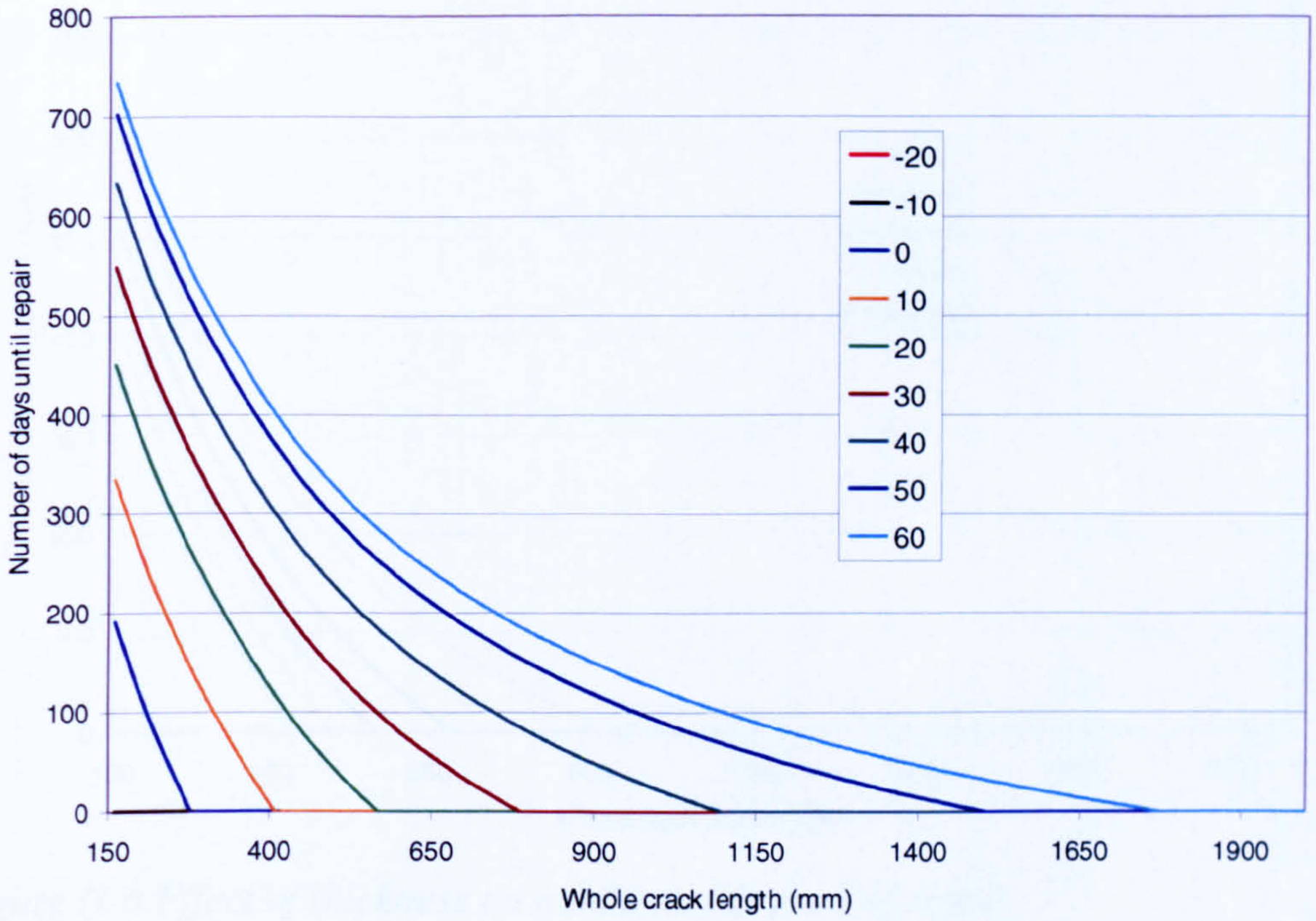

Figure H-4 Effect of temperature relative to Charpy 27J temperature on number of days until repair (no residual stress)

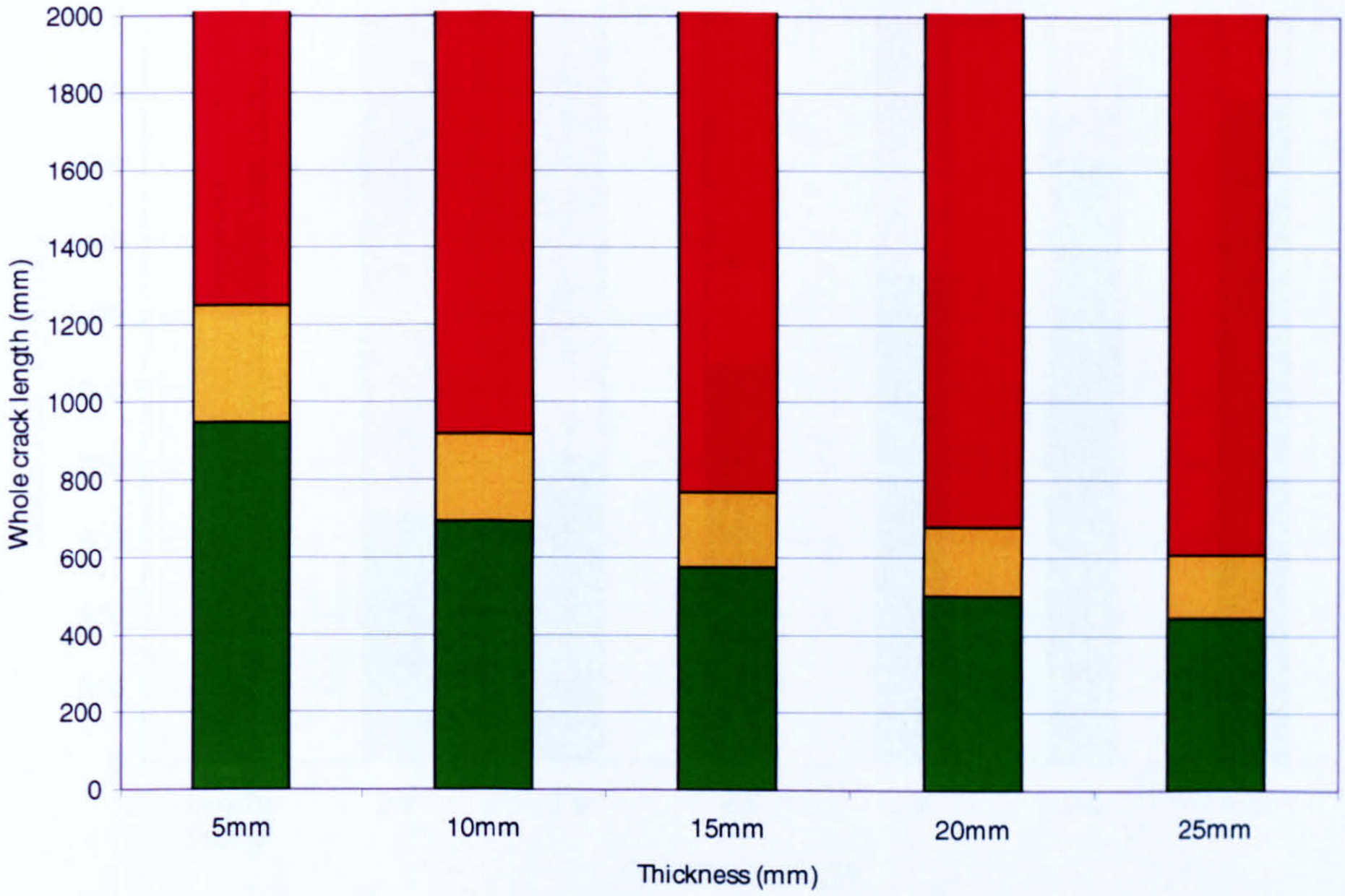

Figure H-5 Effect of thickness on acceptable crack length

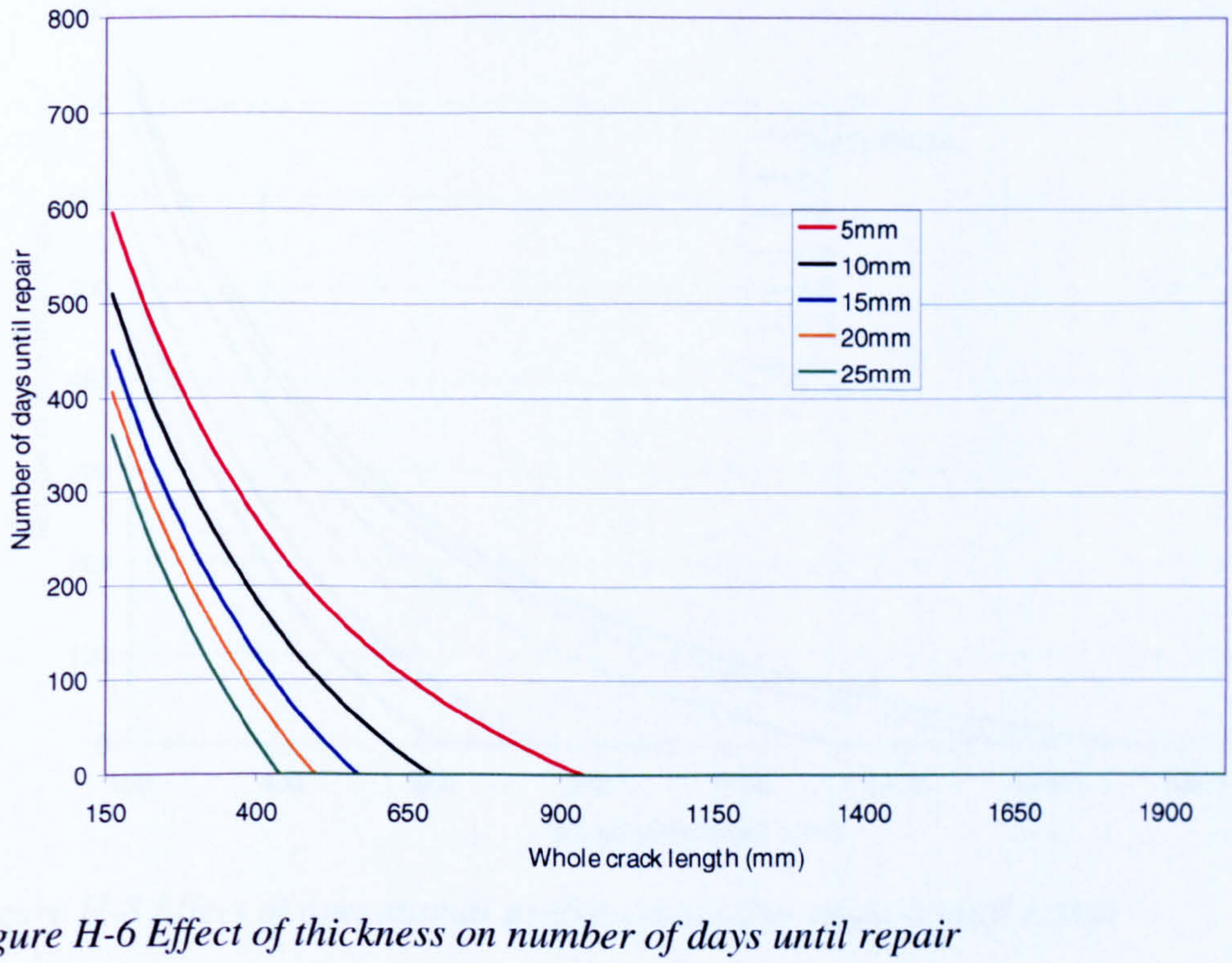

Figure H-6 Effect of thickness on number of days until repair

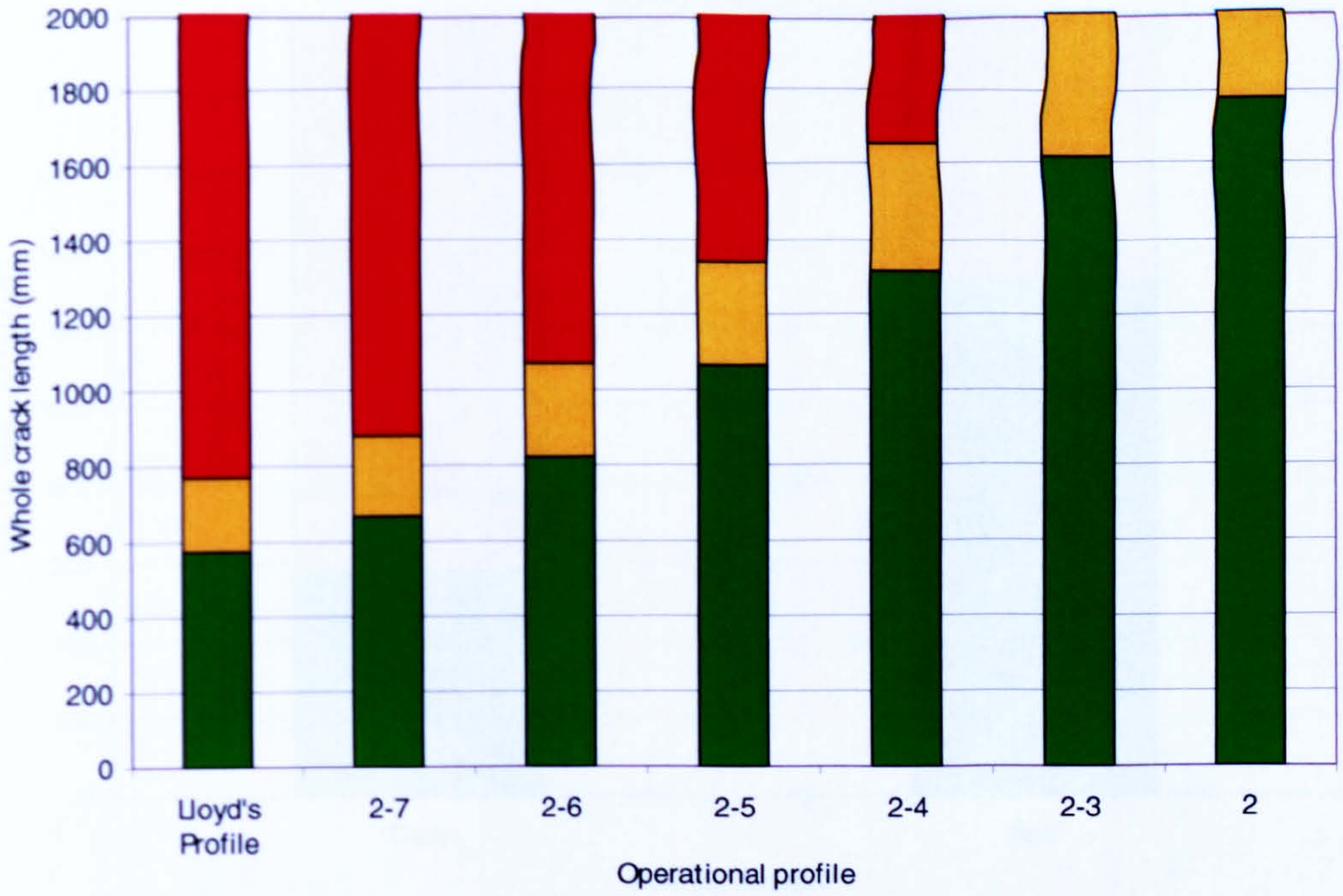

Figure H-7 Effect of operational profile on acceptable crack length

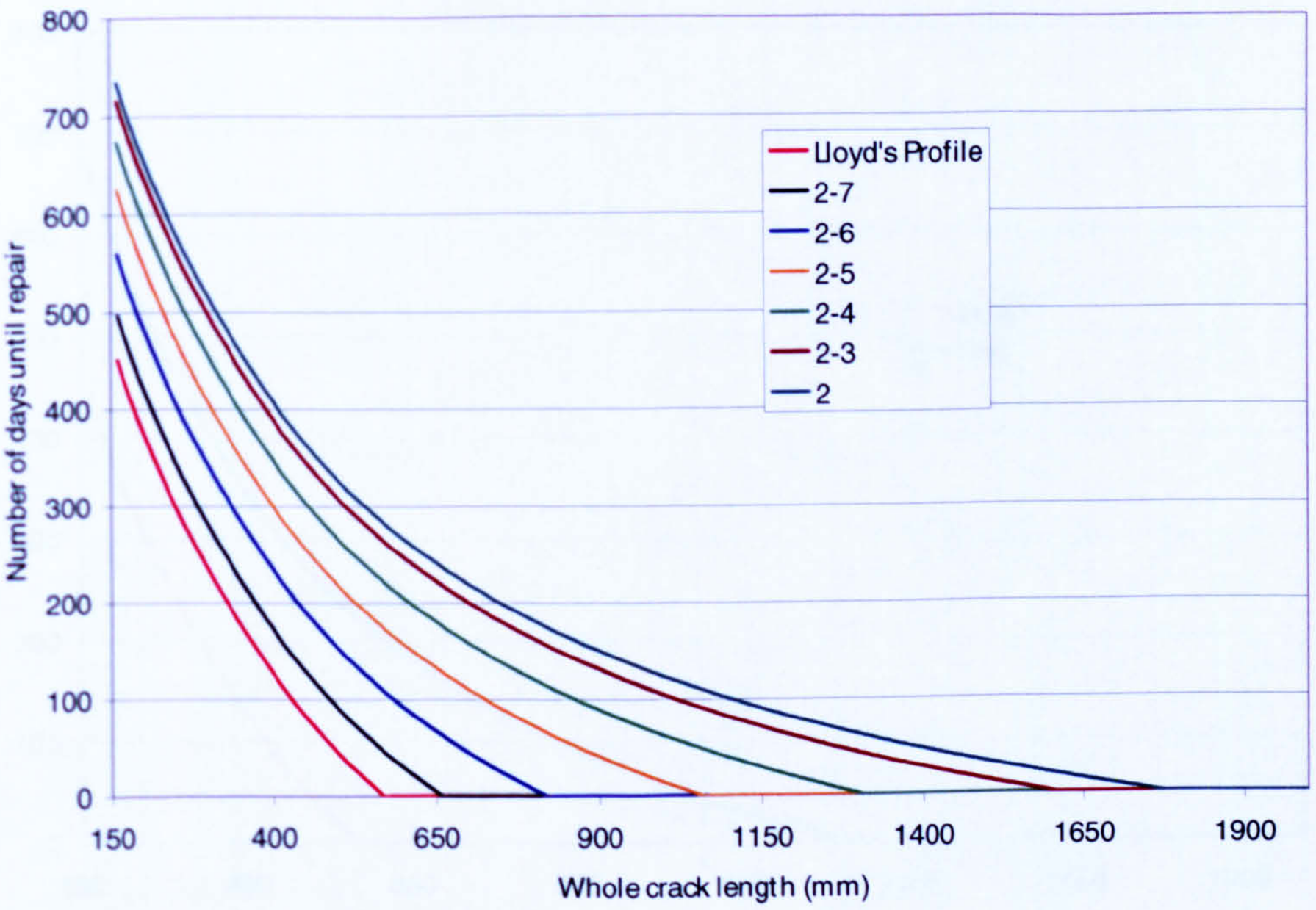

Figure H-8 Effect of operational profile on number of days until repair

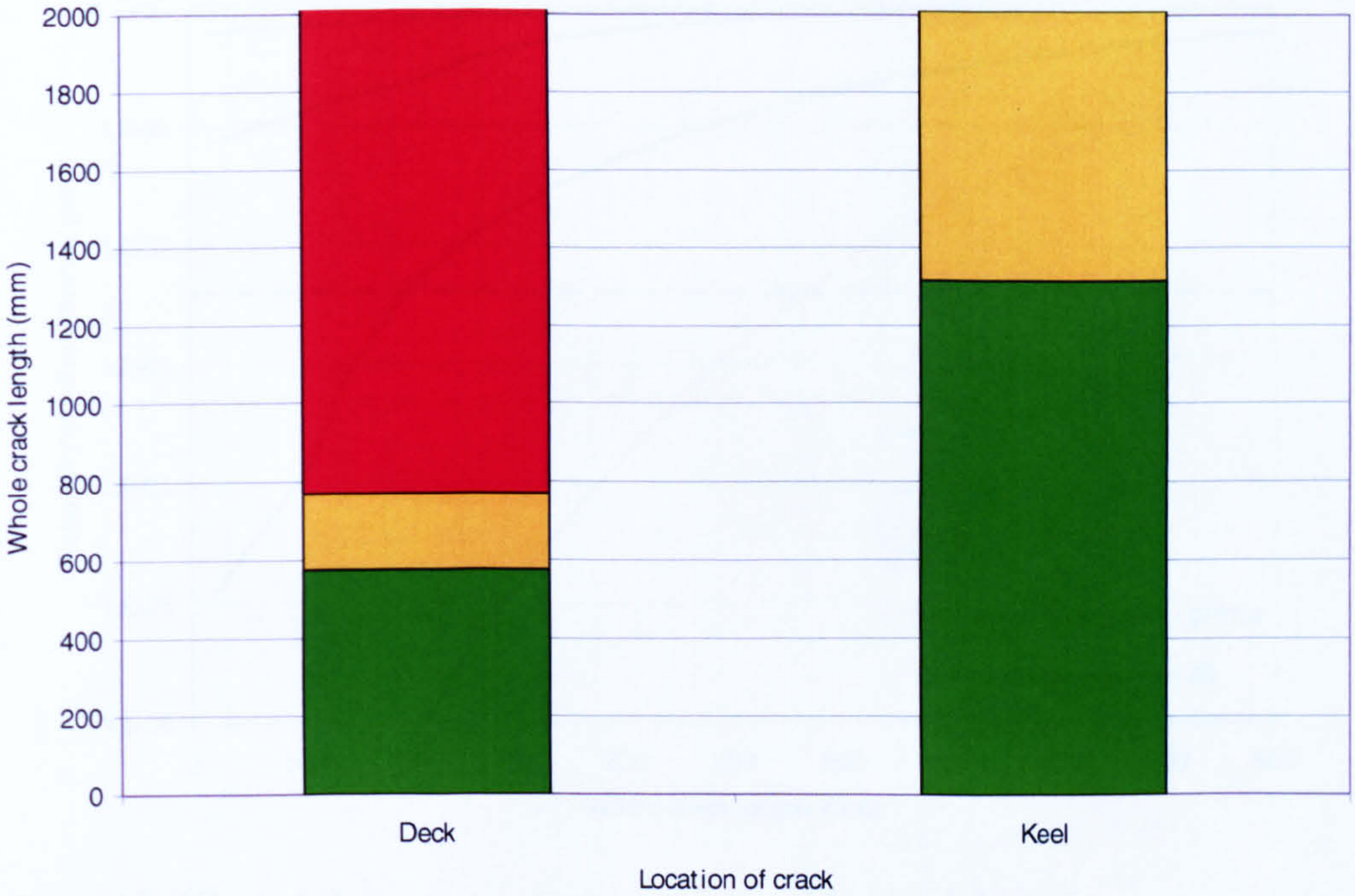

Figure H-9 Effect of location on acceptable crack length

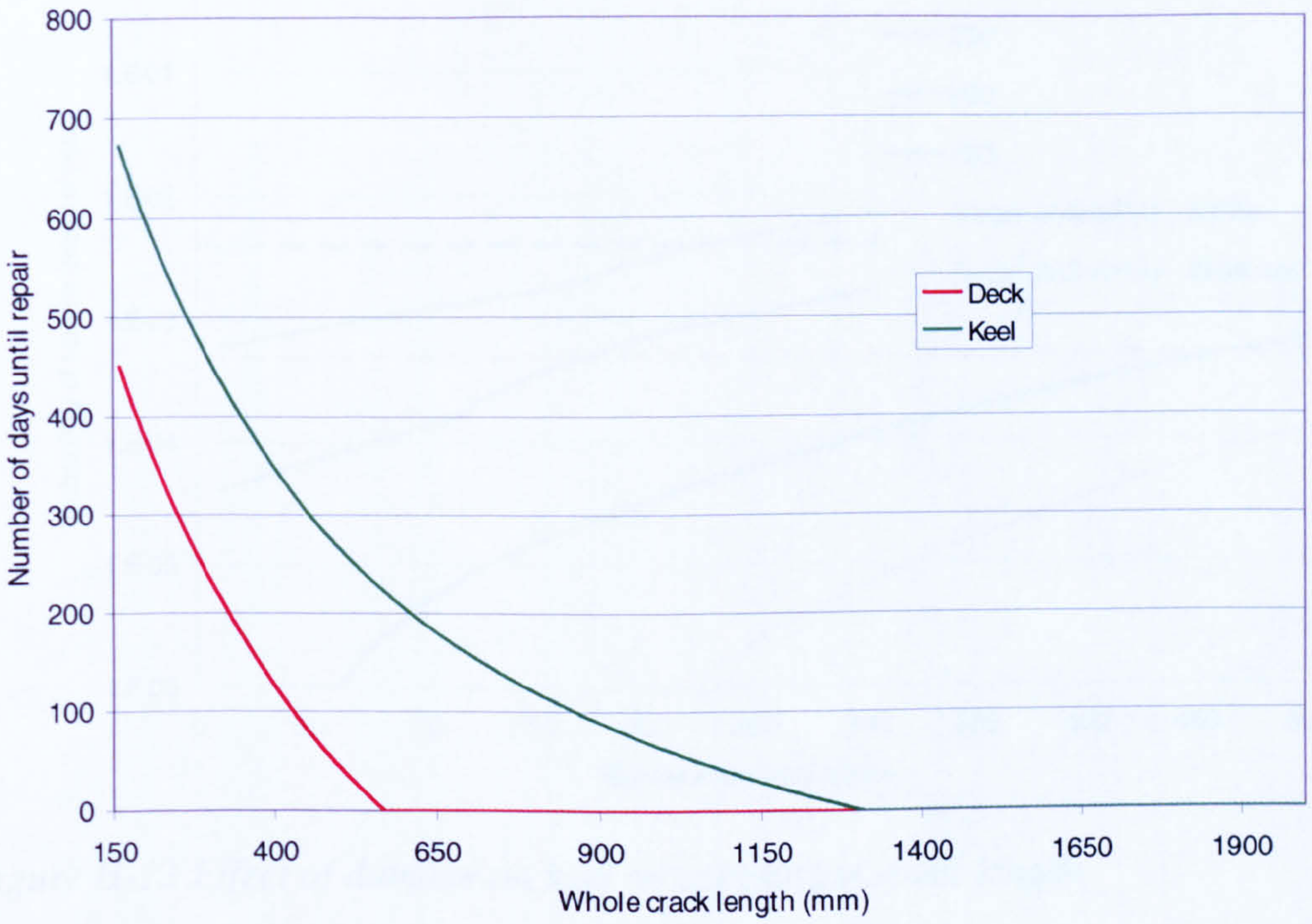

Figure H-10 Effect of location on number of days until repair

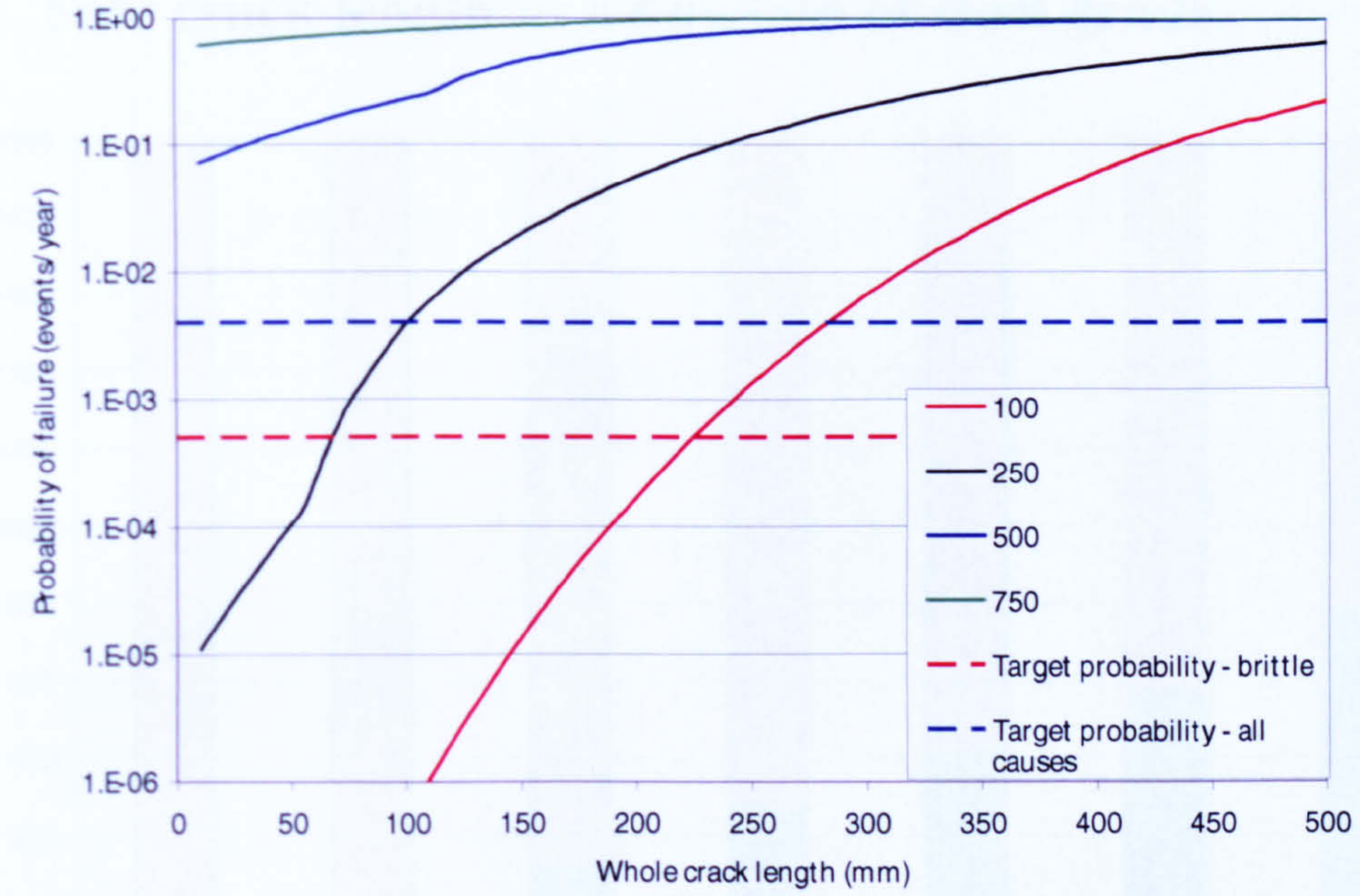

Figure H-11 Effect of damage on deck on acceptable crack length

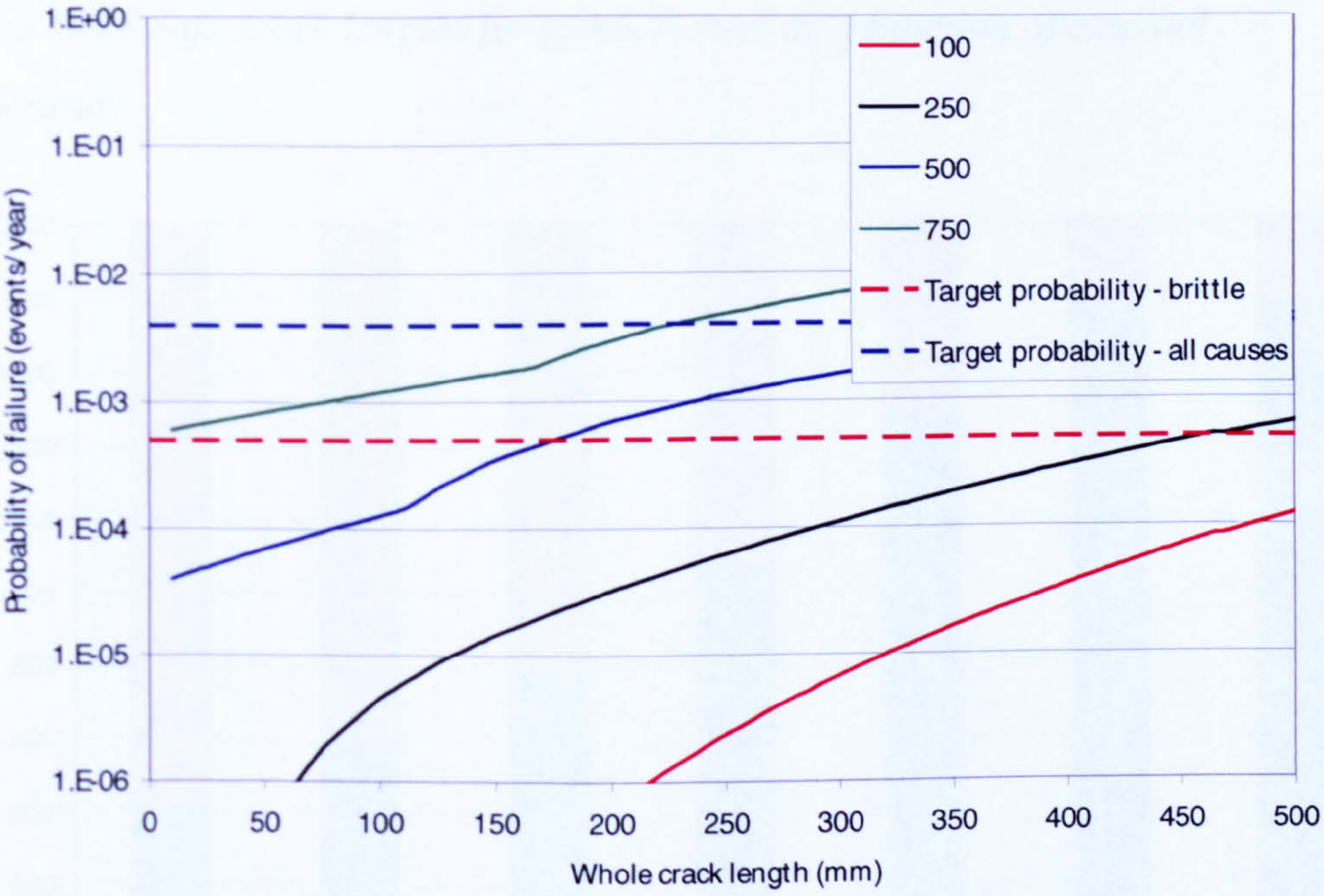

Figure H-12 Effect of damage on keel on acceptable crack length

H.2 Safe crack length as a function of steel grade

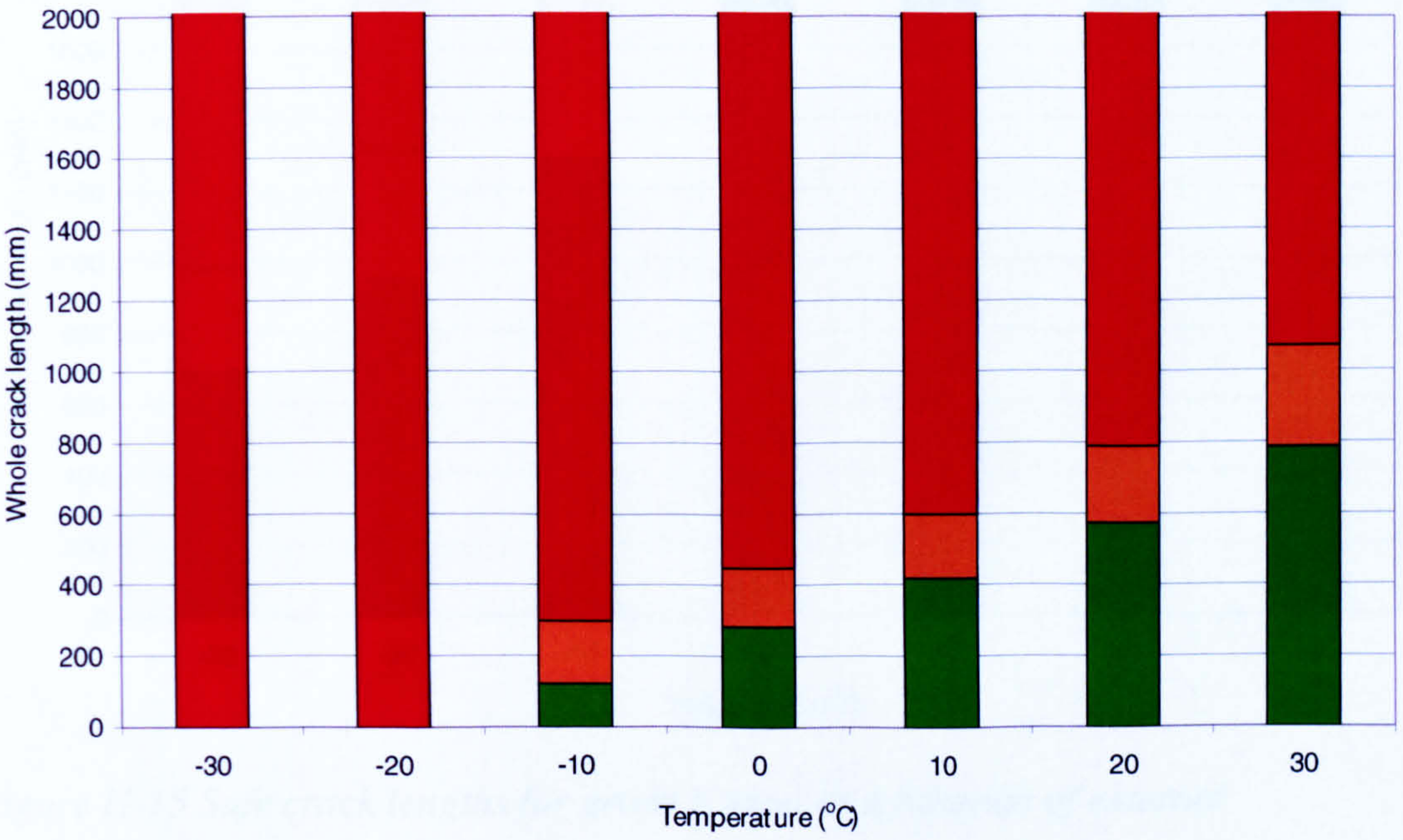

Figure H-13 Safe crack lengths for grade A steel as a function of external temperature

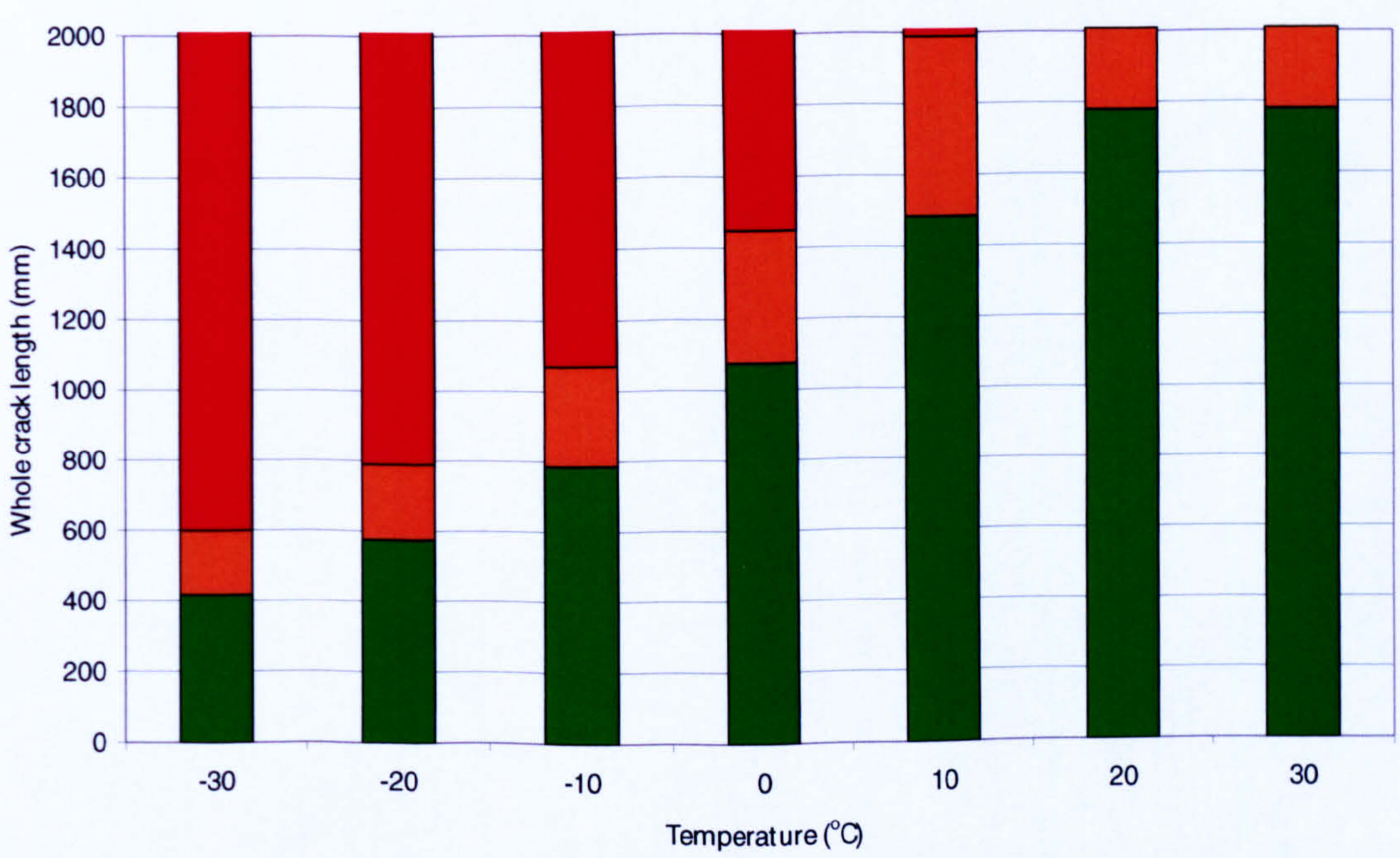

Figure H-14 Safe crack lengths for grade D steel as a function of external temperature

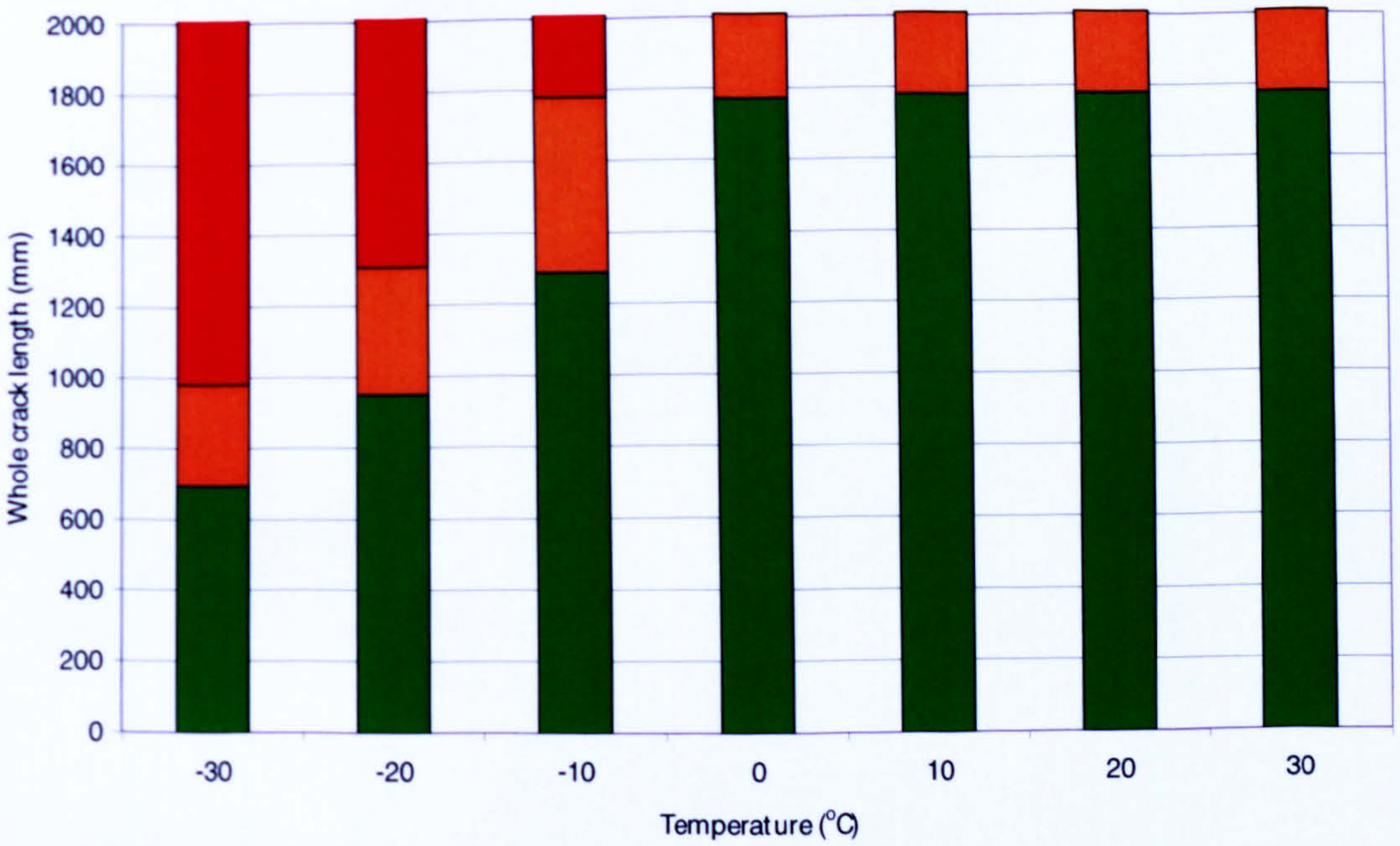

Figure H-15 Safe crack lengths for grade E steel as a function of external temperature